Universiteit Gent
Faculty of Sciences
Dept. of Plant Biotechnology and Bioinformatics

KU Leuven
Faculty of Bioscience Engineering
Centre of Microbial and Plant Genetics

# Network-based identification of driver pathways in clonal systems

## Netwerk-gebaseerde identificatie van causale moleculaire processen in klonale systemen

# Bram Weytjens

Promotors:
Prof. Kathleen Marchal, Universiteit Gent
Prof. Jos Vanderleyden, KU Leuven

Members of the examination board:
Prof. Aurélien Carlier
Prof. Bart Devreese
Prof. Jan Fostier
Prof. Jan Michiels
Prof. Luc De Raedt
Dr. Jimmy Van den Eynden
Dr. Lieven Verbeke

Dissertation presented in partial
fulfillment of the requirements for
the degrees of:
Doctor of Science: Bioinformatics,
and
Doctor of Bioscience Engineering
Academic year 2017-2018

Uitgegeven in eigen beheer, Bram Weytjens, Wijshagen

# Dankwoord

*”No man is an island”*
*-John Donne-*

Biologische netwerken opstellen, data klaarmaken voor analyse, computerprogramma’s ontwikkelen om de data met behulp van voorgenoemde netwerken te analyseren,... het was een uitdaging. Ik ben blij dat ik tevreden kan terugkijken op dit project en dat er concrete toepassingen zijn gepubliceerd die bruikbaar zijn in de praktijk. Maar ik had dit nooit alleen kunnen bereiken. Hier wil ik iedereen bedanken die mij de afgelopen jaren op gelijk welke manier heeft gesteund.

Ik weet nog toen, nu al ongeveer 6 jaar geleden, professor Vanderleyden een project over biologische netwerken kwam voorstellen voor de masterproeven. Het project had weinig tot geen succes omdat biologie noch programmeren echt goed aan bod kwamen tijdens de opleiding burgerlijk ingenieur chemie. Maar gezien mijn interesse in biologie was dat project mij op het lijf geschreven en zo kwam ik terecht bij de groep van professor Kathleen Marchal en was Dries De Maeyer mijn opzichter tijdens mijn master thesis. Dries, jij moet gedacht hebben: ‘Wat gooien ze hier nu binnen?’ Een student die nog nooit van de ‘map‘ of ‘filter‘ functies heeft gehoord en denkt dat ‘Python‘ gewoon de Engelse benaming is voor een slangensoort. Maar je hebt je daar niet bij neergelegd en legde mij met plezier, gevraagd of ongevraagd, alle technische details van zowat alles wat op ons computerscherm verscheen haarfijn uit. Hoewel ik 90% van de tijd vooral overdonderd was door de hoeveelheid informatie die je mij gaf, heeft het er toch toe geleid dat ik vandaag kan zeggen dat ik kan programmeren. Bedankt, Dries! Zonder jouw officieuze programmeerlessen was dit project mij nooit gelukt.

Geen doctoraat zonder promotoren. Bedankt Kathleen voor het gegeven vertrouwen en de kans om dit doctoraat uit te voeren. Het over-en-weer mailen van nieuwe versies van papers zal mij nog lang bij blijven. We zouden toch eens moeten navragen of ”versie 109” een record is voor een wetenschappelijke paper. Ook bedankt professor Vanderleyden om de rol van promotor aan KU Leuven op jou te nemen.

Bio-informatica is een zeer interdisciplinair veld. Dit werk zou dus niet tot stand zijn gekomen zonder de samenwerkingen met collega's uit aanverwante velden. Bedankt Toon S, Sergio P-T, Pieter A, Dries VD en alle anderen voor jullie interesse, enthousiasme en vaak uitgebreide wetenschappelijke discussies.

Verder wil ik nog mijn beide partner instituten, UGent en KU Leuven, bedanken voor het gebruik van hun faciliteiten en iedereen die betrokken is bij het NATAR project, onder leiding van prof. Kevin Verstrepen, voor het delen van ideeën en resultaten tijdens de NATAR meetings en de financiering van dit project.

De boog kan niet altijd gespannen staan. Gelukkig kan ik altijd op mijn vrienden rekenen wanneer het tijd is om te ontspannen. Of het nu gaat om een rustig avondje gezelschapsspelletjes spelen, stijldansen in Bree, op café gaan, knotsgekke vakanties met 'de mannen van Peer' of ons eigen bier brouwen in de kelder. Het zijn stuk voor stuk leuke momenten met geweldige vrienden. Merci allemaal! En Peter en Jo: ooit maken we dat geweldige bier waar we nu al drie jaar naartoe werken.

Natuurlijk mag mijn (schoon)familie hier niet ontbreken. Mama, papa: bedankt voor de steun op alle vlakken de voorbije jaren. Het is dankzij de kansen, de raad en de hulp die ik altijd van jullie gekregen heb dat ik hier ben geraakt. Geert: bedankt voor de leuke momenten en onze seizoensgebonden avonden "Game of Thrones" kijken. Miet en Dominique: bedankt om regelmatig als babysit te fungeren zodat ik de tijd had om aan dit doctoraat te werken.

Tijdens mijn doctoraat heb ik afscheid moeten nemen van mijn nonkel, Jan Weytjens, die altijd een bijzondere interesse in mijn studies en doctoraat had. Jammer genoeg kan je vandaag niet meer op mijn verdediging aanwezig zijn maar bedankt voor alle telefoontjes en gesprekken. Jij wist mij altijd op te beuren als mij iets tegen stak.

Schat, schattebout, liefie, lieveke, kleine. Als er iemand heeft te klagen over dit doctoraat dan ben jij dat wel. De afgelopen jaren waren voor ons uitzonderlijk druk en spannend: trouwen, huisje kopen, een praktijk voor jou opbouwen, de komst van onze lieve schat Elise en dat allemaal terwijl ik vaak nog tot 11 uur 's avonds moest doorwerken. En als er papers binnen moesten zat ik soms tot een gat in de nacht voor mijn computer zodat je in het weekend hoegenaamd ook niks meer aan mij had omdat het dan tijd was om te slapen. Bedankt, schat! Om ook in periodes die voor ons allebei druk waren, een steun voor mij te zijn waarop ik altijd kan terugvallen. Ik ben nu al benieuwd naar ons volgende avontuur.

*Gent, oktober 2017*
*Bram Weytjens*

# Abstract

Highly ethanol-tolerant bacteria for the production of biofuels, bacterial pathogenes which are resistant to antibiotics and cancer cells are examples of phenotypes that are of importance to society and are currently being studied. In order to better understand these phenotypes and their underlying genotype-phenotype relationships it is now commonplace to investigate DNA and expression profiles using next generation sequencing (NGS) and microarray techniques. These techniques generate large amounts of omics data which result in lists of genes that have mutations or expression profiles which potentially contribute to a specific phenotype under research. These lists often include a multitude of genes and are troublesome to verify manually as performing literature studies and wet-lab experiments for a large number of genes is very time and resources consuming. Therefore, (computational) methods are required which can narrow these gene lists down by removing generally abundant false positives from these lists and can ideally provide additional information on the relationships between the selected genes.

Other high-throughput techniques such as yeast two-hybrid (Y2H), ChIP-Seq and Chip-Chip but also a myriad of small-scale experiments and predictive computational methods have generated a treasure of interactomics data over the last decade and a lot of it is now publicly available. By combining this data into a biological interaction network, which contains all molecular pathways that an organism can utilize and thus is the equivalent of the blueprint of an organism, it is possible to integrate the omics data obtained from experiments with these biological interaction networks. Biological interaction networks are key to the computational methods presented in this thesis as they enables methods to account for important relations between genes (and gene products). Doing so it is possible to not only identify interesting genes but also to uncover molecular processes important to the phenotype.

As the best way to analyze omics data from an interesting phenotype varies widely based on the experimental setup and the available data, multiple methods were developed and applied in the context of this thesis.

In a first approach, an existing method (PheNetic) was applied to a consortium of three bacterial species that together are able to efficiently degrade a herbicide but none of the species are able to efficiently degrade the herbicide on their own. For each of the species expression data (RNA-seq) was generated for the consortium and the species in isolation. PheNetic identified molecular pathways which were differentially expressed and likely contribute to a cross-feeding mechanism between the species in the consortium.

Having obtained proof-of-concept, PheNetic was adapted to cope with experimental evolution datasets in which, in addition to expression data, genomics data was available. Two publicly available datasets were analyzed: Amikacin resistance in *E. coli* and coexisting ecotypes in *E.coli*. The results allowed to identify both well-known and newly found molecular pathways involved in these phenotypes.

Experimental evolution sometimes generates datasets consisting of mutator phenotypes which have high mutation rates. These datasets are hard to analyze due to the large amount of noise (most mutations have no effect on the phenotype). To this end IAMBEE was developed. IAMBEE is able to analyze genomic datasets from evolution experiments even if they contain mutator phenotypes. IAMBEE was tested using an *E. coli* evolution experiment in which cells were exposed to increasing concentrations of ethanol. Part of the results were validated in the wet-lab.

In addition to methods for analysis of causal mutations and mechanisms in bacteria, a method for the identification of causal molecular pathways in cancer was developed. As bacteria and cancerous cells are both clonal, they can be treated similar in this context. The big differences are the amount of data available (many more samples are available in cancer) and the fact that cancer is a complex and heterogenic phenotype. Therefore we developed SSA-ME, which makes use of the concept that a causal molecular pathway often has at most one mutation in a cancerous cell (mutual exclusivity). However, enforcing this criterion is computationally hard. SSA-ME is designed to cope with this problem and searches for mutual exclusive patterns in relatively large datasets. SSA-ME was tested on cancer data from the TCGA PAN-cancer project. From the results we could, in addition to already known molecular pathways and mutated genes, predict the involvement of a few rarely mutated genes.

# Nederlandse samenvatting –Summary in Dutch–

Bacteriën die in hogere concentraties ethanol kunnen leven voor de productie van biobrandstoffen, bacteriële pathogen die resistent zijn tegen antibiotica en kankercellen zijn voorbeelden van fenotypes die van belang zijn voor onze maatschappij en die momenteel worden bestudeerd. Om deze fenotypes en hun onderliggende genotype-fenotype relatie beter te begrijpen bestudeert men tegenwoordig het DNA en de expressieprofielen die worden verkregen door middel van next-generation sequencing (NGS) en microarray technieken. Deze technieken genereren grote hoeveelheden omics data hetgeen resulteert in een lijst van genen met interessante mutaties of expressieprofielen die potentieel bijdragen aan het fenotype. Deze lijsten bevatten vaak zeer veel genen. Het is problematisch om deze genen manueel te verifiëren omdat literatuurstudies en laboratoriumexperimenten voor een groot aantal genen veel tijd en middelen vergt. Daarom zijn (computationele) methodes nodig die deze genlijsten kunnen reduceren door, meestal abundante, vals positieve genen te verwijderen. In het ideale geval rapporteren deze methoden ook de relaties tussen de geselecteerde genen.

Andere hoge doorvoer technieken zoals yeast two-hybrid (Y2H), ChIP-Seq en Chip-chip maar ook veel experimenten op kleine schaal en predictieve computationele methodes hebben het afgelopen decennium een schat aan interactomics data gegenereerd. Door deze data te combineren tot een biologisch interactienetwerk, dat alle moleculaire paden bevat die een bepaald organisme kan gebruiken en dus de blauwdruk van dat organisme voorstelt, is het mogelijk om omics data uit experimenten met zulk biologisch interactienetwerk te combineren. Biologische interactienetwerken staan centraal in de computationele methodes die in deze thesis worden voorgesteld omdat ze toelaten om belangrijke relaties tussen genen (en genproducten) in rekening te brengen. Zo doende is het mogelijk om niet enkel interessante genen te identificeren maar ook om moleculaire processen die belangrijk zijn voor een fenotype in kaart te brengen.

De beste manier om omics data van een interessant fenotype te analyseren hangt af van de experimentele opstelling en de beschikbare data. Daarom werden verschillende methodes ontwikkeld en toegepast binnen deze thesis.

Vooreerst werd een bestaande methode (PheNetic) toegepast op een consortium van drie bacteriële soorten die samen in staat zijn om een herbicide efficiënt af te breken maar waarvan geen enkele soort het herbicide op zichzelf efficiënt kan afbreken. Voor elke soort werd er expressiedata (RNA-seq) gegenereerd voor zowel het consortium als de soort in isolatie. Hieruit bleek dat PheNetic moleculaire paden kan identificeren die differentieel geëxpresseerd zijn en wellicht bijdragen tot een cross-feeding mechanisme tussen de soorten in het consortium.

Na het verkrijgen van proof-of-concept werd PheNetic aangepast om experimentele evolutie datasets waarin behalve expressiedata ook genomische data aanwezig is, te analyseren. Twee publiek beschikbare datasets werden geanalyseerd: Amikacine resistentie in *E. coli* en coëxisterende ecotypes in *E. coli*. Uit de resultaten konden reeds beschreven maar ook nieuwe moleculaire paden die belangrijk zijn voor deze fenotypes worden geïdentificeerd.

Experimentele evolutie genereert soms datasets die bestaan uit mutator fenotypes die hoge mutatiesnelheden hebben. Deze datasets zijn moeilijk om te analyseren omdat er veel ruis in zit (de meeste mutaties hebben geen effect op het fenotype). Hiervoor werd IAMBEE ontwikkeld. IAMBEE kan genomische datasets van evolutie-experimenten analyseren, zelfs als ze mutator fenotypes bevatten. IAMBEE werd getest op een *E. coli* evolutie-experiment waarin cellen werden blootgesteld aan stijgende ethanol concentraties. Een deel van de resultaten werd gevalideerd in het laboratorium.

Naast methoden om causale mutaties en mechanismen in bacteriën te analyseren, werd ook een methode ontwikkeld om causale moleculaire paden in kanker te identificeren. Omdat bacteriële cellen en kankercellen beiden klonaal zijn, kunnen ze in deze context als gelijkaardig worden behandeld. De grote verschillen zijn de hoeveelheid data die typisch beschikbaar is (veel meer monsters in kanker) en het feit dat kanker een complex en heterogeen fenotype is. Hiervoor werd SSA-ME ontwikkeld. SSA-ME maakt gebruik van het concept dat een causaal moleculair pad slechts één mutatie heeft in een kankercel (mutuele exclusiviteit). Het toepassen van dit criterium is echter computationeel moeilijk. SSA-ME is ontworpen om om te gaan met dit probleem en zo mutueel exclusieve patronen in relatief grote datasets te vinden. SSA-ME was getest op kankerdata van het TCGA PAN-kanker project. De resultaten lieten toe om, naast reeds gekende moleculaire mechanismen en gemuteerde genen, de betrokkenheid van enkele genen te voorspellen die slechts zelden gemuteerd zijn in kankerpatiënten.

# Table of contents

# List of figures

# List of tables

# Abbreviations

## A

| | |
|---|---|
| AMK | Amikacin |

## C

| | |
|---|---|
| COLOMBOS | Collection of Microarrays for Bacterial Organisms |
| ChIP-Seq | Chromatin immunoprecipitation-sequencing |
| Chip-Chip | Chromatin immunoprecipitation-on-chip |
| cDNA | complementary DNA |
| CDS | Coding DNA Sequence |
| CoMEt | Combinations of Mutually Exclusive Alterations |
| CGC | Cancer Gene Census |
| CNA | Copy Number Alteration |

## D

| | |
|---|---|
| DDBJ | DNA Data Bank of Japan |
| d-DNNF | Deterministic Decomposable Negation Normal Form |

# E

| | |
|---|---|
| eQTL | expression Quantitative Trait Loci |

# G

| | |
|---|---|
| GEO | Gene Expression Omnibus |
| GO | Gene Ontology |

# H

| | |
|---|---|
| HT | High tolerant |
| HINT | High-quality INTeractomes |
| HPRD | Human Protein Reference Database |

# I

| | |
|---|---|
| IAMBEE | Identification of Adaptive Mutations in Bacterial Evolution Experiments |
| INDEL | INnsertion or DELetion |
| ICGC | International Cancer Genome Consortium |

# K

| | |
|---|---|
| KEGG | Kyoto Encyclopedia of Genes and Genomes |
| KO | Knock-out |

| | |
|---|---|
| KAAS | KEGG automatic annotation server |

# L

| | |
|---|---|
| LIMMA | Linear Models for Microarray and RNA-seq Data |

# M

| | |
|---|---|
| MMR | Methyl-directed Mismatch Repair |
| MuSiC | Mutational Significance in Cancer genomes |
| MEMo | Mutually Exclusive Modules in cancer |
| MutSig | Mutational Significance |
| MutSigCV | Mutational Significance CoVariates |
| MES | Mutual Exclusivity Score |
| mRNA | messenger RNA |
| MPIDB | Microbial Protein Interaction DataBase |
| miRNA | MicroRNA |

# N

| | |
|---|---|
| NCBI | National Center for Biotechnology Information |
| NER | Nucleotide Excision Repair |
| NCG | Network of Cancer Genes |
| NGS | Next-Generation Sequencing |
| NMR | Nuclear Magnetic Resonance |

# P

| | |
|---|---|
| PPV | Positive Predictive Value |

| | |
|---|---|
| PCR | Polymerase Chain Reaction |
| PCA | Principal Component Analysis |
| PP | Protein-protein |

# Q

| | |
|---|---|
| qRT-PCR | quantitative Real Time-PCR |
| QTL | Quantitative Trait Loci |

# R

| | |
|---|---|
| ROC | Receiver Operating Characteristic |
| RAST | Rapid Annotation using Subsystem Technology |
| rMES | ranked Mutual Exclusivity Score |
| RNA-seq | RNA sequencing |

# S

| | |
|---|---|
| SSA-ME | Small Subnetwork Analysis with reinforced learning to detect driver genes using Mutual Exclusivity |
| sRNA | small RNA |
| SRA | Sequence Read Archive |
| SNP | Single Nucleotide Polymorphism |
| SIFT | Sorting Intolerant From Tolerant |

# T

| | |
|---|---|
| TAP | Tandem Affinity Purification |
| TCA cycle | TriCarboxylic Acid cycle |

| | |
|---|---|
| TCGA | The Cancer Genome Atlas |
| TSG | Tumor Suppressor Gene |
| tRNA | transfer RNA |

## U

| | |
|---|---|
| Y2H | Yeast two-Hybrid |

## W

| | |
|---|---|
| WGS | Whole genome sequencing |
| WES | Whole exome sequencing |

# 1
# Introduction

In the last decade high-throughput techniques which generate large quantities of omics data have become commonplace as their costs continued to drop [1]. One example is that through Next-generation sequencing (NGS) technologies, the cost of sequencing a human genome, which refers to the DNA molecules in a human cell, has dropped from roughly \$100 million in 2001 to nearly \$1200 in 2015 (**Figure 1.1**). The availability and integration of this omics data has revolutionized a multitude of fields in biology as it lead to a significant increase in our knowledge of systems biology, especially in model oragnisms [2, 3]. But in order to analyze this ever-increasing stream of omics data, further efforts in data curation and multi-omics data integration are needed [4, 5]. This thesis contributes to the latter by the development of methods which integrate interactomics data, in the form of a biological interaction network, with genomics and/or transcriptomics data in order to elucidate the genotype-phenotype relationship underlying a specific phenotype under research [6–8]. This chapter serves as an introduction to some important concept used in this thesis.

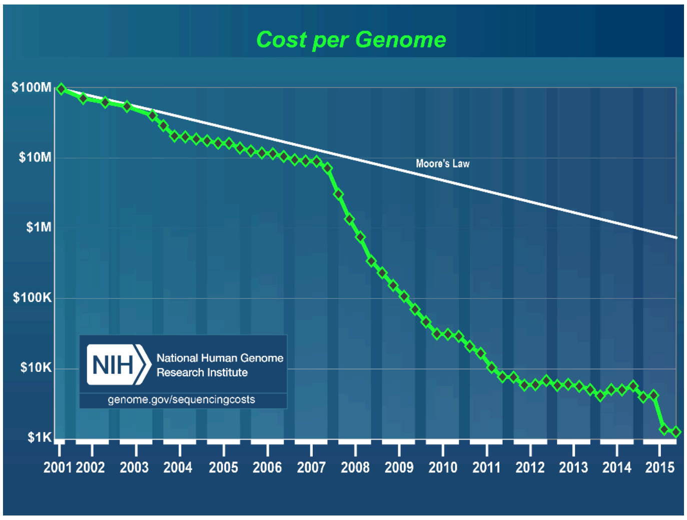

*Figure 1.1:* ***Genome sequencing cost per human genome over time.*** *(source: https://www.genome.gov/images/content/cost pergenome2015_4.jpg)*

## 1.1 The central dogma of molecular biology

Living cells have the ability to perform vital biological functions such as the production of specific enzymes needed for the digestion of food, cellular respiration to produce energy in order to keep the cell alive or cell division needed for growth and procreation. Information on how these functions should be performed is contained within the DNA of each cell. The process of using this information to produce proteins which carry out these functions is known as ”the central dogma of molecular biology” [9] which is explained in the following paragraph.

A living cell contains DNA, which is a double helix structure of which both helices consist solely of four different molecules, called nucleotides. Some parts of DNA contain a specific sequence of nucleotides which can be transcribed into messenger RNA (mRNA) by the cellular machinery. These parts are called genes. This mRNA contains roughly the same information as the DNA for a specific gene but can be translated by ribosomes which use this information in order to produce a protein. The ribosome performs this function by reading the nucleotides of the mRNA molecule in triplets. Each triplet represents a code which maps to a unique amino acid, which is then recruited by the ribosome. Due to the specific order in which these amino acids are recruited, the protein (which is a sequence of amino acids, folded in a specific way) will fold itself. Because mRNA degrades rather quickly after it has been transcribed, using this system a cell can regulate the production of specific proteins and as such react to sudden changes in the environment.

The specific nucleotide sequence of the DNA of an organism is called its genotype and is closely related to the observable traits of the organisms, which together are called the organism’s phenotype. Variation in the genotypes of individuals leads to different proteins being produced and thus to distinct phenotypes between individuals. For example eye colors in humans is largely determined by the alteration of a single nucleotide in several genes [10]. Likewise, a mutation in the DNA of a cell can cause some cellular functions to behave differently or even fail.

As an organism’s environment plays an important role in determining how a cell should behave, the phenotype cannot be fully predicted by only looking at the organism’s genotype but it does play a large role in determining the phenotype. A lot of research, including the research presented in this thesis, tries to identify this genotype-phenotype relationship for a specific trait by looking at how mutations in genes vary with the observed phenotype of an organism [11].

## 1.2 Omics data

The term ”omics” refers to a field of study in biology. Multiple types of omics data exist. Examples include genomics (the study of genomes), lipidomics (the study of lipids), proteomics (the study of proteins) and transcriptomics (the study of RNA). This thesis focuses only on genomics and transcriptomics as those are the omics data sources most commonly generated when trying to disentangle the genotype-phenotype relationship and these data sources were used to develop the proposed methods.

### Genomics data

Genomics data refers to data generated about an organisms’s genome and is thus used to determine the genotype of an organism (the nucleotide sequence of its DNA). Knowing the genotype of an organism under research is of primordial importance when investigating the relationship between an organisms genotype and its phenotype.

Gathering information on the genotype of an organism is called DNA sequencing. This was performed for the first time in 1970 by Ray Wu at Cornell university who partially sequenced DNA from bacteriophage $\lambda$ and 186 DNA [12]. This was later improved so any DNA sequence could be sequenced. It was Frederick Sanger who, in 1977, adopted the sequencing strategy from Wu to create a more rapid way of sequencing DNA [13] which has been the dominant method for DNA sequencing for some time. In fact, the first human genome was sequenced using Sanger sequencing during the human genome project which started in 1990 and was completed in 2003 [14]. Modern efforts which require at least large parts of multiple genomes to be sequenced, such as cancer genome analysis, would have been impossible using Sanger sequencing because it would take up too much time and would be too costly.

Today NGS technologies such as Illumina sequencing and Roche 454 sequencing are used to generate genomics data [15, 16]. The primary advantage of using these methods as compared to the previously used Sanger sequencing is that they are able to produce large amounts of data in small amounts of time with low costs. In general the genome of an organism is first fragmented using enzymes or sonication. These (single stranded) fragments are then immobilized and amplified to create a large concentration of the same fragment in a fixed place. In order to read the sequence of every fragment, one specific nucleotide is added to it at a time and it is detected which complementary nucleotide is added where each time. Because of the large concentration of identical fragments, the signal is strong enough for detection [17]. Using this technique the sequence of all fragments can be determined in parallel which greatly contributes to the amount of data one can generate in a given time.

The result is the sequence of all fragments which constitute the entire genome. These sequences are called ”reads”. As the order of the reads is undefined, the organism’s genome cannot be directly reconstructed from these reads. When no reference genome is available for the organism under research, specific software is used to assemble the reads (put them in the right order), reconstructing the genome [18]. This genome is then normally annotated which means that the positions of genes are determined and their function is inferred based on information from other (closely related) species. Alternatively, when a reference genome is already available, the reads are aligned to the reference genome in order to infer their identity [19].

Often one is interested in the mutations which occurred in the genome during an event, for example before and after an adaptive sweep. This is done by comparing the genome of an evolved organism to the genome of the organism from which it evolved (see the section on evolution experiments). These variants can be SNP’s (single nucleotide polymorphisms), small INDEL’s (INSertions or DELetions of a few base pairs) or larger genomic rearrangements such as translocations or the loss/duplication of large parts of a chromosome. Multiple computational methods are available for variant calling [20–22].

But one is not always interested in sequencing the entire genome, known as whole genome sequencing (WGS). In higher eukaryotes a large fraction of the genome consists of non-coding DNA, which is not translated into proteins. For a lot of studies, just looking at the parts of the genome which are expressed and thus translated into proteins is adequate. This part of the genome is referred to as the ”exome” and sequencing only this part is referred to as whole exome sequencing (WES) [23–25]. However, non-coding DNA can play a role in the functioning of an organism as some is transcribed into RNA (but not further translated into proteins) and this RNA can perform other functions such as inhibiting the translation of other RNA molecules (RNA interference) or help with the recruitment of amino acids to the ribosomes (tRNA). When screening patients for specific genetic diseases an even more concise way of genome sequencing is used in which only one or a couple of specific genes are sequenced and screened for variants known to cause disease, as is done when screening for Huntington’s disease [26].

**Transcriptomics data**

Transcriptomics data refers to the number of mRNA molecules that an organism produces for every gene. As mRNA is translated into proteins by the ribosomes in the cell, mRNA is assumed to be a proxy for the number of proteins produced. Transcriptomics data can thus shed light on the activity of cellular processes. Transcriptomics data are particularly valuable when it is generated together with genomics data for two distinct but related cases (for example before and after a bacteria gains resistance to a specific drug). In such a case it is possible to link the identified mutations to changes in gene expression allowing to identify the mutation(s) responsible for changes in the expression profiles of genes belonging to a specific cellular mechanism (this is called eQTL mapping). Two popular techniques exist for the generation of transcriptomics data: RNA microarrays [27] and RNA-seq [28]. Both techniques are able to quantify the amount of mRNA transcribed for every gene in the genome.

A microarray is a solid plate with a large number of microscopic spots. Each of these spots contains single stranded DNA probes for a specific gene. By submerging the microarray into a pool of single stranded cDNA strains (obtained from the RNA sample under research), hybridization occurs. The probes are designed such that a hybridization event produces an optical result (usually a green or red fluorescent signal) which can be measured. Due to noise and nonlinear characteristics of the optical signals, it is nontrivial to convert the optical signals to a measure which quantifies the amount of mRNA present in the sample [29, 30] and to determine which genes have different expression levels when comparing the results from microarrays of the same organism or strain in two different conditions (which is known as differential expression analysis). Therefore, statistical software is available to solve these issues. Examples of such software include LIMMA [31] and MAANOVA [32].

RNA-seq uses NGS technologies to sequence cDNA, obtained from RNA, instead of the genome. The experimental procedure is thus very similar to genome sequencing. The difference resides in the fact that when performing RNA-seq one is also interested in the quantity of mRNA molecules in the sample instead of only the sequence. Therefore, the resulting reads are mapped to the genome and the number of reads which map to each gene are counted [33]. Because read counts cannot be readily used to compare different samples and thorough statistical analysis is needed to decide which genes are differentially expressed in differential expression analysis, statistical software packages to analyze RNA-seq data are available. They include DeSeq2 [34] and TopHat/Cufflinks [35].

## 1.3 Evolution experiments

Often phenotypes are studied because they are useful in economic applications (for example ethanol resistance for the production of alcoholic beverages or biofuels). In order to study such acquired phenotypes it can be required to study organisms under very specific conditions during multiple generations to assess the relationship between the phenotype and the mutations which arise during adaptation to these conditions. This is impractical to do in nature as it is often impossible to find these conditions, let alone in combination with a suitable organism to study. Therefore, when studying such a phenotype, evolution experiments are widely used [36–38]. While it is possible to conduct evolution experiments in sexual reproducing organisms [39], bacteria are often used due to their short generation times (only about 20 minutes for *E. coli*) which allows to study more generations in the same time frame. Therefore, the evolution experiments described in this section apply to bacteria. Evolution experiments usually start with an ancestral strain which is exposed to a specific environment. Natural selection favors mutations that confer a benefit in the chosen condition leading to improved phenotypes [40]. The environment can be static [41, 42] or gradually increasing in intensity over time [43,44] (**Figure 1.2**).

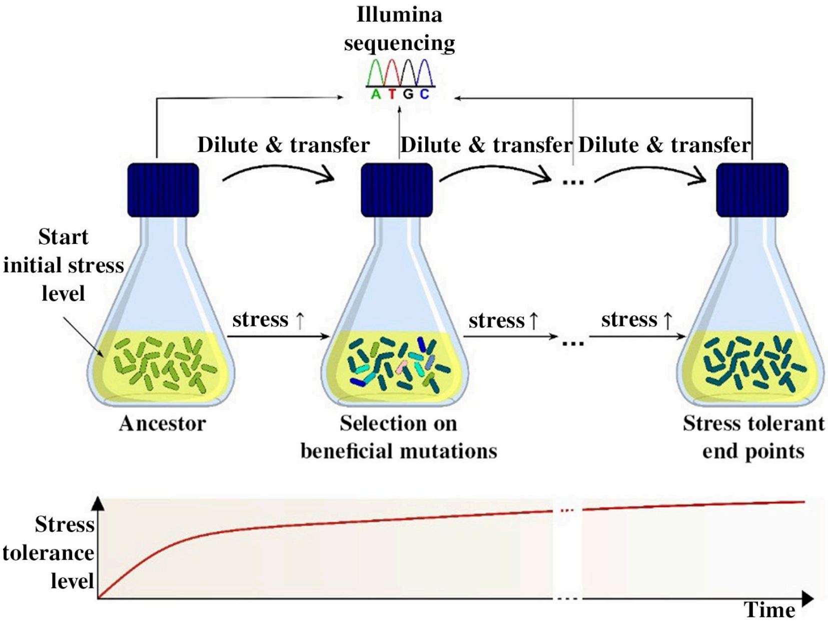

*Figure 1.2:* ***Evolution experiment over time.*** *Initially, an ancestral strain is exposed to a low stress level. When the strain has adapted to the stress level, it is transferred and exposed to a higher stress level. Doing so the strain becomes increasingly more adapted to the imposed stress over time. courtesy of Toon Swings.*

The advantages of performing evolution experiments to study adaptive phenotypes are twofold: 1) the environment to which the strain adapts can be controlled and 2) both the ancestral strain, which does not exhibit the adaptive phenotype, and the adapted strain are available. As such, when omics data are generated, it is possible to focus on the differences between the ancestral strain and the adapted strain.

## 1.4 Cancer

Cancer is a disease of the genome which is caused by aberrant mutations that lead to dysregulation of specific cellular system [45]. This causes an uncontrolled division of the affected cell, leading to the formation and growth of tumors. As tumors thus originate from a patients own cells, it is not trivial to design drugs specifically targeting cancer cells, as can be done with pathogenic bacteria through antibiotics which usually specifically target unique components of bacterial cells. It is thus of importance to understand how aberrant mutations in the (human) genome give rise to cancer in order to identify druggable targets for specific cases [46, 47]. Cancer research is further complicated by the observation that cancer is a very heterogeneous disease, even within cancers with identical primary sites. In this respect it is known that for example within different gastric and breast cancers, amongst others, there exist multiple subtypes each with their own genetic cause, survival rate and response to treatments [48, 49]. This means that knowing the primary site of a tumor is not enough to propose an appropriate treatment and treatment should most likely be based on the genomes of the patient's cancer cells.

Like bacteria, cancer cells have clonal evolutionary properties [50]. In general, tumor progression is controlled by a series of somatic mutations which are acquired during a person's life and that each individually give the cell an increased rate of clonal expansion [51] as these mutations promote uncontrolled divisions. Cells with higher clonal expansion rates will overgrow others and become dominant, forming tumors. Patients which have mutations in their germline (inherited mutations) that contribute to the onset of cancer will typically have higher chances to develop cancer as fewer somatic mutations are needed. Mutations which contribute to healthy cells becoming cancerous can arise in two types of genes: oncogenes and tumor suppressor genes (TSG). Oncogenes are genes which in normal circumstances promote cell growth and division while TSG's are genes involved in mechanisms which counter-act spurious growth such as apoptosis and cell cycle checkpoints [52]. Mutations in oncogenes can lead to an abundance of growth promoting signals while mutations in TSG's can disrupt the cell's control mechanisms [53].

As both technical and ethical problems prohibit the use of evolution experiments to study human cancer, efforts are being made to collect genomics data from multiple patients with similar cancer. Results of such analyses are often stored in (partly) publicly available databases [54]. The most prominent examples are The Cancer Genome Atlas (TCGA) [55] and the International Cancer Genome Consortium (ICGC) [56]. Because genomics data from both cancerous tissue and healthy tissue are usually available, it is possible to focus analysis on somatic mutations.

## 1.5 Biological interaction networks

Networks are currently used in a myriad of disciplines ranging from social networks in business [57] and social sciences [58] to neural networks in machine learning [59]. All these networks have in common that they consist of nodes which represent entities and edges which represent interactions between these entities. Edges can be either directed (the interaction is only valid in one direction) or undirected (the interaction is valid in both directions). In biological networks nodes represent genes and/or gene products (such as proteins or RNA) and edges represent the interactions between these nodes.

Biological networks are seldom homogeneous as different types of interactions are usually present. This is important as different types of interactions have different properties, are discovered using different techniques and are gathered in different databases (see below). More advanced network-based methods also take into account interaction types while analyzing data. Therefore, biological interaction networks are usually multi-layered [60, 61].

The different layers can be subdivided in two groups: physical interactions and functional interactions. Physical interactions are derived from experiments which prove direct physical interactions between genes/gene products. Genes/gene products involved in functional interactions are not proven to physically interact with each other but are associated with each other in other ways. Examples of functional interactions include co-expression when genes share expression profiles in multiple environments [62, 63], predicted interactions in a species by inferring them from known interactions in related species based on phylogeny [64] and text-mined interactions [65,66]. As in physical interaction networks the mechanisms of the interactions are clear and to avoid overconnecting the interaction network, we focus only on physical interaction networks in the context of this thesis (**Figure 1.3**).

The interactomics data required to construct a biological physical interaction network are maintained within a plethora of databases. Usually each database focuses on a specific layer. An important aspect to consider when consulting an interaction database is how the data are curated as each database has its own curation rules [67]. Curation can be high-throughput or literature curated. Literature curated resources contain a large number of small-scale experiments while high-throughput resources contain large-scale experiments. Literature-curated resources are mostly used when benchmarking data mining technologies as the superior reliability of literature curated resources is generally assumed [68]. Another important aspect of an interaction is its reliability. This expresses how likely it is that an interaction exists in reality and is dependent on the experimental technique(s) used to infer the interaction. Note that even if two databases are both literature curated they can have different curation rules and therefore contain different interactions and/or assign different reliabilities to the same interactions. Because of this, efforts such as IMEx, which integrates different databases using identical curation rules, have been made [69].

In the following an introduction to each of the different physical interaction layers is given together with a brief summary of the use of biological subnetworks to analyze omics data.

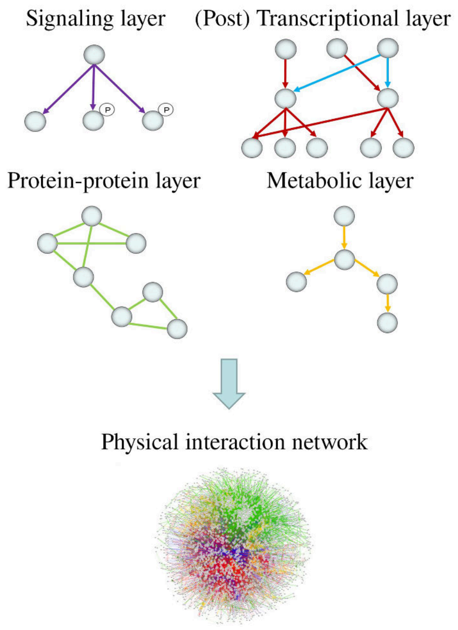

*Figure 1.3:* ***Multi-layered physical biological interaction network.*** *In the context of this thesis, Physical interaction networks are used which consist of multiple layers of physically interacting genes and/or gene products. Here the different layers are depicted at the top of the figure and include a signaling layer, consisting of purple colored signaling interactions such as (de)phosphorylation and (de)methylation, a (post)transcriptional layer consisting of red (protein-DNA) and blue colored (sRNA) post-transcriptional interactions, a protein-protein layer consisting of green colored protein-protein interactions such as protein complexes and a metabolic layer consisting of yellow colored metabolic interactions referring to enzymatic reactions.*

### Protein-protein interactions

In protein-protein (PP) interactions, nodes represent proteins and edges represent a physical binding of the proteins to each other [70]. As experimental techniques to discover PP interactions search for interactions *between* proteins, the direction of PP interactions is always undirected.

Low-throughput methods to detect PP interactions include Nuclear magnetic resonance (NMR) [71], crystallography [72] and spectroscopic methods [73]. High-throughput methods are largely restricted to two-hybrid screens [74] and tandem affinity purification (TAP) tagging [75].

Protein-protein interactions are available in several databases [76] ranging from organism or taxonomic group-specific databases such as the Human Protein Reference Database (HPRD) [77] and the microbial protein interaction database (MPI-DB) [78] which focus on humans and microbes respectively, to databases which contain PP interactions for a large number of organisms such as BioGRID [79] and String [64]. Even efforts which enable users to query multiple PP interaction databases simultaneously have been made (e.g. PSICQUIC [80]).

**(Post)Transcriptional interactions**

(Post)Transcriptional interactions regulate gene expression in cells. In transcriptional interactions the source node of the interaction is a regulator and the end node is a target gene of that regulator [81]. Transcriptional interactions are therefore directed. These interactions regulate translation after transcription and thus involve interfering with mRNA. These are interactions between molecules (such as miRNA or sRNA) and the mRNA of a target gene [82] and are also directed.

Transcriptional interactions are mainly obtained using ChiP-chip [83] or ChIP-seq [84, 85] experimental techniques. But integrating interaction data from multiple Chip experiments does not take the experimental conditions into account. This leads to situations where it is not clear whether different regulators controlling the same gene need to act together to perform a specific regulatory function [86]. Because of this and technical limitations of Chip-chip and ChiP-seq techniques [87], methods have been developed that use expression data together with interaction data in order to infer transcriptional interactions [88, 89].

Databases that contain (post)transcriptional interactions include species-specific databases such as RegulonDB for *E. coli* K-12 [90] and regulatory networks based on ENCODE data for human [91]. Also less specific databases exist such as animalTFDB [92] and RegPrecise which focuses on reconstructing transcription factor regulons in prokaryotes [93].

**Metabolic interactions**

Metabolic interactions represent the metabolism of a cell. Nodes represent enzymes and edges represent the interactions they catalyze. Metabolic interactions are therefore directed.

In recent times, metabolic interactions for a specific organism are not necessarily derived from experiments but rather from hight-throughput genomics data [94, 95]. In general, the genome of the organism is assembled and annotated as to identify genes which code for enzymes [96, 97]. Using highly curated metabolic interactions known from past experiments [98], these genes are then mapped to metabolic interactions. Software tools such as metaSHARK [99] provide an automated way of inferring metabolic interactions from genomics data.

Multiple databases provide metabolic interaction data. Examples are KEGG [100], BRENDA [101] and MetaCyc [102].

**Signaling interactions**

Signaling interactions control essential cellular processes and mediate quick response to changing environments. Examples include post-translational modification of proteins (e.g. (de)phosphorylation [103] and (de) acetylation [104]) and receptor pathways in which a receptor binds to specific molecules and passes the signal down to other cellular processes [105]. The source nodes in signaling interactions are proteins such as kinases, acetylation agents or members of a receptor pathway and the target nodes are the targets of these proteins. the edges are directed.

To study modifications of a single protein, experimental techniques include chromatographic purification or antibody precipitation to obtain samples of, for example, phosphorylated or acetylated proteins [106]. The use of mass-spectrometry methods allows to assess the presence of multiple (de)phosphorylated or (de)acetylated proteins at the same time at different points in time, making it possible to investigate post-translational modification after the pertubation of the environment [107].

Databases which contain signaling interactions include KEGG [100] (small number of signaling interactions for a large number of organisms) and SPIKE [108] (multiple signaling pathways specific for human).

**Weighted interaction networks**

An important aspect for many network-based methods is the concept of a weighted interaction network. In a weighted interaction network each node or edge has a weight assigned to it. This weight can reflect multiple features of the node or edge. Because experimental techniques to infer interactions vary with respect to their accuracy and some edges might have been inferred by multiple experimental techniques, it is not uncommon to assign a weight to the edges which reflects the probability that the interaction is present in the organism [64]. Alternatively, some network-based methods have problems with nodes which have a large number of edges. Most biological networks exhibit a scale-free property with respect to the distribution of the number of interactions each node has [109]. This means that there are many nodes with few interactions but few nodes with a very large number of interactions. Nodes with a very large number of interactions are called ”hubs” and can overconnect the network. Therefore, some network-based methods weight the network based on the network’s topology to mitigate the effects of such hubs [6, 110]. Weights are used by methods as a priori information thereby decreasing the odds of a node/edge to show up in the solution if it has a low weight and vice versa [110–112].

## 1.6 Network-based methods

Currently, biological interaction networks are often used in combination with omics data. How the biological interaction network is used and which data are integrated with the network largely depends on the the research question. Applications include hypothesis generation about a protein’s or gene’s function [113, 114], motif detection, [115] inference of interactions between genes [116], prioritization of gene lists [117] and inference of subnetworks of the interaction network which are involved in a specific phenotype or which are active when exposed to a specific environment [6, 111, 118]. In this thesis, the focus is on subnetwork inference methods and prioritization of gene lists.

The most naive approach would be to identify the most interesting genes from omics data (e.g. mutated genes or genes with high expression values) and map them to the network to see if a subset of them are connected in the network. Subsequent GO enrichment analysis of the connected components [119] could then help to identify the molecular pathways from the set of interesting genes. A more advanced way of doing this would be to first weight the interaction network by assigning scores to the nodes or the edges based on the omics data (e.g. log-fold changes or functional impact scores of mutations). Subnetworks are then inferred by simply selecting the parts of the network which have highest score. These approaches are commonly referred to as ”guilt-by-association” as the premise is that genes which are associated with each other in the network will have similar function [120, 121].

Another approach is to propagate the information over the network, thereby using the network’s topology and in some cases the direction of the edges to diffuse the data through the network. An important added value of diffusion methods as opposed to simply mapping the data to the network is that intermediate nodes, which were not measured or do not show clearly in the data due to technical limitations or their biological properties, can be recovered in this way. Examples include diffusion kernel-on-graphs [122–124].

The network-based methods developed in the context of this thesis explicitly search for biologically relevant paths which are subsequently used to infer the subnetwork of the interaction network that represents the interesting part of the network, given the data. A path is simply a series of consecutive nodes and edges. When searching for paths the directions and types of the interactions are taken into account. For example a path between a mutation and a differentially expressed gene must end with a regulatory edge towards the differentially expressed gene. Based on the experimental data, these paths are then assigned a score. Finally an optimization function is utilized to select the subset of paths which make up the best subnetwork [6, 8, 111, 125].

### Network visualization

Visual inspection of (sub)networks is primordial to interpret the results of network-based methods. To this end multiple software platforms are available such as cytoscape [126], Osprey [127] and BioLayout Express$^{3D}$ [128]. Some of these platforms offer functionality to analyze network properties or to perform enrichment analyses [119, 129, 130].

# 2
# Scientific problem and aim

The methods proposed in this thesis are designed to help analyze data from omics experiments. We address the need for methods capable of analyzing different experimental design and that can cope with large amounts of data, possibly containing a lot of noise. The focus is specifically on the interpretation of genomics and/or transcriptomics data from clonal systems as the analysis of omics data from clonal systems poses additional challenges in comparison with sexual reproducing organisms. This chapter first focuses on these additional challenges as it discusses the scientific problem and secondly gives an overview of the developed methods and explains their aims.

## 2.1 Scientific problem

**Search for molecular pathways**
NGS sequencing enabled rapid characterization of genetic variance between multiple individuals of the same species. Correlating this genetic variation to specific phenotypes or molecular traits using statistical methods, respectively GWAS [131] and eQTL mapping [132], offers potential for the identification and/or prioritization of alleles underlying important properties [133] or diseases [134]. GWAS/e-QTL approaches assume, however, that individuals who have similar phenotypes,

have similar alleles and that enough samples are available to prove correlation.

The assumption that individuals who have similar phenotypes (because for example they are gathered from parallel evolution experiments in which the conditions were identical), have similar alleles is embodied in the fact that traditionally these methods search for recurrently mutated genes. This is a narrow definition of parallelism as mutations in genes belonging to the same molecular pathway can equally well confer the same phenotype [41, 135, 136]. This is especially true for clonal systems which reproduce asexual and therefore DNA exchange between individuals is minimal. Because of this, when a population of clones adapts to a specific environment, individual clones in the population will evolve and adapt independently of each other. This means that when a clone obtains a beneficial mutation, that mutation cannot spread to the offspring of other clones and as such another beneficial mutation in another clone can lead to the formation of subpopulations which have similar phenotypes but different genotypes. This phenomenon is known as clonal interference [137, 138](**Figure 2.1**). As such, when collecting clones from end points in parallel evolution experiments (which have similar phenotypes) the chance of them having identical mutations is lower than would be expected for sexual reproducing organisms. As such, searching for recurrently mutated genes, as is often done [139, 140], might not be adequate. Having access to a large amount of independently evolved samples with similar phenotypes could offset this problem but in reality usually only few samples are available.

This, together with the fact that experiments which exploit sexual reproduction in order to increase the observed mutation frequency in causal genes, such as bulked or pooled segregant analysis [141, 142] is not possible, calls for another strategy to perform genotype-phenotype mapping in clonal systems. As stated earlier, genes belonging to the same molecular pathway can also confer the same phenotype. That is why in this thesis methods are proposed to search for molecular pathways which are recurrently mutated in parallel evolved clonal populations (**Figure 2.2**) instead of consistently mutated genes [41, 135, 136]. In order to do this, it is needed to integrate interactomics data with the obtained genomics (and possible transcriptomics) data in the form of an interaction network which contains data on how the biomolecules within a cell interact with each other.

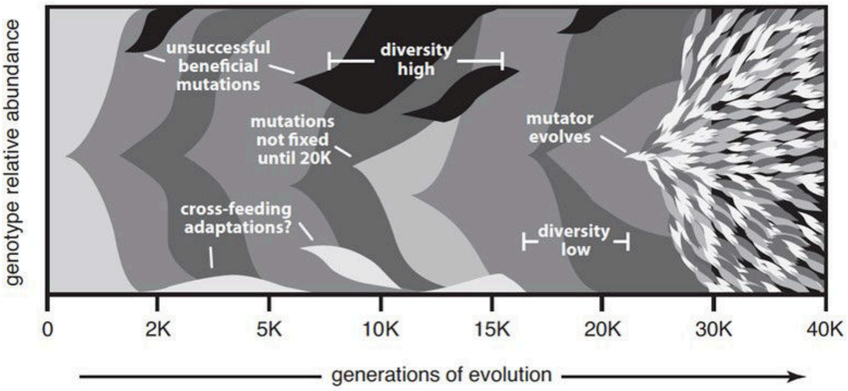

*Figure 2.1:* ***Clonal interference.*** *The relative abundance of genotypes in a clonal population (y-axis) in time (x-axis) during experimental evolution. Different colors depict different subpopulations. Figure taken from Barrick et al. [143].*

### Driver and passenger mutations

When looking at genomics data obtained from an evolution experiment on a clonal system, it is important to note that not all mutations are causal to the observed phenotype. These causal mutations are called ”driver mutations”. While this is also the case in sexually reproducing organisms, in clonal systems, because of clonal interference, typically a smaller fraction of the observed mutations is causal to the phenotype. This is the case because when two driver mutations arise in different individuals within a clonal population at the same time they cannot be recombined in the next generation. Instead these individuals compete with each other and multiple subpopulations arise which have different driver mutations.

In practice this leads to the fact that when a clone acquires a driver mutation, all mutations in the genome of that clone are under positive selection, not just the driver mutation. This is the case because there is no transfer of genetic information between individuals and thus when the clone increases in frequency in the population, so do all of its mutations. Therefore neutral or slightly deleterious mutations which were present at the time of acquiring the beneficial driver mutation will ”hitchhike” with the driver mutation and rise to the same frequency in the population as that driver mutation [144]. These mutations are called ”passenger mutations”. As this can happen in multiple subpopulation at the same time, at lot of passenger mutations will hitchhike and be picked up by variant calling. This results in a low signal-to-noise ratio and, together with the need for searching consistently mutated pathways, makes analysis of genomics data in clonal systems non-trivial.

The search for consistently mutated molecular pathways can cope with the noise from these passenger mutations because it exploits parallelism between independently evolved populations. Driver mutations are likely to be found in molecular pathways related to the adaptive phenotype throughout different independently evolved populations while passenger mutations do not show this consistency (**Figure 2.2**).

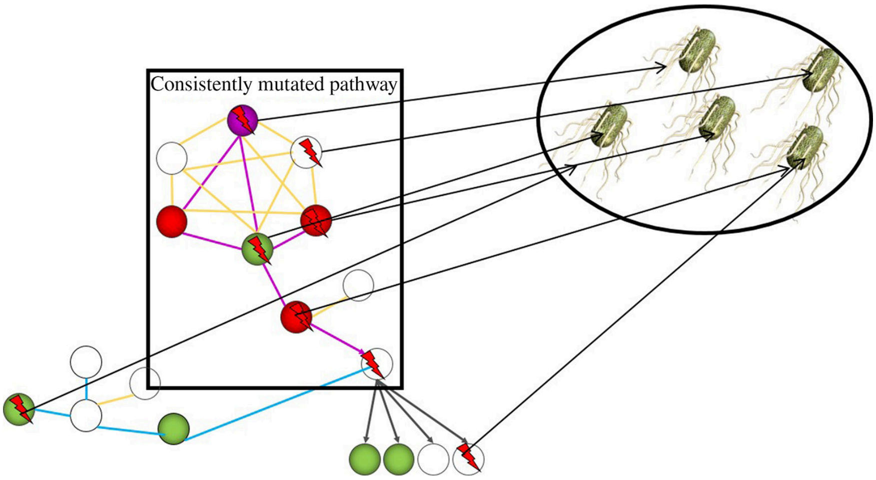

*Figure 2.2:* ***Visual representation of a consistently mutated pathway.*** *Each bacterium represents a clonal system which has adapted to the same condition and thus exhibits a similar phenotype.*

### Hypermutator phenotypes

Clonal populations can sometimes yield hypermutator phenotypes [145–147]. A clone with a hypermutator phenotype has an elevated mutation rate which is often caused by defective mismatch repair systems [148]. Hypermutator phenotypes can be under positive selection because of their increased probability of generating adaptive mutations which are beneficial in a specific environment [149, 150]. However, most of the acquired mutations will be neutral or even slightly deleterious in the specific environment but strongly deleterious in other environments, thereby hampering the ability of the hypermutator phenotype to survive and adapt to other environments [151, 152]. Therefore, mutation rates are strongly regulated and the reversion of mutations which lead to a hypermutator phenotype or the gain of compensatory suppressor mutations can lead to a quick decrease of hypermutator phenotypes within a clonal population [153].

When generating omics data from an evolution experiment which contains (a) population(s) with a hypermuator phenotype, there will be a lot of false positive driver mutations in the omics data as neutral and slightly deleterious mutations, which are prominently present in hypermutator phenotypes, will show up in the data. This makes datasets containing hypermutator phenotypes very hard to analyze, often resulting in the deletion of hypermutator phenotypes from the data or the inability to analyze the dataset entirely.

### The case for cancer

Some cancer genome databases contain up to 2000 patients for one specific cancer type at the time of writing. Because these amounts of data are available for some types of cancer (in bacteria there are usually only between 1 and 20 samples), it is possible to perform GWAS studies [154–156]. However, GWAS studies tend to identify common alleles with low penetrance and are ill-equipped to identify causal mutations which are rare. In addition, the mechanisms underlying the identified mutations are often unclear [157]. Therefore, novel analysis techniques are warranted.

As statistical association analysis techniques such as GWAS use no prior knowledge, the incorporation of prior knowledge in the form of interactomics data (which is abundantly present for human) has potential. Network-based methods are able to account for known interactions between genes when analyzing genomics data, leading to the possible identification of (rare) mutations in which the underlying mechanisms are more clear [8].

### Wet-lab mutations testing

Because epistasis between mutations occurs often [158,159] during evolution, wet-lab testing of a list of interesting mutations is not trivial. As every mutation can potentially influence another mutation, simply testing the mutations one-by-one in the ancestral background will likely only lead to the explanation of part of the phenotype. In principle, every possible combination of identified mutations should be tested in the ancestral background until a minimal set which explains the phenotype completely is found [160]. But this quickly becomes infeasible as even with as few as 4 genes, there are 15 possible combinations to test and this number rises quickly with the number of mutations identified. Therefore, methods which prioritize mutations based on how likely it is that they contribute to the observed phenotype can be very useful as a guidance for which genes and combinations of genes should be tested first.

## 2.2 Aim

The aim of this thesis is to provide computational methods which can help researchers to interpret large genomics and/or transcriptomics datasets. This interpretation includes the use of biological interaction networks to prioritize mutated or differentially expressed genes and the inference of the subnetwork of the biological interaction network which explains the data best. These results will provide researchers in the wet-lab with additional insights into the molecular mechanisms of the phenotype under study and provide a starting point for further experiments. Additionally the results can also be used for hypothesis generation.

More specifically, the aim is to provide methods which are able to analyze experiments from four different experimental designs which each have their own available data and data gathering strategies. In brief, computational methods for the analysis of data from experiments with bacteria were developed and/or tested for the analysis of 1) expression data, 2) genomics data coupled with expression data and 3) only genomics data from hypermutator phenotypes. The fourth experimental design refers to the analysis of a large amount of genomic profiles from cancer patients. A more in-depth overview of the different experimental designs treated in this thesis, together with the specific strategies utilized to tackle them, is provided in the following chapter.

# 3
# Overview of the proposed methods

In order to achieve the aim, in this thesis three different network-based methods were developed and one existing method was tested. Each addresses a specific experimental design in which different data are available. Each method is unique in that it capitalizes on specific biological insights and/or available data while simultaneously dealing with the specific problems of the experimental design. The remainder of the thesis largely consists of the scientific papers of these methods. This chapter is meant to give readers a general overview of the methods and the experimental designs for which they were developed but also to provide insight into the relationships between the different methods.

In chapter 4 subnetwork inference was tested on a transcriptomics dataset using the network-based method PheNetic, which existed prior to this thesis. The method was applied in the context of an ecological study: a consortium of bacteria which occur together in nature is able to degrade the herbicide linuron efficiently while its constituents grown in isolation are not. In this system it was unclear which carbon source(s) support the growth of the primary linuron degrader and how the synergistic interactions between the constituents of the consortium are established. In order to gain insight in these mechanisms, RNA-seq data was generated for both the consortium grown in the presence of linuron as well as for each of its constituents which were grown in isolation and in the presence of linuron or a hydrolysis product of linuron. To this end, differential expression analysis was used to determine the change in expression profiles of genes when comparing consortium conditions to isolation conditions. As limited interactomics data were available for the bacterial species in the consortium, the network was compiled mainly from highly curated metabolic interactions and few signaling interactions. Even when using only limited interactomics data together with differential expression data, it proved feasible to infer a subnetwork of the interaction network which contained molecular processes likely to play a role in the establishment of synergism between the species. PheNetic is able to analyze this dataset by utilizing a sophisticated subnetwork inference procedure. Briefly this works by first weighting the edges of the network based on the differential expression data of the genes and the topology of the network in order to construct a probabilistic subnetwork. Secondly paths between significantly differentially expressed genes in the interaction network are found and assigned a score based on the probabilities of the edges which make up the path (this is called the pathfinding step). Finally probabilistic logic programming is applied to reason about which subset of these paths explains the data best, given an objective function and the scores of the found paths (this is called the optimization step) [161, 162]. This inferred subset of paths is referred to as a the optimal subnetwork of the interaction network.

After the successful application of PheNetic to a transcriptomics dataset it was realized that the rationale of the method could be used in different experimental designs, where different types of omics data are available. This is possible by redesigning both the construction of the probabilistic subnetwork to include the available data and the pathfinding step such that relevant paths are being collected and that the score of a path reflects the probability that the path is involved in the phenotype under research. When these conditions are satisfied, the optimization step which infers the optimal subnetwork can be used as such. Chapters 5 and 6 redefine the construction of the probabilistic subnetwork and the pathfinding step based on the available omics data and the (biological) specificities of different experimental designs to develop new computational methods. A general overview of these methods can be found in figure 3.1.

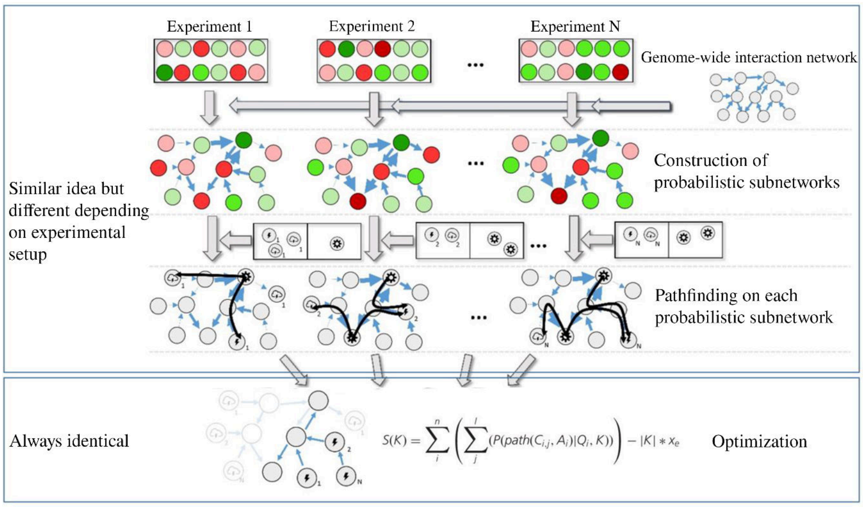
Experiment 1
Experiment 2
...
Experiment N
Genome-wide interaction network
Construction of probabilistic subnetworks
Similar idea but different depending on experimental setup
Pathfinding on each probabilistic subnetwork
Always identical
$S(K) = \sum_{i}^{n}\left(\sum_{j}^{l}(P(path(C_{i,j}, A_i)|Q_i, K))\right) - |K| * x_e$
Optimization

*Figure 3.1:* ***General overview of computational methods used in chapters 4, 5 and 6.*** *In general, for every experiment, first the interaction network is weighted based on the available data (depicted by the variations of gray) to construct a probabilistic subnetwork (probabilities are depicted as the thickness of the edges). Then relevant paths are collected and scored in the pathfinding step. Finally, an optimization function is used to infer the optimal subnetwork. The first two steps are dependent on the available omics data (to weight the probabilistic subnetwork) and the specific biological context of the experimental design (to define what is an interesting path) while the optimization step is always identical, given that adequate definitions can be found for the first two steps.*

In chapter 5 the aim was to develop a network-based method able to analyze coupled expression and genomics (eQTL) data. The focus was specifically on evolution experiments as in those cases differential expression data can be coupled to the mutations obtained during adaptation to a specific environment to find molecular mechanisms which are important for adaptation together with the mutations which are responsible for expression changes in these mechanisms. Additionally, to help wet-lab researchers reconstruct the phenotype efficiently, the aim as expanded to not only identify genes that harbor adaptive mutations but also to prioritize them based on the probability that they are involved in the adaptive phenotype. To this end we adapted PheNetic and tested the new method on two publicly available datasets: one dataset contained four independently evolved strains of *E. coli* K-12 MDS42 in the presence of the drug Amikacin. The other contained a population of *E. coli B REL606* that had been experimentally evolved and now consists of two distinct ecotypes which stabily coexist within the population. Using the new method it was possible to identify previously known molecular mechanisms responsible for Amikacin resistance and cross-feeding between the ecotypes. In addition, the prioritization of the mutated genes corresponded to findings obtained by wet-lab experiments.

In chapter 6 a network-based method named IAMBEE was developed. This method is able to analyze genomics data without having access to coupled expression data. The ability to analyze genomics data in isolation is useful as the cost of performing RNA-seq (which has to be performed at least in triplicate in order to generate reliable results) can be prohibitively large, especially for experiments including a large number of parallel samples and/or the sequencing of multiple time points throughout evolution. Additionally, the method deals with hypermutator phenotypes which are frequently observed in evolution experiments [163, 164]. Datasets including hypermutators are especially hard to analyze, often leading to the exclusion of hypermutators from the dataset or the inability to analyze the dataset at all. By using a specific experimental design and incorporating additional data, the method successfully analyzed a dataset consisting of 16 independently evolved *E. coli* K-12 MG1655 populations, all of which developed a hypermutator phenotype, in the presence of an increasing ethanol concentration.

In chapter 7 a network-based method named SSA-ME was developed to analyze cancer datasets. The big difference in cancer datasets as compared to microbial datasets is the amount of data. In cancer, datasets of several hundred individuals exist while for bacteria there are usually a lot less samples. As such, different biological properties which require the availability of a large number of samples in order to observe them, can be utilized. One such property is mutual exclusivity in cancer. Mutual exclusivity refers to the observation that once a biological pathway involved in oncogenesis has obtained a causal mutation in one of its genes, a second mutation in that pathway will not confer any fitness advantage anymore and will thus not be fixated [165, 166]. Finding such patterns in large datasets is, however, a complex problem as simply testing for all possible combinations of genes is computationally intractable. Therefore, an adaptation of the PheNetic algorithm was not adequate and a completely different network-based method was developed to find patterns of mutually exclusive mutations in large cancer datasets. The method was applied to multiple cancer datasets from the TCGA PAN-cancer project [124] and was able to identify known oncogenic pathways and propose newly found genes which were rarely mutated.

# 4

# Uncovering interspecies interactions from RNA-seq data

## 4.1 Introduction

This chapter presents the analysis of a consortium of three species which together degrade linuron in an efficiënt way but cannot in isolation. To gain insight into which interactions between the constituents of the consortium can explain this observation, RNA-seq data was generated for the consortium and for each of the constituents grown in isolation. After performing differential RNA-seq analysis, PheNetic was used to *analyze the differential expression data* between consortium and isolation conditions for the two most interesting species. together with previous work [6], this chapter represents the proof-of-concept of the network-based methods described in the rest of this thesis.

PA and **BW** analyzed the data, interpreted the results and wrote the manuscript. PA performed the biological experiments, **BW** performed the differential RNA-seq analysis and applied PheNetic. RDM, KM and DS conceptualized the study, designed the experiments, discussed the results and edited the manuscript.

## 4.2 Paper

# Interspecies interactions during linuron mineralization

Albers, P.[†], **Weytjens, B.**[†], De Mot, R., Marchal, K. and Springael, K.(**2017**). Interspecies interactions during linuron mineralization. *tbd*, Submitted.

[†] these authors contributed equally to this paper

### 4.2.1 Abstract

The proteobacteria *Variovorax sp. WDL1*, *Comamonas testosteroni WDL7* and *Hyphomicrobium sulfonivorans WDL6* compose a triple-species consortium that synergistically degrades and grows on the phenylurea herbicide linuron. To acquire a better insight in the interactions between the consortium members and the underlying molecular mechanisms, we compared the transcriptomes of the key biodegrading strains WDL7 and WDL1 grown as biofilms in either isolation or consortium conditions by differential RNA-seq analysis. Differentially expressed pathways and cellular systems were inferred using the network-based algorithm PheNetic. Co- culturing affected mainly metabolism in WDL1. Significantly enhanced expression of *hylA* encoding linuron hydrolase was observed. Moreover, differential expression of several pathways involved in carbohydrate, amino acid, nitrogen and sulfur metabolism was observed indicating that WDL1 gains carbon and energy from linuron indirectly by consuming excretion products from WDL7 and/or WDL6. Moreover, in consortium conditions WDL1 showed a pronounced stress response and overexpression of cell-to-cell interaction systems such as quorum sensing, contact-dependent inhibition and Type VI secretion. Since the latter two systems can mediate interference competition, it prompts the question if synergistic linuron degradation is the result of true adaptive cooperation or rather a facultative interaction between bacteria that coincidentally occupy complementary metabolic niches.

### 4.2.2 Introduction

Mineralization of organic xenobiotic compounds is often performed by microbial consortia by means of metabolic association in which one organism in the consortium converts the organic xenobiotic into metabolites that are degraded by other consortium members [167]. Further degradation of downstream metabolites can enhance the initial degradation step resulting in an overall increased efficiency of mineralization of the organic xenobiotic in which case the metabolic association between consortium members is called synergistic. Members of organic xenobiotic degrading consortia are often heterotrophic organisms that also feed singly on compounds other than the organic xenobiotic. Therefore, it is not always clear whether metabolic association between consortium members is a beneficial interaction that has evolved by cooperative adaptation, at least in part because of this purpose [168], or rather represents a facultative interaction between species that coincidentally occupy complementary metabolic niches. In fact, the evolution of cooperative traits is estimated to be rare in the microbial world [169]. The rare examples of cooperation among bacteria show that the involved bacteria typically have developed specialized molecular mechanisms necessary for synergistic functioning of the consortium, such as co-aggregration or bacterial signaling [170,171]. The identification of such molecular mechanisms can therefore be indicative of the evolution of cooperation between bacterial consortium members.

A consortium that synergistically degrades an organic xenobiotic compound has been described for mineralisation of the widely used phenylurea herbicide linuron [172]. The consortium was enriched from an orchard soil with a history of linuron treatment and originally consisted of five to six species with functional redundancy. The consortium can be reduced to three partners, i.e. strains *Variovorax sp.* WDL1, *Comamonas testosteroni* WDL7 and *Hyphomicrobium sulfonivorans* WDL6, that together provide all steps of the catabolic pathway for linuron mineralisation [172]. Metabolic association, i.e., the exchange of linuron metabolites, has been identified as the major driver for synergistic linuron degradation by the consortium. *Variovorax sp.* WDL1 hydrolyzes linuron into 3,4-dichloroaniline (3,4-DCA) and *N,O*-dimethylhydroxylamine (*N,O*-DMHA) using the phenylurea hydrolase HylA [172, 173]. Although WDL1 contains dca and ccd clusters encoding for the further degradation of 3,4-DCA to 3-oxoadipate via a chlorocatechol intermediate, 3,4-DCA is degraded inefficiently by WDL1. Instead, 3,4-DCA and *N,O*-DMHA are excreted by WDL1 and used as carbon and energy source by WDL7 and WDL6, respectively [172]. An overview of linuron degradation by the consortium is depicted in **Figure 4.1**. When the consortium is grown as a biofilm on linuron as the sole carbon, nitrogen and energy source, the removal of 3,4-DCA by WDL7 increases the rate of linuron hydrolysis by strain WDL1 whereas *N,O*-DMHA degradation by WDL6 has no effect on linuron hydrolysis. Therefore, WDL7 is considered to act as a mutualistic partner of WDL1 whereas WDL6 is suggested to have a rather commensal role [174]. The metabolic interaction between the three strains is further reflected in their close co-localization when grown as biofilms on linuron [174]. Conservation of species composition of linuron-degrading consortia as suggested by the isolation of such consortia from geographically separated and physico- chemically different soils [174] and from molecular ecology studies [167, 174, 175], underlines the ecological relevance of this multi-species bacterial organization. Although metabolic association during linuron degradation appears the major driving force of the consortium composition and functionality, we do not know whether other interactions underlie the synergistic degradation of linuron. For instance, it is not yet clear which carbon source(s) support the growth of the primary linuron degrader strain WDL1 in the consortium.

Neither do we know whether contact dependent and/or independent mechanisms drive the establishment of synergistic interactions between the consortium members, and which could be indicative of true cooperative adaptation [168].

Differential transcriptomics using next generation Illumina RNA-seq, in which global gene expression is compared between strains when grown in consortium and in isolation, has been recently successfully used to identify candidate genes relevant for interspecies interactions in both artificially composed consortia [176] and in syntrophic consortia [177–180]. In its first application to scrutinize an organic xenobiotic-degrading consortium, we used differential RNA-seq to identify molecular mechanisms mediating synergistic interactions between the members of the linuron-degrading consortium consisting of *Variovorax sp.* WDL1, *C. testosteroni* WDL7 and *H. sulfonivorans* WDL6, grown as biofilms. Focus was on mutualistic partners WDL1 and WDL7 for which gene expression was compared between consortium and monoculture biofilms fed with linuron or 3,4-DCA as the sole carbon and energy source.

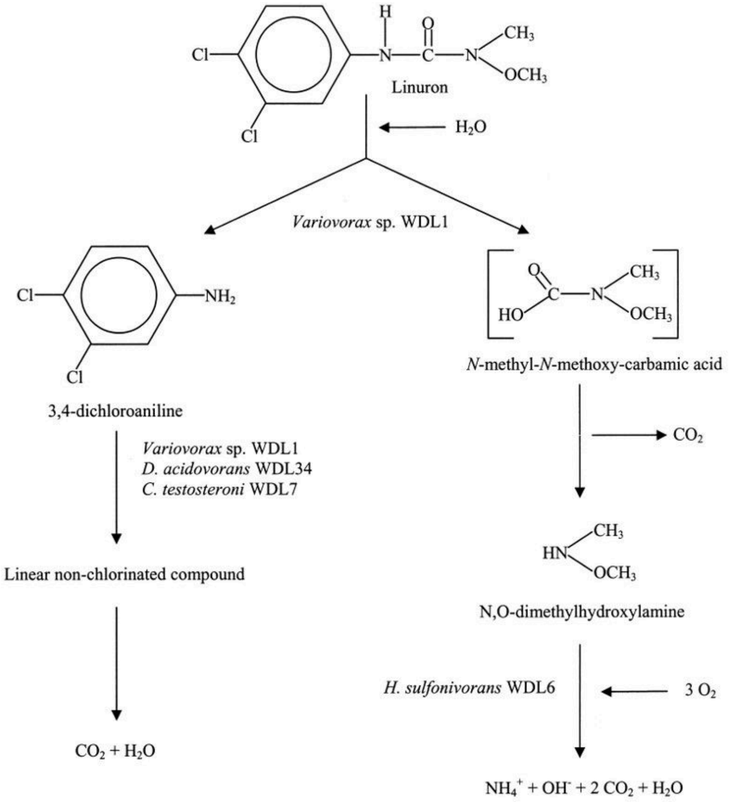

*Figure 4.1:* ***Overview of linuron degradation by the triple-species consortium.*** *Figure taken from Dejonghe et al. [172]*

### 4.2.3 Results

#### 4.2.3.1 Linuron and 3,4-DCA degradation performance of consortium and monoculture biofilms

For differential gene expression analysis, biofilms of the consortium containing WDL1, WDL6 and WDL7 as well as monoculture biofilms of WDL1 and WDL7 were grown on inorganic nitrogen-containing mineral medium (MMO) [172] supplemented with linuron or 3,4-DCA as the sole carbon source. The synergistic degradation of linuron by the consortium was evident from the linuron degradation efficiency of consortium biofilms compared to this of WDL1 monoculture biofilms (**Figure 4.2 A**). The latter degraded linuron inefficiently and effluent concentrations never dropped below 96% of the linuron influent concentration. In the consortium biofilms, the linuron effluent concentration started to decrease after two weeks of operation. After 29 days, steady-state conditions were attained with linuron effluent concentration stagnating around 35% of the influent concentration. Minor accumulation of 3,4-DCA was observed in both consortium and WDL1 monoculture biofilms, never exceeding 3% and 2% (molar equivalent) of the linuron influent concentration, respectively. In WDL7 monoculture biofilms fed with 3,4- DCA, effluent 3,4-DCA concentrations started to decrease after two days of operation. After 4 days, steady-state degradation was obtained and effluent 3,4-DCA concentrations remained around 14% of the influent concentration (**Figure 4.2 B**).

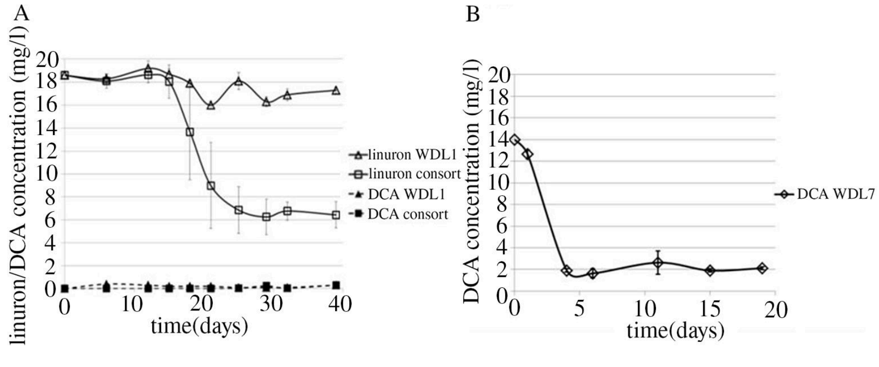

*Figure 4.2: **Time lapse effluent concentrations of metabolites. A)** Time lapse effluent concentrations of linuron (solid lines) and 3,4-DCA (dotted lines) in flow channels containing WDL1/WDL7/WDL6 consortium (squares) and WDL1 monoculture biofilms (triangles). **B)** Time lapse effluent concentration of 3,4-DCA in flow channels containing WDL7 monoculture biofilms (diamonds). Each data point with error bar represents the mean and standard deviations of three replicate systems.*

*Table 4.1:* ***Summary of sequencing results and read alignment of the different RNA-seq libraries.***

| | **Replicate** | **# read pairs** | **# filtered read pairs (Phred score > 30)** | **# uniquely mapped read pairs** | **# read pairs uniquely mapped to CDS** | **# read pairs uniquely mapped to rRNA** |
|---|---|---|---|---|---|---|
| WDL1 | 1 | 8.090.000 | 7.921.052 | 6.491.448 | 26.258 | 6.032.872 |
| WDL7 | 1 | 1.360.000 | 1.329.361 | 1.169.256 | 12.466 | 1.077.552 |
| WDL7 | 2 | 470.000 | 463.034 | 420.385 | 6.008 | 384.077 |
| WDL7 | 3 | 3.330.000 | 3.248.923 | 2.783.049 | 41.470 | 2.478.562 |
| Consortium | 1 | 15.850.000 | 15.441.928 | 13.920.873 | 107.069 | 13.080.821 |
| Consortium | 2 | 25.040.000 | 24.490.945 | 22.529.095 | 227.025 | 14.805.214 |
| Consortium | 3 | 20.590.000 | 20.005.138 | 18.442.744 | 134.644 | 17.227.266 |
| Total | | 74.720.000 | 72.900.381 | 65.756.850 | 554.940 | 55.086.363 |

#### 4.2.3.2 Overall analysis and validation of RNA-seq data

Samples for transcriptome analysis were taken after two weeks of steady linuron or 3,4-DCA degradation. Sequencing of all cDNA libraries resulted in a total of 74 million read pairs (**Table 4.1**). Monoculture and consortium libraries had been multiplexed in a 1:5 concentration ratio for sequencing which was reflected by the numbers of reads from consortium libraries being higher than those from monoculture libraries. However, the number of read pairs between replicates were highly variable (**Table 4.1**). After the trimming step, read pairs were mapped on the compiled genome sequences of strains WDL1, WDL6 and WDL7. A challenge for performing RNA-seq analysis using transcript data from mixed cultures is the risk that reads will be mapped erroneously to orthologous genes present in the other strains. Therefore, reads that show non157 unique alignment on the compiled triple-species reference genome sequence were discarded. Results show that on average only 9 (± 1)% of the reads of the consortium samples were as such discarded. Finally, 76 to 88% of the read pairs in the samples could be unambiguously mapped on the compiled triple-species reference genome sequence (**Figure 4.3**). Despite the rRNA depletion treatment, on average 88% of these retained read pairs aligned with rRNA genes. The percentage of retained read pairs that mapped to CDSs was low for all samples: 0.4% for the WDL1 monoculture biofilm, 1.1-1.5% for the three WDL7 monoculture biofilms, and 0.7-1.0% for the three consortium biofilms. The number of read pairs mapping to CDSs ranged from 6.008 to 227.025 which is lower than what was observed in comparable studies (300.000-1.000.000 read pairs) [179, 181]. Rarefaction curve analysis (**Figure 4.4**) showed that despite the low number of mapped read pairs, the number of expressed CDS detected in the consortium samples and one WDL7 monoculture sample (50%-66%) was close to the estimated asymptotic value of 70%. On the other hand, the sequencing depth for two WDL7 monoculture replicates and the WDL1 monoculture sample only covered the expression of 26%-40% of the genes, indicating that for those samples a part of the genes with low expression levels remained undetected. Overall, gene expression values obtained for biological replicates of the different samples were highly correlated, with a Pearson correlation (R) of on average 0.99 between pairs of WDL1 in consortium samples, of 0.93 for pairs of WDL7 in consortium samples, and of 0.97 between the WDL7 monoculture samples. RNA-seq inferred differential expression levels observed between consortium and monoculture conditions were reassessed by qRT-PCR for five genes of WDL1 (*hylA*, *dcaQ*, *ccdC* and *phoA*) and four genes of WDL7 (*pcaF*, *glxR*, *pilM*, *pilY1* and *yrbC*). Those genes were selected as they were considered as potentially involved in interspecies interactions based on annotation (*hylA*, *dcaQ*, *ccdC*, *pcaF*, *pilY1*) and/or because their RNA-seq-inferred differential expression levels ranged from underexpression (*pcaF*) over non-differential (*dcaQ*, *ccdC*, *phoA*, *pilY1*, *yrbC*) to overexpression (*hylA*, *glxR*, *pilM*) in consortium conditions. qRT-PCR and RNA-seq based values showed a high Pearson correlation (R = 0.97) (**Supplementary Figure S4.1**). The high reproducibility between similar samples and the confirmation of RNA-seq-based differential expression by means of qRCR indicates that one WDL1 monoculture sample is sufficient for correctly analyzing the differential response of WDL1 to consortium growth.

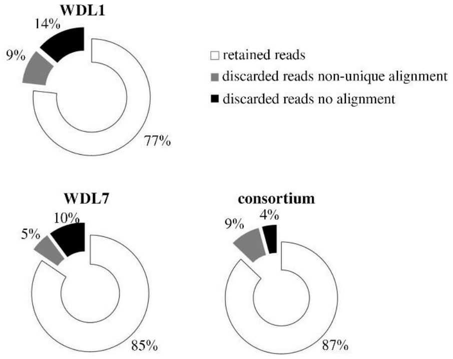

*Figure 4.3:* ***Average percentages of retained and discarded RNA-seq read pairs.*** *Read pairs obtained with one WDL1 monoculture (WDL1), three WDL7 monoculture (WDL7) and three consortium (consortium) biofilm samples after mapping the read pairs to the compiled triple-species reference genome of Variovorax sp. WDL1, C. testosteroni WDL7 and H. sulfonivorans WDL6.*

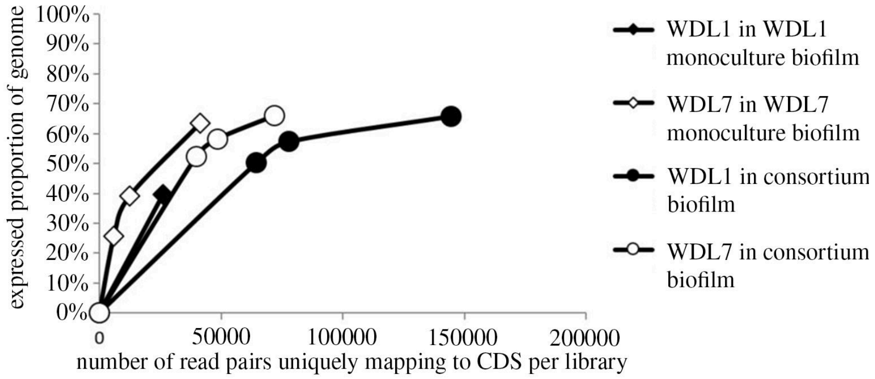

*Figure 4.4:* ***Rarefaction curves.*** *The curves show the proportion of CDSs of the genome of WDL1 or WDL7 that were expressed (with read pair count $\geq 1$) in the monoculture and consortium biofilms (as determined by RNA-seq) as a function of the number of read pairs uniquely mapping to CDSs of WDL1 or WDL7: expressed proportion of WDL1 genome in the WDL1 monoculture biofilms (black diamond), expressed proportion of WDL1 genome in the WDL1/WDL6/WDL7 consortium biofilms (black circles), expressed proportion of WDL7 genome in the WDL7 monoculture biofilms (white diamonds) and expressed proportion of WDL7 genome in the WDL1/WDL6/WDL7 consortium biofilms (white circles).*

#### 4.2.3.3 Transcriptional responses in *Variovorax sp.* WDL1 when grown in consortium conditions

In WDL1, 1372 CDSs showed differential expression between monoculture and consortium conditions. The differentially expressed CDSs were functionally categorized based on KEGG orthology (**Figure 4.5**) and PheNetic was used to find pathways underlying the differentially expressed genes (**Figure 4.6**). Only a few genes of catabolic clusters involved in linuron degradation in WDL1 were differentially expressed. The linuron hydrolase gene *hylA* in WDL1 appeared more than 100-fold overexpressed in consortium conditions, while all three genes of the oxoadipate catabolic operon (pcaFIJ) required for converting the linuron metabolite 3197 oxoadipate into TCA cycle intermediates (K01031, K00632 and K01032), were 2-to 4-fold underexpressed in consortium conditions (**Figure 4.6; Table 4.2**). All other genes putatively involved in linuron degradation to TCA intermediates, i.e., all genes belonging to the dcaQT-A1A2B gene cluster encoding the 3,4-DCA multicomponent dioxygenase and the ccdCFDE gene cluster encoding conversion of chlorocatechols to 3-oxoadipate were not differentially expressed between consortium and monoculture conditions. The dcaQTA1A2B-, ccd-, and pca-clusters represented about 11%, 5% and 0.2%, respectively, of the total number of transcript read pairs mapping with CDSs in both consortium conditions and monoculture conditions indicating their high expression in WDL1 regardless of the strain was grown alone or together with WDL7 and WDL6 (results not shown). The results further showed that overall, general cell metabolism was altered in WDL1 in consortium conditions compared to monoculture conditions. When grown in consortium conditions, 351 enzyme encoding genes were differentially expressed genes in WDL1. About 17% of these genes (61 CDS) were involved in carbohydrate metabolism (**Figure 4.5**) and several carbohydrate metabolizing pathways were selected by PheNetic (**Figure 4.6**). For an in-dept analysis of the found molecular pathways and their genes, we refer to **Appendix A**.

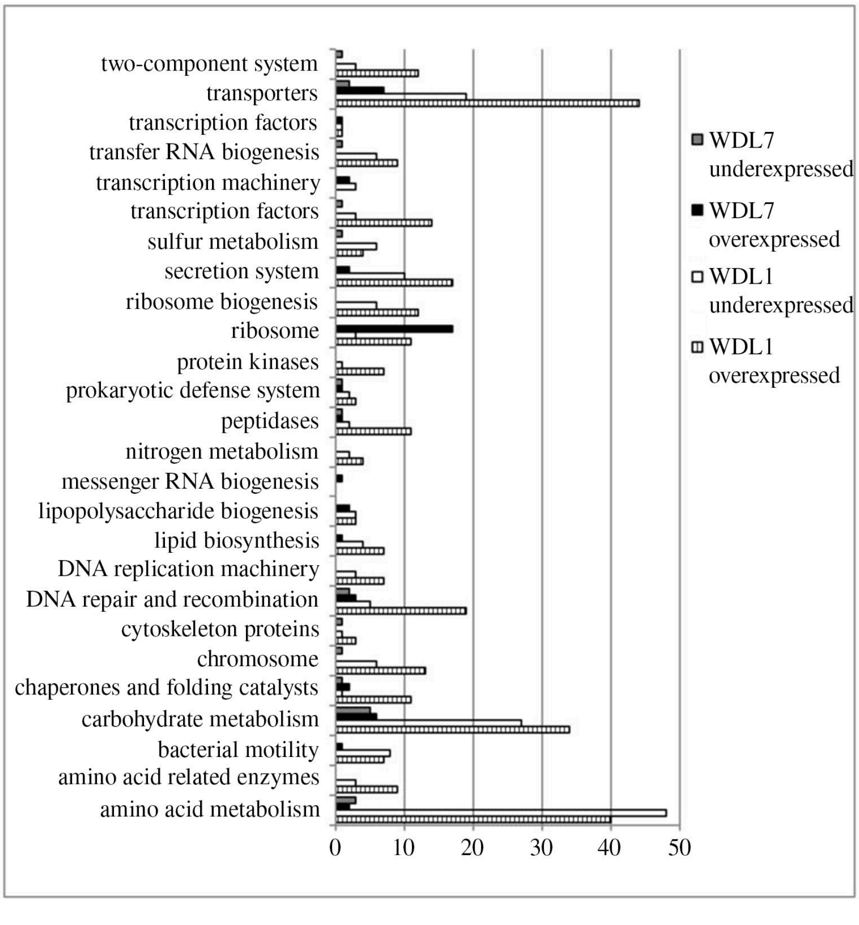

*Figure 4.5: **KEGG orthology based functional categorization of CDSs.** This figure depicts the number of CDSs in several functional categories that are over-or under-expressed in WDL1 or WDL7 when grown in WDL1/WDL7/WDL6 triple-species biofilms compared to their growth in monoculture biofilms.*

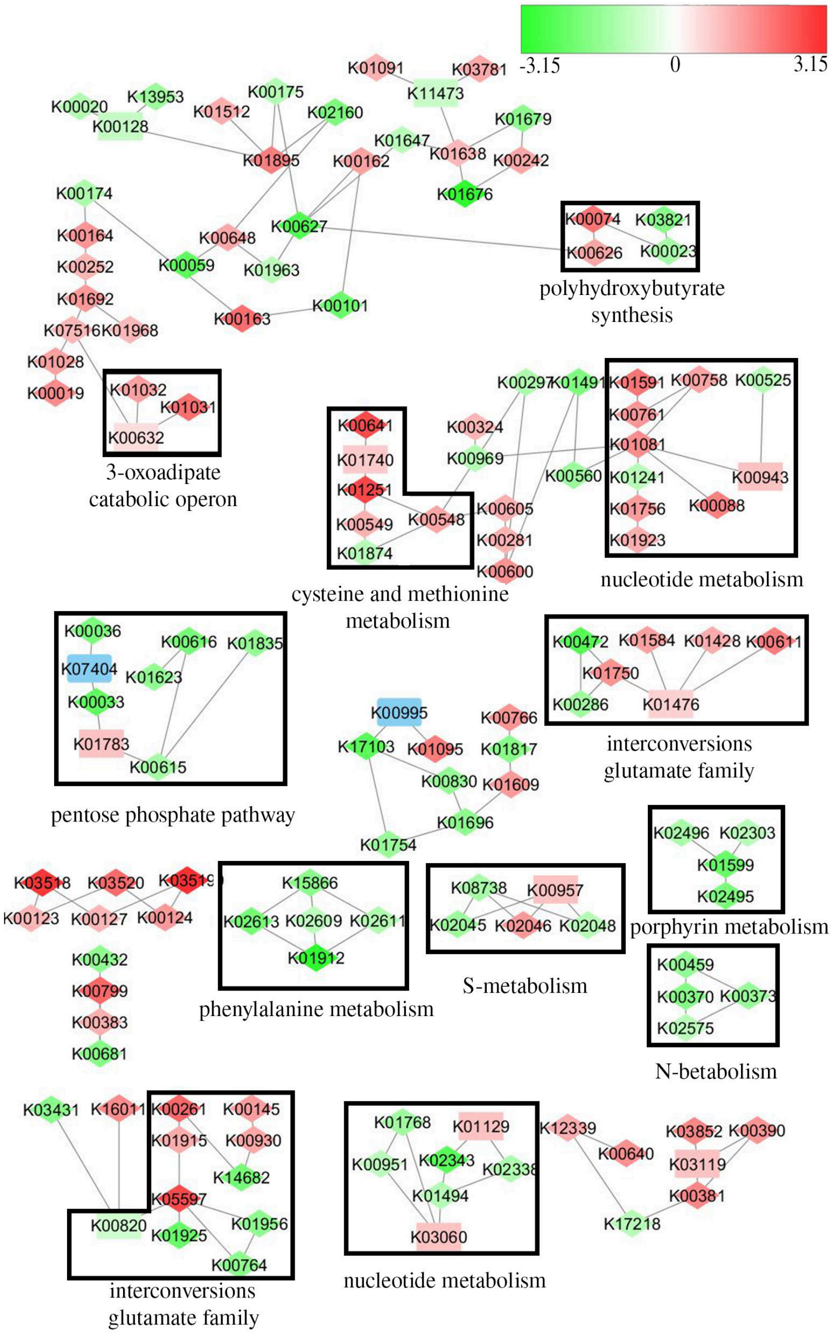

*Figure 4.6:* ***Molecular pathways differentially expressed between consortium and monoculture conditions for WDL1 as inferred by PheNetic.*** *This figure shows all genes and interactions between genes inferred by PheNetic. Log2-fold change in expression is indicated on a color scale from green to red, with red signifying underexpression in consortium conditions and green representing overexpression in consortium conditions. Blue-highlighted genes are genes for which no transcripts were recorded. Genes that are differentially expressed (|Log2-fold change| $\geq$ 1) are indicated by diamond shapes. Discussed pathways are boxed and annotated.*

#### 4.2.3.4 Transcriptional responses elicited in *C. testosteroni* WDL7 when grown in consortium biofilms

Only 169 CDSs in WDL7 showed differential expression when comparing monoculture with consortium conditions. Similar to WDL1, only a few genes of the gene clusters predicted to be involved in 3,4-DCA degradation, were differentially expressed in WDL7. The *dcaB* gene of the dcaQTA1A2B cluster encoding the oxygenation of 3,4-DCA in WDL7 was twofold underexpressed in consortium conditions. Furthermore, in contrast to WDL1, only *pcaF* of the pcaFIJ operon, i.e., the gene encoding acetyl-CoA acetyltransferase was threefold underexpressed in consortium conditions (**Table 4.2**). However, the latter was not confirmed by transcriptional fusion reporter analysis (**Supplementary Figure S4.2 A**). *catAB*, *CMBL* and *tfdF* encode conversion of chlorocatechol to 3-oxoadipate in WDL7 [182], and were not differentially expressed between consortium and monoculture conditions. As in WDL1, most DCA catabolic genes (dcaQTA1A2, *catAB*, *CMBL*, *tfdF* and *pcaIJ*) were not differentially expressed and all DCA catabolic genes represented together more than 25% of the transcript reads indicating a high expression of the DCA catabolic pathway in WDL7.

One system that was selected by PheNetic as clearly underexpressed in WDL7 under consortium conditions was the high affinity cbb3-type cytochrome c oxidase (K00404, K00405, K00406; **Figure 4.7; Table 4.2**). None of the other three terminal respiratory oxidase gene clusters in WDL7 showed altered expression in consortium conditions compared to monoculture conditions. For an in-dept analysis of the found molecular pathways and their genes we refer to **Appendix A**.

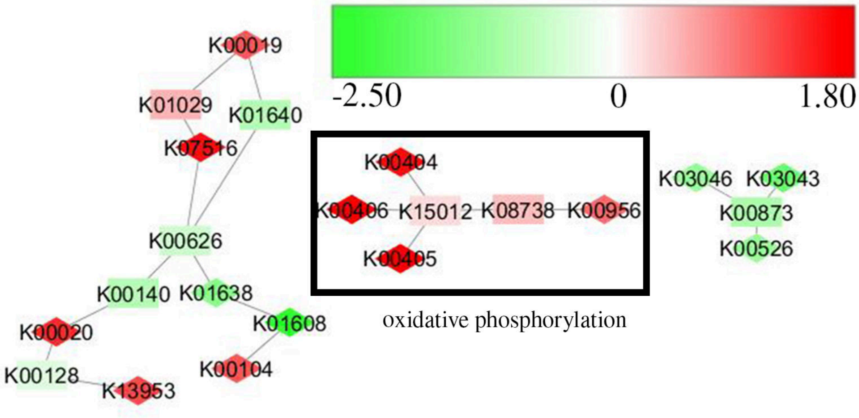

*Figure 4.7:* ***Molecular pathways differentially expressed between consortium and monoculture conditions for WDL7 as inferred by PheNetic.*** *Log2-fold change in expression is indicated on a color scale from green to red, with red signifying underexpression in consortium conditions and green representing overexpression in consortium conditions. Genes that are differentially expressed (|Log2-fold change| ≥ 1) are indicated by diamond shapes. Discussed pathways are boxed and annotated.*

*Table 4.2:* ***Log2-fold change values for genes belonging to discussed molecular pathways.***

| Knumber/gene name | Log2-fold change monoculture-consortium | Knumber/gene name | Log2-fold change monoculture-consortium |
|---|---|---|---|
| | **WDL1** | | |
| **linuron catabolism** | | **nitrogen metabolism** | |
| *hylA* | -6.8 | K00459 | -1.6 |
| K00632/*pcaF* | 1.3 | K00373 | -1.6 |
| K01032/*pcaJ* | 1.4 | K00370 | -1.8 |
| K01031/*pcaI* | 2.1 | K07673 | -2.2 |
| **polyhydroxybutyrate synthesis** | | K07712 | -1.4 |
| K00626 | -1.2 | K07708 | -2.2 |
| K03821 | -1.8 | K03320 | -1.4 |
| K00023 | -1.3 | K02575 | -1.0 |
| **cysteine and methionine metabolism** | | K01915 | 1.2 |
| K12339 | 1.2 | **sulfur metabolism** | |
| K00548 | -1.7 | K00390 | 1.6 |
| K01251 | 2.7 | K00381 | 1.8 |
| K00549 | 1.1 | K00957 | 0.9 |
| K00789 | 2.7 | K02046 | 1.5 |
| K00641 | 2.6 | K02048 | -1.1 |
| K00640 | 1.6 | K02045 | -1.5 |
| **glutamate family** | | K03147 | 3.7 |
| K05597 | 2.7 | K03154 | 2.2 |
| K01925 | -2.3 | **heat shock regulon** | |
| K01956 | -1.7 | K04043/*dnaK* | -1.3 |
| K00764 | -1.7 | K04077 | -1.2 |
| K01915 | 1.2 | K11907/*clpB* | -2.8 |
| K00472 | -2.6 | K03705/*hrcA* | -1.7 |
| K00286 | -1.4 | K04079*htpG* | -1.3 |
| K01750 | 1.6 | *dnaJ* | -1.7 |
| K01584 | 1.4 | K07263 | -1.6 |
| K01428 | 1.2 | K03089/*rpoH* | -1.1 |
| K00611 | 1.9 | K04078 | -1.4 |
| **DNA repair/recombination** | | K13993 | -1.9 |
| K01142 | -2.1 | K03687/*grpE* | 1.4 |
| K04764 | -1.2 | **nucleotide metabolism** | |
| K00567 | 1.7 | K01591 | 2.0 |
| K03702 | -1.4 | K00761 | 1.5 |
| K01972 | -1.9 | K01081 | 1.7 |
| K03703 | -2 | K01241 | -1.1 |
| K04485/*recA* | -1.5 | K01756 | 1.4 |
| K03553 | 1.0 | K01923 | 1.2 |
| K02343 | -2.5 | K00758 | 1.2 |

| | | | |
|---|---|---|---|
| K10563 | -2.3 | K00525 | -1.1 |
| K00525 | -1.1 | K00088 | 1.9 |
| K03574 | -1.3 | K00951 | -1.0 |
| K10979 | -1.3 | K02343 | -2.5 |
| K01971 | -1.3 | K02338 | -1.2 |
| K10979 | -1.4 | K01494 | -1.1 |
| K03724 | -1.2 | **type VI secretion system** | |
| K03582 | -1.9 | K11893 | -1.5 |
| K10860 | -1.1 | K11891 | -1.3 |
| K02338 | -1.2 | K11890/*impM* | -1.4 |
| K03584 | -1.1 | K11903 | -1.7 |
| K03554 | -1.1 | K11900/*impC* | -1.6 |
| K03530 | -1.1 | K11901/*impB* | -1.6 |
| **CDI** | | K11907/*clpB* | -2.8 |
| K15125 | -1.0 | K11904/*vgrG* | -2.8 |
| putative CDI antitoxin | -1.1 | K11906/*vasD* | -1.0 |
| K15125 | -1.4 | **quorum sensing** | |
| **porphyrin metabolism** | | K18098/*luxR family* | -3.9 |
| K02496 | -1.3 | K18096/*luxI* | -1.7 |
| K02303 | -1.1 | **pentose phosphate pathway** | |
| K01599 | -2.3 | K00615 | -1.3 |
| K02495 | -2.0 | K00033 | -2.4 |
| | | K00036 | -2.0 |
| | | K00616 | -2.1 |
| | | K01623 | -1.6 |
| | | K01835 | -1.6 |
| | **WDL7** | | |
| **glycerate biosynthesis operon** | | **cytochrome c oxidase** | |
| K01608 | -2.2 | K00406/*CcoP* | 1.8 |
| K00042 | -2.3 | K00405/*CcoO* | 1.9 |
| K01816 | -1.9 | K00404/*CcoN* | 1.7 |
| **linuron catabolism** | | | |
| K00632/*pcaF* | 1.7 | | |
| *dcaB* | 1.0 | | |

## 4.2.4 Discussion

### 4.2.4.1 Co-culturing of strains modulates additional metabolic pathways in the linuron-degrading consortium

As reported above, we recently observed that WDL1 consists of a linuron-hydrolyzing and a DCA-oxidizing subpopulation. Considering that the linuron-hydrolyzing WDL1 subpopulation retrieves no energy nor carbon from linuron hydrolysis, its growth on linuron in consortium conditions can only be explained by the uptake and metabolism of alternative carbon sources produced by the other consortium members during linuron degradation. Cross-feeding and growth on compounds other than linuron metabolites is indeed supported by the many differentially expressed genes, particularly in WDL1, that can be linked to the exchange of metabolites with their environment. Firstly, the high number of genes coding for functions involved in transport and two-component systems in WDL1 that are overexpressed in consortium conditions (**Figure 4.5**), likely reflects a substantial change in the chemical composition of the local environment surrounding WDL1 cells. Since the three consortium members are closely associated when grown together as a biofilm [174], each strain is confronted with the metabolic footprint of the other strains. The metabolic footprint, i.e., the ensemble of metabolites in the extracellular space as a result of uptake of nutrients and the excretion of metabolites, was previously shown to be, among other factors, a species specific trait [183, 184]. A similar change in expression of genes coding for membrane proteins in multispecies biofilms of soil bacteria was observed before [185]. Secondly, the altered expression of genes encoding enzymes involved in metabolic pathways (**Figure 4.5**) is similarly indicative of cross-feeding between the consortium members. Amino acids appear as one such type of molecules exchanged in the consortium as suggested by the altered expression in WDL1 of genes involved in amino acid metabolism and transport, but also by a change in expression of genes involved in nitrogen regulation, uptake of inorganic nitrogen and assimilation via glutamine synthetase (**Table 4.2**). Differential expression of genes involved in nitrogen metabolism in bacteria as a response to multiculture growth was previously observed and suggested to be associated with the exchange of amino acids or other nitrogen containing compounds between consortium partners [178, 180, 186, 187]. Interestingly, addition of amino acids was previously shown to enhance degradation of linuron in monocultures of linuron-degrading Variovorax strains that were recovered from linuron-degrading consortia with compositions similar to the tripartite WDL1/WDL6/WDL7 consortium [174]. Alternatively, the altered nitrogen metabolism in WDL1 can be merely a consequence of the loss of 3,4-DCA as the nitrogen- delivering metabolite of linuron degradation by the WDL1 cells in consortium conditions, due to the more efficient uptake by WDL7. The underexpression of genes involved in the biosynthesis of sulfur-containing compounds such as thiamine, methionine and cysteine in consortium conditions in WDL1 (**Table 4.2**) could point towards a lower dependence on de novo synthesis of these compounds when they are obtained from other strains in consortium conditions. This was also observed previously in a cyanobacterial-heterotrophic co-culture [180].

Compared to WDL1, WDL7 shows a less extensive metabolic response upon co-culturing. Only a clear overexpression of the glycerate biosynthesis gcl operon was observed in WDL7 during consortium growth (**Table 4.2**). This operon was shown to be induced by glyoxylate in Escherichia coli [188], suggesting that WDL7 senses a higher concentration of glyoxylate when grown in consortium conditions and thus that glyoxylate is a candidate metabolite that WDL7 could receive during consortium growth. As WDL7 does not show a strong change in regulation of metabolic pathways between growth conditions, 3,4-DCA seems to remain the main carbon and energy source of WDL7 both in monoculture and consortium biofilm conditions. In contrast to the non-differential expression of metabolic pathways in WDL7, its growth rate does seem to increase in consortium conditions based on the abundant overexpression of one third of WDL7 genes encoding for ribosomal proteins. This has been described before in other consortia and was suggested to be a metric of in situ growth rate [177, 189]. A higher growth rate is also expected for WDL1 in consortium conditions from the increase of DNA synthesis [190].

#### 4.2.4.2 Co-culturing of consortium strains triggers a stress response in WDL1

Growth in consortium conditions engenders the overexpression of stress related proteins in WDL1, like the heat shock regulon (**Table 4.2**). Some of these molecular chaperones were also found to be overexpressed in a phototrophic bacterial consortium [187] and in a halophilic co-culture of closely related strains [189] indicating that a stress response upon co-growth of strains mutually benefiting from the interaction is not unique to the linuron-degrading consortium. Also several genes involved in DNA repair and recombination appear to be upregulated indicating that increased DNA damage occurs in WDL1 under consortium conditions (**Table 4.2**). DNA damage can be caused by change in metabolic activity resulting in an enhanced production of reactive oxygen species that are continuously generated during metabolism [191] but can also be caused by exogenous agents such as toxins [192]. On the other hand, increased DNA repair and recombination might also be due to the increased DNA synthesis in WDL1 in consortium conditions as indicated by the underexpression of degradation of purine and pyrimidine nucleotides and overexpression of formation of deoxynucleotides (**Table 4.2**). Nevertheless, coexistence in the linuron-degrading consortium appears to be experienced by WDL1 as a stressful situation implying that the ecological interactions between the consortium members are more complex than merely the exchange of metabolites.

#### 4.2.4.3 Potential involvement of cell-to-cell interactions in shaping the linuron degrading consortium

In this study, we observed two types of contact-dependent interaction systems (T6SS, a Type VI secretion system and CDI) that were overexpressed in consortium conditions in WDL1 (**Table 4.2**). In both T6SS and CDI, toxic effector proteins and antitoxins form a functional pair and mediate growth inhibition of neighboring competitor cells that do not produce the identical toxin/antitoxin pair [193, 194]. The T6SS and CDI systems might be used by WDL1 for contact-dependent interference competition with WDL6 and WDL7. However, CDI and T6SS can also mediate cooperation and communication between bacteria expressing the same toxin-antitoxin system in which case they are immune to each others toxins and are called ”self” -bacteria. Alternative ecological roles beyond competition have been proposed for CDI and T6SS, where the toxin protein could be interpreted as a contact-dependent signal molecule by ”self” -bacteria. In this way, toxin-antitoxin systems can contribute to community architecture, but they can also enforce cooperative behavior in ”self”-bacteria when the toxin-antitoxin pair is co-regulated with genes coding for social traits by killing self-bacteria that do not express social traits [193]. In that context, it was recently shown that the CDI system of *Burkholderia dolosa* alters gene expression in *Burkholderia thailandensis* showing that self-bacteria can belong to different species as long as they produce the same toxin-antitoxin pair [194]. However, we only identified T6SS or CDI toxin or antitoxin genes in WDL1 and not in the other consortium members.

### 4.2.5 Conclusion

Using a differential transcriptomic approach, we revealed that next to metabolic association between the members of a linuron-degrading consortium, additional cross-feeding interactions are expected to be present and that amino acids are one type of metabolites that are possibly exchanged between the consortium members that in particular are used by WDL1 for growth. In comparison to WDL7, WDL1 shows a more extensive response upon co-culturing with WDL6 and WDL7, including the increased expression of *hylA* encoding linuron hydrolase which can be directly linked with enhanced linuron degradation and a stress response. Furthermore, several cell-to-cell interaction systems were overexpressed that could be involved in interspecies signaling such as quorum sensing, contact-dependent inhibition and Type VI secretion. Whether or not those signaling systems contribute to the well-functioning of the consortium remains to be elucidated. On the contrary, Type VI secretion and contact-dependent inhibition could also be used by WDL1 in interference competition with WDL6 or WDL7. This raises the question if synergistic linuron degradation by the consortium involves true adaptive cooperation or is rather a byproduct of selfish interactions between the consortium strains that are competing for other nutrients and space. The apparent experience of stress by WDL1 favors the latter hypothesis. Furthermore, a large number of differentially expressed genes in WDL1 and WDL7 were coding for hypothetical, putative and unknown proteins which was also observed in similar studies with other consortia [181, 189, 195]. These uncharacterized proteins might include novel functions that are important for the well-functioning of consortia and their study is of interest for gaining more insight in the synergistic mechanisms in bacterial consortia.

### 4.2.6 Experimental procedures

#### 4.2.6.1 Bacteria, media and biofilm growth conditions

Biofilms were grown at 25 °C in a continuous flow chamber system (BioCentrum DTU, Denmark) as described by Breugelmans et al. [174]. *Variovorax sp.* WDL1 (LMG 27260), *C. testosteroni WDL7* (LMG 27261) and *H. sulfonivorans WDL6* (LMG 27262) cell suspensions for inoculation were prepared as described by Horemans et al. [196]. Consortium biofilms and WDL1 monoculture biofilms were grown on MMO [197] supplemented with 20 mg $L^{-1}$ linuron. Monoculture biofilms of WDL7 were grown on MMO supplemented with 14 mg $L^{-1}$ 3,4- DCA. Consortium biofilms as well as WDL1 and WDL7 monoculture biofilms were grown in triplicate. Triplicate non-inoculated control systems for abiotic removal of linuron or 3,4-DCA were operated in parallel. At regular time intervals, one ml effluent samples were taken, centrifuged at 10,000 g for 5 min, and the supernatant stored at -20°C prior to HPLC analysis of linuron and 3,4-DCA concentrations as described [198]. The theoretical maximal accumulated concentration of 3,4-DCA in linuron-fed biofilms was calculated as the molar equivalent of the linuron influent concentration, i.e., the concentration of 3,4-DCA in case all linuron is converted into 3,4-DCA. Consortium and WDL1/WDL7 monoculture biofilms were harvested after two weeks of steady-state linuron and/or 3,4-DCA degradation. In all experiments, linuron and 3,4-DCA PESTANAL analytical standards (99.9 %; Sigma-Aldrich, Belgium) were used.

#### 4.2.6.2 Determination of differential gene expression values

Sequences were trimmed to only retain bases with a PHRED quality score of at least 30 near their ends using Trimmomatic version 0.32. For every replicate separately, the trimmed reads were aligned against a triple-species reference genome sequence consisting of the compiled genome sequences of strains WDL1, WDL6 and WDL7. Bowtie 2 version 2.2.6 was used for the alignment of paired-end data. Read pairs aligning at different positions in the triple-species reference genome with identical mapping scores were classified as ambiguous and discarded. When a read pair mapped only one time discordantly, i.e. only one of the reads from the pair mapped uniquely to the triple species reference genome, that read was considered as mapped and retained. Simply discarding ambiguous reads would reduce the estimated expression level of genes with similar sequences and hence result in false expression rates [199]. Therefore, we adapted a method developed by Ilut et al. [199] in which for each gene a scaling factor is calculated that adjusts the expression levels inferred from read counts to account for the likelihood of undercounting expression of genes with similar sequences. For both WDL1 and WDL7 only 0.3% of the genes had a scaling factor different from 1, meaning this adjustment has an insignificant effect on the analysis. The calculated scaling factors for all genes in WDL1 and WDL7 can be found as supporting information (**Supplementary Table S4.1**). To generate read counts for each gene in consortium and monospecies conditions, the number of retained read pairs were counted in every sample using HTseq version 0.6.1 for strand specific paired-end reads using intersection_nonempty as overlap resolution mode [33]. Differential expression of genes between consortium and mono-species conditions was obtained using the DEseq2 package in R [34]. The independent filtering setting was used in order to increase experiment-wide power and the BenjaminiHochberg correction was used to correct for multiple hypothesis testing. To check if sequencing depth was sufficient, we adapted a method used in biodiversity sampling studies [200], by plotting the proportion of identified coding sequences (CDS) of the WDL1 or WDL7 genome that were expressed (read pair count = 1) as a function of the sampling size in consortium and monoculture RNA-seq libraries. The sampling size was expressed as the number of read pairs that uniquely mapped to CDS of WDL1 or WDL7 in each library. Genes were called differentially expressed between consortium and monoculture conditions when |log 2 fold change| = 1. We did not take into account the p-values of the differential expression analysis as this would be too restrictive. This was shown before to be a valid approach to analyze differential transcriptomic data [42, 180, 201]. While this approach is more prone to false positives, this is offset by the subsequent pathway analysis which is more robust to false positives.

#### 4.2.6.3 Differential gene expression analysis

Analysis of differentially expressed genes was based on the Kyoto Encyclopedia of Genes and Genomes (KEGG) orthology classification of proteins (http://www.genome.jp/kegg/). KEGG identifiers for the coding sequences (CDS) of the three genomes of the consortium members were obtained by exporting the amino acid sequences of all CDS from the RAST server and uploading them on the KEGG automatic annotation server (KAAS) (http://www.genome.jp/tools/kaas/). To unveil pathways and other cellular systems underlying the differentially expressed genes between consortium conditions and isolated conditions for both WDL1 and WDL7, the network-based algorithm PheNetic [6] and the Search Brite tool for functional classification using KEGG orthology [202] were both used. PheNetic searches for common pathways between differentially expressed genes based on an interaction network. The used interaction networks in WDL1 and WDL7 consisted of metabolic, (de)methylation, and (de)phosphorylation interactions from KEGG [202] version 80.0. For WDL1 and WDL7, respectively interactions documented in any of four Variovorax strains (*V. paradoxus S110*, *V. paradoxus EPS*, *V. paradoxus B4* and *Variovorax sp. PAMC 2877*) and any of two *C. testosteroni* strains (*CNB-2*, *TK102*) were used. The standard parameters were applied, run mode was set to ”downstream” and the cost was set to 0.15 for WDL1 and 0.1 for

WDL7. These costs were determined by running a sweep over the cost parameter. In order to avoid selecting noise, identified pathways consisting of at most three genes were discarded The subsystem tool from RAST [203] was used to look for additional genes with no KEGG identifier that could be linked with the differentially expressed pathways and other cellular systems. The RNA-seq derived expression of four genes of WDL1 (*hylA*, *dcaQ*, *catA* and *phoA*) and five genes of WDL7 (*pcaF*, *glxR*, *pilM*, *pilY1* and *yrbC*) were validated by real time quantitative PCR (qRT-PCR). For detailed information, see Supporting Experimental Procedures.

For information on draft genome sequencing of the consortium members, RNA extraction and library prep an how differential transcription was verified, we refer to the Additional experimental procedures in **Appendix A**

### 4.2.7 Acknowledgements

This work was funded by IWT (Innovation by Science and Technology) project SB/101628, by KU

Leuven project OT/10/030, FWO project n°G.0371.06 and the Inter-University Attraction Pole (IUAP) ”$\mu$-manager” of the Belgian Science Policy (BELSPO, P7/25). We thank A. Sanchez, B. Horemans, B. zturk and V. Nolla Ardevol for advice and assistance. The authors declare no competing interests.

# Supplementary

## 4.2.8 Supplementary figures and tables

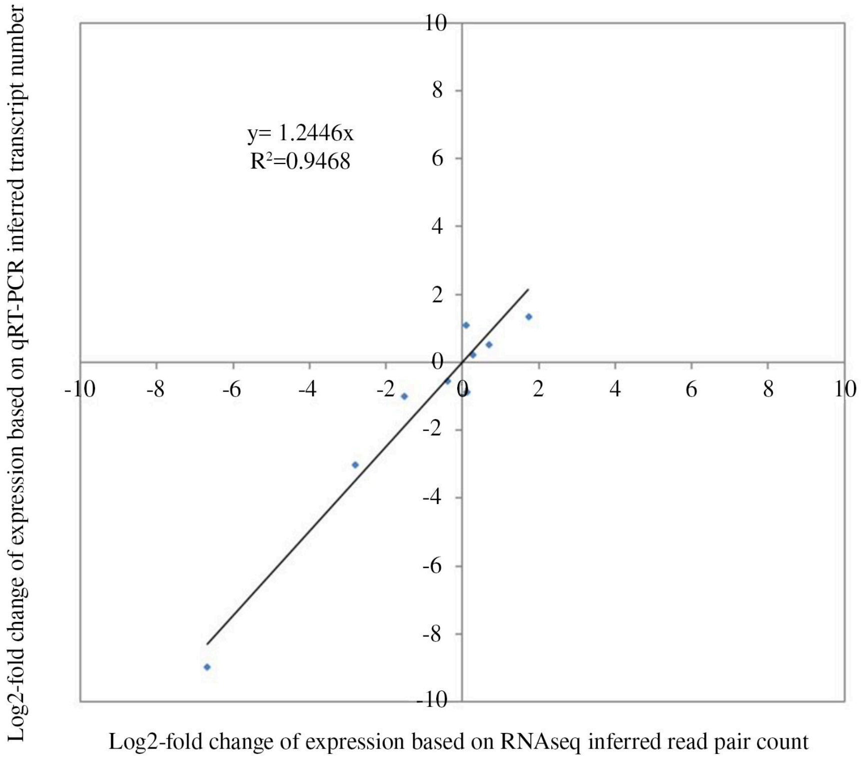

*Figure S4.1:* ***RNA-seq data validation.*** *Correlation between RNA-seq and qRT-PCR data of four genes of WDL1 and five genes of WDL7 showing log2-fold change of gene expression in monoculture versus consortium conditions.*

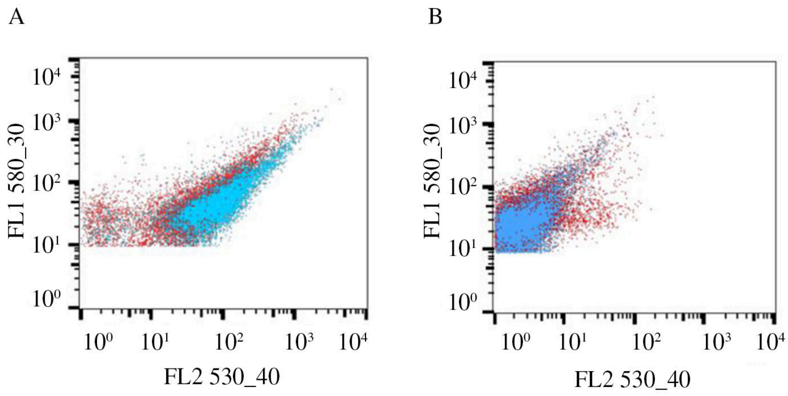

*Figure S4.2:* ***Phenetic inferred map of porphyrin metabolism*** *Flow cytometric profiles of WDL7-Rfp transcriptional gene fusions assessing differential gene expression from* ***A)*** *the promotor region of the oxoadipate catabolic pca operon and* ***B)*** *the promotor region of the glycerate biosynthesis gcl operon, grown in consortium conditions (red dots) vs monoculture conditions (blue dots). Both promotor regions are in fusion with gfpmut3.1 in pRU1097. The dot plot profiles show the amount of green fluorescence (excitation 488 nm, emission filter FL02 (530/40)) on the x-axis, while red fluorescence (excitation 488 nm, emission filter FL01(580/30)) is shown on the y-axis.*

*Table S4.1:* ***Only non-1 scaling factors are depicted. Scaling factors for all other genes are equal to 1.***

| **peg ID WDL 1** | **scaling factor** | **peg ID WDL 7** | **scaling factor** |
|---|---|---|---|
| $ID = fig\vert 6666666.13192.peg.1$ | 0 | $ID = fig\vert 6666666.13171.peg.1$ | 0 |
| $ID = fig\vert 6666666.13192.peg.2$ | 0 | $ID = fig\vert 6666666.13171.peg.2$ | 0 |
| $ID = fig\vert 6666666.13192.peg.3$ | 0 | $ID = fig\vert 6666666.13171.peg.3$ | 0 |
| $ID = fig\vert 6666666.13192.peg.4$ | 0 | $ID = fig\vert 6666666.13171.peg.4$ | 0 |
| $ID = fig\vert 6666666.13192.peg.3689$ | 0.142516872 | $ID = fig\vert 6666666.13171.peg.5$ | 0.16307947 |
| $ID = fig\vert 6666666.13192.peg.5$ | 0.16307947 | $ID = fig\vert 6666666.13171.peg.2839$ | 0.2271777 |
| $ID = fig\vert 6666666.13192.peg.6$ | 0.497746273 | $ID = fig\vert 6666666.13171.peg.6$ | 0.497746273 |
| $ID = fig\vert 6666666.13192.peg.10$ | 0.501577287 | $ID = fig\vert 6666666.13171.peg.10$ | 0.501577287 |
| $ID = fig\vert 6666666.13192.peg.8$ | 0.643989552 | $ID = fig\vert 6666666.13171.rna.57$ | 0.571813511 |
| $ID = fig\vert 6666666.13192.rna.47$ | 0.804181185 | $ID = fig\vert 6666666.13171.rna.12$ | 0.643989552 |
| $ID = fig\vert 6666666.13192.peg.4835$ | 0.946582804 | $ID = fig\vert 6666666.13171.peg.11$ | 0.804657629 |
| $ID = fig\vert 6666666.13192.rna.44$ | 0.951161462 | $ID = fig\vert 6666666.13171.peg.2499$ | 0.963350785 |
| $ID = fig\vert 6666666.13192.peg.11$ | 0.963350785 | $ID = fig\vert 6666666.13171.peg.4167$ | 0.978855513 |
| $ID = fig\vert 6666666.13192.peg.6989$ | 0.969519019 | $ID = fig\vert 6666666.13171.peg.8$ | 0.980474665 |
| $ID = fig\vert 6666666.13192.peg.3037$ | 0.97631723 | $ID = fig\vert 6666666.13171.peg.7$ | 0.985572588 |
| $ID = fig\vert 6666666.13192.peg.7290$ | 0.978653829 | | |
| $ID = fig\vert 6666666.13192.peg.7$ | 0.978855513 | | |
| $ID = fig\vert 6666666.13192.peg.5723$ | 0.985004686 | | |
| $ID = fig\vert 6666666.13192.peg.6754$ | 0.991871676 | | |
| $ID = fig\vert 6666666.13192.peg.6992$ | 0.996460627 | | |
| $ID = fig\vert 6666666.13192.peg.4902$ | 0.99970856 | | |

# 5

# Prioritization of driver genes and pathways from eQTL data

## 5.1 Introduction

In this chapter an adaptation of the network-based method PheNetic, which was used in the previous chapter, is presented. This adapted version is specifically designed to analyze differential expression data *together with* genomics data (eQTL data). As such the method uses a biological interaction network to uncover which mutated genes lead to significant changes in the expression profile of molecular pathways. On top of the identification of causal mutated genes and molecular pathways, the method also ranks the observed mutation based on their likelihood to be causal to the phenotype. By testing the method on two publicly available datasets which had previously been analyzed using literature research and wet-lab experiments, it was possible to automatically reconstruct the results and propose new causal mutations.

DDM and **BW** conceptualized the study, developed the method, analyzed the data, interpreted the results and wrote the manuscript. LDR and KM conceptualized the study, discussed the results and edited the manuscript.

## 5.2 Paper

# Network-based analysis of eQTL data to prioritize driver mutations

De Maeyer, D.$^\dagger$, **Weytjens, B.**$^\dagger$,De Raedt, L., Marchal, K. (**2016**). Network-based analysis of eQTL data to prioritize driver mutations. Genome biology and evolution, 8(3): 481-494.

$^\dagger$ these authors contributed equally to this paper

### 5.2.1 Abstract

In clonal systems, interpreting driver genes in terms of molecular networks helps understanding how these drivers elicit an adaptive phenotype. Obtaining such a network-based understanding depends on the correct identification of driver genes. In clonal systems, independent evolved lines can acquire a similar adaptive phenotype by affecting the same molecular pathways, a phenomenon referred to as parallelism at the molecular pathway level. This implies that successful driver identification depends on interpreting mutated genes in terms of molecular networks. Driver identification and obtaining a network-based understanding of the adaptive phenotype are thus confounded problems that ideally should be solved simultaneously. In this study, a network-based eQTL method is presented that solves both the driver identification and the network-based interpretation problem. As input the method uses coupled genotype-expression phenotype data (eQTL data) of independently evolved lines with similar adaptive phenotypes and an organism-specific genome-wide interaction network. The search for mutational consistency at pathway level is defined as a subnetwork inference problem, which consists of inferring a subnetwork from the genome-wide interaction network that best connects the genes containing mutations to differentially expressed genes. Based on their connectivity with the differentially expressed genes, mutated genes are prioritized as driver genes. Based on semi-synthetic data and two publicly available data sets, we illustrate the potential of the network-based eQTL method to prioritize driver genes and to gain insights in the molecular mechanisms underlying an adaptive phenotype.

### 5.2.2 Introduction

Because of their short generation times, large population sizes and quasi clonal behavior, experimental evolution of micro-organisms offers great potential for trait selection and testing evolutionary theory [204, 205]. Evolution experiments start from a single clone propagated for many generations under a predefined conditional set up, defined as the selection regime. As the organisms propagate they gradually accumulate genetic variation (SNPs, INDELs, etc.). Some of this variation will cause a clonal fitness increase and a concomitant selective sweep, which ultimately increases population fitness. The acquired genetic variation can be identified in the evolved lines of the population through sequencing. Genes containing mutations that are fixed in the population, that reach a high frequency in the population, or of which the origin coincides with an increase in fitness [135, 136, 206] are pinpointed as likely drivers, where a driver in this context is defined as any gene carrying adaptive mutations, that in isolation or in combination with other drivers can elict a fitness increase and concomittant clonal expansion. In most evolution studies however, a mechanistic understanding of how the selected driver mutations elicit the adaptive phenotype is still lacking. Such a mechanistic interpretation depends on correctly identifying and interpreting driver genes in terms of the genome-wide interaction network of the organism of interest in order to find the molecular pathways that drive the observed adaptive phenotype. The identification of the driver genes is in itself not trivial because during a selection sweep, passenger mutations, i.e. mutations that do not contribute to the phenotype, are likely to hitchhike to fixation along with driver mutations [150]. Furthermore, because under strong selection pressures hyper mutators frequently arise [153, 207], the ratio of driver genes to passenger genes can become low, further complicating the identification of driver genes. To identify driver genes, one can exploit parallelism of mutations at the gene/nucleotide level. Genes observed to be recurrently mutated in independently evolved lines with a similar phenotype are more likely to be drivers [41, 136]. However, independently evolved lines can also acquire similar adaptive phenotypes by mutations in different genes that affect the same molecular pathways [41, 135, 136], rather than by sharing exactly the same mutations or mutated genes. Identifying driver genes underlying an observed phenotype thus requires identifying mutational parallelism between independently evolved lines at the molecular pathway level [208–211]. In other words, driver gene identification and acquiring a network-based understanding of the adaptive phenotype are confounded problems that have to be solved simultaneously. In this study, we illustrate how a network-based method in combination with coupled genotype-expression phenotype data (eQTL data) of parallel evolved lines can aid in simultaneously prioritizing driver genes and providing a network-based interpretation of the molecular mechanisms underlying the evolved adaptive traits. To this purpose the network-based eQTL method uses an organism-specific genome-wide interaction network, compiled from publicly available interactomics data [60, 61] to drive the search for mutational consistency at the pathway level. By generating a semi-synthetic experimental evolution benchmark, the ability of the method to prioritize driver genes is demonstrated. To illustrate the performance of both driver gene prioritization and network-based interpretation of the data in a real setting, the method is applied to eQTL data obtained from two previously described evolution experiments in Escherichia coli. The first data set aims at identifying the adaptive pathways that gave rise to improved Amikacin resistance in four independently evolved lines [201]. The second data set focuses on unveiling the molecular interactions between two distinct ecotypes that evolved from a common ancestor in the long term evolution experiment of Lenski et al. [212]. For both data sets the method prioritizes driver genes that contribute to the adaptive phenotypes and unveils their molecular modes of action.

### 5.2.3 Materials and Methods

#### 5.2.3.1 Network-based eQTL method

The eQTL analysis method is based on the probabilistic logical querying language ProbLog [213]. To simultaneously prioritize driver genes and unveil adaptive molecular pathways, elicited by these driver mutations, the driver gene identification problem is reformulated as a decision theoretic subnetwork inference problem [161] over multiple probabilistic networks $Q_i$, derived from the genome-wide interaction network $G$. The method consists of three steps (**Figure 5.1**):

#### 5.2.3.2 Construction of probabilistic networks

For each of the parallel evolved lines i of an evolution experiment, the genome-wide directed interaction network $G$ is converted into a probabilistic network $Q_i$ by assigning to each edge a weight that reflects the probability the edge is playing a role under the assessed condition, given the differential expression data as depicted in **Figure 5.1 A**. To this end, per node the probability is calculated that an expression value at least as extreme as the one associated with that node would be observed by chance, given the null hypothesis that the expression value of the gene which corresponds to the node is not significantly differentially expressed, is true. Calculation is performed using a two-tailed p-test assuming that the log2 fold changes follow a normal distribution $N(\mu,\sigma)$ [214,215]. By standardizing this distribution to N(0,1) this probability can be calculated for any differential expression value $D_{gene}$ using **Equation 5.1** in which $Z_{gene}$ corresponds to the standard score associated with $\mathrm{D_{gene}}$.

$$P_{gene} = \begin{cases} P(X > Z_{gene}) + P(X < -Z_{gene})\ if\ Z_{gene} > 0 \\ P(X < Z_{gene}) + P(X > -Z_{gene})\ if\ Z_{gene} < 0 \end{cases} GivenN(0,1) \tag{5.1}$$

As in the network-based eQTL method the edges, not the nodes, are weighted, the value $P_{gene}$ is propagated to the edges that terminate in it. A high value for the probability that a specific edge is involved in a specific experimental condition is assigned to edges that terminate in highly differentially expressed genes.

Therefore, *1-*$P_{end\,gene}$ will be assigned to all edges. Using the cumulative normal distribution of $N(\mu,\sigma)$ which is written as $\phi(\mu,\sigma)$, this can be simplified as shown in **Equation 5.2**.

$$P_{edge} = (|0.5 - \phi_{(\mu,\sigma)} * (D_{end_gene})|) * 2 \tag{5.2}$$

Where $D_{end\,gene}$ is the differential expression data of the end gene of the interaction. If no differential expression data is available for $D_{end\,gene}$, $P_{edge}$ is set to 0.5.

#### 5.2.3.3 Pathfinding in probabilistic networks

Each probabilistic network $Q_i$ allows for determining the probability of connectedness between a gene $C_{i,j}$, from a set of genes $C_i$, and a gene set $A_i$, defined as $P(path(C_{i,j},A_i)|Q_i)$. This probability of connectedness expresses how likely it is that there exists a path that connects the gene $C_{i,j}$ to any gene in the gene set $A_i$, in the probabilistic network $Q_i$. A path between two nodes is a sequence of consecutive edges from the genome-wide interaction network that connects these two nodes and for which all edges are directed in the same direction. The probability of such a path is simply the product of the probabilities of the edges it contains. In the proposed eQTL setting each gene $C_{i,j}$ is defined as significantly differentially expressed in evolved line i and gene set $A_i$ is the set of mutated genes obtained from evolved line *i*. A path connects a significantly differentially expressed gene to genes mutated in the same evolved line. The rationale behind this is that the significantly differentially expressed genes are effects of mutations and thus connect to the "causal" mutations through the probabilistic network. The probability of connectedness $P(path(C_{i,j},A_i)|Q_i)$ represents the probability with which the differential expression of $C_{i,j}$ can be induced by the set of mutations, given the probabilistic interaction network $Q_i$ and quantifies which mutations are most likely to cause the differential expression of $C_{i,j}$.

#### 5.2.3.4 Inference of the optimal subnetwork by combining the data from all evolved lines

Identifying driver mutations from a set of independent end points with the same phenotype corresponds to inferring a single subnetwork $K_{optimal}$ over all independent end points that best connects the significantly differentially expressed genes $C_{i,j}$ and the set of mutations $A_i$ for all end points together as depicted in **Figure 5.1 C**. A subnetwork $K$ of a network $G$ is defined as a subset of the edges in $G$ together with the nodes occurring in the selected edges. Note that a subnetwork in this context can thus consist of any number of disconnected parts of the original network *G*. For each subnetwork *K* from *G* the probability of connectedness changes to $P(path(C_{i,j},A_i\ )|Q_i,K)$ as paths that are valid in $Q_i$ are not necessarily valid in a subnetwork *K*. Therefore, the probability of connectedness changes to $P(path(C_{i,j},A_i)|Q_i,K)$ when working with subnetworks *K*, denoting that the edges along the path have to be present in both $Q_i$ and *K*. Each subnetwork *K* should be scored based on the sum of probabilities that there exists a path between each significantly differentially expressed gene $C_{i,j}$ in $C_i$ and the list of mutated genes $A_i$, for each independently evolved line *i*, out of a total of n independently evolved lines as described in **Equation 5.3**. Between different end points it is expected that the same adaptive pathways are triggered (parallel evolution). Also, within every end point separately, multiple paths are expected to be found in regions with many significantly differentially expressed genes that are likely to be important for the phenotype. Therefore, paths between driver genes selected from different end points and their respective sets of differentially expressed genes should overlap in the optimal subnetwork. By restricting the size of the network through a cost based on the number of edges $|K|$ in the subnetwork the method will preferentially select these overlapping paths. This edge cost can be modulated using the cost factor $x_e$. $K_{optimal}$ is defined as the subnetwork that has the maximum possible value of the score function *S(K)*:

$$S(K) = \sum_{i}^{n}(\sum_{j}^{l}(P(path(C_{i,j},A_i)|Q_i,K))) - |K| * x_e \tag{5.3}$$

Computing the probability that there exists a path between two nodes in a probabilistic network is known as the two-terminal reliability problem, which is NP-hard. This explains why there is no known efficient exact inference algorithm and why we employ an approximation algorithm to compute $P(path(C_{i,j},A_i)|Q_i)$. This probability is approximated by using only the *N* most likely paths of maximal length *l* between the differentially expressed gene $C_{i,j}$ and any mutated gene of $A_i$ [162,213]. The resulting paths (for all $C_i$) are then represented as a Boolean formula (as in probabilistic logic programming languages [213]): each path corresponds to a conjunction of the edges that are present in the path, and a set of such paths corresponds to the disjunction of the conjunctions corresponding to these paths. This formula is then compiled into an equivalent deterministic Decomposable Negation Normal Form (d-DNNF) using knowledge compilation techniques [216]. The advantage of the d-DNNF is that it contains the same information as the original set of paths and that it can efficiently be evaluated in polynomial time for each subnetwork *K* [217]. Selecting such a subnetwork K corresponds to setting all edges not in *K* to false when evaluating the d-DNNFs. The optimal subnetwork $\mathrm{K}_{\mathrm{optimal}}$ is determined by sampling different subnetworks *K* from *G* by performing a random-restart hill climbing optimization as outlined in [161]. Note that, as $K_{optimal}$ is a subset of *G*, $K_{optimal}$ is not necessarily connected.

#### 5.2.3.5 Driver gene prioritization

Because subnetworks obtained using a higher edge are more enriched in driver genes than subnetworks obtained using a low edge cost (higher PPV, more stringent conditions) and subnetworks detected at high edge costs are in general contained within the ones retrieved at lower edge costs, mutated genes are prioritized based on the highest edge cost for which they are still selected (i.e. ranks of mutated genes are based on the most stringent condition under which they are still selected). The reason for this is that mutated genes that are detected at the highest edge cost (most stringent parameter) represent the most pronounced signals in the data. Mutated genes that represent weaker signals (mutations that explain less of the expression data) are only retrieved at less stringent edge parameter costs. To this end, for each data set multiple optimal subnetworks are inferred using a gradually decreasing edge cost, i.e. a parameter sweep over the edge cost. Mutated genes that are retrieved using a high edge cost are strongly connected to the expression phenotype and thus receive the lowest (best) rank. Note that this prioritization strategy can result in assigning identical ranks to different mutated genes. These prioritized mutated genes, together with the inferred subnetworks are visualized by depicting the union of all edges and nodes present in the different inferred subnetworks.

#### 5.2.3.6 Parameter settings

To infer subnetworks the maximum length of a path is set to four edges based on both biological [218, 219] and computational considerations. To approximate the probability of connectedness $P(path(C_{i,j},A_i|Q_i,K)$ the 20-best paths were used that connect each differentially expressed gene $C_{i,j}$ to the set of mutated genes $A_i$. The edge cost parameter determines the size of the inferred subnetwork and forces the selection of overlapping paths. The behavior of the edge cost is characterized on a semi-synthetic data set as indicated in the result section. As described in the driver gene prioritization paragraph, a parameter sweep of the edge cost was performed in order to prioritize the mutated genes. As lower edge costs do not affect ranks of genes prioritized at higher edge costs, the choice of the lower bound on the edge cost does not interfere with the results of the highest ranked genes. For convenience and visualization purposes we choose a cut-off on the sweep at a cost that corresponds to finding a network of no more than 120 nodes. Conversely, when setting the conditions too stringent i.e. very high edge cost, subnetworks can no longer be inferred. Therefore, as smallest edge cost we chose the most stringent value at which a subnetwork could be inferred. This resulted in a parameter sweep of the edge cost from 1.75 to 0.25 for the AMK resistance data set and from 0.975 to 0.025 for the co-existence ecotypes data set. The edge cost sweep was performed with a step size of 0.025. Note that the upper limit of the edge cost in the sweep corresponds to the value for which no subnetwork was inferred anymore.

#### 5.2.3.7 Data sets

**Semi-synthetic benchmarking set**

The semi-synthetic benchmark data set was based on data published by Stincone et al. (publicly available from Gene Expression Omnibus under accession number GSE13361) assessing for 27 *E. coli* K-12 MG1655 single gene knock-out strains involved in acid resistance, the expression profiles relative to a wild type *E. coli* K-12 MG1655 [220]. Levels of differential expression of single gene knock-out strains (27 strains) with respect to the reference were obtained from COLOMBOS [221]. As no repeats were available for the different experiments, and thus no relevant p-values were available, significantly differentially expressed genes were determined as genes having a log2 fold expression change larger than 2. For each KO strain, the knocked out gene was considered a known driver gene and the measured levels of differential expression as the corresponding expression phenotype. Five of those strains, namely *phoH*, *cadB*, *ycaD*, *spy*, *yjbJ* and *grxA*, were discarded for benchmarking, because these genes only have incoming interactions in the genome-wide interaction network or, in the case of *yjbJ*, are not present in the interaction network. In addition the experiment corresponding to the *hns* KO strain was removed as the COLOMBOS database did not contain the appropriate data. For each of the remaining 20 strains the presence of passenger genes was mimicked by randomly selecting a nucleotide position in the reference genome and mapping this position to a gene. Passenger mutations had to obey following conditions: 1) randomly selected genes did not belong to the set of driver genes and 2) they were connected in the genome-wide interaction network with outgoing interactions. The number of passenger mutations assigned to each data set was selected from a binomial distribution with n, the total number of selected mutations, being equal to 9 and p, the chance of adding a passenger mutation, being equal to 0.5. On average this mimics an addition of 5 passenger mutations with a standard deviation of 1.5 for each of the 20 strains in each data set. This way the total number of mutated genes in the semi-synthetic data set is of the same order of magnitude as the number of passenger mutations per driver mutation observed in real data sets [41,201,206].

**AMK resistance data set**

The genomic data for the four amikacin resistant strains was obtained from Suzuki et al [201]. Raw sequencing data was available at the DDBJ Sequence Read Archive under accession number PRJDB2980. Only the Illumina reads were used. The data of the four Amikacin resistant lines was mapped to the ancestral *E. coli* K-12 MDS42 strain using bowtie2 [19]. SNPs and small INDELs were called using freebayes [222] while large INDELs were called using Pindel [20]. This resulted in a total of 59 mutations throughout the four strains. These mutations were mapped to genes as follows: mutations within the coding region of a gene were mapped to the encoded gene, mutations in intergenic regions were mapped to the closest gene if there was a gene within 250 bp of the intergenic region. This resulted in 51 mutated genes. Of these 51 mutated genes, 41 could be mapped to the *E. coli* K-12 MDS42 reference genome. Normalized expression data for each of the four Amikacin resistant strains and the ancestral line was obtained from GEO under accession code GSE59408. Differentially expressed genes were defined as genes having an absolute log2 fold expression change value higher than 2. This cut off value was selected as no repeated measurements were available and thus no p-values could be calculated. Differential expression values were obtained between the Amikacin resistant strains and an ancestral line.

**Coexisting ecotypes data set**

Genomic data was obtained from Plucain et al [212]. Mutations present in both clones of the same ecotype, but not in clones of the other ecotype, were selected as candidate driver mutations that could explain the origin of speciation into the observed coexisting ecotypes. It was hereby assumed that potential driver mutations are likely to be ecotype-specific, as mutations common to all clones most likely originated before divergence of the ecotypes. This resulted in the selection of 87 candidate driver mutations, which could be mapped to 86 potential driver genes. The mapping of mutations to genes was taken from Plucain et al. [212]. Of those 86 genes, 62 genes could be mapped to the *E. coli* B REL606 genome-wide interaction network which were used as input. As expression phenotype we used the degree to which gene expression differed between respectively the L and S ecotype as determined by microarray experiments performed by Le Gac et al. [223] (publicly available from GEO under accession number GSE30639). Microarrays of 6 biological replicates of the L ecotype, 6 biological replicates of the S ecotype and 5 biological replicates of the ancestor were available. Using PCA analysis one microarray of the S ecotype and one microarray of the ancestor were found to be outliers and were discarded from subsequent analyses (**Supplementary Figure S5.1**). The LIMMA package [224] was used to identify the degree of differential expression between the ecotypes. As for this data set repeated measurements for the expression data were available, significantly differentially expressed genes are defined as genes having a p-value of maximum 0.05 and an absolute value of log2 fold change of minimal 0.75. The cut off on the log2 fold change was taken lower than in the other data sets as here we impose an additional cut off on the p-value.

#### 5.2.3.8 Genome-wide interaction networks

In this paper a genome-wide interaction network refers to a comprehensive representation of current interactomics knowledge on the organism of interest. Networks are represented as graphs *G(N,E)* in which nodes *N* correspond to genetic entities (genes, proteins or sRNAs) and edges *E* to the interactions between these entities. Every edge is assigned an edge type, indicating the molecular layer to which the interaction represented by the edge belongs (e.g. protein-DNA, protein-protein, metabolic or signaling interactions). Depending on its type and provided the proper information is available, an edge will be added as a single directed interaction (e.g. protein-DNA interactions, sRNA-DNA, kinase-target, etc.) or two directed interactions (protein-protein interactions, undirected metabolic interactions, etc.).

*Table 5.1:* ***Data sets used to compile the Escherichia coli genome-wide interaction networks.***

| **interaction type** | **E. coli** K12 MG1655 | **E. coli** B REL606 | **E. coli** K12 MDS42[a] |
|---|---|---|---|
| Protein-protein | 2737 | 27282 | 2534 |
| Protein-DNA | 4492 | 3415 | 3890 |
| Sigma | 727 | 1225 | 592 |
| Metabolic | 2798 | 5146 | 2530 |
| (de)Phosphorylation | 44 | 38 | 44 |
| Srna | 213 | 2 | 171 |
| Size (edges) | 11011 | 12554 | 9761 |
| Size (nodes) | 2732 | 2643 | 2422 |

[a] The *E. coli* K12 MDS42 network was derived from the *E. coli* K12 MG1655 network by deleting all edges connecting genes that do not exist in *E. coli* K12 MDS42.

An overview of the genome-wide interaction networks used in this study for the three different *E. coli* strains: *E. coli* K-12 MDS42, *E. coli* B REL606 and *E. coli* K-12 MG1655 is given in **Table 5.1**. To compile these networks metabolic interactions and (de)phosphorylation interactions were derived from KEGG [225] version 72.1, protein-DNA, sigma interactions and sRNA-DNA interactions from RegulonDB version 8.6 [90] and high-confidence physical protein-protein interactions from String [226] version 10. Interactions involving *RpoD*, the primary sigma factor, were removed from these interaction networks as *RpoD* regulates over half of the genes in the interaction network.

### 5.2.4 Results

#### 5.2.4.1 Method overview

A network-based eQTL method was devised to simultaneously prioritize driver genes and unveil molecular pathways involved in the adaptive phenotype. As input the method requires a genome-wide interaction network of the organism of interest and coupled genotype-expression phenotype (eQTL) data for a set of independently evolved lines (strains/populations) with similar phenotypes (**Figure 5.1**). The expression phenotype is defined as the level of differential expression of every gene between an evolved line and a reference. To prioritize driver genes, all genes from the end points carrying allelic variants (hereafter referred to as mutated genes) will be assessed for their ability to explain the adaptive expression phenotype. Hereto the method infers from the genome-wide interaction network the subnetwork that best connects the mutated genes in each of the evolved lines to the set of significantly differentially expressed genes in the corresponding evolved lines, assuming that 1) the expression phenotype is at least partially a consequence of the driver mutations and 2) the adaptive molecular pathways, but not necessarily the driver genes, are to some extent similar, resulting in parallelism at the molecular pathway level.

An overview of the proposed network-based eQTL method is given in **Figure 5.1**. The method consists of three steps (see 5.2.3). In a first step (**Figure 5.1 A**) the genome-wide interaction network is for each evolved line separately converted into a condition-specific probabilistic network using the expression data of the corresponding evolved line. These condition-specific probabilistic networks are subsequently, in a second step (**Figure 5.1 B**), used to find all paths between mutated and significantly differentially expressed genes for each evolved line separately. A path is here defined as a sequence of consecutive edges in the genome-wide interaction network. These paths represent possible molecular mechanisms by which mutations could induce the observed pattern of differential expression. In the third step (**Figure 5.1 C**) all these paths are analyzed together to find the optimal subnetwork, which aims at selecting the subnetwork of the genome-wide interaction network that captures the molecular mechanisms that drive the adaptive phenotype common to all evolved lines. The optimization enforces the selected subnetwork to have two properties. First, it selects the subnetwork that contains the most likely paths that explain the connection between the mutated and differential expressed genes. Second, it enforces the network to contain parallel molecular pathways between the different evolved lines. The optimal subnetwork thus contains the molecular mechanisms likely to drive adaptation. Possible driver mutations which occur in the optimal subnetwork are prioritized based on the strength of their connectivity with downstream effects and their involvement in parallel molecular pathways (see 5.2.3).

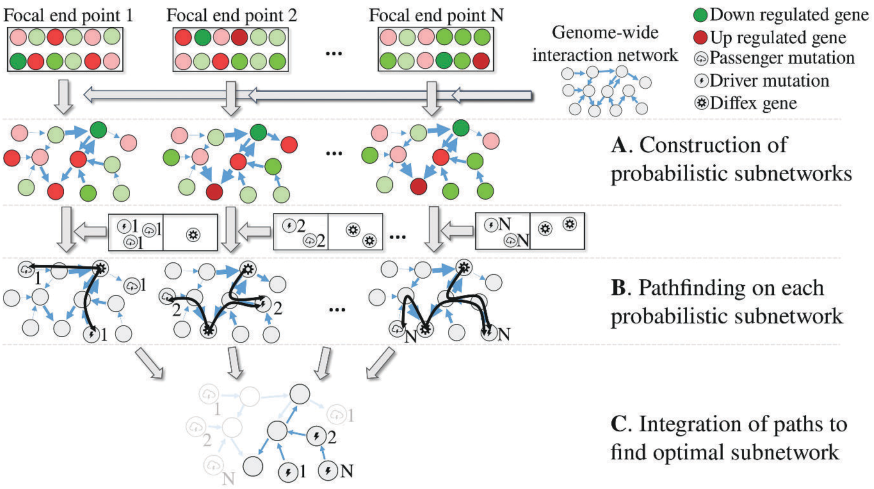
Focal end point 1
Focal end point 2
...
Focal end point N
Genome-wide interaction network
Down regulated gene
Up regulated gene
Passenger mutation
Driver mutation
Diffex gene
A. Construction of probabilistic subnetworks
1
2
N
B. Pathfinding on each probabilistic subnetwork
C. Integration of paths to find optimal subnetwork

*Figure 5.1:* ***Overview of the network-based eQTL method.*** *The input of the method consists of respectively coupled genotype and expression phenotype data for a set of evolved lines with the same phenotype and a genome-wide interaction network. Red and green indicate respectively over- and under expression with respect to a reference. Genes that are considered to be significantly differentially expressed (called diffex genes in the legend of the figure) according to a test statistic, are indicated by a specific symbol as displayed on the figure legend. Mutated driver and passenger genes are indicated with two different symbols as displayed on the legend. The numbering of each mutated gene indicates the evolved line in which this mutated gene occurred.* ***A****. Construction of the end point specific probabilistic subnetworks: for each evolved line the genome-wide interaction network is converted into a probabilistic subnetwork by assigning to each edge in the genome-wide interaction network a weight that is interpreted as the probability that the edge has an influence on the assessed phenotype. These weights depend on the level of differential expression of the terminal node of the edge. Genes that are more differentially expressed (darker red/green) will give rise to higher weights on the edges (indicated by the width of the edge).* ***B****. Pathfinding in each of the probabilistic subnetworks. The mutated and significantly differentially expressed genes occurring in each of the evolved lines are mapped to the corresponding end point specific probabilistic subnetworks. For each significantly differentially expressed gene all possible paths from this gene to all mutated genes in the same end point are searched for (paths are shown as black curves).* ***C****. Optimal subnetwork selection. Optimization is performed by integrating the paths found in all end point specific probabilistic networks according to a predefined cost function that positively scores the addition of paths connecting pairs of mutated genes-differentially expressed genes observed in any of the end points, but that penalizes the addition of edges. As a result, paths that are strongly connected to the expression phenotype and that overlap with each other are selected as the optimal subnetwork.*

#### 5.2.4.2 Performance of network-based eQTL method on a semi-synthetic data set

To assess the performance of prioritizing causal mutations by the network-based eQTL method, a semi-synthetic benchmark data set was constructed based on a previously published knock-out expression profiling experiment. This study assesses differential expression profiles between 20 knock-out strains with altered fitness in acidic conditions and the wild type *E. coli* K12 strain. To mimic the eQTL set up, each of the knocked out genes was considered a ”driver gene” and the presence of passenger genes was simulated by adding a number of randomly selected genes to each knock-out data set (see 5.2.3). Differential expression profiles between each knock-out strain and the wild type were derived from the original publication data (see 5.2.3). The performance of the network-based eQTL method was measured in terms of correctly distinguishing driver from passenger genes.

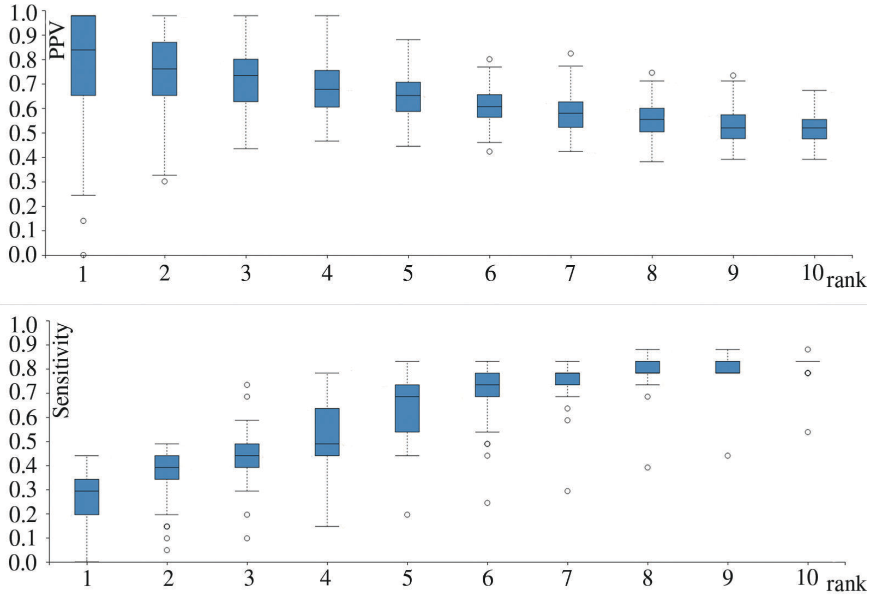

*Figure 5.2:* ***Performance assessment of the network-based eQTL method on the semi-synthetic data set based on data from 100 randomizations.*** *Data of all selected mutated genes at specific ranks are presented as Tukey boxplots. Note that multiple mutated genes can have identical ranks as ranks are assigned based on the maximal edge cost for which a mutation is present within the subnetwork and thus multiple mutated genes can have identical maximal edge costs for which they are present within the subnetwork. The upper plot shows the positive predictive value (PPV, fraction of the selected mutations which are true positives, i.e. driver mutations) in terms of the ranks of the selected mutations. It can be seen that low ranks have higher PPV values. Note that at rank 1 the variance is high. This is because inferred subnetworks for rank 1 are small, and therefore more prone to random effects. i.e. the selection of one additional false positive in a particular random set largely affects the PPV. Solutions are clearly less variable from rank 2 onwards. The lower plot shows the sensitivity (fraction of all possible true positives selected) in terms of the ranks of the selected mutations. Sensitivity increases with rank, implying a trade-off between PPV and sensitivity.*

The main parameter of the method is the edge cost, i.e. the cost for selecting an edge in the inferred subnetwork (see 5.2.3). As a lower amount of mutated genes will be selected using a higher edge cost, mutated genes can be prioritized by the maximum edge cost for which they are selected. This allows assigning a rank for every selected mutated gene based on the maximum edge cost. This prioritization is motivated by the fact that mutations which are selected at high edge costs need to be better connected to the expression and/or have a higher degree of parallelism with other mutations than mutations which are selected at lower edge costs. This reasoning was tested by analyzing the semi-synthetic data set for a wide range of edge costs (see 5.2.3 for specific parameter settings). As can be seen in **Figure 5.2**, the positive predictive value (PPV) is high for low ranks and decreases for higher ranks, meaning mutated genes having low ranks are likely to be driver genes. Furthermore the sensitivity clearly increases with increasing rank, leading to a trade-off between selecting few passenger mutations and selecting many driver mutations. Even for high ranks, results are still better than a random selection of genes as this would correspond to a PPV of 0.2 (on average for every driver gene, 4 passenger genes were added).

#### 5.2.4.3 Unveiling the molecular mechanisms underlying Amikacin resistance

We applied the eQTL analysis on the eQTL data set from the study of Suzuki et al. [201]. In this study four independent *E. coli* MDS 42 lines were grown in the presence of the aminoglycoside antibiotic until all four strains attained increased Amikacin resistance compared to the parental strains. The network-based eQTL method was applied using the genome-wide interaction network of *E. coli* MDS 42 and the data of the 4 parallel evolved strains (see 5.2.3). Out of 41 mutated genes, we prioritized 12 as potential drivers based on their association with the expression data (**Table 5.2**). The inferred adaptive pathways containing those prioritized genes are visualized in **Figure 5.3**.

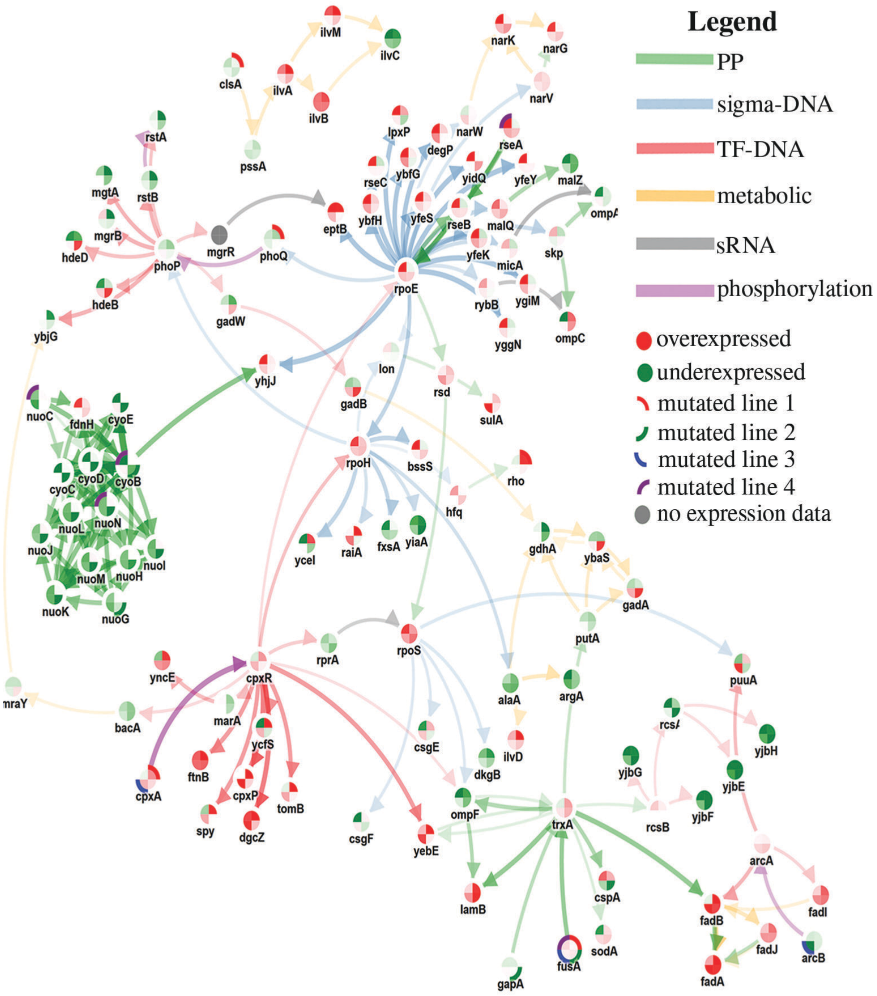

*Figure 5.3: **Visualization of subnetworks inferred from the Amikacin resistance data set.** The visualization was created by merging separate inferred subnetworks resulting from a parameter sweep of the edge cost from 0.25 to 1.75. The width of an edge displays the stringency at with the edge was selected (the wider the edge the more stringent the condition. More Stringent conditions correspond to higher edge costs). Node borders are subdivided into four parts in order to visualize in which line a mutation occurred (evolved lines compared to ancestral line). The inner color of the nodes is also subdivided into four parts where each part represents the degree of differential expression in the corresponding line. Overexpression means that the gene was expressed more in the evolved strain as compared to the ancestral strain. The colors of the edges represent the edge types.*

One very plausible driver mutation is *fusA*, encoding the elongation factor G which is consistently carrying a missense mutation in all 4 strains (mutational consistency at gene level). Mutations in the *fusA* ortholog have previously been found to confer aminoglycoside resistance in *Staphylococcus aureus* [227]. Prioritized genes that are also plausible candidate drivers are those that are consistently mutated at pathway level. Examples of those are the highly prioritized genes *cyoB*, *nuoG*, *nuoN* and *nuoC*, affected in lines 2 and/or 4 by nonsense or frameshift mutations. These genes are members of the electron transport chain which are known to down regulate the protein complexes to which they belong (NADH dehydrogenase or terminal oxidase, see **Supplementary Figure S5.2**) implying an involvement of the electron transport chain in the adaptive phenotype. *cpxA* is another likely driver as it shows mutational consistency at gene level in two lines (lines 1 and 3). *cpxA* is a sensor kinase that is known to regulate the *cpx* response in conjunction with the transcription factor *cpxR*. The mutations in *cpxA* seem to result in lines 1 and 3 in an activation of the *cpx* response with the targets of *cpxR* being overexpressed compared to the ancestral strain. This increased *cpx* response has previously been found to have an effect on the electron transfer chain [228]. These results are consistent with what is described in the original paper of Suzuki et al. [201] and are in line with the knowledge that Amikacin uptake is dependent on proton-motive force [229]. Our results confirm these previous findings although the different lines seem to be triggered through two different molecular systems, either by directly affecting the electron transfer chain or through mutations in *cpxA*. In addition to genes associated with the proton motive force, the method prioritizes additional genes, such as *rseA* explain a large part of the expression phenotype and therefore receive a high rank. However, as a mutation in the anti-sigma factor which inhibits *rpoE* leads to large effects on the expression phenotype and other independently evolved lines do not show effects in molecular pathways associated with *rseA* or *rpoE*, we would need more data to completely rule out the *rseA* mutation in line 4 being a false positive.

#### 5.2.4.4 Unveiling the molecular mechanisms of coexisting ecotypes in glucose-limited minimal medium

A second test case consisted of transcriptomics data and genomics data, described respectively by Plucain et al. [212] and Le Gac et al. [223]. These data sets provide the molecular characterization at generation 6500 of *Ara-2*, one of the 12 populations that were evolved in the *E. coli* long term evolution experiment in glucose minimal medium [36, 143]. By this time the ancestral line had diverged into two distinct, stable ecotypes [223]. Associated studies by Rozen et al. [230–232] showed that the L ecotype grows faster on glucose, but secretes byproducts that S can exploit, implying a cross-feeding mechanism between the L and S ecotypes that can explain their stable coexistence. Plucain et al. experimentally identified a minimal set of mutations. Two S-specific mutations in respectively *arcA* and *gntR* and one in *spoT*, shared by both the L and S strains that when reintroduced together in the ancestral strain were sufficient to mimic the evolved S ecotype in invading and stably coexisting with the L ecotype. However, the fitness level of this reconstructed S ecotype was lower than the fitness level of the evolved S ecotype [212], suggesting that additional mutations play a role in establishing the phenotype of the evolved S ecotype. Both the L and S ecotypes are hyper mutators and have accumulated a large number of mutations. Such setting complicates the identification of the correct driver genes. By applying the network-based eQTL method on this coupled genomics-transcriptomics (eQTL) data [212,223] (see 5.2.3), we tested to what extent we could successfully prioritize the known important driver genes in a data-driven way and could identify missing drivers explaining the adaptive phenotype. The network-based eQTL method resulted in prioritizing 11 mutated genes out of 62 identified mutated genes (**Table 5.2**, **Figure 5.4**).

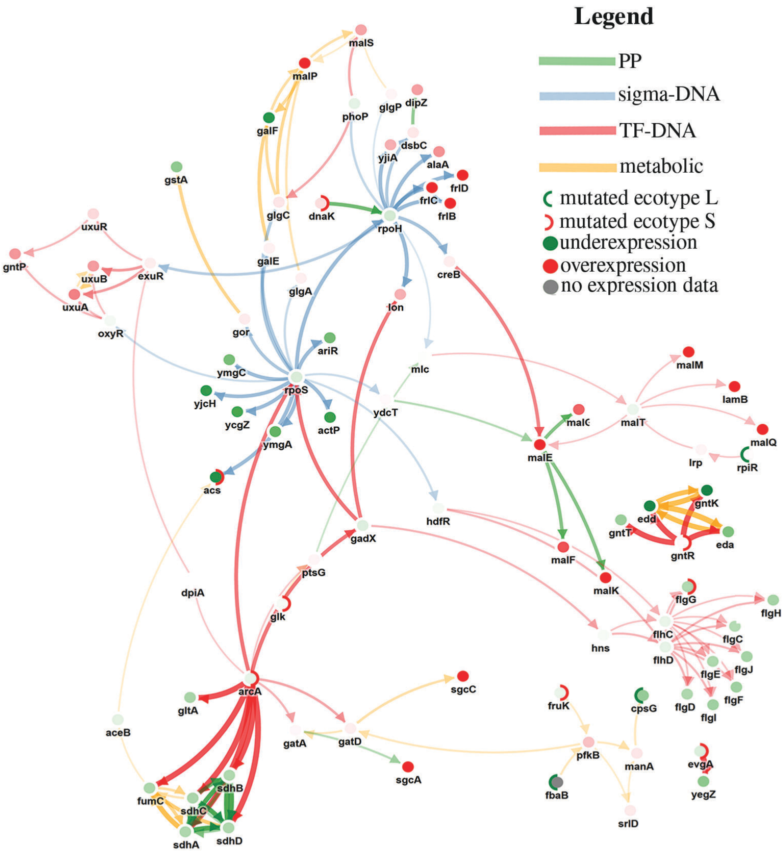

*Figure 5.4:* ***Visualization of subnetworks inferred from the coexisting ecotypes data set.*** *The visualization was created by merging separately inferred subnetworks resulting from a parameter sweep of the edge cost from 0.025 to 0.975. The width of the edges represents the maximal mutation cost for which these edges were selected. The width of the edge displays the stringency at with the edge was selected (the wider the edge the more stringent the condition. More Stringent conditions correspond to higher edge costs). Node borders are subdivided into two parts in order to visualize in which strain a mutation occurred. The inner color of the nodes represents the degree of differential expression (L ecotype compared to S ecotype thus overexpression means that there was more expression in the L ecotype). The colors of the edges represent the edge types.*

Given the available data, we could only focus on identifying drivers that originated after the divergence between both ecotypes. Using this input data we were able to successfully prioritize the driver genes originally identified by Plucain et al., which are *arcA* and *gntR*, but not *spoT* as this mutation was present before the divergence of the two ecotypes. The selected subnetwork (**Figure 5.4**) shows that, consistent with the prioritized mutations in *arcA* and *gntR*, the TCA cycle and the Entner-Doudoroff pathway are up-regulated in S as compared to L. (**Supplementary Figure S5.3** and **Supplementary Figure S5.4**). **Figure 5.4** shows how the S-specific mutation in *gntR* is responsible for the observed up regulation of the Entner-Doudoroff pathway (*gntT*, *gntK*, *edd*, *eda*). As *gntT* is a gluconate transmembrane transporter protein, the inferred subnetwork provides an explanation of one of the previously described mechanisms of the cross-feeding phenotype [231] in which the gluconate released by the L ecotype is metabolized by the S ecotype. The S-specific mutation in the *arcA* gene relates to the S-specific up regulation of the TCA cycle (*gltA*, *fumC*, *sdhC*, *sdhD*, *sdhA*, *sdhB*). *ArcA* was previously found to be repetitively mutated in strains of fast switching phenotypes [233], meaning that the S ecotype could have a fast switching phenotype.Besides the already previously prioritized adaptive alleles, the method could prioritize several additional mutated genes. *acs*, carrying an S-specific mutation in a cis binding site element known to promote *acs* expression [234] was prioritized. Consistently, the network shows how *acs* is highly up-regulated in the S-strain as compared to the L strain. *acs* is an extracellular acetate scavenger involved in the conversion of acetate to acetyl coenzyme which implies that, in addition to gluconate, acetate might also be (partly) responsible for the cross feeding phenotype between L and S. Acetate consumption has previously been linked to the origin of cross-feeding phenotypes in experimental evolution [150, 206]. Interestingly an intergenic mutation associated to *dnaK* in the S ecotype appears highly prioritized (**Table 5.2**). Overexpression of the gene *dnaK*, a heat shock chaperone, has previously been found to mitigate the effect of deleterious mutations in hyper mutators [235]. Although in our network this mutation does not lead to significantly higher expression levels of *dnaK*, the mutation could indirectly interfere with e.g. the stability of the mRNA and as such affect protein expression [236], hereby protecting both hyper mutator strains. For the S ecotype the molecular mechanism involved in triggering the coexistence phenotype are clear, the mechanism of the L ecotype in the coexistence phenotype is, given the available data, less obvious. However, the *uxuA* and *uxuB* genes are more pronouncedly expressed in the L strain than in the S strain. Both genes are involved in catalyzing the reaction of D-fructuronate to 2-dehydro-3-deoxy-D-gluconate, which could play an important role in gluconate cross-feeding.

*Table 5.2:* ***Selected mutated genes prioritized as driver genes.***

| AMK resistance | | | | Coexisting ecotypes | | | |
|---|---|---|---|---|---|---|---|
| **Gene name** | **rank$^a$** | **Line** | **type** | **Gene name** | **rank$^a$** | **Line** | **type** |
| CyoB | 1 | 2,4 | frameshift | gntR | 1 | S | missense |
| CpxA | 2 | 1,3 | missense | arcA | 1 | S | missense |
| NuoG | 3 | 2 | nonsense | evgA | 1 | S | missense |
| rseA | 3 | 4 | nonsense | dnaK | 2 | S | intergenic |
| nuoN | 3 | 4 | In-frame del | acs | 3 | S | intergenic |
| nuoC | 4 | 4 | missense | flgG | 4 | S | synonymous |
| fusA | 5 | 1,2,3,4 | missense | fbaB | 5 | L | missense |
| phoQ | 6 | 1 | missense | cpsG | 5 | L | Large del |
| arcB | 7 | 3 | Frameshift del | fruK | 6 | S | missense |
| gapA | 8 | 2 | missense | rpiR | 7 | L | intergenic |
| ClsA | 9 | 1 | missense | glk | 7 | S | intergenic |
| rho | 10 | 1 | missense | | | | |

### 5.2.5 Discussion

Here we present a network-based eQTL method that exploits parallelism between independently evolved lines to search for mutational consistency at the molecular pathway level. Because the method searches for parallel molecular pathways between the different evolved lines, these identified driver mutations are likely to be adaptive. In the context of this paper this adaptive effect is different from directly affecting fitness as some of the adaptive mutations will elicit their effect on the phenotype only in the presence of additional adaptive mutations (epistasis). Key to the method is the use of the interaction network to guide the search. The method belongs to the class of subnetwork selection methods that have been used to interpret differential expression data on networks [110,237,238], for gene prioritization [239] or for linking KO genes or genes from a genetic screen to an expression phenotype [118, 240], but that have not yet been used to solve the combined problem of searching for molecular pathway consistency in independently evolved clones and driver gene identification. Several recent studies in cancer have shown how searching for mutational consistency at pathway level between independently evolved samples can aid in prioritizing drivers. These methods use genomic information as input and identify driver genes as genes carrying somatic mutations that are frequently mutated in different tumor samples and/or that are in each others neighborhood in a human genome-wide interaction network [123,241–243] and/or that display patterns of mutual exclusivity over different tumor samples [244,245]. All of the abovementioned techniques rely mainly on genomic information and are applicable only when large numbers of independent samples are available (in a cancer setting often at least 1000 tumor samples are available [55]. This in contrast to evolution experiments in micro-organisms which contain too few independently evolved samples (clones) to directly apply the abovementioned data-driven methods that mainly rely on genotype data. Therefore, we combine molecular profiling data (expression data) with genomic data to increase the signal of mutational consistency at the molecular pathway level. This compensates partly for the number of evolved samples usually available in studies on microbial clonal systems. Because of the eQTL setting drivers that affect expression are more likely to be identified. Based on the few eQTL studies that have been performed it appears that at least in microbes adaptive mutations often result in a sometimes marginal but significant expression response compared to their (immediate) ancestor [246, 247]. Furthermore, In contrast to the statistical and diffusion based methods used in cancer research, we have developed a method that can more explicitly exploit prior information to drive the search for drivers. To that end our method relies on a probabilistic subnetwork selection technique that in a first pathfinding step uses an explicit path definition to find paths in a weighted (by expression data) and annotated probabilistic subnetwork. This allows integrating prior and/or condition specific data on the biological process of interest to steer the search towards specific parts of the genome-wide interaction network by exploiting the directionality of the network and the properties of the edges to define biologically relevant paths and by assigning prior weights to the edges of the network that are likely to be active under the assessed conditions. The optimization function actively searches for overlap in the selected subnetworks allowing to detect mutational consistency at molecular pathway level, despite even a low number of independently evolved lines. The required overlap between paths can be tuned using the edge cost parameter. Driver mutations exhibit a high degree of mutational consistency at the molecular pathway level. Therefore, using a high edge cost, which forces the selection of subnetworks with a large overlap between paths over the different evolved lines, leads to fewer false positives amongst the identified driver mutations. On the semi-synthetic data set it was illustrated how a sweep on the edge cost parameter can be used to successfully prioritize the most likely candidate drivers. Using two biological data sets, the potential of applying the method on eQTL data for studying the molecular mechanisms underlying adaptive traits was illustrated. From a large number of potential mutations the method was able to select previously identified driver mutations. In addition to this, potential driver mutations could be identified and verified with literature. The potential of the method to distinguish passengers from driver mutations was also shown on mutator phenotypes, where a large amount of passenger mutations are present but where the method was able to rank the previously identified driver genes as highly likely to be driver genes. It is important to note that even if few mutations are available, it is often not clear which of those are the drivers (as is illustrated in the case of the Amikacin resistance) and which are potentiating mutations. Microbial systems are not guaranteed to display mutational consistency at gene level, solely relying on mutational consistency of the same mutation in independent lines to identify drivers might fail. Because of this, the experimental identification of drivers is tedious as it requires reintroducing all possible individual driver mutations and, in case of complex phenotypes, their possible combinations in the ancestral strain [150]. As illustrated with the biological test cases, the combination of an eQTL setting with the dedicated network-based approach allows to drastically reduce the list of possible driver genes. Using a dedicated network-based analysis to an eQTL data sets is key to better understanding basic concepts of microbial evolution. Experimental evolution has become an important experiment in wet-lab practice to study interesting phenotypes, e.g. the role of epistasis [158, 159, 248, 249] or to understand the degree to which parallelism occurs [41, 135, 158, 206]. Interpreting identified drivers in terms of the molecular interaction network can potentially contribute to a better understanding of why epistasis or parallelism occurs beyond the level of mutational consistency. An illustration of such parallelism was shown in the analysis of the Amikacin dataset, where based on only 4 independently evolved lines, the network method was able to identify two different mechanisms by which strains alter their proton motive force to lower Amikacin uptake. Each of these mechanisms was identified by exploiting parallelism at molecular pathway level. Interestingly both mechanisms, one involving direct mutations in the electron transport chain and one involving mutations in *cpxA*, appeared mutually exclusive i.e. strains had either mutations in their electron transfer chain or in *cpxA* but never simultaneously in both. This shows that the network-based eQTL method is not only able to successfully exploit parallelism, but also allows identifying convergent ways of evolution that lead to the same adaptive phenotype. In this study we presented a network based analysis method that exploits public interactomics knowledge to analyze eQTL data sets. The results of this method provide a simultaneous prioritization of driver mutations and an understanding of the adaptive phenotype at the molecular pathway level. This method exploits the potential of coupled genotype-expression data sets to study experimental evolution and bacterial trait selection in bacteria.

### 5.2.6 Acknowledgements

This work was supported by Ghent University Multidisciplinary Research Partnership Bioinformatics: from nucleotides to networks; Fonds Wetenschappelijk Onderzoek-Vlaanderen [grant numbers G.0329.09, 3G042813, G.0A53.15N]; Agentschap voor Innovatie door Wetenschap en Technologie (IWT) [NEMOA, to D. De Maeyer]; and the Katholieke Universiteit Leuven [grant number PF/10/010] (NATAR).

# Supplementary

## 5.2.7 Supplementary Figures

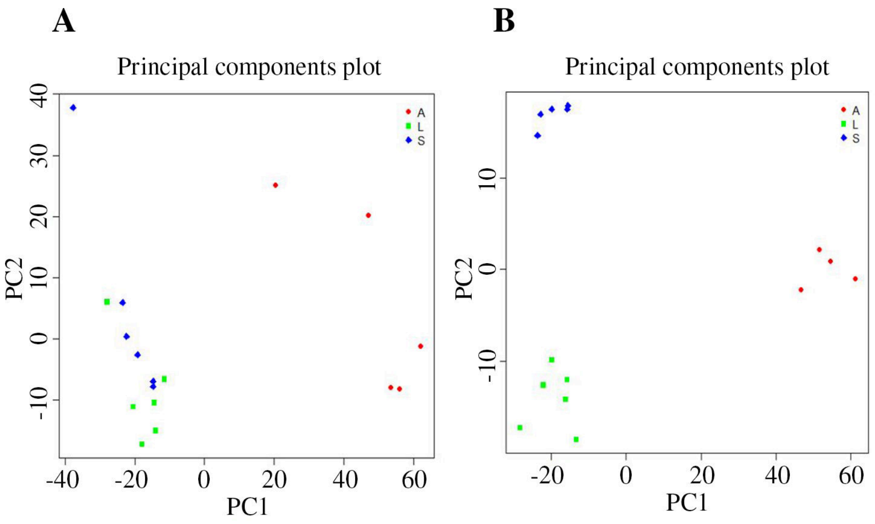

*Figure S5.1:* ***PCA analysis of transcriptomics data of the coexisting ecotypes data set as obtained from Le Gac et al. [223].*** *Genes are treated as variables, strains as observations. Dots of identical shape and color represent replicate cultures. Circular/red dots represent ancestral strains, square/-green dots represent L ecotypes and diamond shaped/blue dots S ecotypes. It is expected that dots of equal shape and color will group together because ideally they should exhibit identical expression levels for each gene.* ***A)*** *PCA plot of the observations on the first two PCs. Except for two outliers (one ancestral and one S ecotype) observations group together according to their label.* ***B)*** *PCA plot of the observations on the first two PCs after removing the outliers from the data set. As can be seen, the observations group together far better according to their label when removing the outliers. To reduce noise on the part of the transcriptomics data, the two microarrays corresponding to the outlier observations were discarded.*

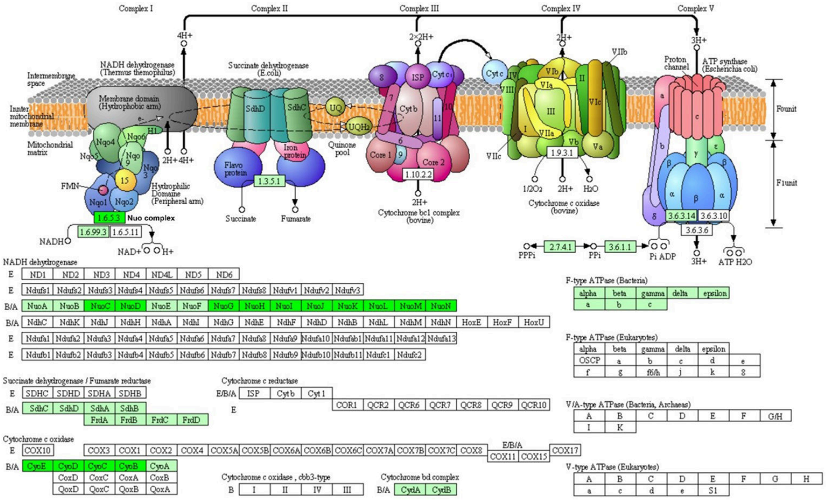
Complex I
Complex II
Complex III
Complex IV
Complex V
Intermembrane space
Inner mitochondrial membrane
Mitochondrial matrix
NADH dehydrogenase (Thermus themophilus)
Membrane domain (Hydrophobic arm)
Hydrophilic Domaine (Peripheral arm)
Nuo complex
Succinate dehydrogenase (E.coli)
Flavo protein
Iron protein
Quinone pool
Succinate
Fumarate
Cytochrome bc1 complex (bovine)
Cytochrome c oxidase (bovine)
Proton channel
ATP synthase (Escherichia coli)
F0 unit
F1 unit
1.6.5.3
1.6.99.3
1.6.5.11
1.3.5.1
1.10.2.2
1.9.3.1
3.6.3.14
3.6.3.10
3.6.3.6
2.7.4.1
3.6.1.1
NADH
NAD+
H+
PPPi
PPi
Pi ADP
ATP H2O
NADH dehydrogenase
E ND1 ND2 ND3 ND4 ND4L ND5 ND6
B/A NuoA NuoB NuoC NuoD NuoE NuoF NuoG NuoH NuoI NuoJ NuoK NuoL NuoM NuoN
B/A NdhC NdhK NdhJ NdhH NdhA NdhI NdhG NdhE NdhF NdhD NdhB NdhL NdhM NdhN HoxE HoxF HoxU
Succinate dehydrogenase / Fumarate reductase
E SDHC SDHD SDHA SDHB
B/A SdhC SdhD SdhA SdhB
FrdA FrdB FrdC FrdD
Cytochrome c reductase
E/B/A ISP Cytb Cyt1
Cytochrome c oxidase
E COX10 COX3 COX1 COX2 COX4 COX5A COX5B COX6A COX6B COX6C COX7A COX7B COX7C COX8 COX11 COX15 COX17
B/A CyoE CyoD CyoC CyoB CyoA
CoxD CoxC CoxA CoxB
QoxD QoxC QoxB QoxA
Cytochrome c oxidase, cbb3-type
Cytochrome bd complex
B/A CydA CydB
F-type ATPase (Bacteria)
alpha beta gamma delta epsilon
a b c
F-type ATPase (Eukaryotes)
V/A-type ATPase (Bacteria, Archaea)
V-type ATPase (Eukaryotes)

*Figure S5.2:* ***Mapping of the inferred subnetwork from all four lines of the Amikacin resistance data set to the oxidative phosphorylation from KEGG pathways.*** *Light green boxes correspond to genes/gene products present in E. coli MDS 42.Green boxes correspond to genes/gene products present in the inferred subnetwork which are down regulated as compared to the ancestral strain. It can be seen that NADH dehydrogenase and cytochrome oxidase complexes are down regulated in the AMK resistant strains.*

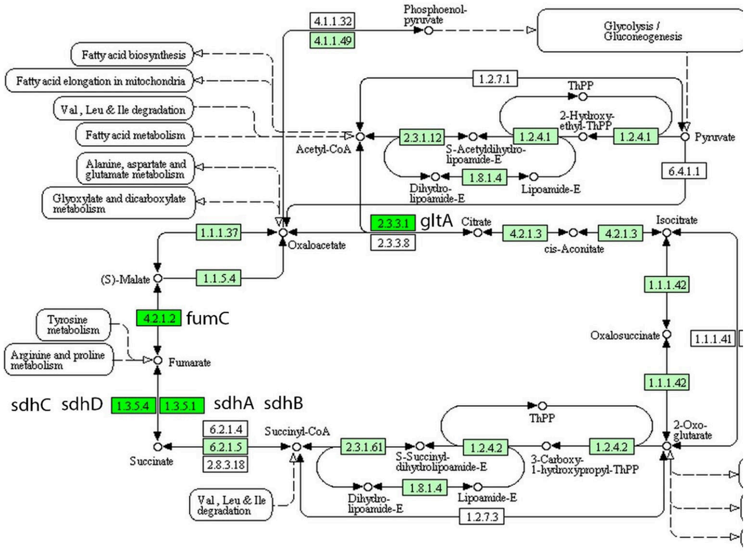

*Figure S5.3:* ***Mapping of the inferred subnetwork from the coexisting ecotypes data set to the TCA cycle from KEGG pathways.*** *Light green boxes correspond to genes/gene products present in E. coli B REL606. Green boxes correspond to genes/gene products present in the inferred subnetwork and up-regulated in the S ecotype as compared to the L ecotype. It can be seen that multiple components of the TCA cycle are up-regulated in the S ecotype as compared to the L ecotype.*

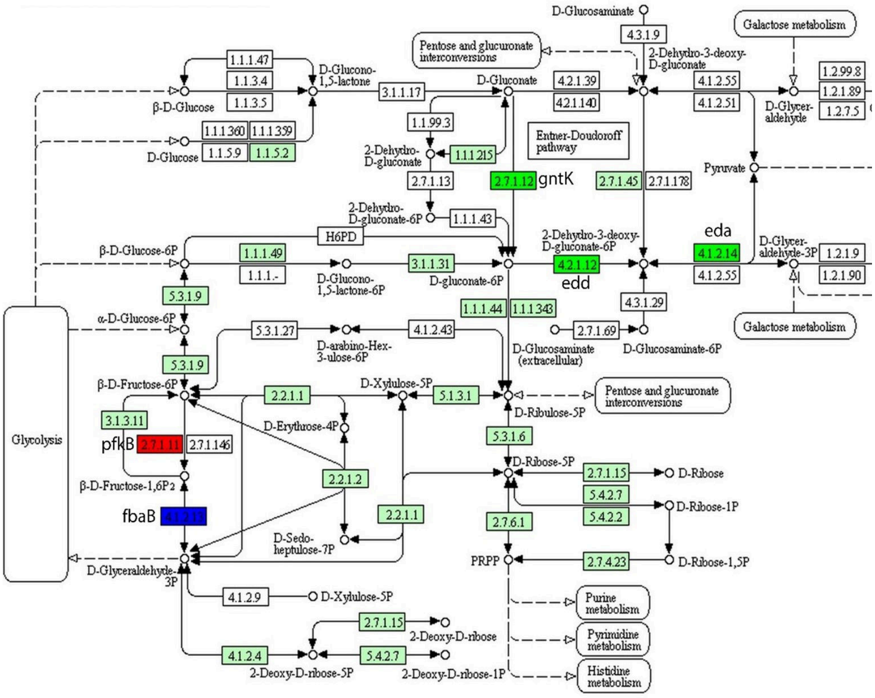

*Figure S5.4:* ***Mapping of the inferred subnetwork from the coexisting ecotypes data set to the pentose phosphate pathway from KEGG pathways.*** *Light green boxes correspond to genes/gene products present in E. coli B REL606. Green boxes correspond to genes/gene products present in the inferred subnetwork and up-regulated in the S ecotype as compared to the L ecotype. Red boxes correspond to genes/gene products present in the inferred subnetwork and overexpressed in the L ecotype as compared the S ecotype. Blue boxes correspond to genes/gene products present in the inferred subnetwork and mutated in the L ecotype. It can be seen that multiple components of the Entner-Doudoroff pathway are up-regulated in the S ecotype as compared to the L ecotype implying S-specific uptake of gluconate.*

# 6 Ranking of driver genes and pathways from genomics data

## 6.1 Introduction

This chapter describes IAMBEE, a network-based method which was specifically designed for use with evolution experiments in which genomics data is available before and after an adaptive sweep. In such an experimental set-up, data on the increase in frequency of every mutation during the adaptive sweep is available. By combining this data with information about the functional effects of each mutation and correcting for possible samples which exhibit a mutation rate which is much higher than the other samples, IAMBEE can prioritize molecular pathways which harbor adaptive mutations. It is shown that IAMBEE can lead to additional insights in the acquisition of a specific trait. For example, in this chapter mutual exclusivity of mutations on the level of molecular pathways was found in an evolution experiment in which *E. coli* was exposed to ethanol.

TS and **BW** conceptualized the study, analyzed and interpreted the results and wrote the manuscript. TS designed and performed the biological experiments, **BW** designed IAMBEE and used it to analyze the sequence data. CB helped in performing the biological experiments. NV, JM and KM conceptualized the study, designed the experiments, discussed the results and edited the manuscript.

## 6.2 Paper

# Network-Based Identification of Adaptive Pathways in Evolved Ethanol-Tolerant Bacterial Populations

Swings, T.[†], **Weytjens, B.**[†], Schalck, T., Bonte, C., Verstraeten, N., Michiels, J.[§] and Marchal, K.[§] (**2017**). Network-based identification of adaptive pathways in evolved ethanol-tolerant bacterial populations. Molecular Biology and Evolution, msx228.

[†] these authors contributed equally to this paper
[§] these authors contributed equally to this paper

### 6.2.1 Abstract

Efficient production of ethanol for use as a renewable fuel requires organisms with a high level of ethanol tolerance. However, this trait is complex and increased tolerance therefore requires mutations in multiple genes and pathways. Here, we use experimental evolution for a system-level analysis of adaptation of *Escherichia coli* to high ethanol stress. As adaptation to extreme stress often results in complex mutational datasets consisting of both causal and non-causal passenger mutations, identifying the true adaptive mutations in these settings is not trivial. Therefore, we developed a novel method named IAMBEE (Identification of Adaptive Mutations in Bacterial Evolution Experiments). IAMBEE exploits the temporal profile of the acquisition of mutations during evolution in combination with the functional implications of each mutation at the protein level. These data are mapped to a genome-wide interaction network to search for adaptive mutations at the level of pathways. The 16 evolved populations in our dataset together harbored 2286 mutated genes with 4470 unique mutations. Analysis by IAMBEE significantly reduced this number and resulted in identification of 90 mutated genes and 345 unique mutations that are most likely to be adaptive. Moreover, IAMBEE not only enabled the identification of previously known pathways involved in ethanol tolerance, but also identified novel systems such as the AcrAB-TolC efflux pump and fatty acids biosynthesis and even allowed to gain insight into the temporal profile of adaptation to ethanol stress. Moreover, this method offers a solid framework for identifying the molecular underpinnings of other complex traits as well.

### 6.2.2 Introduction

Experimental evolution offers great potential to gain insights into the molecular mechanisms that contribute to the acquisition of complex traits [149, 205, 250]. Previously, experimental evolution has been used not only to study the mechanisms underlying clinically [251–253] or industrially relevant phenotypes [254], but also to improve key industrial traits for the production of advanced evolutionary engineered strains [254]. Laboratory evolution experiments usually start from a single clone that is cultivated for prolonged periods of time in predefined conditions. During this period of time, natural selection favors mutations that confer a benefit in the chosen condition leading to improved phenotypes [40]. Fitness is tracked over time and clones displaying increased fitness are genotyped to identify the underlying mutations [255]. While some phenotypes are established by only one or just a few mutations, complex traits often lead to complex mutational profiles, severely complicating identification of the causal adaptive mutations [256].

In this study, we used experimental evolution to study high ethanol tolerance in the bacterium *Escherichia coli*. Usually, microbial ethanol production capacity is severely limited by the toxic effect of ethanol itself. Therefore, higher ethanol tolerance and increased ethanol production are inherently linked [257, 258]. Even though understanding and improving this trait is vital for strain engineering, it has been challenging to fully elucidate the underlying mechanisms. Previous studies have identified single genes [259, 260] as well as epistatically interacting genes [261] involved in higher ethanol tolerance. However, tolerance to ethanol is clearly a complex trait established by the interaction of multiple genes and pathways [259–263] and a broad understanding of ethanol tolerance in *E. coli* is currently lacking. Moreover, in a previous study we found that hypermutation drives evolution under severe stress, such as ethanol stress, to enable adaptation of at least some individuals to avoid extinction [44]. An increased mutation rate was found in all high ethanol tolerant populations and resulted in a higher ratio of passenger versus adaptive mutations, leading to an extremely complex mutational profile. Consequently, this increased complexity impedes the ability to statistically distinguish between true adaptive mutations and passenger mutations.

In most studies, this distinction between adaptive and passenger mutations is based on identifying mutations or mutated genes that recurrently emerge in independent evolutionary lines [139, 264–268]. This narrow definition of parallelism assumes that only frequently mutated genes contribute to an adaptive phenotype. However, in populations that evolve independently, there is no guarantee that exactly the same mutation or even the same mutated gene is responsible for the observed adaptive phenotype. Affecting the same pathway through different and not necessarily frequently mutated genes might equally well induce the same adaptive phenotype [41, 135, 136]. Rather than identifying recurrent mutations, one can search for consistently mutated molecular pathways, assuming that adaptive mutations will hit the same adaptive pathways in independently evolved populations, while passenger mutations will be spread randomly over the genome. Approaches that search for consistent changes in molecular pathways are typically network-based and have been applied successfully, mainly in the context of cancer genomics [8, 124, 269, 270] but not yet for the mapping of genotypes to complex traits in clonal micro-organisms such as bacteria.

To cope with the specificities of clonal evolution experiments that aim to study complex traits, we developed a novel network-based method, IAMBEE. IAMBEE exploits the information gained from the trajectory of individual mutations along the evolution experiment to reduce the complexity of identifying adaptive pathways/genes. Our experimental set-up combined with this unique network-based approach resulted in the identification of several adaptive pathways that conferred ethanol resistance in *E. coli*. The role of the 30S ribosomal subunit pathway [271, 272] as well as the osmotic stress response pathway (*ompR*/*envZ*) [273, 274] were confirmed. In addition, newly predicted molecular mechanisms such as the multidrug efflux pump AcrAB-TolC and the fatty acid biosynthesis pathway were experimentally validated. These results demonstrate the value of IAMBEE to analyze complex mutational datasets including even datasets resulting from a hypermutator phenotype, to obtain a comprehensive overview of the pathways and its specific mutated components involved in the establishment of the trait.

### 6.2.3 Results

### 6.2.4 Ethanol tolerant populations display a hypermutator phenotype

We set up an evolution experiment in which 16 independent *E. coli* populations were experimentally evolved under increasing ethanol concentrations (**Figure 6.1**). Changes in ethanol tolerance due to accumulation of beneficial mutations were tracked in time to obtain a fitness trajectory for each population (**Supplementary Figure S6.1**). These trajectories show remarkable selective sweeps between 5% and 6% ethanol tolerance (further referred to as the initial selective sweep) and from 6% to 6.5% ethanol tolerance (further referred to as the second selective sweep). Populations were sampled right before and right after each increase in ethanol tolerance and were subjected to pooled sequencing. Primary analysis of the data showed that each of the ethanol tolerant populations evolved a hypermutation phenotype. In depth study of this observation led to the conclusion that near-lethal conditions require rapid adaptation of at least some individuals to avoid extinction of the population [44]. Hypermutation considerably facilitates rapid adaptation by increasing the mutational supply rate thereby increasing the probability to acquire a beneficial mutation [44, 249, 275]. While hypermutation enables adaptation, it also leads to complex mutational profiles with multiple mutations in random genes [140], further impeding identification of causal mutations. In our dataset of 16 evolved populations a total of 2286 mutated genes, containing 4470 unique mutations were detected. To identify causal mutation despite this complexity, we developed a method that overcomes the limitations of only identifying recurrent mutations.

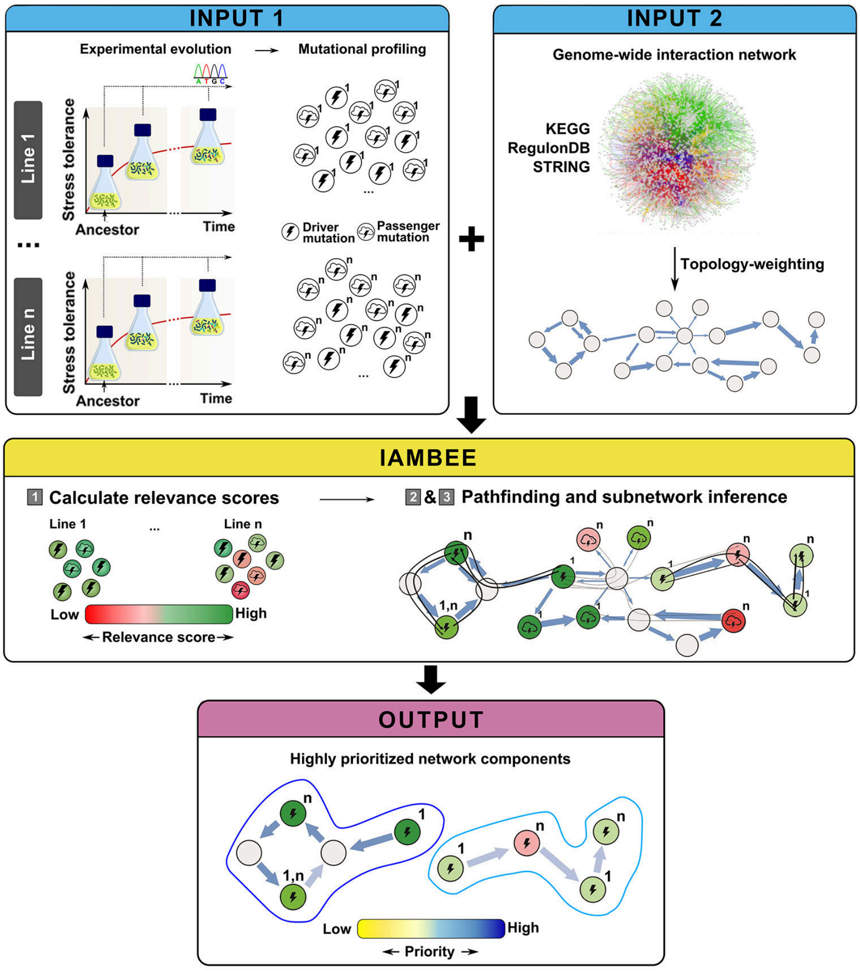

*Figure 6.1:* ***Set-up of the experiment, data acquisition and workflow of adaptive pathway identification.*** *A first input consists of all mutations observed in independently evolved populations before and after a selective sweep. As a second input, an interaction network is used which is topology-weighted in order to account for hubs. This network is constructed using publicly available datasets. Subsequently, IAMBEE maps all mutated genes (input 1) to this topology-weighted interaction network (input 2) and calculates a relevance score for each mutation (green genes have higher and red genes lower relevance scores). The details on the calculation of these relevance scores are shown in* ***Figure 6.2****. The relevance scores of the genes (nodes in the network) as well as the weights of the edges (interactions between genes), which are derived from the topology-weighting, are used to weight the paths (shown as black lines) between mutated genes from different populations found in the pathfinding step. Thick black lines represent paths that contain genes that have a high probability to be involved in the phenotype while thin black lines depict paths with low probability. Finally, a subnetwork inference step takes place which selects a subset of these paths in such a way that as many as possible paths connecting genes with large relevance scores are selected, but which is forced to select a sparse subnetwork as it minimizes the number of edges included. The result is that overlapping paths tend to be chosen and this leads to the selection of recurrently mutated connected subnetwork components. As a final output IAMBEE shows the inferred subnetwork containing highly prioritized network components that represent the identified adaptive pathways underlying the observed phenotype.*

### 6.2.5 Exploiting parallel evolution to identify adaptive pathways

To distinguish between adaptive and passenger mutations and to identify pathways underlying complex traits we have developed IAMBEE, which integrates prior information on gene interactions (i.e. an interaction network) with the specificities of the experimental design. Key to the concept of IAMBEE is the use of multiple independently evolved populations to search for recurrently mutated molecular pathways. This search is driven by the interaction network and based on a decision theoretic subnetwork inference problem [6, 7]. However, given the high mutation rate and the relatively low number of indpedently evolved populations, additional information in the form of functional impact scores of the individual mutations is needed to drive the analysis. We hereby assume a priori that not all mutations are equally likely to be involved in the adaptive phenotype. Mutations that increase in frequency during a selective sweep and/or that have a functional impact on the protein in which they occur, are more likely to be involved in the phenotype. **Figure 6.1** gives a conceptual overview of IAMBEE. The input consists of called mutations from multiple, independently evolved populations and a genome-wide interaction network of the organism of interest. After topology-weighting the interaction network to downweight the effect of hubs on the final solution (see Materials and Methods), IAMBEE proceeds in three steps (**Figure 6.1**): 1) the relevance score is calculated for each mutated gene in each population. The relevance score consists of three components. The first component describes the change in frequency of the mutation during a selective sweep in the population. Mutations that increase in frequency during a selective sweep are more likely to be adaptive than mutations that decrease in frequency. However, not necessarily all adaptive mutations will increase in frequency during a sweep (e.g. potentiating mutations) and conversely passenger mutations that hitchhike with driver mutations will also increase in frequency [144]. Therefore, the frequency change component is complemented with a second component: the functional impact score. The functional impact score reflects the effect of the mutation on the function of the protein. Mutations that are likely to alter a proteins function are more likely to be adaptive. A last component of a mutations relevance score relates to the mutation rate of the population in which the mutation occurs: we assume that mutations that originate from populations with a significantly higher mutation rate than the other populations should contribute relatively less to the final solution as they contain a larger number of passenger mutations (more noise) and a mutation of such a line should thus exhibit a stronger signal in order to be selected. A detailed overview of the calculation of the relevance scores by IAMBEE is shown in **Figure 6.2** and is described in Materials and Methods. 2) The pathfinding step embodies the search for paths, which are defined as consecutive sets of edges connecting mutated genes from different populations, on the topology-weighted interaction network. These paths are weighted based on the relevance scores of the involved mutations and the weights of the edges involved in the path. The weight of a path reflects the degree of belief that the path is involved in the adaptive phenotype. 3) Subnetwork inference (optimization strategy) is subsequently used to select a subset of the paths found during the pathfinding step. This subset is selected such that a maximum number of mutated genes with high relevance scores are included but a minimal number of edges is selected. This means that overlapping paths are more easily selected as they share edges, which reflects the search for molecular pathways that are consistently mutated throughout independently evolved populations. The resulting subset of paths makes up a subnetwork that consists of multiple connected components which are parts of molecular pathways. For a more detailed explanation of these steps, we refer to the methods section.

#### 6.2.5.1 Validation of IAMBEE using synthetic data

To validate and characterize IAMBEE, we generated 100 synthetic datasets, each with randomly selected adaptive and passenger mutations (**Supplementary methods**). Running IAMBEE on one of these datasets with a specific parameter setting resulted in a subnetwork containing prioritized mutated genes. Every synthetic dataset was run with 50 different parameter settings ranging from settings which result in small subnetworks to settings which result in larger subnetworks. As in this synthetic setting the true adaptive mutations (true positives) are known, we used PPV (the ratio of true positives to the total number of prioritized mutations) and sensitivity (the number of true positives to the total number of true positives in the dataset) as performance criteria. Results showed that, as expected for a method that makes relevant non-random predictions, small subnetworks have a high PPV at the expense of a lower sensitivity and subnetworks (of any size) rarely have both low sensitivity and PPV (**Supplementary Figure S6.2**). This indicates that users should start exploring small solutions when identifying candidates for experimental validation while progressing to larger solutions allows gaining a more complete pathway level insight into the adaptive phenotype but risks identifying false positives. This information is also included in the output of IAMBEE where more opaque edges represent edges which are involved in both small and large solutions (high PPV) while less opaque edges are only involved in small solutions (lower PPV) (**Figure 6.3**, **Figure 6.4**).

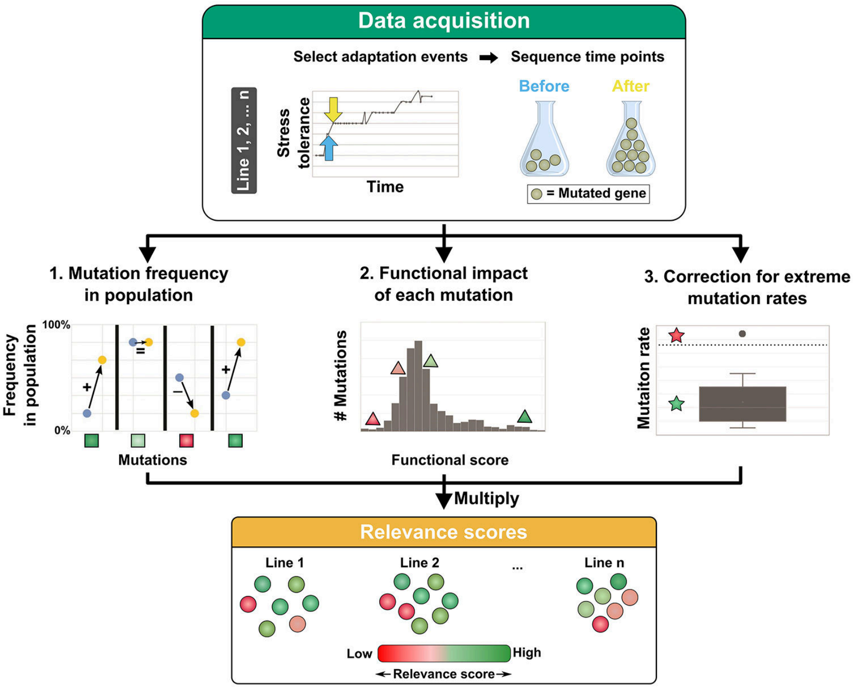

*Figure 6.2:* ***Calculation of the relevance scores for each mutation by IAMBEE.*** *In the data acquisition step, a selective sweep of interest is chosen from an evolution experiment involving multiple parallel evolved populations. Samples taken at time points just before (blue arrows) and just after (orange arrows) this selective sweep are sequenced and mutations are called. For every mutation, a functional impact score and frequency change in the population are determined by the IAMBEE software. The frequency change is derived from the degree to which the mutation changes in frequency before (blue) and after (orange) the selective sweep. Genes with mutations that rise in frequency have higher frequency increase scores (green square) while a low frequency increase score is assigned to genes with mutations that decrease in frequency in the population (red squares). Next, a functional impact score is assigned to each mutation by using SIFT4G ( [276]). Genes with mutations having a high functional impact score are depicted with green triangles and vice versa. In addition, populations with a mutation rate that is significantly higher than the mutation rates of the other populations are detected. The relevance of mutated genes in populations with a significantly higher mutation rate are corrected (red star) to avoid overrepresentation of mutations from these populations. Finally, combining a genes frequency score, functional impact score and the correction for mutation rates allows calculating a relevance score for every mutated gene in every population. Mutated genes with a high relevance score (green circles) are more likely to harbor mutations that increase in frequency during the selective sweep, have high functional impact scores and are not involved in a population with significantly higher mutation rate than the rest of the populations.*

#### 6.2.5.2 Network-based analysis unravels adaptive pathways for high ethanol tolerance

We pooled the mutation data observed in the 16 different lines for respectively the first and second selective sweep and applied IAMBEE to the pooled data of each sweep to unveil pathways that drive increases in ethanol tolerance during each of the sweeps. We identified connected components that were common to both sweeps and components that were unique to each of the sweeps. Identified connected network components representative of adaptive pathways or at least parts of adaptive pathways are shown in **Figure 6.3** and **Figure 6.4**, respectively. 32 connected network components, involving 108 genes harboring 228 mutations, were prioritized by IAMBEE out of a total of 1646 mutated genes harboring 2511 mutations in 16 populations. Likewise, in the second selective sweep 22 connected components, involving 90 genes harboring 345 mutations, were prioritized by IAMBEE out of a total 2286 mutated genes harboring 4470 mutations in the same 16 populations. 15 of these connected components were partly or entirely selected in both sweeps (**Supplementary Figure S6.3**). The fact that both unique and shared clusters are detected for each selective sweep demonstrates fundamental differences between initial adaptation to high ethanol stress and prolonged exposure to increasing ethanol concentration. Below, we describe important identified connected network components and their putative roles in ethanol tolerance. A more detailed overview and description of all identified ethanol tolerance related pathways is given in the supplementary results of **Appendix B**.

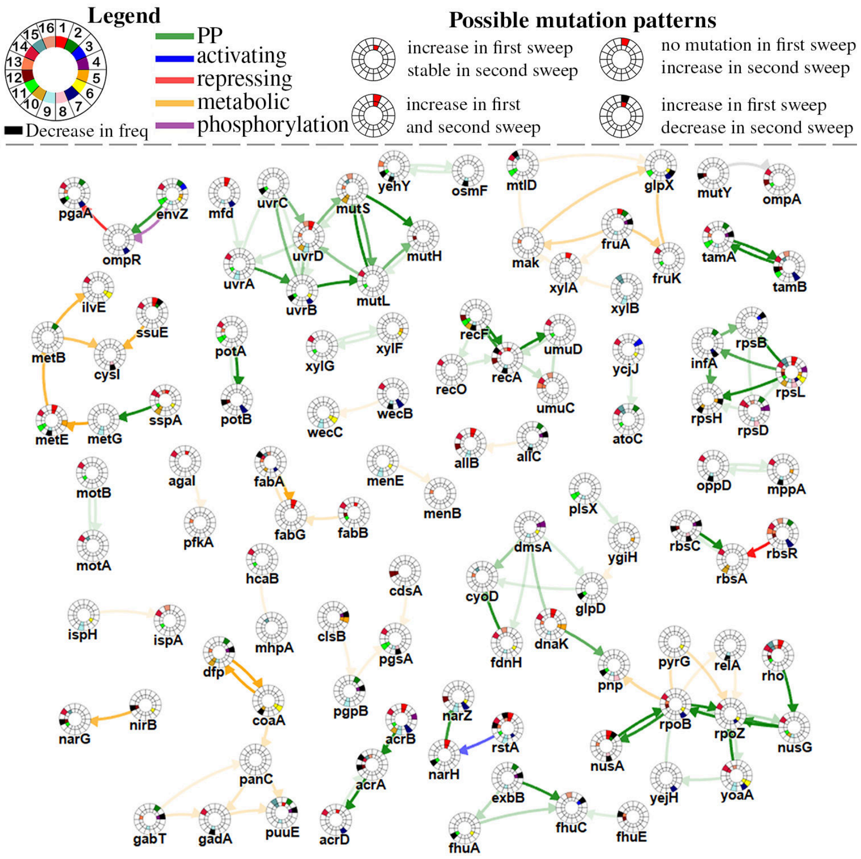

*Figure 6.3: **Subnetwork consisting of multiple connected components inferred by analyzing the mutation data observed in all 16 populations during the initial selective sweep.** Nodes represent genes and edges represent interactions between the genes. Around each node an inner and an outer circle is indicated, which are both divided in 16 equal parts, representing mutations in population HT1 to population HT16 (see legend). A colored part of the inner circle represents a mutation which increases in frequency during an initial selective sweep for that gene in the corresponding population while a colored part of the outer circle represents a mutation which increases in frequency during the second selective sweep in that same population. An overview of all possible mutation patterns can be found at the top of the figure (note that as the outcome of the initial selective sweep is compared to the ancestral strain, it is impossible for a mutation to decrease in frequency during an initial selective sweep). The color of the edges represents their type (see legend). The opacity of the edges represents the maximum edge cost for which those edges were selected (a measure for the degree of belief that the interaction is implicated in the adaptive phenotype). Opaque edges are selected in cases with high edge costs (high degree of belief) while edges with low opacity are only selected in cases with low edge costs (lower degree of belief). The online version of the resulting subnetwork is provided in the online version of this paper.*

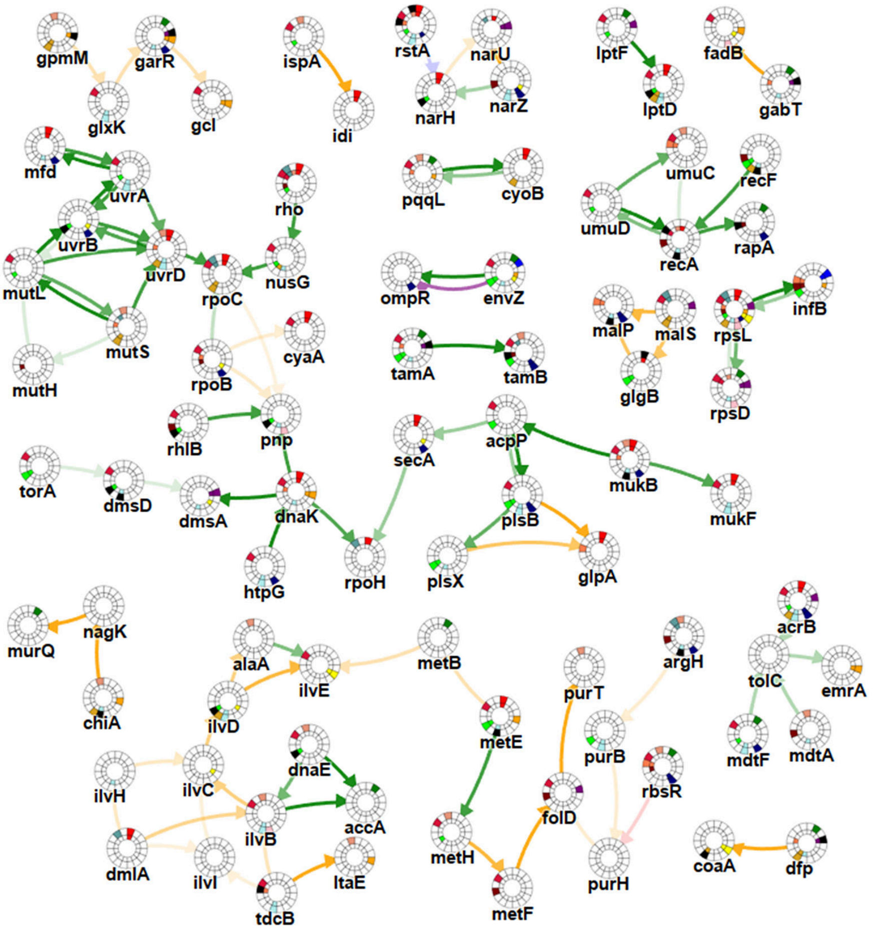

*Figure 6.4*: ***Subnetwork consisting of multiple connected components inferred by analyzing the mutation data observed in all 16 populations during the second selective sweep.*** *Nodes represent genes and edges represent interactions between the genes. Colors of the nodes and the edges are identical to* ***Figure 6.3****. The online version of the resulting subnetwork is provided in the online version of the paper.*

#### 6.2.5.3 The fatty acids biosynthesis pathway is selected exclusively for initial adaptation

An important network component that was exclusively identified in the initial selective sweep is the fatty acid biosynthesis pathway, encoded by the *fab* genes. The prioritization of this pathway in the initial, but not in the subsequent selective sweep, means that most mutations in the *fab* genes were already fixed in the latter step, explaining why they were not selected as being adaptive in the second selective sweep. This early fixation of *fab* mutations indicates that changing the fatty acid composition in the membrane is an initial adaptation strategy, but does not suffice to confer resistance to higher concentrations of ethanol. Both *fabA* and *fabB* accumulated mutations in different parallel populations. The amount of unsaturated fatty acids eventually present in the membrane depends on the competition for intermediates at the FabA branch point in the pathway [277–279]. Mutations in either the *fabA* gene itself or in genes downstream (*e.g. fabB* or *fabG*) can permanently change the ratio saturated versus unsaturated fatty acids thereby changing the fluidity of the membrane. Changes in membrane composition, such as the ratio of saturated versus unsaturated fatty acids, have previously been reported to affect ethanol tolerance [280, 281] although mutations in the *fab* genes have not been associated with ethanol resistance in the past.

To validate whether mutations in the *fab* genes affect membrane composition, we compared fatty acid content of selected strains harboring these mutations with that of the wild type (**Figure 6.5**). When exposed to 5% ethanol, the percentage unsaturated fatty acids in wild-type cells increases 2-fold (**Figure 6.5a**). This observation corroborates previous results showing ethanol-induced inhibition of saturated fatty acid synthesis [280]. The percentage unsaturated fatty acids in the absence of ethanol in the two mutant populations harboring a *fabA* (HT15) and a *fabB* (HT12) mutation equals that of the wild-type ancestor. However, in the mutant populations subjected to 5% ethanol the percentage unsaturated fatty acids also increases, but not to the same extent as for the wild type (**Figure 6.5b**). This difference suggests a direct effect of the identified *fab* mutations on the ethanol-induced shift in saturated versus unsaturated fatty acids ratio. Increased proportions of unsaturated fatty acids fluidizes the membrane. Mutations in the *fab* genes possibly counteract this shift to become more tolerant against ethanol by maintaining structural rigidity of the membrane.

#### 6.2.5.4 Pathways involved in both initial and consecutive adaptation

Several highly prioritized pathways conferring tolerance to ethanol were identified in both the initial and second sweep. When a pathway is selected in both sweeps, typically only few genes are prioritized in the initial sweep, whereas newly acquired mutations are prioritized in the second sweep (**Figure 6.3**, **Figure 6.4**).

**Multidrug efflux pumps**

One network component of particular interest is linked to multidrug efflux complexes. The genes *acrA*, *acrB* and *acrD*, encoding the AcrAB-TolC and the AcrAD-TolC multidrug efflux pump were found to be frequently mutated during the initial selective sweep. Multidrug efflux pumps usually consist of three parts: an inner-membrane transporter, such as AcrB, a membrane fusion protein such as

AcrA and an outer-membrane transport channel such as TolC. AcrD, like AcrB, binds to AcrA and forms a complex with TolC to constitute a multidrug efflux pump. Despite their association with tolerance to organic solvents [282–284], efflux pumps have to our knowledge not yet been specifically linked to ethanol tolerance. To validate the role of the efflux pump in ethanol tolerance, we constructed a deletion mutation in *acrB*, one of the subunits of the AcrAB-TolC multidrug efflux pump that accumulated most mutations. Indeed, the Δ*acrB* deletion mutant has an increased growth rate compared to the wild-type ancestor under 5.5% ethanol stress (**Figure 6.6**). Moreover, the relative difference in growth compared to the wild type increases with the ethanol percentage in the medium (**Supplementary Figure S6.3**).

Whereas *acrA*, *acrB* and *acrD* are mutated in the initial selective sweep, during the second selective sweep additional mutations occurred in *mdtA* and *mdtF*. MdtA, like AcrA, is a membrane fusion protein in the MdtABC-TolC multidrug efflux pump [285, 286]. MdtF is the counterpart of AcrB and acts as a transporter in the MdtEF-TolC multidrug efflux pump [287]. The mutations in *mdtA* and *mdtF* that rise in frequency during the second selective sweep frequently occurred in populations that already harbored a mutation in the AcrAB-TolC efflux pump

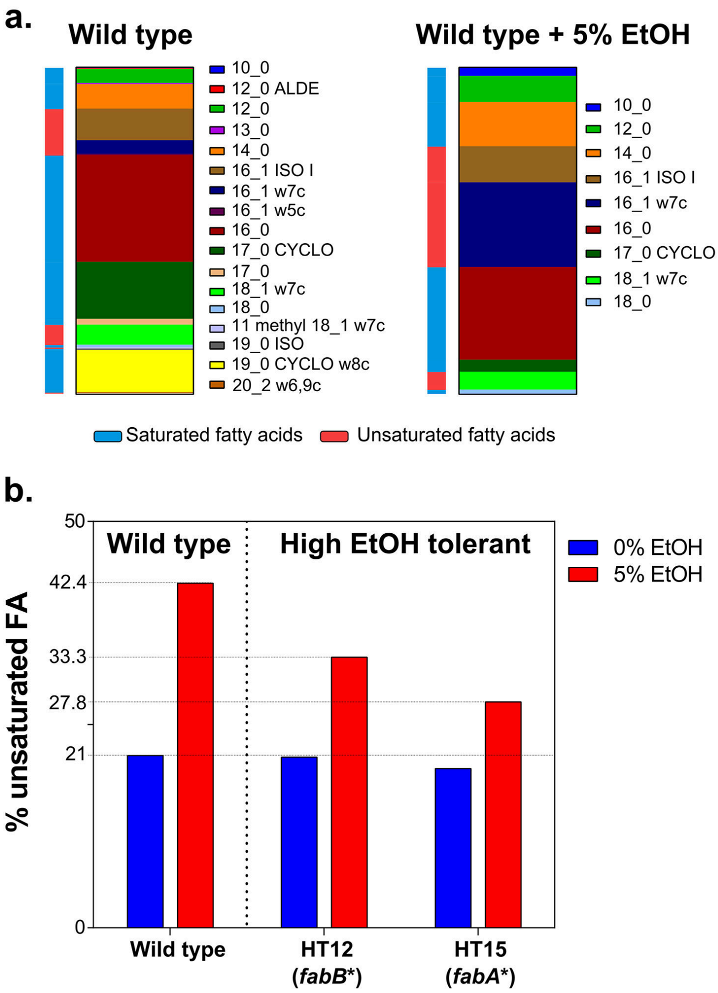

*Figure 6.5:* ***Effect of fab mutations on the percentage of unsaturated fatty acids in the plasma membrane. a****, The membrane composition of E. coli changes dramatically when grown in the presence of 5% ethanol. Especially the proportion of palmitoleic acid (16_1 w7c) increases considerably, while the proportion of palmitic acid (16_0) decreases. Additionally, we can see that the larger fatty acids with chain lengths higher than 18 disappear. A switch to shorter chain length is also part of the response to ethanol stress. The first number in the name of the fatty acids denotes the length (or number of C-atoms) in the chain. The second number denotes the number of double bonds: a zero means a saturated fatty acid and a 1 or 2 means a mono- or di-unsaturated fatty acid. The "w" followed by a number shows the position of the double bond, while the "c" means cis instead of trans.* ***b****, The total percentage of unsaturated fatty acids in the wild type doubles upon exposure to ethanol. In the two high ethanol tolerant populations, in which we identified mutations in fabA and fabB the percentage of unsaturated fatty acids still increases, but less pronounced compared to the wild type. These results demonstrate that rewiring of unsaturated fatty acid biosynthesis through involved genes, such as fabA and fabB can confer high tolerance to ethanol.*

originating from the earlier selective sweep (4 out of 7). Subsequent mutations in paralogous AcrAB-TolC and MdtABC-TolC multidrug efflux systems thus are likely to enable gradual adaption and further improve fitness under high ethanol concentrations. Intriguingly, even though TolC is the common outer membrane channel for all above mentioned efflux pumps no mutations occurred in the *tolC* gene, suggesting that only the inner membrane transporter and fusion protein are altered to increase fitness under ethanol stress.

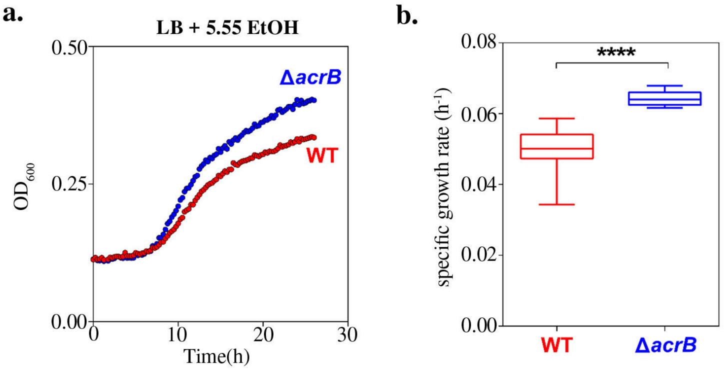

*Figure 6.6:* ***Effect of acrB deletion on growth under high ethanol stress. a****, The graph shows the growth of both the wild-type strain and the acrB deletion mutant under 5.5% ethanol stress. The ΔacrB mutant grows faster and reaches a higher carrying capacity (higher final optical density) under these conditions.* ***b****, The growth curves were fitted using the Gompertz equation and specific growth rate was extracted. The acrB deletion mutant has a significantly increased growth rate compared to the wild type. Both growth rates were statistically compared using an unpaired two-sided Students t-test (n=6, box = median, whiskers = min to max, ****: p<0.0001). These results confirm a selective advantage of the ΔacrB mutant compared to the wild type.*

## DNA repair

One highly prioritized pathway includes several genes involved in DNA repair mechanisms, such as the methyl-directed mismatch repair pathway (MMR, *mutS*, *mutL* and *mutH*), the nucleotide excision repair pathway (NER, *uvrA*, *uvrB* and *uvrC*) and the DNA helicase encoded by *uvrD* which is involved in both the MMR and NER pathways. Mutations in these pathways explain the observed higher mutation rates that were observed in the evolution experiment. Prioritization of this network component substantiates our previous work where we demonstrated the crucial role of mutations in the mismatch repair pathway for adaptation to ethanol under high stress conditions [44].

#### 6.2.5.5 Pathways exclusively involved in the second adaptation step

One smaller network component that was exclusively, but highly, prioritized in the second selective sweep consist of two genes *fadB* and *gabT*. FadB plays a role in fatty acid oxidation and is regulated by FadR [288]. Interestingly, a *fadR* deletion mutant was also recently found to increase organic solvent tolerance [289] pointing to a similar process.

Several additional identified pathways that have never been linked to ethanol tolerance before, but that might influence this trait are discussed in **Appendix B**. In conclusion, we state that IAMBEE is able to detect previously known as well as new adaptive pathways. The identified adaptive pathways in ethanol tolerance might serve as a basis for future strain improvement efforts.

#### 6.2.5.6 Indications for epistasis at the pathway level

Remarkably, adaptive mutations in the fatty acid pathways tend to occur in a mutual exclusive way: 8 populations have mutations in *fadB-gabT*, 9 populations have mutations in the *fabA-B* system, 2 populations (HT13 and HT14) have mutations in both pathways and only 1 population (HT3) has no mutations in either of the respective pathways. Strikingly, this would imply negative epistasis at the pathway level, *i.e.* a mutation in either pathway increases ethanol resistance but mutations in both mechanisms do not lead to a greater increase in resistance. The incomplete pattern of mutual exclusivity in HT14 can be explained by the fact that both the mutation in *fabA* (present in 50% of population) and *fadB* (present in 12% of population) are not fixated in the population. Therefore, it is possible that these mutations exist in different subpopulations. As was the case in the co-occurrence of mutations in the *acrAB-tolC/fab* pathway, the incomplete pattern of mutual exclusivity in HT13 could be explained by the fact that the *fabA* mutation is situated towards the end of the *fabA* protein (7 amino acids near the end), which makes it likely that this mutation is not functionally relevant. Indeed, by determining the membrane composition we confirmed that the percentage of unsaturated fatty acids in absence and in response to 5% ethanol did not differ from the wild-type strain, suggesting that this particular mutation does not contribute to higher ethanol stress by changing the membrane composition (**Supplementary Figure S6.4**).

Additionally, mutations in the AcrAB-TolC efflux pump tend to co-occur with mutations in the previously mentioned *fab* pathway. From the 10 populations which have a mutation in *acrAB-tolC* and the 9 populations which have a mutation in the *fab* pathway, 8 populations overlap. According to the mutational trajectories, mutations in both pathways arise during the same selective sweep (5%-6%) in 7 populations. Only in one population (HT10), the mutation in *acrAB-tolC* was obtained late during the second selective sweep, following an earlier mutation in the *fab* pathway. Only population HT13 had a *fabA* mutation but not a mutation in *acrAB-tolC*. Again, this specific mutation in *fabA* is located at 7 amino acid residues near the end of the FabA protein (**Supplementary Figure S6.4**).

#### 6.2.5.7 Comparison with per gene mutation frequency approach

To show the value of the network-based approach of IAMBEE, we compared our results with those obtained by a frequency-based approach which ranks genes based on the number of populations in which they were mutated (**Figure 6.7**, Supplementary file available in supplementary data of the originally published online version of this paper). Although our method does not explicitly search for genes that are recurrently mutated across populations, it also prioritizes most of the frequently mutated genes which are associated with ethanol resistance (*e.g. rpsL* and *envZ*). We subsequently tested whether mapping the frequently mutated genes (136 and 153 for respectively the first and the second selective sweep) to the genome-wide interaction network also allowed identifying adaptive pathways. Connected components identified in this way show (**Supplementary Figure S6.5** and **Supplementary Figure S6.6**) that adaptive pathways which were identified by IAMBEE, such as the fatty acid biosynthesis pathway, *fadB-gabT* and *acrAB-tolC*, are largely or completely missed. This can be explained by the fact that these pathways are composed of genes that are not necessarily frequently mutated (*e.g.* some connecting genes were only found mutated in one or two populations). By exploiting all mutated genes over the network using information from mutational trajectories and functional impact scores IAMBEE can, in contrast to the frequency-based approach, extract adaptive pathways consisting of less frequently mutated but highly connected genes (**Table 6.1**). However, as IAMBEE is network-based it is possible that some genes are missed because they are not present in the network (*e.g. marC* and *tqsA* [283, 290]). Nevertheless, this does not outweigh the benefit of IAMBEE to retrieve more complete pathways and to be able to reason about the temporal aspects of mutation acquisition, which is not possible by simply assuming that the most frequently mutated genes are the only driver genes.

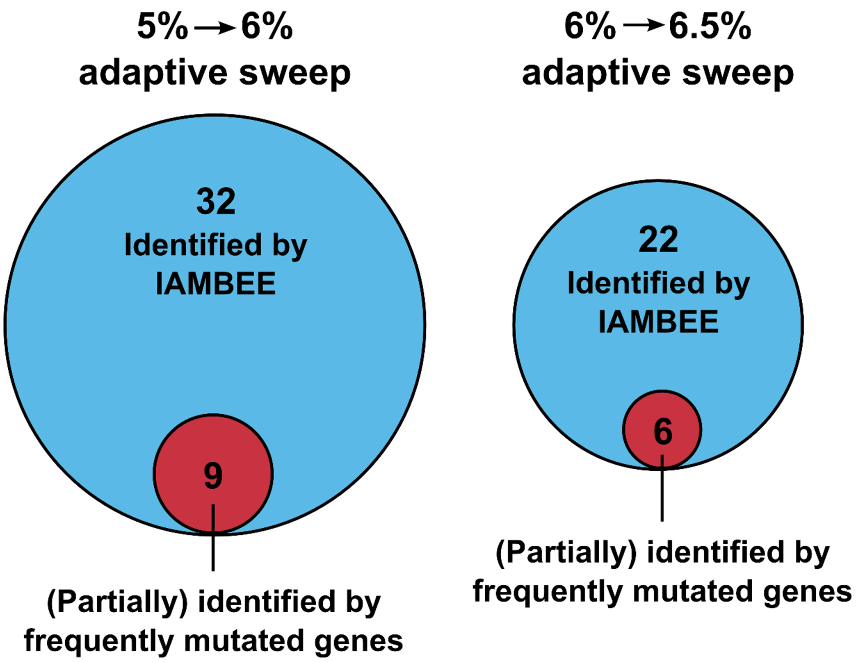

*Figure 6.7:* ***Comparison of the output generated by IAMBEE with the per gene mutation frequency approach.*** *By performing a pooled analysis of the mutation data observed in the 16 populations during respectively the first and second selective sweep IAMBEE identified respectively 32 and 22 connected network components. The alternative method using exclusively the number of mutations per gene allowed (partial) identification of respectively 9 and 6 connected network components in the first and second selective sweep. This result clearly demonstrates that only a fraction of the involved adaptive pathways are identified by using the approach that only takes into account frequently mutated genes. By combining mutation frequency data and functional impact scores, IAMBEE enables identification of the network components underlying an adaptive phenotype. More details on the specific connected network components prioritized by both approaches are given in* ***Table 6.1*** *and* ***Supplemental Figures S6.5 and S6.6****.*

*Table 6.1:* ***Comparison between IAMBEE and the commonly used frequency-based approach.***
*A pathway is partly present when at least one gene of the pathway was included.*

| Prioritized subnetworks | | | | | |
|---|---|---|---|---|---|
| **5% to 6% adaptive sweep** | | | **6% to 6.5% adaptive sweep** | | |
| Pathways | IAMBEE | Frequently mutated genes | Pathways | IAMBEE | Frequently mutated genes |
| *nar*G-*nirB* | √ | Partially | *fadB-gabT* | √ | × |
| *ispAH* | √ | × | *dnaK-pnp* | × | Partially |
| *potAB* | √ | × | *mutHLS-uvrABD-mfd* | √ | Partially |
| *wecBC* | √ | × | *rho-nusG-rpoBC* | √ | Partially |
| *rbsACR* | √ | Partially | *plsB-plsX-glpA* | √ | × |
| *fhuAEC* | √ | × | *rpsLD-infB* | √ | Partially |
| *umuCD* | √ | × | *tamAB* | √ | √ |
| *agaL-pfkA* | √ | × | *mukBF-acpP* | √ | × |
| *allBC* | √ | × | *malSP-glgB* | √ | Partially |
| *sspA metBEG ssuE* | √ | × | *ispA-idi* | √ | × |
| *pgsA* | √ | × | *acrB-mdtAF-tolC-emrA* | √ | × |
| *acrABD* | √ | Partially | *umuCD-recAF* | √ | × |
| *motAB* | √ | × | *dfp-coaA* | √ | × |
| *envZ-ompR* | √ | × | *glxK-gpmM-garR-gcl* | √ | × |
| *xylFG* | √ | × | *iptDF* | √ | × |
| *fruA-xylA* | √ | × | *rstA-narHUZ* | √ | × |
| *oppD-mmpA* | √ | × | *nagK-murQ-chiA* | √ | × |

| | | | | | |
|---|---|---|---|---|---|
| *rpsBHLD infA* | √ | Partially | *envZ-ompR* | √ | × |
| *rpoZ-rho- rpoB-nusAG-pnp* | √ | Partially | *ilvB-dnaE-accA* | √ | × |
| *mutHLS* | √ | Partially | *ilvCDEH-alaA* | √ | × |
| *fabABG* | √ | × | *metBEFH* | √ | × |
| *mutY-ompA* | √ | × | *purBHT-rbsR* | √ | × |
| *rstA-narHZ* | √ | √ | | | |
| *atoC* | √ | × | | | |
| *yehH-osmF* | √ | × | | | |
| *mhpA-hcaB* | √ | × | | | |
| *menEB* | √ | × | | | |
| *tamAB* | √ | √ | | | |
| *dnaK-glpD* | √ | Partially | | | |
| *plsX-ygiH* | √ | × | | | |
| *coaA-dfp* | √ | × | | | |
| *puuE-gadA-gabT-panC* | √ | × | | | |

### 6.2.6 Discussion

Evolution experiments have been successfully used to identify the role of specific genes in an adaptive phenotype [201, 252]. However, genetic data derived from parallel evolution experiments is usually interpreted by looking at the mutation frequencies of the individual genes. Especially when dealing with complex traits, these studies do not necessarily yield insight into the complex interactions of the genes that contribute to the adaptive phenotype. Key to unraveling the genetic mechanisms underlying high ethanol tolerance is the development of a dedicated analysis method. IAMBEE is unique in prioritizing adaptive mutations by combining information on each individual mutation inferred from functional impact scores and relative frequency increases during a selective sweep, with information on the interactions between genes (a genome-wide interaction network). Using our newly developed method, we were able to prioritize multiple pathways that were recurrently mutated in different independent high ethanol tolerant populations. Among the highly prioritized pathways, those related to translation, anti-termination and amino acid metabolism were previously associated with high ethanol tolerance. Recovering these well-known pathways confirms the ability of IAMBEE to identify true adaptive pathways.

On top of those well-known systems, we identified a yet undescribed role for multidrug efflux pumps in the continuous adaptation to high ethanol stress and the role of fatty acid metabolism in allowing the cell to cope with the toxic effects of ethanol on the membrane [291]. Related to the latter mechanism, binding and penetration of ethanol into the lipid bilayer increases membrane fluidity [292], thereby inducing secondary effects, such as osmotic stress [293–295]. Response to osmotic stress has previously been shown to induce alterations of the membrane composition including cis-to-trans isomerization of unsaturated fatty-acids as a short-term response [278] and alteration of the ratio of saturated versus unsaturated fatty acids as a long-term response [280,281]. Both changes to the membrane composition can result in denser packing of the fatty acids thereby increasing the rigidity of the membrane which enables the cell to withstand the toxic effect of ethanol [261, 292]. Although there has been confusion about the effect of unsaturated fatty acids on ethanol tolerance [280, 281, 296], we provide evidence that tempering the shift to higher ratios of unsaturated fatty acids confers higher resistance to ethanol (**Figure 6.5**). We could indeed show that mutations in representative genes of the *fab* pathway resulted in increased ethanol tolerance by affecting the ratio of saturated versus unsaturated fatty acids.

As IAMBEE is designed to be used in combination with a dedicated experimental set-up, which includes sequencing of the evolving populations before and after a selective sweep, it is possible to gain insight in the temporal profile of adaptation. Using this unique feature of the method we found that mutations in the fatty acid biosynthesis pathway occur early in the evolutionary trajectory of ethanol resistance in *E. coli* while mutations in other pathways have less strict temporal constraints. In this context, we also found that mutations in respectively the pathway for fatty acid biosynthesis (*fabA*, *fabG* and *fabB*) and a pathway involved in fatty acid oxidation (*gabT*, *fadB*) were mutually exclusive while having high coverage (15 out of the 16 populations had a mutation in either pathway). This implies that fatty acids play a pivotal role in ethanol tolerance, but that either a mutation in one of the two pathways does not lead to a significant increase in fitness if a mutation in the other pathway is already present (negative epistasis) or that having a mutation simultaneously in both pathways is lethal (synthetic lethality as an extreme form of negative epistasis). In contrast, mutations in the fatty acid biosynthesis pathway (*fabA*,*fabG* and *fadB*) and the AcrAB-tolC efflux pump (*acrA* and *acrB*) significantly co-occur, suggesting positive epistasis between these pathways.

When compared to a naive approach which is based on recurrence of mutations across experiments at the level of individual genes, it is obvious that IAMBEE offers not only the advantage of being able to identify adaptive mutations which are not frequently mutated but also to interpret adaptive mutations and epistasis at the level of pathways. As such, IAMBEE is very useful and meets the need for adequate tools to analyze highly complex mutational datasets.

### 6.2.7 Conclusions

Experimental evolution can readily yield insight in complex traits assuming low complexity of the resulting mutational profiles. However, in the case of complex traits and especially when hypermutation arises, evolution experiments often lead to complex mutational profiles with high rates of passenger mutations that are difficult to interpret. Traditionally, adaptive genes are identified by counting the number of mutations per gene across independently evolved populations. While this approach is valid in some datasets, in complex mutational profiles it neglects less frequently mutated genes, resulting in the inability to generate a broad understanding of the adaptive phenotype. Therefore, we developed IAMBEE, a method that exploits the interaction network, combined with information from mutational trajectories and functional impact scores, to identify adaptive genes and pathways from complex mutational datasets. By applying IAMBEE to an evolution experiment consisting of 16 independently evolved *E. coli* populations subjected to increasing ethanol concentrations, pathways that were previously linked to high ethanol resistance as well as novel pathways, which were experimentally validated, could be identified. In conclusion, IAMBEE is a powerful tool that successfully allows to generate a broader understanding of (complex) traits that could not be fully elucidated so far.

### 6.2.8 Materials and Methods

#### 6.2.8.1 Data acquisition

#### 6.2.8.2 Functional impact scores and frequency of mutations

To calculate functional impact scores for each mutation we used SIFT scores which were calculated using the SIFT4G annotator version 2.2 with the *E. coli* (GCA_-000005845.1.21) database [276]. Note that while SIFT scores were used in this paper, any functional impact score measure can be inserted in IAMBEE. As IAMBEE tries to identify the causal molecular pathways which lie at the basis of a selective sweep, mutations which decrease in frequency during a selective sweep are not taken into account. Therefore, we have to determine when a mutation ”decreases” in frequency. As the precision of frequency calling of mutations is finite, the naive way of viewing all mutations with a negative frequency increase as ”decreasing” is not valid. This would discard too many mutations which remained stable or, most of the time, were fixed previously in the population. As these mutations could be potentiating mutations, we do not want to discard them. Because of this, and the specifications of the CLC variant caller (a required significance of 1%), we viewed all mutations with a decrease in frequency of at least 2% as decreasing. All mutations in both selective sweeps, together with their SIFT scores and their increase in frequency during the selective sweep are given in Supplemental file 1 which is available in the online version of this paper.

#### 6.2.8.3 Genome-wide interaction network

We used a directed genome-wide interaction network of *E. coli* K-12 MG1655 compiled from (de)-methylation, (de)phosphorylation and metabolic interactions from KEGG version 80 [100,225], protein-DNA, sigma factor binding and sRNA-DNA interactions from regulonDB version 9.2 [297] and protein-protein interactions from STRING version 10 (RRID:SCR_005223) [64]. To reduce the number of false positive interactions in the interaction network, only direct (physical) associations with a score of at least 0.8 were retained from STRING. Interactions involving the primary sigma factor RpoD were removed as RpoD regulates over half of the genes in the interaction network. Furthermore, self-edges were deleted. The final genome-wide interaction network contains 2678 nodes (genes) and 14702 edges (interactions between genes/sRNAs), representing about 63% of *E. coli* K-12 genes. This interaction network is supplied together with IAMBEE at http://bioinformatics.intec.ugent.be/IAMBEE.

#### 6.2.8.4 Construction of the probabilistic genome-wide interaction network

IAMBEE is guided by a directed genome-wide interaction network with the nodes representing genes and the edges representing interactions between these genes. A topology-based weighting of the genome-wide interaction network was performed to reduce the effect of hubs in the subsequent analysis steps: a power law distribution [298] was estimated based on the out-degrees of the nodes in the interaction network. Next, a sigmoidal function was constructed using as inflection point the out-degree that corresponded to the 90th percentile. This leads to following topology-based weighting of each edge between node *i* and node *j* [6]:

$$weight_{(i,j)} = \frac{1}{1+e^{\frac{out\_degree(i)\text{-}inflection\_point}{\frac{inflection\_point}{6}}}} \tag{6.1}$$

This sigmoidal function is utilized to mainly down-weight interactions originating from large hubs while avoiding to penalize interactions involving nodes with low out-degrees. The value 6, which together with the inflection point value dictates the slope of the sigmoidal, was chosen as such because it led to good results when used with multiple bacterial interaction networks (results not shown). As bacterial interaction networks tend to follow similar scale-free distributions it is expected that this sigmoidal will perform well on other bacterial interaction networks as well.

For the materials and methods on the used experimental evolution setup, the sequencing and mutation calling and the mapping of mutations to genes we refer to **Appendix B.2**.

### 6.2.9 IAMBEE

#### 6.2.9.1 Calculation of relevance scores

Not all mutations are equally likely to be involved in the adaptive phenotype. Therefore, a relevance score was assigned to each mutation based on its estimated functional impact on the coding/promoter sequence and based on its relative increase in frequency in the population during a fitness increase. The functional impact score reflects how likely a mutation causes a functional change in the resulting protein(s). Here it is based on the degree of conservation of amino acid residues in sequence alignments from closely related sequences using the SIFT algorithm (RRID:SCR_012813) ( [276, 299, 300]). To derive frequency increases, for each population the adaptive trajectory (e.g. fitness profile) is used to delineate selective sweeps (sudden jumps in fitness or an increase in adaptation towards the experimental conditions). The frequency increase of a mutation is equal to the difference of its frequency in the population just after and just before the sweep. To assess the relative importance of a mutations frequency increase or functional impact score, we first estimate both the distribution functions, based on the frequency increase/impact score of all mutations from all evolved populations. As neither the functional impact score distribution, nor the frequency increase distribution is expected to follow any known mathematical distribution, the distributions are estimated using a nonparametric cumulative distribution function (MathWorks 2017). As synonymous mutations would skew the distribution of the functional impact scores towards low functional impact scores, which could result in assigning relatively high relevance scores to mutations with poor functional impact scores, synonymous mutations are removed from the data when estimating the functional impact distribution function. Note that because some synonymous mutations do have relevant functional impact scores they are not discarded but only ignored when estimating the functional impact distribution. While the functional impact distribution function is estimated using all mutation data from all evolved populations, the frequency increase distribution is estimated on a per-population basis as the population dynamics can differ between populations. This means that one functional impact distribution is estimated, while the number of frequency increase distributions is equal to the number of parallel evolved populations are estimated. Based on these distributions a relevance score is calculated for each mutated gene in each population as follows:

$$\begin{aligned} relevance(S,n) = {} & (1 - \mathit{eCDF}_{fun}(Functional\_score(S,n))) \\ & \times \mathit{eCDF}_{freq,n}(Frequency\_increase(S,n)) \end{aligned} \tag{6.2}$$

with *eCDF*$_{fun}$*(Functional_score(S,n))* the value of the cumulative distribution function of the functional impact scores for the mutation in gene S in population n with the most deleterious functional impact score (note the $1-$*eCDF*$_{fun}$*(Functional_-score(S,n))*. This is needed as we use SIFT scores which are low when the mutation is deleterious.), *eCDF*$_{freq,n}$*(Frequency_increase(S,n))* the value of the cumulative distribution function in population n of the frequency increases for the mutation in gene S in that population with the highest frequency increase. *relevance(S,n)* is a value between 0 (gene *S* is unlikely to be relevant towards adaptation in population *n*) and 1 (gene *S* is very likely to be relevant towards adaptation in population *n*). Genes without mutations are assigned the mean functional impact score and frequency increase when calculating their relevance.

Furthermore, if the dataset contains populations with a mutation rate which is significantly higher than the mutation rates of the other populations, the search for paths in the pathfinding step (see following paragraph) would be skewed towards this population (**Table 6.2**). In order to reduce the impact of this feature without completely discarding these populations, a correction factor for each population is calculated. To detect populations with significantly higher rates we use the modified z-score for outlier detection ( [301]) as follows:

$$\begin{gathered}
\textit{modified Z-score}\,(n) = \frac{0.6745 \times (mutations\,(n) - median\,(n_1,\ldots,n_i))}{MAD(n)} \\
MAD(n) = median\,(|mutations(n) - median(n_1,\ldots,n_i)|)
\end{gathered} \tag{6.3}$$

with *mutations(n)* the number of mutations in population $n$, $median(n_1,\ldots,n_i)$ the median number of mutations in a population and *MAD(n)* the mean absolute deviation of population $n$. Note that in the original publication the modified Z-score is defined as the absolute value of the measure used in this paper. We intentionally left out the absolute value to avoid down weighting populations with few mutations. Populations with a significantly higher mutation rate are defined as populations having a modified Z-score of at least 3.5 [301]. From this modified Z score a population specific correction factor is calculated, based on a parameter p which sets the upper limit for the correction factor. In our analysis we set this to 3 to have an upper limit of 0.85 but based on how a user would like to deal with populations having significantly higher mutation rates, the factor can be anywhere between 0 and 3,5:

$$correction(n) = \begin{cases} \frac{p}{\textit{modified Z-score(n)}} & \textit{if modified Z-score(n)} \geq 3.5 \\ 1 & \textit{else} \end{cases} \tag{6.4}$$

Due to the modified Z score, the correction factor intrinsically assigns a lower value to outlier populations when the study contains a larger number of independent populations, hereby largely removing populations with high mutation rates to reduce noise when a large number of independent populations is present while largely retaining them, as in that case they will be needed to exploit parallelism, if only few populations are present. The relevance score and the correction factor are integrated into a single score for every mutated gene in every population. This is implemented as follows:

$$corrected\_relevance(S,n) = relevance(S,n) \times correction(n) \tag{6.5}$$

With $S$ a mutated gene in population $n$

*Table 6.2:* ***Percentage of paths found at the end of the pathfinding step on the data obtained for the second selective sweep, with and without correction for significantly higher mutation rates.*** *It can be seen that the correction inhibits the most prominent outlier (HT14) from consuming nearly a fourth of all paths.*

| Population | Without correction | With correction | # mutations |
|---|---|---|---|
| HT1 | 7.86 | 9.12 | 324 |
| HT2 | 3.66 | 2.43 | 142 |
| HT3 | 0.73 | 1.82 | 79 |
| HT4 | 2.01 | 4.26 | 124 |
| HT5 | 3.29 | 5.17 | 113 |
| HT6 | 4.02 | 9.12 | 164 |
| HT7 | 7.68 | 4.26 | 342 |
| HT8 | 1.28 | 3.34 | 82 |
| HT9 | 10.97 | 13.68 | 621 |
| HT10 | 4.75 | 3.95 | 195 |
| HT11 | 11.33 | 15.81 | 478 |
| HT12 | 3.29 | 7.90 | 164 |
| HT13 | 5.12 | 8.81 | 157 |
| HT14 | 23.95 | 1.82 | 1121 |
| HT15 | 4.94 | 6.69 | 184 |
| HT16 | 5.12 | 1.82 | 180 |

#### 6.2.9.2 Pathfinding between mutated genes

All genes with at least one mutation in any independent population are mapped on the topology-weighted genome-wide interaction network. Subsequently, all possible paths originating from a mutated gene in a population and ending in any other gene which is mutated in another population, are enumerated. A path is defined as a series of consecutive edges in the interaction network. We exclude paths between mutated genes in the same populations, reasoning that because of the clonality a single mutation in a pathway will confer most of its fitness advantage [8] and including paths between mutated genes within one population would not be informative as this does not reflect parallel evolution.

Each path is assigned a probability which reflects the degree of belief that the path is associated with the adaptive phenotype under study. This probability takes into account the weights of the edges which make up the path (calculated based on the network topology in the previous step) and the corrected relevance scores from both the start gene and the terminal gene of the path (calculated based on the frequency increase and the functional impact score of both genes in the data preparation step). Only the relevance scores of the start gene and the terminal gene are considered because whether or not intermediate genes are mutated should not be taken into account. If they were taken into account, even one passenger mutation in the middle of an interesting molecular pathway would severely decrease the probability of every found path in that molecular pathway. This leads to the following equation for the probability of a path:

$$\begin{aligned} probability(S,n,E,m)_{(S\neq E,n\neq m)} = \prod_{(i,j)\in P} weight_{(i,j)} \times relevance(S,n) \\ \times relevance(E,m) \end{aligned} \tag{6.6}$$

with *(S,n,E,m)* the path which starts in gene *S*, which is mutated in population *n* and terminates in gene *E*, which is mutated in population *m*. *P* is the collection of edges which make up the path and *(i,j)* is the edge from node *i* to node *j*.

Enumerating all possible paths is computationally expensive and leads to a prohibitively large computational cost in the subsequent subnetwork inference step. Therefore, the following heuristics are used:

1. Based on biological considerations [218, 219] the maximum path length is set to four.
2. From all possible paths originating from a mutated gene in a specific population, only the 25 paths with highest probabilities are retained.

#### 6.2.9.3 Subnetwork inference and prioritization of molecular pathways

The final step of the analysis is the inference of a subnetwork containing the molecular pathways responsible for the adaptive phenotype. This subnetwork consists of a subset of the paths selected in the previous step. This subset of paths is obtained by optimizing the following function:

$$S(K) = \sum_{n\in R}(\sum_{S\in Q_n}(P(path(mut_{S,n}, mut_{all})|probabilities, K))) - |K| \times x_e \tag{6.7}$$

Where *S(K)* is the score of the selected subnetwork and needs to be maximized, $|K|$ is the number of edges selected, $x_e$ is the imposed cost for each edge, *R* is the collection of strains, $Q_n$ the collection of mutated genes in *n* and $P(path(mut_{S,n}, mut_{all}))$

| *probabilities,K*) is the probability that there exists a path between a mutated gene S in population n and any other mutated gene in any other population, given the degrees of belief (probabilities) of all found paths in the pathfinding Step and the selected subnetwork *K*. The calculation of this term is a generalization of the two-terminal reliability problem [302,303] and the implementation of the search for the highest scoring subnetwork, according to this optimization function is explained in chapter 5 of this thesis as the exact same strategy was used. Note that the optimal subnetwork, which is the selected subnetwork with the highest score *S(K)*, is not necessarily a connected graph.

As the complexity of this problem inhibits a deterministic solution, a greedy hill-climbing heuristic is used in which the previously found paths get sampled pseudo-randomly based on the overlap the paths have with each other: Overlapping paths are more likely to be sampled together. As this procedure is probabilistic in nature, the procedure is repeated 20 times and the best solution with respect to the optimization score *S(K)* is used as the solution.

The $x_e$ parameter is an important parameter as it incentives IAMBEE to primarily select overlapping paths with high probabilities because doing so a single edge can be used multiple times while the cost for selecting this edge only has to be paid once. This is biologically relevant as molecular mechanisms in which multiple (partly) overlapping paths with high probabilities are found, are likely mechanisms of interest for a specific selective sweep.

Setting the $x_e$ parameter is not trivial as its optimal value is dataset specific. If $x_e$ is set too high the subnetwork will be small and multiple causal molecular pathways are likely missed. Conversely if $x_e$ is set too low the subnetwork will be too large and of little practical use as the fraction of false positives in the solution increases (**Figure 6.2**). Therefore, instead of calculating the optimal subnetwork for one specific cost, we perform a parameter sweep over the $x_e$ parameter and summarize the results in the form of a network, which is obtained by taking the union of all found optimal subnetworks and where the edges are prioritized based on the maximum edge cost for which they are still included in an optimal subnetwork. This means that edges with a high priority (visualized in the output as opaque edges) get selected even when the edge cost $x_e$ is high. This is useful as the PPV (positive predictive value) of a subset of opaque edges is higher (Synthetic data in **Subsection 6.2.5.1**) and thus a good starting point for experimental validation.

#### 6.2.9.4 Parameter setting

The parameters of IAMBEE were set as follows for both jumps in ethanol tolerance: The path length was kept at the default value of 4 and the maximum number of paths between every pair of mutated genes was kept at the default value of 25.

The sweep over the edge cost parameter $x_e$ was set from 0.1 to 1.5 in steps of 0.025 and the maximum size for an optimal subnetwork to be accepted was set to 80 (in terms of nodes) in order to keep the resulting subnetwork small enough to interpret manually.

#### 6.2.9.5 Validation of IAMBEE features

To show the importance of the different features of IAMBEE, which include mutation frequencies, functional scores, a correction factor for populations with extreme mutation rates and the use of an interaction network, the method was adjusted several times to exclude one feature each time. Each of these adjusted versions of IAMBEE was applied to the synthetic dataset. PPV and sensitivity plots were constructed (*Supplemental Figure S6.2*) and demonstrated that each feature led to an increase in performance. The results are discussed in **Supplemental Methods**.

### 6.2.10 Acknowledgments

We thank S. Xie for providing the *E. coli* SX4 ancestor strains.

### 6.2.11 Availability of data and material

The genome sequencing dataset generated and analyzed during the current study are available in the SRA repository of NCBI, **PRJNA380734** (https://www.ncbi.nlm.nih.gov/bioproject/380734). IAMBEE is can be found at http://bioinformatics.intec.ugent.be/IAMBEE.

### 6.2.12 Competing interests

The authors declare no competing financial interests. The funding sources were not involved in study design, data collection and interpretation, or the decision to submit the work for publication.

# Supplementary

## 6.2.13 Supplementary methods

### 6.2.13.1 Synthetic data

As complete and reliable gene sets of causal mutations for complex traits are rarely available and previous methods do not advocate the analysis of experimental evolution data in complex traits from clonal organisms, we used synthetic datasets to illustrate that IAMBEE can identify causal mutated genes and mechanisms. For the construction of the synthetic datasets, the same *E. coli* MG1655 genome-wide interaction network as used in the analysis of the ethanol tolerance dataset was used. Each synthetic dataset was constructed by randomly choosing a number of populations between 5 and 30 to simulate a wide range of possible evolution experiments with different amounts of data. In order to make sure that IAMBEE will have to deal with hypermutators in at least some datasets, each population has a 15% chance of being a hypermutator. Each normal population has a random number of mutated genes between 5 and 40 [289] while each hypermutator population harbors a random number of mutated genes between 100 and 200 [41]. The causal mechanisms are determined by randomly sampling a gene together with all of its outgoing interactions from the interaction network. Isolated genes are withheld. The union of all genes involved in the sampled interactions is labeled as the causal mechanism. As the complexity of traits vary, for each dataset 1 to 5 causal mechanisms are present. For every causal mechanism, every population has a 50% chance to have a mutation in a random gene from that causal mechanism with the additional constraint that parallel evolution is, at least to some extent, present and thus every causal mechanism has at least two mutations from two different populations. For obvious reasons, every population is forced to have at least one causal mutation. To determine the frequency increase and the functional impact score data for each mutated gene in every population in a synthetic dataset, we sample from respectively the frequency increase data and the functional impact score data of the mutations implicated in the used *E. coli* MG1655 ethanol tolerance dataset in the main paper. As the used mutation rates for a synthetic data are based on non-synonymous mutations, we only sample from non-synonymous mutations in the ethanol tolerance dataset. Because the ethanol tolerance dataset is dominated by passenger mutations, we randomly sample from all mutations when setting the frequency increase and functional impact score for the synthetic passenger mutations. When setting these values for the synthetic adaptive mutations, we sample only from the mutations which are amongst the 20% highest frequency increase/-functional impact score. 100 such synthetic datasets were created and analyzed with identical settings as the *E. coli* MG1655 ethanol tolerance experiment, using a parameter sweep over the edge cost parameter from 0.05 to 2.45 in steps of 0.05.

The results are depicted in **Supplementary Figure S6.7**.

#### 6.2.13.2 Using synthetic data to validate IAMBEE features

In order to validate and disentangle the contribution of the different features of IAMBEE (mutation frequency, functional data, correction factor and the network) we performed the same analysis on the synthetic data with different versions of IAMBEE, each time leaving out one feature. Note that in the case of leaving out the network, subnetworks are not inferred but instead the genes were ranked based on their relevance scores and e.g. a solution of size 5 for a specific synthetic dataset consists of the 5 highest ranked genes in that synthetic dataset. These results are depicted in **Supplementary figure S6.2**. As can be seen, in general PPV and sensitivity are both higher in the original version of IAMBEE. This means that the resulting subnetworks of the original version will overall contain a higher proportion of adaptive mutations and that the original version is more likely to find (nearly) all adaptive mutations. This is especially true for the relatively smaller subnetworks which is important as the prioritization of interactions is based on the assumption that mutations found in small subnetworks are more likely to be adaptive mutations. From the plots of PPV in terms of sensitivity it can be seen that few subnetworks have both low sensitivity and low PPV (which are bad solutions) in the original version of IAMBEE while other versions generate more bad solutions. These results indicate that, even in simple synthetic datasets where adaptive mutations are guaranteed to have high scores for frequency increase and functional impact score, all features of IAMBEE contribute to better results.

## 6.2.14 Supplementary figures

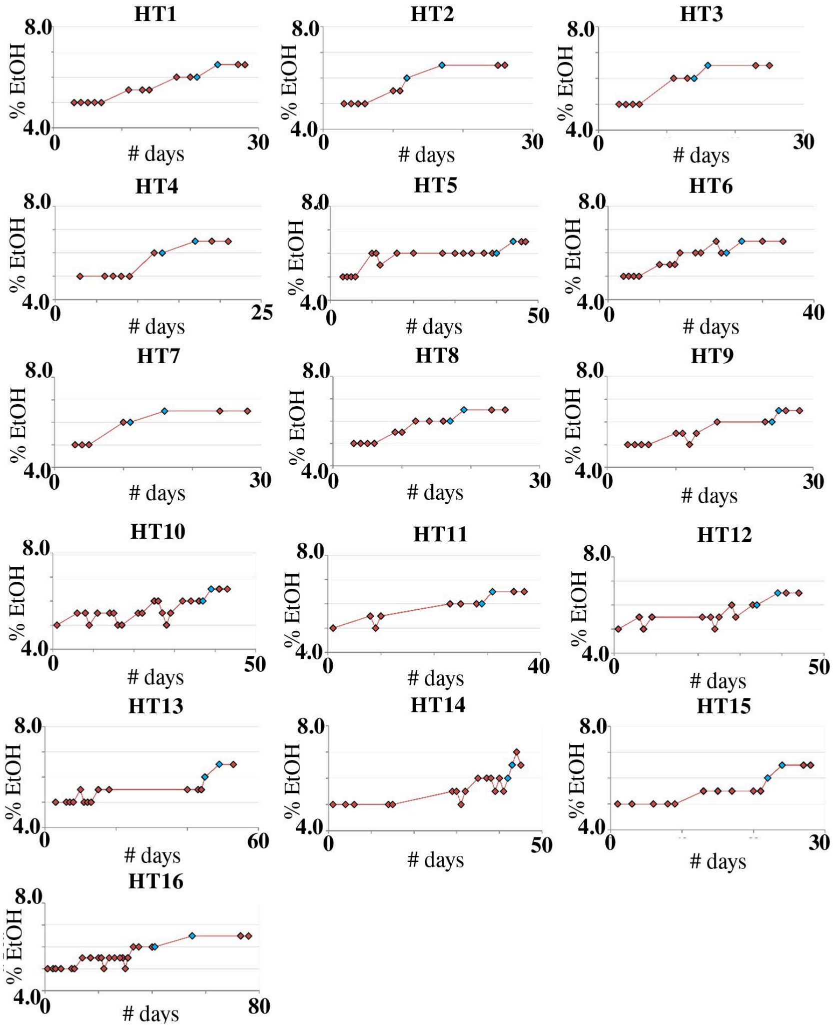

*Figure S6.1:* ***Ethanol tolerance profiles of HT populations.*** *For each population the changes in ethanol tolerance due to accumulation of beneficial mutations were tracked in time to obtain a fitness trajectory. Each red diamond represents an intermediate time point during the evolution experiment. At these time points the population showed growth to an optical density of 0.2 or higher. Depending on the time necessary to obtain this optical density the concentration of ethanol was either increased, kept unchanged or decreased. The blue diamonds represent the time points that correspond to the second selective sweep. The pooled sequences of the time points before and after both selective sweeps were used as datasets for the implementation of IAMBEE.*

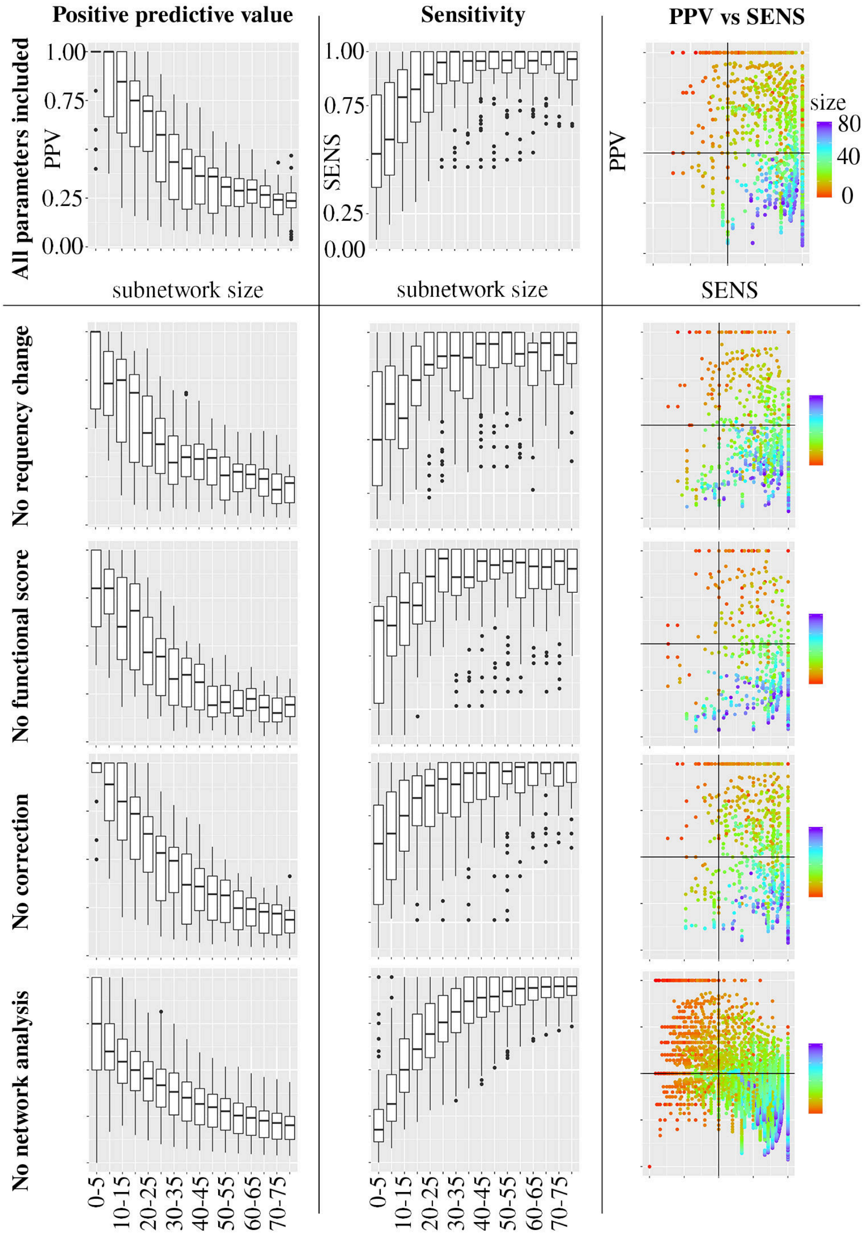

*Figure S6.2:* ***Synthetic data analysis results.*** *PPV plots, sensitivity plots and PPV in terms of sensitivity plots from the analysis of 100 synthetic datasets using 50 different parameter settings per synthetic dataset. Results with sizes larger than 80 are not shown. Every row depicts a slightly different version of IAMBEE. The top row shows the results for the normal version of IAMBEE while in the other rows one feature of IAMBEE is left out each time (see labels). Left column: Box plots for the PPV in terms of different ranges of subnetwork sizes. Small subnetworks tend to have high PPV while larger subnetworks tend to have lower PPV. Middle column: Box plots for the sensitivity in terms of different ranges of subnetwork sizes. Small subnetworks tend to have low sensitivity while larger subnetworks tend to have high sensitivity. Right column: Plot of PPV in terms of sensitivity. Each dot represents an optimal subnetwork from a specific synthetic dataset and a specific parameter setting (edge cost). Size is reflected through the colors of the dots.*

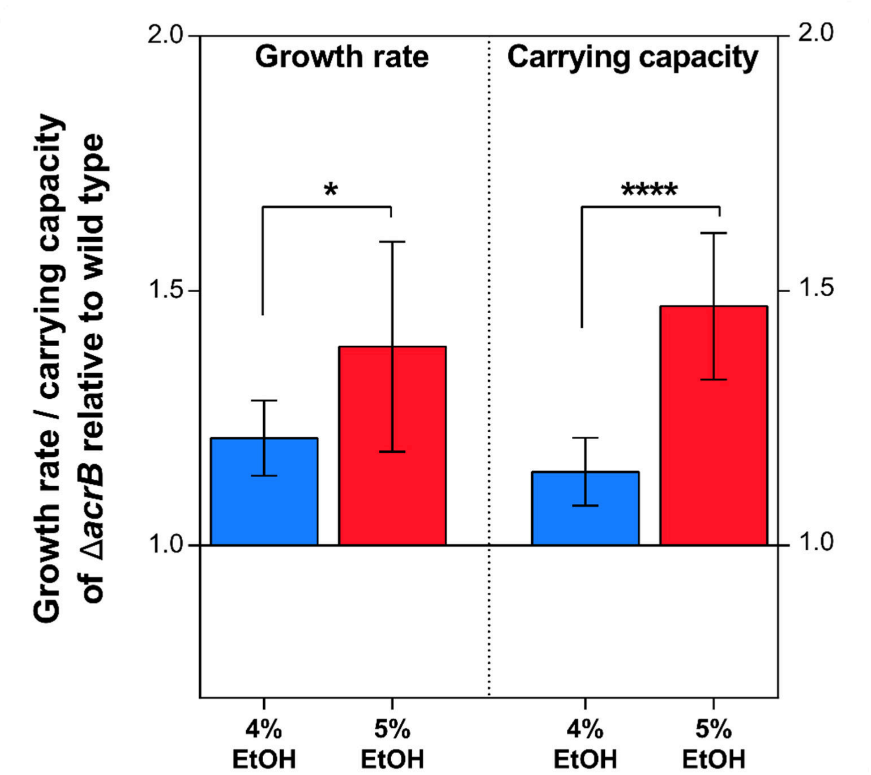

*Figure S6.3:* ***Growth advantage of a ΔacrB mutant under ethanol stress increases with the concentration of the stress.*** *The graph shows both the relative growth rate (left) and the relative carrying capacity (right; the relative number of cells that can be supported by the environment indefinitely) of the ΔacrB mutant compared to the wild type under 4% ethanol (blue) and 5% ethanol stress (red). Increased concentration of ethanol result in a significantly higher growth benefit reflected by a higher relative growth rate as well as a higher carrying capacity. Relative growth rates and relative carrying capacities were statistically compared using an unpaired two-sided Students t-test (n=9, average ± s.d., *: p<0.05; ****: p<0.0001).*

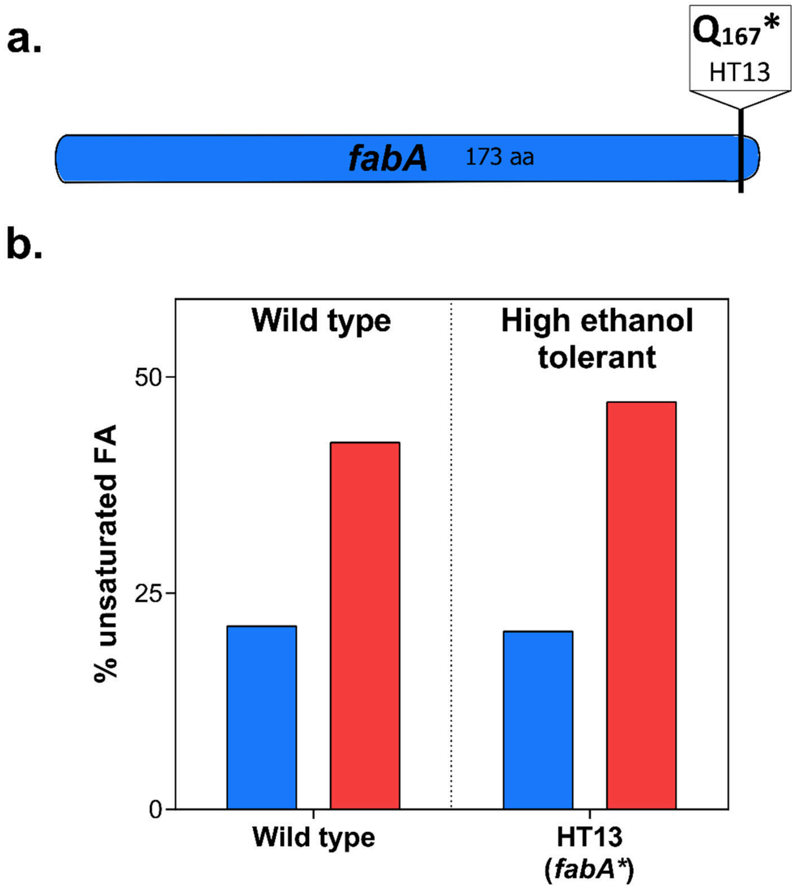

*Figure S6.4:* ***fabA mutation in HT13 does not affect the shift in percentage unsaturated fatty acids in response to ethanol. a****, The amber mutation in fabA identified in population HT13 is located near the end of the FabA protein.* ***b****, Membrane analysis in the absence and presence of 5% ethanol shows no decrease in shift to unsaturated fatty acids for population HT13 compared to the wild type. This was the case in other high tolerant populations HT12 and HT15 (Figure 5). Therefore, the fabA mutation in HT13 might not influence ethanol tolerance through altered changes in unsaturated fatty acids ratio as response to 5% ethanol stress.*

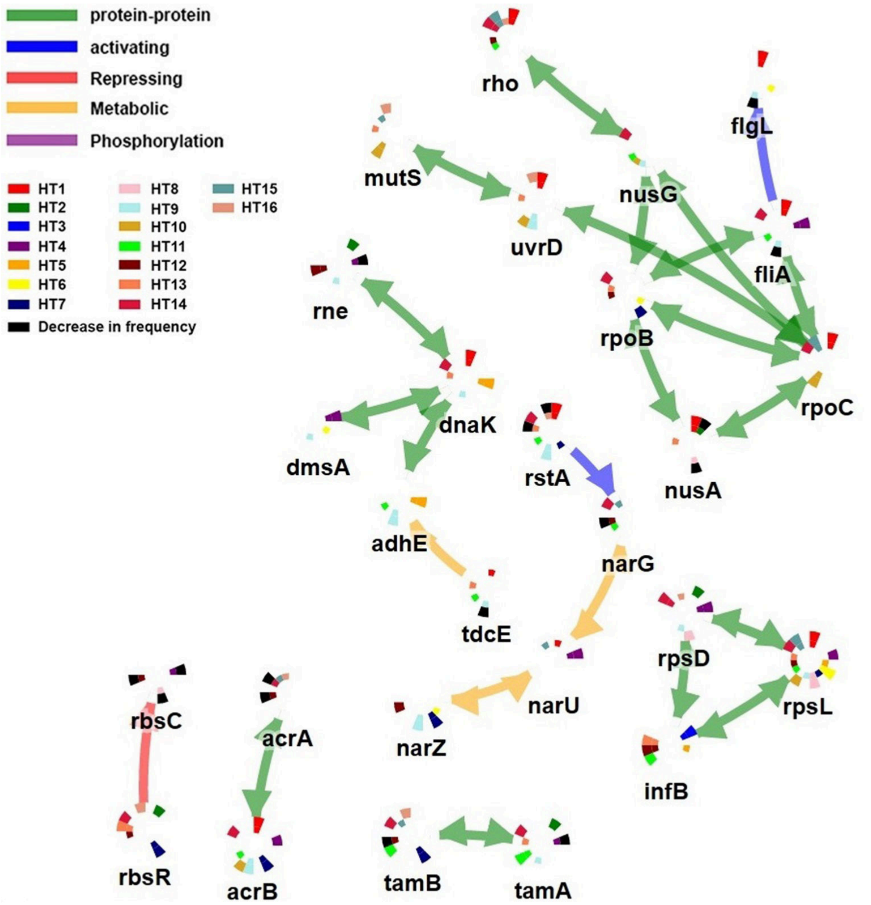

*Figure S6.5:* ***Results of mapping the mutations identified with the frequency-based approach for the initial selective sweep on the interaction network.*** *All genes with at least one mutation in three different populations were mapped. Nodes represent genes and edges represent interactions between the genes. The color of the edges represents their type (legend). Around each node there are an inner and an outer circle, which are both divided in 16 equal parts, representing population HT1 to population HT16 (clockwise). The inner circle is colored in case the corresponding population has a mutation in the gene at the 6% ethanol time point. The outer circle is colored in case the corresponding population has a mutation which increases during the second selective sweep. In case the outer circle is black in the position corresponding to a specific population, the mutation in the gene decreased in frequency during the second selective sweep. In case there is a mutation at the 6% ethanol time point which remains stable during the second selective sweep the inner circle is colored but the outer circle is white in the part corresponding to the specific population.*

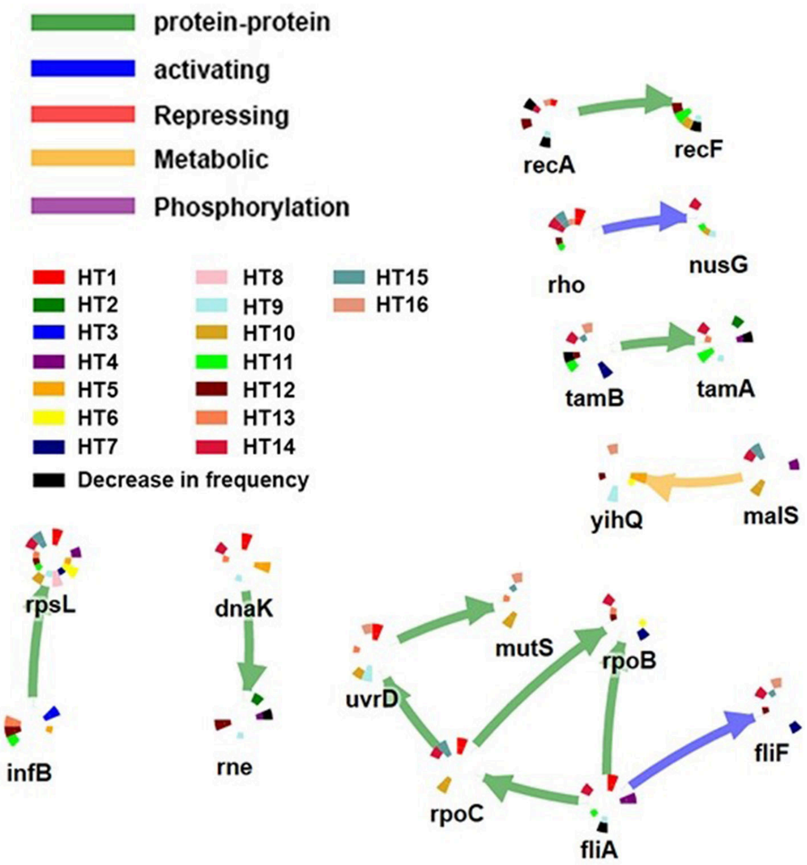

*Figure S6.6:* ***Results of mapping the mutations identified with the frequency-based approach for the second selective sweep on the interaction network.*** *All genes with at least one mutation in three different populations were mapped. Nodes represent genes and edges represent interactions between the genes. Colors of the nodes and the edges are identical to* ***Supplementary Figure S6.5****.*

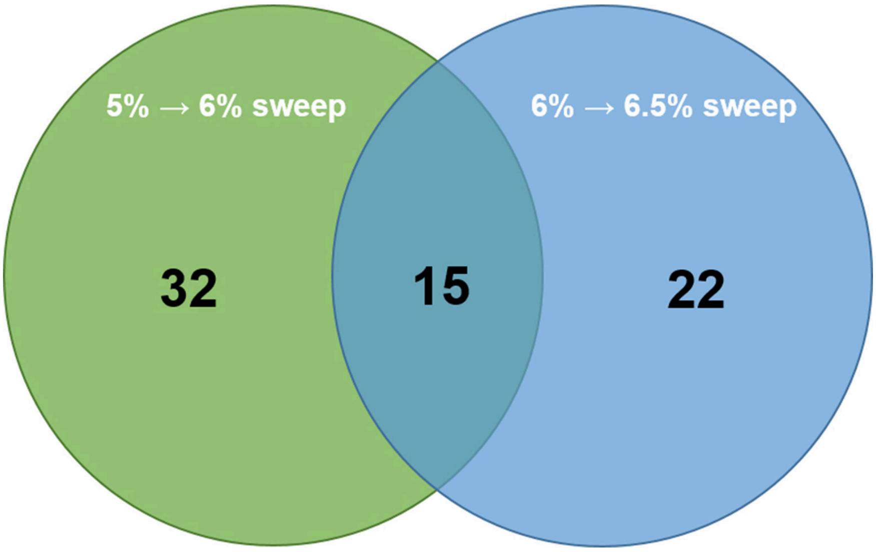

*Figure S6.7:* ***Degree to which pathways identified in the two distinct ethanol sweeps overlap.*** *For each selective sweep the identified connected network components identified by IAMBEE are represented. If two connected components identified in distinct sweeps overlapped in two or more genes this component was considered to overlap between both sweeps. Mutations in overlapping network components are likely to driving the adaptation to higher ethanol tolerance, while components unique to one of the two selective sweeps are likely necessary for either early adaptation or fine-tuning higher tolerance in later steps of the evolution.*

# 7

# Mutual exclusivity to detect cancer driver genes

## 7.1 Introduction

This chapter presents the development of SSA-ME, a network-based method which can analyze large genomic datasets in the context of cancer. SSA-ME uses the concept of mutual exclusivity to patterns of mutual exclusive mutated genes within the dataset. As mutual exclusivity is computationally expensive to calculate, SSA-ME uses a biological interaction network and a reinforcement learning heuristic to restrict the search space and produce an approximate but adequate result within reasonable time. SSA-ME was tested on all cancer datasets belonging to PAN-cancer [55] and was able to predict the involvement of a couple of rarely mutated genes.

SPT, **BW**, DDM and KM conceived the study. SPT, **BW** and DDM developed the SSA framework. SPT and **BW** developed, tested and analyzed the performance of the SSA application to mutual exclusivity. SPT, BW and KM wrote the manuscript. All authors reviewed the manuscript.

## 7.2 Paper

# SSA-ME Detection of cancer driver genes using mutual exclusivity by small subnetwork analysis

Pulido-Tamayo, S.†, **Weytjens, B.**†, De Maeyer, D., Marchal, K. (**2016**). SSA-ME Detection of cancer driver genes using mutual exclusivity by small subnetwork analysis. Scientific Reports, 6: 36257.

† these authors contributed equally to this paper

### 7.2.1 Abstract

Because of its clonal evolution a tumor rarely contains multiple genomic alterations in the same pathway as disrupting the pathway by one gene often is sufficient to confer the complete fitness advantage. As a result, many cancer driver genes display mutual exclusivity across tumors. However, searching for mutually exclusive gene sets requires analyzing all possible combinations of genes, leading to a problem which is typically too computationally complex to be solved without a stringent a priori filtering, restricting the mutations included in the analysis. To overcome this problem, we present SSA-ME, a network-based method to detect cancer driver genes based on independently scoring small subnetworks for mutual exclusivity using a reinforcement learning approach. Because of the algorithmic efficiency, no stringent upfront filtering is required. Analysis of TCGA cancer datasets illustrates the added value of SSA-ME: well-known recurrently mutated but also rarely mutated drivers are prioritized. We show that using mutual exclusivity to detect cancer driver genes is complementary to state-of-the-art approaches. This framework, in which a large number of small subnetworks are being analyzed in order to solve a computationally complex problem (SSA), can be generically applied to any problem in which local neighborhoods in a network hold useful information.

### 7.2.2 Introduction

Because of internationally coordinated efforts such as TCGA [55, 304] and ICGC [56], a vast number of cancer datasets are publicly available. Using these datasets to identify mutations and pathways driving cancer phenotypes has become an active field of research [165, 245, 305, 306].

Efforts to search for driver genes in cancer tend to use single-gene tests, e.g. identification of significantly mutated genes based on background mutation rates (MutSigCV [264], MuSiC [265]), identification of genes which are enriched in mutations with high functional impact (Oncodrive-FM [305]) or identification of genes involved in tumorigenesis based on the spatial distribution of their mutations (somInaClust [307]). Most single-gene methods heavily rely on recurrent mutations in single genes across samples, thereby risking to miss rarely mutated genes.

Other methods do not perform their analysis at single gene level, but at the level of gene sets by exploiting the clonal properties of cancer. Tumorigenesis and tumor progression follow a clonal evolutionary model [308–311]. This has two consequences: first different tumors evolve independently. It has been shown that different tumors evolve by triggering the same driver pathways but not necessarily by affecting the same genes. Tumors thus display recurrent mutations at pathway level rather than at single gene level. A second property of the clonal evolutionary model is mutual exclusivity. In this view, the disruption of a single gene in a molecular pathway often yields the complete fitness advantage associated with disruption of that pathway, making additional mutations in the same pathway redundant11. This evolutionary property can be exploited to understand cancer mechanisms and identify driver mutations by searching for groups of genes that display mutual exclusivity with each other (i.e. groups of genes which have mostly one mutation per tumor).

A first series of methods that analyze gene sets assume that, because of the clonal properties of cancer cells, recurrent mutations should occur at the pathway level rather than at single gene level. These methods search for gene sets rather than single genes that display a certain property (high functional impact score, high frequency of mutations) and that are closely connected on an interaction network. This connectivity constraint reduces the search space in possible number of genes sets that have to be evaluated. As these methods (e.g. HotNet2 [124]) rely on propagating information on an interaction network, they require information to be defined at the gene level (e.g. mutation frequency or gene scores).
A second series of methods make use of the mutual exclusivity property to analyze gene sets. They usually search for patterns of mutually exclusive genes (e.g. Dendrix [245], MultiDendrix [244] and CoMEt [312]). The identification of groups of genes showing mutual exclusivity across patients in large datasets has already been proven useful for the detection of driver mutations/pathways in single cancer types such as triple-negative breast cancer [313], Lung Adenocarcinoma [244] and in a pan-cancer setting [124, 314]. Due to the combinatorics properties of the problem, these methods apply stringent upfront filtering to be able to analyze the data.

Some methods combine both clonal properties i.e. they search for mutual exclusivity and for recurrently mutated pathways (sets of mutually exclusive genes that tend to occur in pathways). However, because the mutual exclusivity information can only be defined at the level of gene sets and not at the level of single genes, using the network does not sufficiently constrain the combinatorics of the problem. Because these methods have to analyze a large number of combinations of genes, the problem typically gets computationally too complex to be solved. Consequently, these methods use upfront filtering to reduce this computational complexity, thereby reducing the number of genes to analyze. Doing so, methods as MEMo [165] and mutex [269] filter upfront based on mutational frequency and are thus unable to take into account rarely mutated genes.

In order to provide a framework to assess mutual exclusivity while incorporating biological pathway information without the need for stringent upfront filtering, we developed SSA-ME (Small Subnetwork Analysis with reinforcement learning to detect driver genes using Mutual Exclusivity). SSA-ME is a computational tool that searches for genes that show mutual exclusivity and that are closely connected on an interaction network to prioritize drivers. It uses a novel methodology named Small Subnetwork Analysis with reinforcement learning (SSA) that divides a complex problem, i.e. finding driver genes that exhibit mutual exclusivity, into many simpler ones by calculating measures for mutual exclusivity in many small subnetworks. By solving these simpler problems iteratively, each time biasing the search space based on results of previous iterations, SSA-ME can prioritize potential driver genes with linear algorithmic complexity. This, in principle, allows it to process large input datasets in short computational times and therefore, in contrast to previous approaches, requires little upfront filtering.

To assess the performance of SSA-ME we analyzed each of the 12 TCGA Pan-Cancer tumor types [314]. Despite adding many more mutations to the input, we could prioritize well-known drivers that are found to be recurrently mutated in different tumors. However, in addition to prior findings we could prioritize several genes that displayed mutual exclusivity and pathway connectivity with well-known drivers, but that were rarely mutated in the different tumors and were missed by other methods that search for mutual exclusivity.

### 7.2.3 Results

#### 7.2.3.1 SSA-ME implementation

To identify cancer driver genes, we developed SSA-ME, a method that searches for small subnetworks of the interaction network containing mutated genes that show mutual exclusivity. SSA-ME approaches the complex problem of detecting driver genes by solving many independent and less complex sub-problems. In each sub-problem the method scores a set of genes which are close to each other in the interaction network for mutual exclusivity. SSA-ME scores many of these small subnetworks for their potential to contain genes exhibiting mutual exclusivity. Using these small subnetwork scores in a reinforcement learning framework allows prioritizing individual genes that are likely involved in the cancer phenotype.

The method is outlined in **Figure 7.1**. SSA-ME searches the local neighborhood around a set of predefined seed genes. In this case, the seed genes correspond to all genes mutated in at least one sample. In each iteration step of the algorithm, genes in the neighborhood of a seed gene are selected into a small subnetwork with a chance proportional to their gene scores (which are chosen to be uniformly distributed in the first iteration). These small subnetworks are subsequently scored based on the mutual exclusivity signal of the genes in each small subnetwork. Individual gene scores are updated proportional to the mutual exclusivity scores of the selected small subnetworks to which they belonged. Updating of the gene scores modifies the likelihood with which each gene will be selected in subsequent iteration steps. The iterative process continues until the method converges to a solution or a maximum number of iterations is reached. The output of SSA-ME consists of a ranked list of prioritized potential drivers supported by bootstrap and an interactive network visualizing the prioritized drivers together with supporting files compatible with Cytoscape [126].

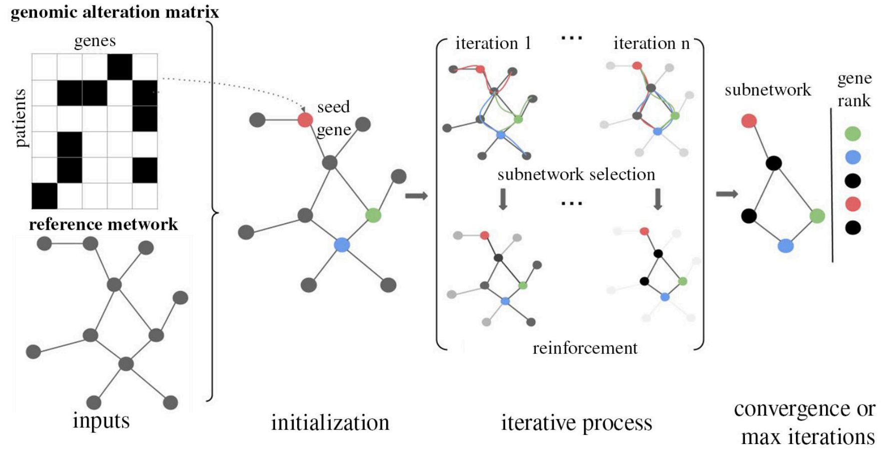

*Figure 7.1: **Overview of SSA-ME.** The input consists of a matrix containing genomic alterations (i.e. mutations or copy number alterations, among others) across patients (depicted as black tiles) and a human reference network. In a first initialization step, every gene which has at least one genomic alteration across all patients is selected as a seed gene (colored genes in the network). The gene scores (represented as the opacity of the genes in the networks) are uniformly set to a value of 0.5. In every subsequent iteration step, small subnetworks will be generated, starting at every seed gene. Every gene adjacent to the small subnetwork has a chance proportional to its score to be incorporated in the small subnetwork. When a certain size has been reached the small subnetwork generation will stop and a score for each selected small subnetwork will be calculated based on the mutually exclusivity pattern found within this small subnetwork. At the end of every iteration step these small subnetwork scores will be used to update gene scores, altering the chance of genes to be incorporated into the small subnetwork in subsequent iteration steps. Upon convergence it can be seen that a few genes have high scores while others have scores close to 0. Genes are ranked based on their gene scores which reflects their potential to belong to a mutual exclusivity pattern.*

#### 7.2.3.2 Performance on simulated data

To evaluate the robustness of the method with respect to the used reference network, we applied SSA-ME on a simulated dataset in combination with a high quality human reference network and underconnected/overconnected versions of this reference network (with respectively 10%, 25% and 50% of the network edges being deleted or added). Per network, 100 simulations were performed. Each simulated dataset contained a target gene set of mutually exclusive genes consisting of maximally 20 genes that are connected on the reference network and that were mutated in 30% of the samples (see **Materials and Methods**).

Applying SSA-ME on each simulated dataset resulted in a ranked gene list. The top x% of the gene list were considered as driver genes. Performance was evaluated by plotting the sensitivity versus the specificity where the sensitivity is defined as the percentage of genes belonging to the target gene set that was retrieved amongst the x% highest ranked genes and the specificity is defined as the proportion of genes not present in the target gene set that were correctly classified as non-drivers. The results are shown in **Figure 7.2 A** for the highest ranked genes as this is the range that is of biological relevance (correctly identifying positives). The full ROC plot and the sensitivity/PPV plots can be found in **Supplementary Figure S7.1**.

(**Figure 7.2 A**) indicates that the best performance is obtained using the reference network without added or deleted edges, as for the same relative increase in sensitivity less false positives are predicted (lower relative increase in 1-sensitivity). The method shows in general a high resilience of the results to using an overconnected network. In this case the method is capable of successfully prioritizing most of the genes in the mutually exclusive gene set with a low number of false positives (which is the range we envisage when only showing the values of the 1-specificty between 0 and 0.01). With an underconnected network the maximal sensitivity that can be reached will get restricted as some of the genes that show mutual exclusivity can no longer be connected in the network.

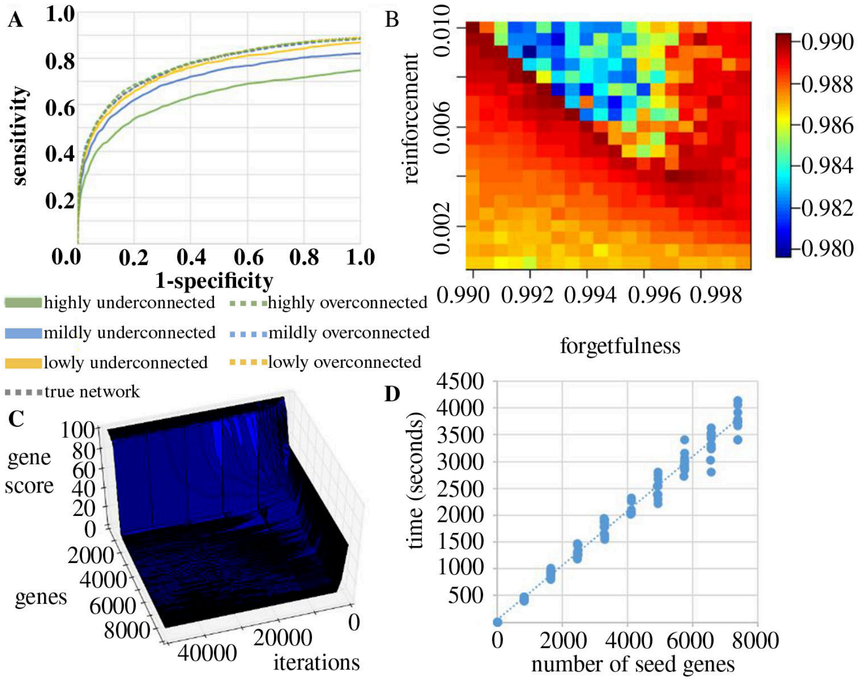

*Figure 7.2: **Performance on Simulated Data. A)** Robustness of the predictions with respect to the used reference network. The X-axis represents 1-specificity and the Y-axis represents sensitivity (ROC curve). Underconnected networks lead to lower performance while overconnected networks result in similar, although lower, performance as compared to the performances obtained with the original network. Note that, for clarity reasons, the range of the x-axis is restricted to [0, 0.01]. **B)** Heat map depicting parameter sensitivity. Area under the ROC curve (AUC) values for every analyzed parameter pair are depicted. Warm colors depict higher AUC values while cold colors depict lower AUC values. It can be seen that the best performance is achieved on the diagonal for combinations of reinforcement and forgetfulness of 1. **C)** Plot visualizing convergence and stability of convergence of gene scores. The X-axis represents the number of performed iterations, the Y-axis displays all genes in the reference network (black lines in the plot) and the Z-axis represents the gene scores. All genes start on the right side with a gene score of 0.5. Most of them converge fast to 0 or 1. As no inflecting lines are observed, convergence is stable. Results are shown on a plot depicting scores for all genes at every iteration step. **D)** Plot showing linear time complexity of the algorithm with respect to the number of seed genes. Each dot on the plot represents the time to convergence of a separate run. Per tested number of seed genes, 10 simulations were performed. Results were obtained by running the algorithm on one single processor Intel(R) Xeon(R) CPU E5-2670 0 2.60GHz.*

To assess the sensitivity of the method versus its parameter settings we ran SSA-ME on the same simulated data each time using a different combination of the reinforcement and forgetfulness parameters. Reinforcement determines the maximal value by which a gene score can be increased in the next iteration. Forgetfulness determines the fraction of the gene score that is retained in each subsequent iteration. Hereby reinforcement values were varied from 0.0005 to 0.0100 in steps of 0.0005. Forgetfulness values varied from 0.99 to 0.9995 in steps of 0.0005. Note that values of the forgetfulness closer to 1 imply that less is forgotten and values of reinforcement are consistently lower than the ones of the forgetfulness to ensure that only true positives will be reinforced. For each parameter combination 10 simulated datasets were analyzed. The performance per parameter combination was assessed using the mean value of the area under the ROC curve (**Figure 7.2 B**). In general, a low performance is obtained if the forgetfulness is relatively low compared to the reinforcement. In those settings false positives might become reinforced relatively more than some weak or isolated true positives. However, when the forgetfulness is close to 1, the performance is more robust to the choice of the reinforcement value. Alternatively, when the forgetfulness is too high compared to the reinforcement, true positives retain too little gene score which results in a more random selection of nodes, hence incorporating more false positives. Best performances were obtained on the diagonal where the sum of the values of $r$ and $f$ is close to one: $r$+$f$ = 1. In most cases, a combination where the sum of the reinforcement and the forgetfulness is higher than one results in lower performances because then again the reinforcement becomes relatively high compared to the forgetfulness, resulting in relatively more false positives.

To show that the method converges to a stable solution, we ran it on one simulated dataset for 50.000 iterations. **Figure 7.2 C** shows that the method exhibits a consistent behavior, i.e. after a gene obtains a high gene score, it will remain consistently high or vice versa. Furthermore, this figure shows that the algorithm converges, provided a sufficient number of iterations have been performed.

To analyze its complexity with respect to the number of seed genes, we ran SSA-ME on 10 different simulated datasets, each time using an increasing number of seed genes (ranging from 1 to 8000 genes). Datasets contained incrementally more added seed genes. Seed genes were added gradually according to the frequency with which they were found mutated in the different tumor samples, hereby assuming that the most frequently mutated genes are the ones that in a real setting would also be prioritized as the most promising seeds. These runs were repeated on 10 different simulated datasets. Results are visualized in **Figure 7.2 D** and clearly show the linear complexity of the algorithm with respect to the number of seed genes.

#### 7.2.3.3 Analysis of TCGA data

To test the biological relevance of SSA-ME, we applied it to each of the Pan-Cancer TCGA cancer datasets [314]. In this section we primarily focus on the well-studied Breast cancer dataset as a benchmark but also show the most interesting results of the Pan-Cancer analysis. All remaining Pan-Cancer TCGA results can be found in the online version of this paper.

For the analysis we used a high quality human interaction network (see **Materials and Methods**). As seed genes we used all genes carrying at least one somatic mutation or copy number alteration in any of the samples. After running SSA-ME, genes were prioritized as putative drivers based on their ranks by using a cut-off on the ranked list. This cut-off was chosen to provide a good trade-off between sensitivity and precision (i.e. an adequate positive predictive value (PPV) based on the genes present in the Cancer Gene Census (CGC) [315] as true positives) (**Figure 7.3 A**). Note that the PPV represents a lower boundary on the actual number of true positive predictions as all genes not present in the CGC are regarded as false positives. This is particularly true in this analysis because CGC defines known cancer genes merely based on their somatic mutational load: This excludes genes implicated in cancer based on expression values, epigenetics, germline variants and amplifications/deletions if it is deemed that the amplification/deletion cannot be attributed to a single or a few genes with a sufficient amount of evidence [315].

In the breast cancer dataset, we identified 34 potential driver genes. **Figure 7.3 B** displays these genes in the form of an interaction network where the nodes are genes and the edges are interactions connecting them. Because of the nature of the method this prioritized gene list contains putative drivers, but also linker genes that connect genes showing mutual exclusivity but that are not mutated themselves in any of the breast cancer samples. These linker genes are therefore not drivers within the available tumor samples, but have driver potential as they were found to connect drivers through the network.

Most of the prioritized genes (26 out of 34) have previously been mentioned in catalogues of genes implicated in cancer (CGC, NCG or the most relevant Malacard) (**Supplementary Table S7.1**). 2 genes of 26 (*CDC42* and *BCL2L1*) were selected as linker genes (i.e. did not display alterations in the breast cancer dataset). *CDC42* is a candidate cancer driver according to NCG and is also listed in the Breast cancer malacard. *BCL2L1* is mainly associated with colorectal cancer and lung cancer [316–318] through gene expression changes and is also selected as a driver mutation in other TCGA datasets (see below). This confirms the driver potential of the identified linker genes. Amongst the prioritized genes, 9 are rarely altered (in ¡ 1% of the samples, at most 10 alterations in the breast cancer dataset, i.e. *BCL2L1*, *CDC42*, *DDX5*, *AKT1*, *VAV2*, *EPHA2*, *CRK*, *UFD1L*, *NGFR* and *APC*), indicating our method is able to also prioritize genes with few genomic alterations. For genes with such low mutational load it is impossible to statistically or visually prove mutual exclusivity. These rarely mutated genes are retrieved by SSA-ME, despite having few mutations, when they exhibit at least partial mutual exclusivity with the surrounding genes in the network. If these surrounding genes exhibit sufficient mutual exclusivity with each other, the rarely mutated gene is selected based on its association with that pattern of mutual exclusivity. The fact that of the 10 rarely mutated genes, 5 (*BCL2L1*, *CDC42*, *DDX5*, *AKT1* and *APC*) are listed in cancer gene databases indicates such association-based selection is useful.

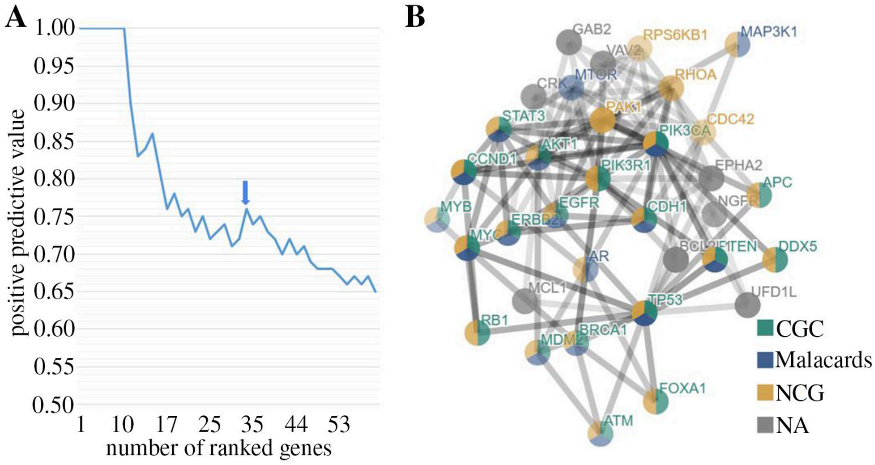

*Figure 7.3:* ***Application of SSA-ME on TGCA Breast Cancer dataset. A)*** *Determination of the number of genes to be prioritized as cancer drivers. Genes were ranked according to their gene score obtained by SSA-ME. The X-axis represents the number of genes in the list of prioritized genes obtained by setting a cut-off on the rank. The Y-axis represents the positive predictive value (PPV) for the genes present in each list that corresponds to a given rank threshold. The PPV is defined as the number of true driver genes prioritized divided by the number of prioritized genes. Note that the true driver genes are defined as all genes present in CGC. At the chosen threshold (arrow) 34 potential cancer drivers were prioritized.* ***B)*** *Subnetwork obtained after using SSA-ME on the TGCA breast cancer dataset. Genes are represented by nodes. If the gene had been associated with cancer, this is indicated by the color of the database in which the association was described. Gray genes correspond to genes not present in the Census of Cancer Genes, Malacards (breast cancer) or the Network of Cancer Genes database. The size of the node reflects the number of samples in which a gene was found mutated.*

To uncover the driving force behind the selection of the prioritized genes, the five small subnetworks with the highest mutual exclusivity scores (see **Materials and Methods**) were retained for each prioritized gene. As an illustrative example the mutual exclusivity pattern of the union of these networks is shown for *EPHA2*, one of the prioritized genes that was rarely mutated in breast cancer and not listed in any of the used reference cancer databases. The *EphA2* receptor is involved in multiple cross-talks with other cellular networks including EGFR, FAK and VEGF pathways, with which it collaborates to stimulate cell migration, invasion and metastasis [319]. We did prioritize *EPHA2* as a driver in breast cancer, despite its relatively low number of mutations. This because it showed (near) perfect mutual exclusivity with the well-known drivers *PIK3CA*, *GAB2*, *PAK1* and *RPS6KB* and all members of the PI3K pathway known to act downstream of *EPHA2*. These results were confirmed by the visualization of the mutual exclusivity patterns at pan-cancer level (**Figure 7.4**). The clear mutual exclusivity of *EPHA2* with the aforementioned genes at pan-cancer level are mainly due to the contribution of the Head and Neck squamous cell carcinoma tumor samples (HNSC) in which *EPHA2* was found to be more frequently mutated. Consistently, *EPHA2* was also highly prioritized by our analysis of the HNSC dataset (see Supplementary Material available in the originally published online version of this paper). The illustrative example shown in **Figure 7.4** also demonstrates that although SSA-ME is not designed to retrieve the largest mutual exclusive subnetwork, the selected small subnetworks that drive the selection of the prioritized genes do show mutual exclusivity. Note that *PAK1* and *GAB* are by definition not mutually exclusive as they belong to the same amplicon (see **Supplementary results**).

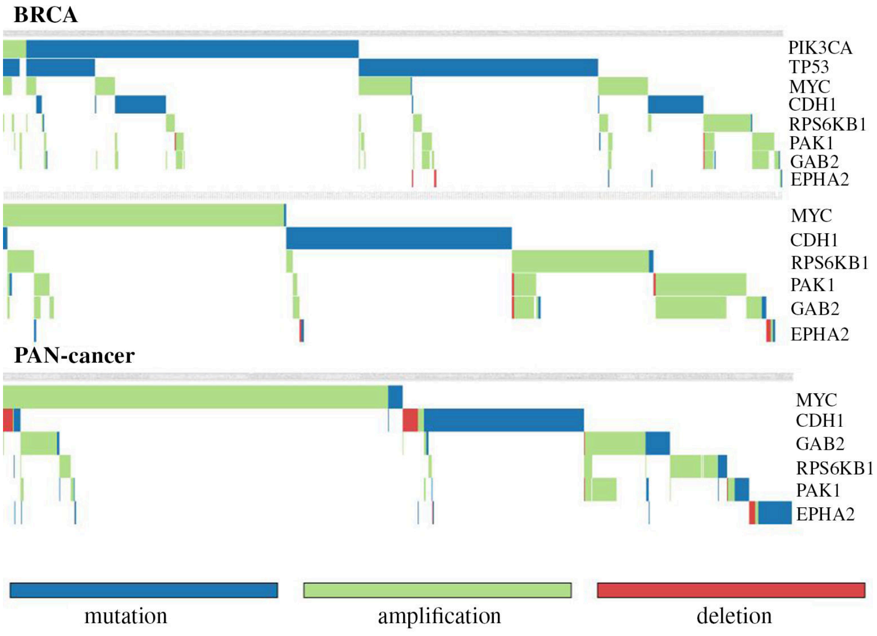

*Figure 7.4: **Mutual exclusivity pattern for EPHA2.**Green tiles depict copy number gains, orange tiles depict somatic mutations and red tiles depict losses of copy number. The top figure is the mutual exclusivity pattern for EPHA2 in the breast cancer dataset. The middle figure is the same pattern but with PIK3CA and TP53 left out in order to allow zooming in on the least frequently mutated genes. The bottom figure provides the pan-cancer view of the pattern detected in breast cancer (also with PIK3CA and TP53 left out). Patterns were created with Gitools [320].*

**Figure 7.5** shows that the somatic mutations carried by the 34 prioritized genes follow a CADD [321] score distribution significantly higher (Wilcoxon rank sum test, W= 44197000, p= 2.2x10-16) than the CADD score distribution of all present somatic mutations, pointing towards the functional relevance of at least some of the mutations carried by the predicted drivers. Of the 34 ranked genes, 10 genes were not listed in cancer gene databases (*VAV2*, *EPHA2*, *BCL2L1*, *CRK*, *GAB2*, *TPS6KB1*, *UFD1L*, *NGFR*, *MCL1* and *PAK1*) based on CGC version 77, NCG 5.0 or the Malacards Breast Cancer category version 1.11.724. To further investigate these putative cancer drivers, we compared the distributions of the mutual exclusivity scores of the small subnetworks derived from respectively the real and randomized data to which the putative driver genes belonged (**Supplementary**

**Figure S7.2**). These results indicate that the mutual exclusivity scores of the subnetworks from which the prioritized genes were derived were always significantly higher in the real than in the randomized data, even when accounting for the fact that the mutual exclusivity scores decrease globally when using randomized data (**Supplementary Table S7.2**).

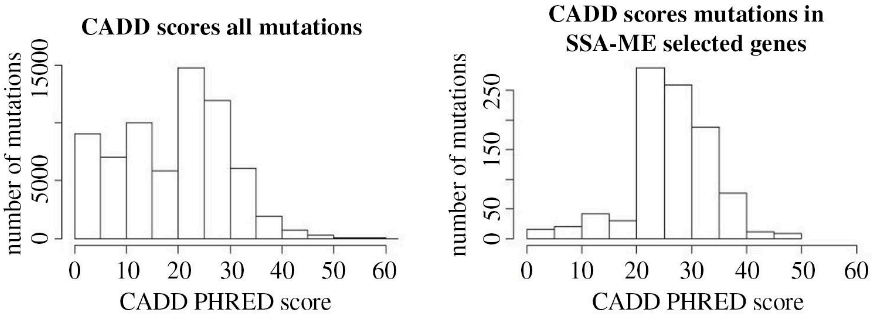

*Figure 7.5:* ***Analysis of selected genes.*** *CADD score distribution of all mutations (left histogram), and of the set containing the mutations in the genes prioritized by SSA-ME (right histogram). The X-axis depicts the CADD score and the Y-axis depicts the frequency of mutations having a CADD score within a certain range.*

We also ran SSA-ME on the remaining 11 Pan-cancer datasets (see supplementary materials in the online version of this paper). In order to identify promising candidate driver genes, we identified the genes that were recurrently prioritized as driver genes in different Pan-cancer datasets. Interesting prioritized genes include *VCAN* (identified in STAD, LUAD, BLCA and fell just out of PPV cutoff in UCEC), *UBE2I* (identified in OV, STAD and fell just out of PPV cutoff in HNSC) and *BCL2L1* (identified in OV, BLCA, COADREAD, LUAD, UCEC and LUSC). *BCL2L1* was selected in 7 out of 12 analyzed cancers. While it was selected as a linker gene in BRCA, it has primarily gain of copy numbers in OV, BLCA, COADREAD, LUAD, UCEC and LUSC. Further literature-based evidence for the most interesting putative driver genes from the BRCA dataset and the PAN-cancer dataset can be found in **Supplementary results** and **Appendix C** respectively.

#### 7.2.3.4 Comparison with other methods

To compare SSA-ME to other methods, we obtained the results of MutSigCV [264], MutSig2CV [322], Mutex [269] and Oncodrive-FM [305] when run on the TCGA Breast cancer data. MutSigCV and MutSig2CV are representatives of single-gene prioritization methods that test whether a gene is mutated more than expected by chance. Oncodrive-FM prioritizes by searching for genes that are enriched in mutations with a high functional impact. Mutex searches for mutual exclusivity modules using a reference network.

We used the positive predictive value using genes mentioned in CGC as true positives to compare the performance of the different methods to each other. These results are depicted in **Figure 7.6 A**. From this it can be seen that SSA-ME performs about equally well as its competitors given the evaluation criteria. In all cases the methods will be penalized for finding relevant novel predictions not present in CGC. As the known drivers might be biased towards unknown properties (e.g. mutational recurrence) it is hard to predict which methods will be affected most by false negatives in CGC. The relative under/over performance of certain methods over other methods should therefore be interpreted with care.

**Figure 7.6 B** shows to what extent the different methods prioritize the same genes. For each method we selected from the top 61 ranked genes (61 is the number of genes ranked by SSA-ME after bootstrapping on the top 100 ranked genes prior to bootstrapping) only those present in CGC and we show their overlap. We used genes present in CGC to reduce the number of false positives for this analysis. As expected, the more similar the concept of two methods, the more similar their results. The single gene methods MutSigCV and Mutsig2CV are comparable and SSA-ME shows the highest relative overlap with Mutex as both methods are network-based and use mutual exclusivity. However, in general SSA-ME selects several known cancer genes that were not selected by any of the other methods (58% of genes selected by SSA-ME), indicating the complementary of SSA-ME to the other methods in selecting drivers. The complementarity with single gene methods is understandable given that SSA-ME uses different properties (mutual exclusivity of a gene set rather than frequency-based properties of single genes). Part of the difference between SSA-ME and Mutex can be explained by the difference in filtering (we can find more genes as we do not need to apply a stringent criteria). Remaining differences might relate also to the fact that Mutex uses, as an integral part of the method, a directed signaling network different from the interaction network used by SSA-ME. Note that the genes selected by SSA-ME show a very low number of mutations in some genes. For example, of the 18 genes selected only by SSA-ME, 7 genes contained less than five mutations compared to just one of the 19 genes selected only by MutSig2CV and MutSigCV together. This indicates that SSA-ME is complementary to the other methods in finding rarely mutated driver genes.

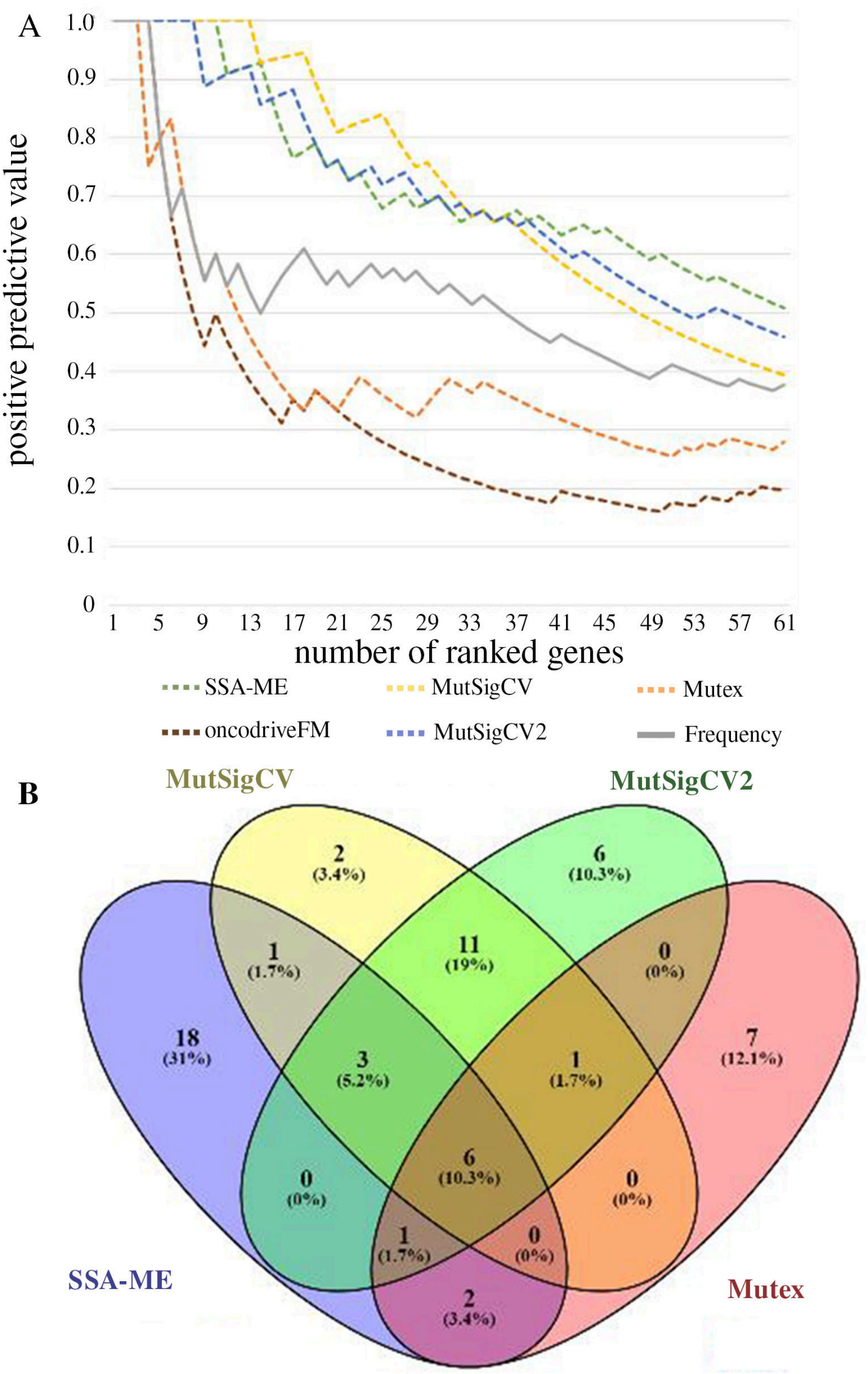

*Figure 7.6:* ***Comparison between SSA-ME and related methods. A)*** *The positive predictive value (PPV) of the results of multiple methods when analyzing the breast cancer dataset. The PPV is defined as the number of true driver genes prioritized divided by the number of prioritized genes. Note that the true driver genes are defined as all genes mentioned in CGC.* ***B)*** *Overlap of prioritized driver genes between the different methods. Venn diagram created with VENNY [323]*

A widely used method that is conceptually most similar to SSA-ME is MEMo as it also uses mutual exclusivity over an interaction network. However, we were not able to run MEMo on the used datasets so we could not directly include it in the comparison described above. In order to compare the results with MEMo, we ran SSA-ME on the 2012 TCGA BRCA data using the same criteria to filter the input data as was used in the original MEMo publication. It can be shown that we are able to find largely the same results in this case. The main advantage of SSA-ME compared to MEMo is that SSA-ME can be run on larger, much less stringently upfront filtered, datasets. The result of this comparison is in Supplementary Notes.

### 7.2.4 Discussion

We introduce SSA-ME, a tool for prioritizing cancer driver genes using mutual exclusivity with SSA (Small Subnetwork Analysis). SSA is a small subnetwork analysis technique with reinforcement learning which solves a complex combinatorial search problem over an interaction network by calculating, in this case, measures for mutual exclusivity in many small subnetworks. The framework can be generically applied to any problem in which local neighborhoods in a network hold useful information.

Here we applied SSA to prioritize cancer driver genes that are in each others neighborhood in the interaction network and at the same time display mutual exclusivity across different tumor samples (referred to as SSA-ME). To overcome the inherent high algorithmic complexity posed by its combinatorial nature, the problem of identifying drivers is iteratively solved and in each iteration multiple small subnetworks are independently analyzed for mutual exclusivity. All results of these small subnetwork analyses are used in subsequent steps to bias the search space. The advantage of splitting the complex problem into multiple less complex problems, is that SSA-ME is not restricted by the number of mutated genes in the input data. By circumventing the stringent filtering strategy that is required by most other methods to evaluate mutual exclusivity, SSA-ME can identify drivers that are rarely mutated. These mutations are normally lost when an upfront filtering is used based on the mutation frequency across samples.

When prioritizing drivers by searching for closely connected genes on an interaction network that exhibit mutual exclusivity, the incompleteness of the interaction network might lead to an underestimation of the number of potential driver genes. Missing edges in the interaction network could refrain the method from connecting some driver genes. Given we search for small subnetworks, our method shows resilience towards incomplete or underconnected networks as was shown by the simulated data and was able to find drivers even when mutual exclusivity had been heavily disrupted.

The search for small subnetworks comes at the expense of never explicitly searching for the largest patterns of mutual exclusivity. Such largest patterns of mutual exclusivity can only be approximated by merging small subnetworks with high scores to which a prioritized gene belongs. They provide a good approximation but there is no guarantee that all genes within such pattern are mutual exclusive with each other.

The performance of SSA-ME in terms of a positive predictive value based on known genes associated with cancer was comparable to widely used methods. An important observation is the fact that, while the SSA-ME and the other driver identification methods share some findings, SSA-ME was also able to prioritize a large number of genes not found by any other method, indicating the complementarity between SSA-ME and the other methods. In contrast to the single-gene methods, SSA-ME relies also on the use of the interaction network and mutual exclusivity. As compared to MEMo and Mutex, which use an interaction network and mutual exclusivity, SSA-ME is the only method that can deal with a large number of input mutations and is therefore able to use mutual exclusivity to drive the gene prioritization.

### 7.2.5 Materials and Methods

#### 7.2.5.1 SSA-ME

Small Subnetwork Analysis with reinforcement learning to detect driver genes using Mutual Exclusivity (SSA-ME) is an algorithm that uses an interaction network to detect driver genes by exploiting mutual exclusivity in cancer. To accomplish this, SSA-ME performs two independent functions in an iterative manner: small subnetwork selection/scoring and reinforcement learning. Each gene (node) in the interaction network is initialized with a uniform gene score. Then, iteratively: starting from a set of seed genes, small subnetworks are selected favoring genes with high gene scores. Each selected small subnetwork is then scored based on how well the genes composing the small subnetwork exhibit mutual exclusivity. Genes that consistently belong to small subnetworks with high mutually exclusivity scores are more likely to be selected in subsequent iterations. This will lead to high gene scores for genes which are involved in local gene sets showing mutual exclusivity, and therefore are possible drivers. The pseudocode describing the algorithm can be found in **Figure 7.7**.

**Initialization**
The algorithm is initialized by giving each gene (node) an initial gene score of 0.5. A static list of seed genes is defined that contains genes which are possibly driver mutations. Any type of biologically relevant filtering can be used to generate such gene list. In the context of this paper, seed genes are defined as all genes that were

found to be altered in at least one sample (tumor).

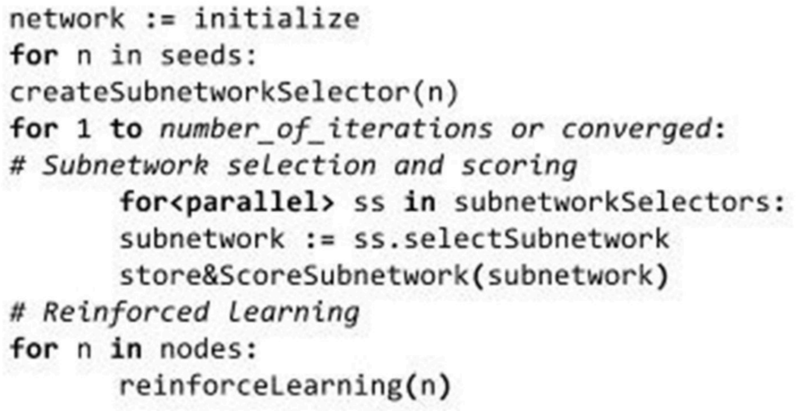

```
network := initialize
for n in seeds:
createSubnetworkSelector(n)
for 1 to number_of_iterations or converged:
# Subnetwork selection and scoring
      for<parallel> ss in subnetworkSelectors:
      subnetwork := ss.selectSubnetwork
      store&ScoreSubnetwork(subnetwork)
# Reinforced Learning
for n in nodes:
      reinforceLearning(n)
```

*Figure 7.7:* ***Pseudocode of SSA-ME algorithm.***

**Small subnetwork selection and scoring**

Within each iteration step small subnetworks of equal size are selected. Starting from every seed gene, subnetworks are selected by subsequently adding a gene which is connected to the current subnetwork, expressing the assumption that mutually exclusive genes are likely to be located in the same adaptive pathway. In order to evaluate gene sets of different sizes for mutual exclusivity, the size of the small subnetworks varies from 3 to 6 genes between iterations. The probability of adding a gene to a small subnetwork is proportional to the gene scores of genes connected to the small subnetwork. Once constructed, each small subnetwork receives a mutual exclusivity score (MES). Each sample (tumor) contributes to this score with a weight that is inversely related to the number of genes from the small subnetwork that were found mutated in that sample using following equation:

$$MES(sn) = \sum_{v \in V} \sqrt{\sum_{s \in S} \frac{1}{m(s,v,V)}} \tag{7.1}$$

Where *V* are the genes present in small subnetwork *sn* ordered according to the number of samples in which these genes were found to be mutated (from large to small). *S* is the set of samples pending to contribute to the mutual exclusivity score. Initially *S* includes every sample with a mutation in one of the genes in the small subnetwork, but every time a sample is used to calculate *m(s,v,V)* it is removed from *S*. In this way a sample can only contribute once to *MES(sn)*. *m(s,v,V)* is the number of genes in $V$ which are mutated in sample $s$ with the restriction that sample $s$ must have a mutation in $v$, otherwise sample $s$ is not yet used to calculate *m(s,v,V)*. *m(s,v,V)* will be equal to 1 if the genes in patient $s$ are all members of a perfect mutual exclusive pattern and $|V|$ if all genes in $s$ are also mutated in all other samples. The square root allows giving relatively higher mutual exclusivity scores to small subnetworks for which each gene is mutated in approximately the same number of samples (**Figure 7.8**). When an unambiguous ordering of the samples is not possible due to an identical number of mutated genes in multiple patients, *MES(sn)* is calculated for every possible ordering and the resulting *MES(sn)* is taken as the mean of these results. Next, the MES are ranked from highest to lowest and their ranks are divided by the maximum rank (**Figure 7.8**). We end up with a ranked MES (rMES) between zero and one where zero refers to the small subnetwork having the least evidence for mutual exclusivity and one refers to the small subnetwork having the most evidence for mutual exclusivity.

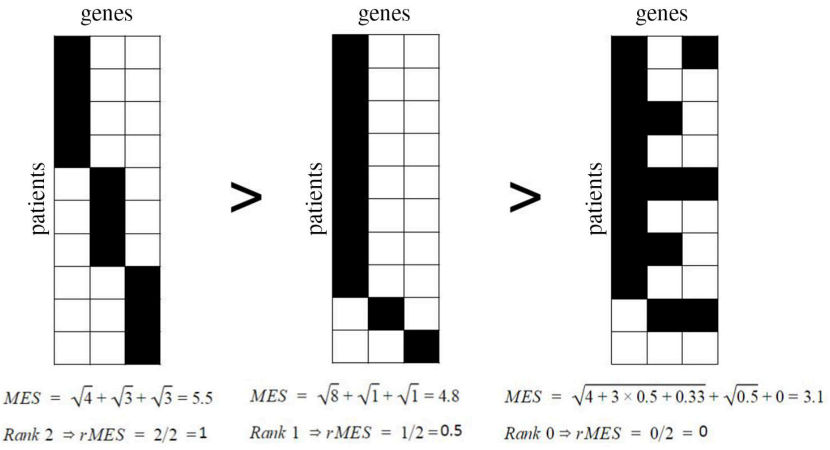

*Figure 7.8:* ***Calculation of MES and corresponding rMES scores for three different small subnetworks.*** *Genes which make up the small subnetwork are represented as columns, patients are represented as rows. Genes with alterations in a specific patient are depicted as black tiles. Small subnetworks exhibiting perfect mutually exclusivity patterns (two most left small subnetworks) have higher rMES scores than small subnetworks with non-perfect mutual exclusivity patterns (most right small subnetwork). Also, small subnetworks having a more uniform distribution of gene alterations across patients have higher rMES scores as shown by the two most left small subnetworks.*

### Reinforcement learning

Using the rMES for each small subnetwork, the reinforcement learning step updates gene scores based on two parameters: reinforcement and forgetfulness. The reinforcement is a parameter that determines the maximal value by which a gene score can be increased in the next iteration. The reinforcement is multiplied by the highest rMES score of all small subnetworks to which the gene belongs, so the gene score of genes which are consistently in small subnetworks with high rMES scores will further increase with iterations. The forgetfulness determines the fraction of the gene score that is retained in every subsequent iteration. This means that part of the gene score is effectively lost every iteration step and thus the gene scores of genes having persistently low scores will go to zero. To calculate gene scores, the following formula is used:

$$g_{i+1} = g_i * f * [1 + r * \max_{sn \in SN_g} rMES(sn)] \tag{7.2}$$

Where $\mathrm{g_i}$ is the gene score at iteration $i, f$ is the forgetfulness, $r$ the reinforcement and $\mathrm{SN_g}$ the set of small subnetworks containing the gene. If the gene score resulting from the formula is larger than 1, it is topped off at 1 as the maximal gene score can never be larger than 1. The default parameters of the method are forgetfulness $f$=0.995, reinforcement $r$=0.005 and 5000 iterations. In general, the sum of forgetfulness and reinforcement should be close to 1 and the reinforcement should be small (smaller than 0.01). This because small values for forgetfulness or large values for reinforcement would make the algorithm prone to stochastic effects. Note that genes which are not part of any small subnetwork are assigned a value of zero for *max rMES(sn)*.

In a final step we assign a rank to each gene that reflects the possibility of it being a driver gene. Hereto we exploit the fact that driver genes that exhibit mutual exclusivity tend to have a consistent increase in their gene score between iterations over time. Genes are ranked according to the maximal gene score they reach and in case of ties are based on how fast their score converges.

**Bootstrapping**

In order to eliminate predicted driver mutations which are likely artefacts of specific samples in the data, we perform a bootstrap analysis. Here, we randomly sample with replacement an equal number of tumor samples as in the original dataset and run SSA-ME on this new dataset. Each bootstrap dataset will contain some duplicate samples but will also lack some samples from the original dataset. For each dataset we generate and evaluate 1000 bootstrap datasets. We then evaluate these results by assessing at which minimal rank threshold (the rank threshold is the highest (worst) rank still considered in the calculation of the bootstrap support across all bootstrap results) a gene can attain a bootstrap support of 95% (selected in at least 95% of bootstrap results). We do this by gradually increasing the rank threshold. The final rank of the genes is based on the order in which this 95% bootstrap support is attained by the genes, the highest ranked gene being the gene which attained a bootstrap support of 95% using the most strict minimal rank threshold.

#### 7.2.5.2 Simulated data

To assess the performance of SSA-ME we used simulated data. The set of true positive driver genes was defined first by creating a target gene set of mutual exclusive genes which in biological terms corresponds to a driver pathway. The target gene set was generated using a random walker with restart (5% restart chance) to select genes from the local network neighborhood of a randomly selected gene until 20 interactions have been visited in a high quality human reference network. This high quality human reference network was composed of HINT [324] version 3, Interactome (HI-II-14) [325] and Reactome [326] interaction data.

To mimic real tumor data, we counted the number of mutated genes present in each tumor sample in the TCGA 2012 study and assigned an equal number of alterations to random genes, thus conserving the distribution of mutated genes per sample. We added mutually exclusive mutations to genes present in the target gene set in 30 % of the samples. Each sample had 5% chance to also be mutated in any of the other genes belonging to the mutually exclusivity gene set as we allowed for non-perfect mutual exclusivity module.

To evaluate the robustness of the method with respect to the used reference network, multiple simulated datasets were analyzed for different degrees of connectedness in the high quality human reference network: highly underconnected (50% of the edges were deleted from the reference network), mildly underconnected (25% of the edges deleted), lowly underconnected (10% edges deleted), original network (i.e. the high quality human reference network), lowly overconnected (10% additional random edges added to the reference network), mildly overconnected (25% additional edges) and highly overconnected (50% additional edges). We generated 100 different simulated datasets per network and ran SSA-ME. Performance was measured by receiver operating characteristic (ROC) curves.

To assess parameter sensitivity, we tested the effect of using different parameter combinations on the performance. This included 400 simulations for all combinations of reinforcement r (from 0.0005 to 0.0100 in steps of 0.0005) and forgetfulness f (from 0.99 to 0.9995 in steps of 0.0005). Performance for each parameter combination was measured using the area under the curve (AUC).

#### 7.2.5.3 TCGA Data

TCGA data was downloaded from GDAC Firehose [327–329]. We used somatic mutations annotated by MutatorAssesor [330] together with copy number alterations (CNAs) inferred with GISTIC [331]. We removed samples containing more than 500 genomic alterations to avoid taking into account hypermutator samples. In our analysis only copy number altered genes in samples with high-level thresholds (threshold 2 in GISTIC) for amplifications/deletions and for which copy number alteration showed a positive correlation ($q < 0.05$) with expression data were used. Prioritization results were obtained by running SSA-ME on a non-stringently filtered input set, consisting of all genes having at least one genetic alteration (mutation or amplification/deletion) in the dataset. As a high quality human reference network we compiled information data from HINT [324] version 3, Interactome (HI-II-14) [325] and Reactome [326]. Results for MutSigCV and MutSig2CV were downloaded from GDAC Firehose [332, 333]. Results for Mutex were taken from supplementary of the original paper [269]. Results for Oncodrive-FM were obtained by running Oncodrive-FM using default settings and functional impact scores (SIFT [334], mutation assessor [330] and PolyPhen2 [335]).

#### 7.2.5.4 Patterns of mutual exclusivity

SSA-ME searches for small subnetworks that display a high degree of mutual exclusivity. To visualize the patterns of mutual exclusivity for any prioritized gene, SSA-ME selects the five best subnetworks (with highest MES score) to which that prioritized gene belongs. In many cases the five best small subnetworks to which the prioritized gene belongs, overlap and thus the union of these genes is used as a pattern of mutual exclusivity with the prioritized gene. However, as we do not explicitly impose the constraint that within such a union there should be mutual exclusivity, there is no guarantee that all genes within the retrieved pattern are mutually exclusive. It is perfectly possible that such a union consist of two separate patterns of mutual exclusivity, each involving the prioritized gene.

### 7.2.6 Acknowledgements

The authors would like to thank Lieven Verbeke for the useful comments and discussions.

Funding: Ghent University Multidisciplinary Research Partnership Bioinformatics: from nucleotides to networks; Fonds Wetenschappelijk Onderzoek-Vlaanderen (FWO) [G.0329.09, 3G042813, G.0A53.15N]; Agentschap voor Innovatie door Wetenschap en Technologie (IWT) [NEMOA and the personal fellowship of Dries de Maeyer]; Katholieke Universiteit Leuven [PF/10/010] (NATAR)

### 7.2.7 Additional Information

The authors declare no competing financial interests.

### 7.2.8 Availability of materials and data

SSA-ME software is available at https://github.com/spulido99/SSA. CADD scores version 1.3 were downloaded from http://cadd.gs.washington.edu/. The TCGA Pan-Cancer datasets are publicly available at https://gdac.broadinstitute.org/.

# Supplementary

## 7.2.9 Supplementary results

### 7.2.9.1 Comparison with MEMo

In order to compare the results of SSA-ME with those of MEMo, a method that searches for mutual exclusivity patterns using an interaction network, we obtained the results from MEMo on the TCGA 2012 breast cancer dataset [304] and ran SSA-ME on the same TCGA 2012 dataset, which was obtained directly from the TCGA breast cancer analysis portal. To maximize comparability between our results and those of MEMo, we reproduced to the best possible extent the filtering approach and network of the original MEMo study to run SSA-ME.

The used network is a non-curated network consisting of Reactome [326], Panther [336], KEGG [337], INOH [338] and interactions from non-curated sources like high-throughput derived proteinprotein interactions, gene co-expression, protein domain interaction, GO annotations, and text-mined protein interactions [339]. The genetic alteration data was prepared according to the description in the original paper, i.e. only retaining genes that were altered in at least ten samples.

Just like Mutex, MEMo is primarily designed to detect patterns of mutual exclusivity but does not explicitly extract drivers. To compare the results of MEMo with these of SSA-ME and because of the high similarity of the mutual exclusivity patterns detected by MEMo in the original paper (patterns consisting of maximally 8 genes that varied in most cases in no more than one gene), we collapsed the 23 genes of all patterns found by MEMo and depicted them as a network (**Supplementary Figure S7.3 A**). The subnetwork obtained by SSA-ME consisted of 33 genes (applying a FDR cutoff, as described in the main text) of which 18 were also found in the MEMo network (**Supplementary Figure S7.3 B**). 5 genes retrieved by MEMo were not detected by SSA-ME: 3 genes (*NBN*, *CHECK2* and *MDM4*) because they were no longer present in the filtered list we used as input, whereas they must have been present in the original input of MEMo: in contrast to what has been described in the original TGCA paper we found these genes to be mutated in less than 2 samples and therefore removed them from our analysis, the score of *ATM* just fell below the chosen threshold of the ranked list of SSA-ME (*ATM* ranked 36 whereas with the chosen cut-off we only retained the 33 top ranked genes) and *ATK3* was truly missed in our analysis as the small subnetworks to which it belonged never received consistently high scores during subsequent iteration steps.

On the other hand, we found 10 additional genes that were not retrieved by MEMo. Some of these additional genes had previously been associated to breast cancer (*AR* and *ESR1*) or to cancer in general (*MUC4* and *CCDN1*). The reason why we detect more genes than MEMo is partially due to the choice of the cutoff, but also because of the inherent differences in selection criteria between the methods: MEMo searches for patterns of mutual exclusivity in which all genes need to be mutually exclusive which each other (have to pass a permutation test) whereas the mutual exclusivity criteria of SSA-ME are less stringent. Also, our method does not require stringent filtering which leaves the possibility of selecting rarely mutated genes.

These results thus show that SSA-ME is able to reproduce largely the same results as MEMo, provided the same input data are used. Genes that are highly ranked by MEMo are also highly ranked by SSA-ME.

#### 7.2.9.2 Literature-based evidence for predicted cancer drivers in the breast cancer dataset

Of the 34 ranked genes, 8 genes were not listed in cancer gene databases (*MCL1*, *GAB2*, *RPS6KB1*, *CRK*, *NGFR*, *EPHA2*, *VAV2* and *UFD1L*) based on CGC version 77, NCG 5.0 or the Malacards Breast Cancer category version 1.11.724. These genes are discussed below. Some of these are well known cancer drivers not reported in CGC, because they contain CNVs rather than somatic mutations. For selected genes which are not listed in cancer gene databases, for which the mutations are mainly SNPs and which have at least 20 SNPs in all pan-cancer datasets combined (to ensure the pattern can be visually convincing), we show the uncovered mutual exclusivity profiles (*EPHA2* and *VAV2* showed).

*MCL1* was found frequently (64 times) amplified in the dataset. *MCL1* is involved in apoptosis modulation and signaling [340]. Its alterations by CNVs have been reported in literature before [341]. It has been associated with a number of cancers because of its involvement in the regulation of apoptosis versus cell survival [342].

Both *GAB2* and *PAK1* were frequently amplified (respectively 58 and 61 times) in the TCGA breast cancer dataset. Both genes belong to the same amplicon as the well-known breast cancer driver *CCND1* [343], which was in concordance also frequently amplified. However, because it cannot be excluded that more genes in the same amplicon are causal to cancer and because *CCND1*, *GAB2*, and *PAK1* each show a strong mutual exclusivity with a subset of selected genes closely related in the network, each of them might act independently from one another as a true driver. Whereas both *CCND1*, a regulatory protein involved in mitosis, and *PAK1*, a protein belonging to the family of serine/threonine p21-activating kinases that are involved in cytoskeleton reorganization and nuclear signaling, have been reported in at least one of the cancer related databases, *GAB2* is not. *GAB2* was prioritized because of its mutual exclusivity and close network connectivity with amongst others *PIK3CA*, *PTEN* and *EPHA2* (**Figure 7.4**). *GAB2* is a scaffolding adapter protein that transduces cellular signals between receptors (tyrosine kinase receptors) and intracellular downstream effectors (*PI3K*, *SpH2*) and is required for efficient *ErbB2*-driven mammary tumorigenesis and metastatic spread by acting downstream of *ErbB2* [321, 344]. Interestingly, it was also shown that a focal amplification of *GAB2* independently of *CCND1* in breast tumors contributes to diverse oncogenic phenotypes in breast cancer by activating, amongst others, the PI3K pathway, further confirming the role of *GAB2* as primary driver in breast cancer [345].

*RPS6KB1* was found to be frequently (77 times) amplified in the TCGA breast cancer dataset. *RPS6KB1*, encoding a ribosomal S6 kinase 1 (S6K1) is a member of the frequently mutated PI3K pathway and has been reported to be involved in cell proliferation and protein translation. A link between the S6K1 function and cancer was suggested by the finding that *RPS6KB1* resided in the chromosomal region 17q22-17q23 and was often amplified in lung and breast cancers [346,347].

Other genes we prioritized were not listed in cancer gene databases but were previously associated with cancer because of their expression behavior expression.

The signaling adaptor protein *Crk* has been shown to play an important role in various human cancers. In the used breast cancer dataset *CRK* only had one SNP. The CRK family proteins all act as molecular bridges between tyrosine kinases and their substrates and modulate the specificity and stoichiometry of signaling processes. Evidence suggests that cellular Crk proteins are overexpressed in human tumors and that expression levels correlate with aggressive and malignant behavior of cancer cells [348]. Using RNAi-mediated knockdown, Fathers et al. [349] have shown in their study that *CRK* is required for cell migration and invasion of metastatic breast cancer cells in vitro and for metastatic growth in vivo. However, a mechanistic understanding of Crk proteins in cancer progression in vivo is still lacking, partly because of the highly pleiotropic nature of Crk signaling [350].

*NGFR* (nerve growth factor receptor). It had 1 SNP in the BRCA dataset. *NGFR* inactivates p53 by promoting its *MDM2*-mediated ubiquitin dependent proteolysis and by directly binding to its central DNA binding domain and preventing DNA-binding activity. Biologically, cancer cells hijack the negative feedback regulation of p53 by *NGFR* to their growth advantage, as down regulation of *NGFR* induces p53-dependent apoptosis and cell growth arrest as well as suppressed tumor growth [351]. Overexpression of *NGFR* has been observed in many metastatic cancers and promotes tumor migration and invasion [352–354].

The *EphA2* receptor is involved in multiple cross-talks with other cellular networks including EGFR, FAK and VEGF pathways, with which it collaborates to stimulate cell migration, invasion and metastasis [355]. It had 7 mutations in the BRCA dataset (3 SNPs, 1 amplification and 3 deletions). While its overexpression has been correlated to stem-like properties of cells and tumor malignancy as for instance in colon cancer, less information is available on the role of *EPHA2* as a driver gene. We did prioritize *EPHA2* as a driver in breast cancer, despite its relatively low number of mutations. This because it showed (near) perfect mutual exclusivity with, amongst others, the well-known drivers *PIK3CA*, *PTEN*, *GAB2* and *RP6KB1*, and all members of the PI3K pathway known to act downstream of *EPHA2*. A recent study shows that rare SNPs in receptor tyrosine kinases, amongst which *EPHA2*, can be associated with negative outcome. This further points towards the clinical relevance of these less frequently mutated drivers [356]. See (**Figure 7.4**) for the retrieved mutual exclusivity pattern of EPHA2 in BRCA and in all pan-cancer datasets.

*VAV2* was also prioritized in the breast cancer dataset but rarely mutated (only 2 mutations in BRCA). *VAV2* is a gene involved in altering cell shape and migration and has previously been associated with metastasis in breast cancer [304]. It was prioritized because of its association with *PIK3CA* and *ERBB2*, a signaling subnetwork that was shown in literature to be involved in ovarian tumor cell migration and growth through activation of PI3K in HER2 ovarian tumors. This activation leads to the recruitment of actin and actinin to *ERBB2*, which then colocalizes with the VAV2 guanine nucleotide exchange factor to induce Rac1 and Ras signaling and the concomitant activation of ovarian tumor cell migration and growth [357]. See (**Supplementary Figure S7.4**) for the retrieved mutual exclusivity pattern of *VAV2*.

*UFD1L* was prioritized in BRCA but has only 1 SNP. As there is only limited evidence to support the involvement of *UFD1L* in tumorigenesis [358] we cannot rule out *UFD1L* is a false positive.

### 7.2.10 Supplementary figures and tables

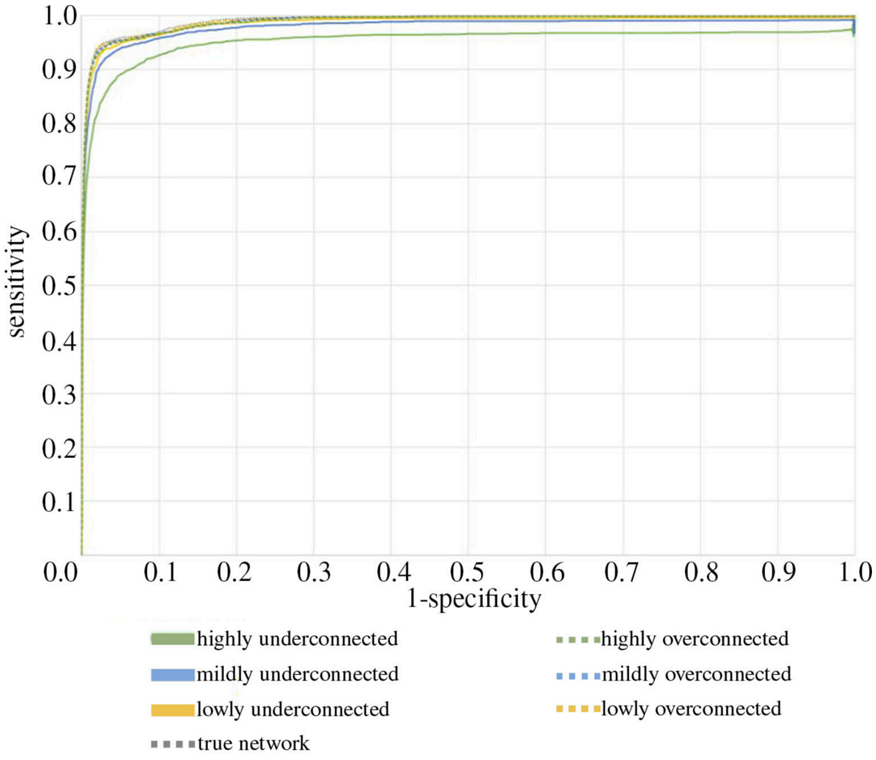

*Figure S7.1:* ***Robustness of the predictions with respect to the used reference network.*** *The X-axis represents 1-specificity and the Y-axis represents sensitivity. Underconnected networks result in a lower performance while overconnected networks result in similar, although lower, performance to the true network. Complete ROC curve.*

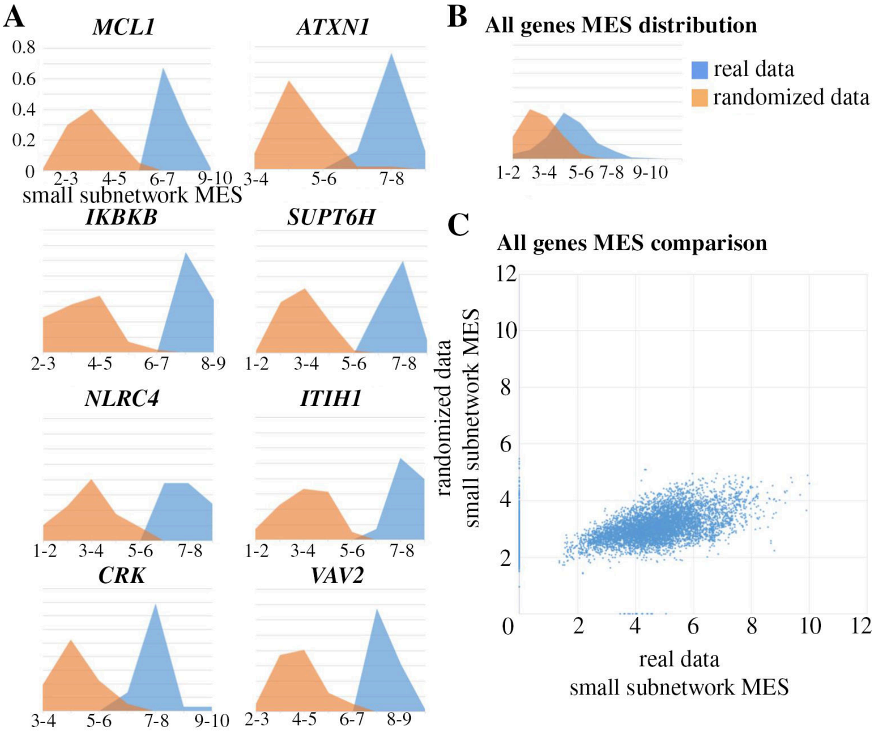

*Figure S7.2:* ***Differences in mutual exclusivity scores of small subnetworks derived from respectively real and randomized datasets.*** *Note that in order to have complete information about the mutual exclusivity scores of the small subnetworks to which a specific gene can be assigned we, for each randomized dataset and also for the real data, ran the algorithm 100 times and each time retained the mutual exclusivity score of the subnetwork with which that gene is associated upon convergence of the method. This leads to the score distributions depicted in these figures.* ***A)*** *Distributions of mutual exclusivity scores of the small subnetworks in randomized datasets (orange) and the real dataset (blue) for some putative driver mutations prioritized by SSA-ME.* ***B)*** *Distribution of mutual exclusivity scores of the small subnetworks in randomized datasets (orange) and the real dataset (blue) for all genes.* ***C)*** *Graph showing per gene the average score of the small subnetworks it belonged to upon convergence of the algorithm as derived from the real data (X-axis) and from the randomized data (Y-axis). Mutual exclusivity scores are normalized by the size of the small subnetworks. Randomization were performed by shuffling gene names. See (**Supplementary table S7.2**) for the confidence intervals of the differences in mutual exclusivity scores between randomized datasets and the real dataset for the putative driver genes and all genes together.*

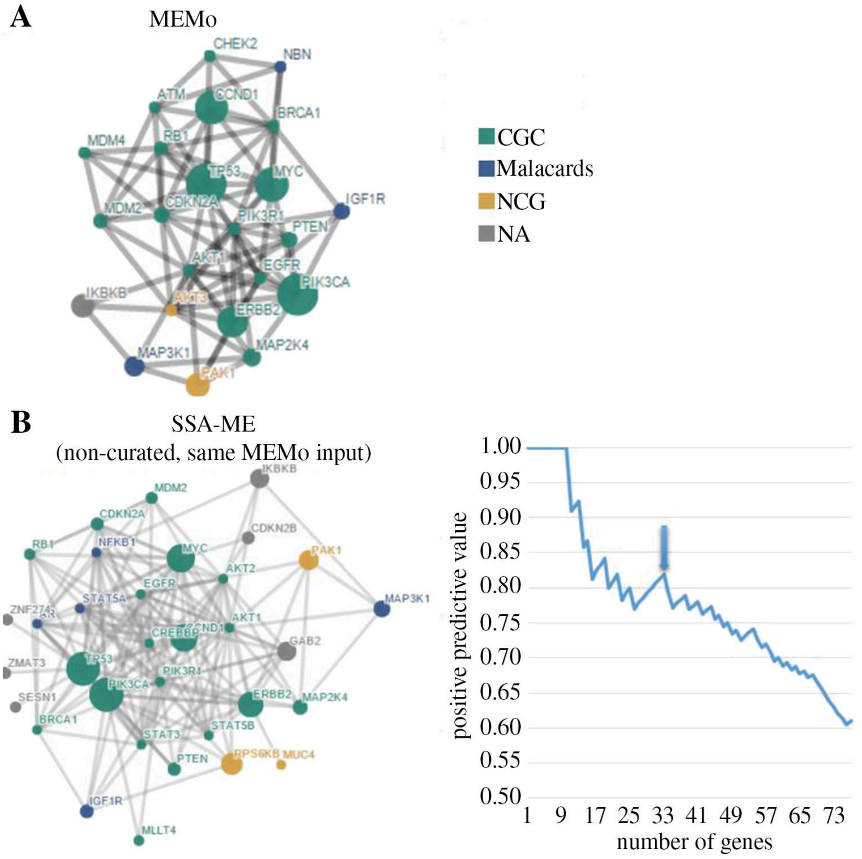

*Figure S7.3: **Comparison between SSA-ME and MEMo.** Prioritized driver networks obtained by MEMO as retrieved from the original mutually exclusive modules outlined in the breast cancer TCGA paper (**Panel A**) and obtained by SSA-ME using the filtered data (**Panel B**). Genes are represented as nodes. Colors refer to the databases in which associations of the indicated genes with breast cancer or cancer have been described. Gray genes were not found to be associated with breast cancer/cancer according to the used reference databases. The right figure in panel B represents the PPV analysis of results obtained by SSA-ME. The Y-axis represents the PPV according to the reference databases. The X-axis represents the number of genes in lists of prioritized genes of increasing order. The size of the gene list was determined by ranking the genes according to their gene scores and counting the number of genes with a rank lower than a given threshold. The Arrow indicates the thresholds that was chosen to select the genes in the network. We choose the threshold on the ranked list so that an adequate trade-off between sensitivity and precision was obtained.*

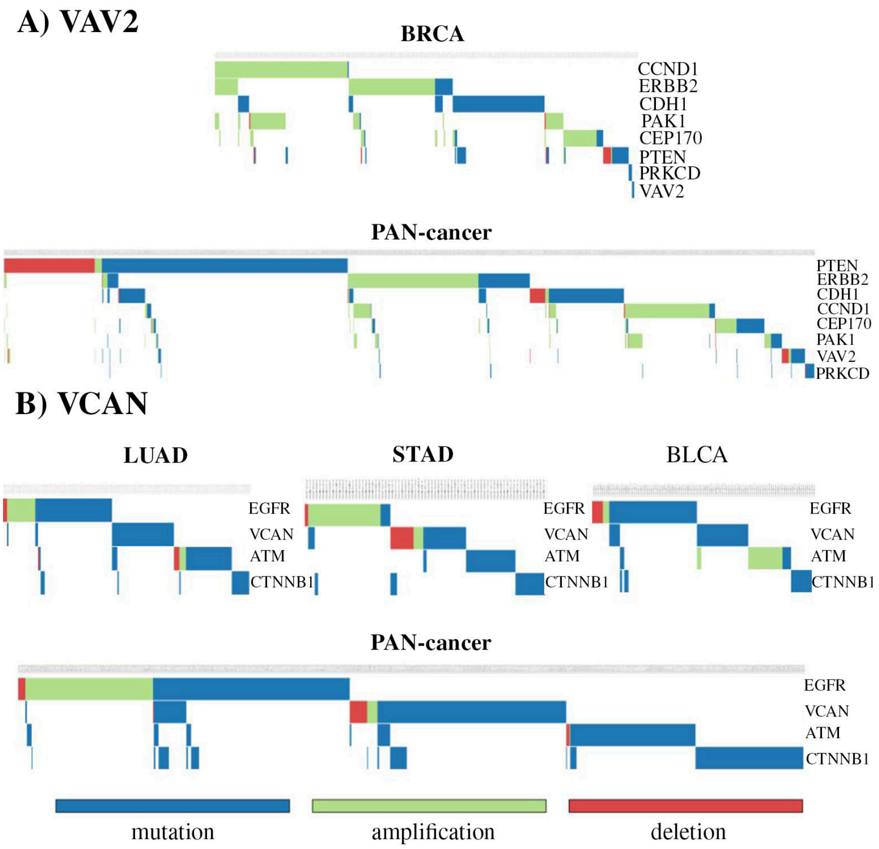

*Figure S7.4:* ***Mutual exclusivity patterns of selected genes.*** *Green tiles depict copy number gains, blue tiles depict somatic mutations and red tiles depict losses of copy number for all these patterns.* ***A)*** *Mutual exclusivity pattern of VAV2. The top figure visualizes the pattern in the BRCA dataset in which the pattern was originally detected. The bottom figure provides the pan-cancer view of the same pattern. TP53 and PIK3CA, which were also part of the pattern, were omitted from the visualization to allow zooming in on the less frequently mutated genes.* ***B)*** *Mutual exclusivity patterns of VCAN. Top panel shows the pattern in each of the three pan-cancer datasets in which the pattern was prioritized (LUAD, STAD and BLCA). The bottom figure provides the pan-cancer view of the same pattern. The genes shown correspond to the intersection of the genes present in the 5-best small subnetworks which showed highest mutual exclusivity values for each dataset in which VAV2 was prioritized (LUAD, STAD and BLCA). TP53 which was also part of the pattern but was omitted from the visualization to allow zooming in on the less frequently mutated genes.*

*Table S7.1:* ***Ranked genes for the BRCA dataset.*** *For every gene it was checked if it was present in a database of known (or putative) cancer genes (CGC,NCG or Malacards).*

| GeneSymbol | CGC | NCG | Malacards |
|---|---|---|---|
| PIK3CA | TRUE | TRUE | TRUE |
| TP53 | TRUE | TRUE | TRUE |
| CCND1 | TRUE | TRUE | TRUE |
| MYC | TRUE | TRUE | TRUE |
| PTEN | TRUE | TRUE | TRUE |
| PAK1 | FALSE | TRUE | FALSE |
| PIK3R1 | TRUE | TRUE | FALSE |
| CDH1 | TRUE | TRUE | TRUE |
| DDX5 | TRUE | TRUE | FALSE |
| ERBB2 | TRUE | TRUE | TRUE |
| RPS6KB1 | FALSE | TRUE | FALSE |
| UFD1L | FALSE | FALSE | FALSE |
| RB1 | TRUE | TRUE | FALSE |
| APC | TRUE | TRUE | FALSE |
| STAT3 | TRUE | TRUE | TRUE |
| GAB2 | FALSE | FALSE | FALSE |
| EPHA2 | FALSE | FALSE | FALSE |
| FOXA1 | TRUE | TRUE | FALSE |
| EGFR | TRUE | TRUE | TRUE |
| VAV2 | FALSE | FALSE | FALSE |
| MAP3K1 | FALSE | TRUE | TRUE |
| CRK | FALSE | FALSE | FALSE |
| BRCA1 | TRUE | TRUE | TRUE |
| AKT1 | TRUE | TRUE | TRUE |
| NGFR | FALSE | FALSE | FALSE |
| MDM2 | TRUE | TRUE | TRUE |
| RHOA | FALSE | TRUE | FALSE |
| MCL1 | FALSE | FALSE | FALSE |
| MYB | TRUE | TRUE | TRUE |
| ATM | TRUE | TRUE | TRUE |
| CDC42 | FALSE | TRUE | FALSE |
| BCL2L1 | FALSE | FALSE | FALSE |
| MTOR | FALSE | FALSE | TRUE |
| AR | FALSE | TRUE | TRUE |

*Table S7.2:* ***95% confidence intervals for the difference in mutual exclusivity scores between randomized data sets and the real data set.****Note that, as the 95% confidence intervals of any putative driver gene does not overlap with the 95% confidence interval of all genes together, the putative driver genes are involved in small subnetworks with significantly higher mutual exclusivity scores than expected by chance.*

| **GENE** | | **95% confidence Interval** |
|---|---|---|
| all data | 1.777 | 1.788 |
| MCL1 | 4.940 | 5.594 |
| VAV2 | 3.344 | 3.843 |
| CRK | 2.519 | 2.958 |

## 7.3 Critical reflections and future work

The above manuscript shows that a method which uses an interaction network to find sets of genes that are mutually exclusive in a (large) population of cancer patients is useful and that an objective function to uncover such gene sets, that trades of mutual exclusivity and coverage, is adequate to fulfill this task.

While the proposed method has proven its value, after publication algorithm was reassessed and certain aspects were identified which could be improved. As this would benefit the general applicability of the method and possibly allow the method to analyze larger datasets with higher accuracy and precision, these aspects are being re-implemented at the time of writing in the form of a new algorithm which nevertheless adheres to the same foundations as SSA-ME, being the trade-off between mutual exclusivity and coverage. This section enumerates and discusses these aspects.

In order to solve the highly combinatorial problem of finding sets of genes which exhibit mutual exclusivity, SSA-ME uses a reinforcement learning approach based on the ideas of ant colony optimization which were originally applied to solve the traveling salesman problem, which is also a combinatorial problem [359, 360]. As explained in the manuscript, this involves a multitude of agents which traverse the network in multiple rounds and in each round decide which edges to take based on a dynamic gene score which is assigned to the nodes. At the end of each round the gene scores are updated based on the extent to which the node was part of an important gene set (based on an objective function). After some time the agents only visit the ”important” parts of the network and the involved genes will have high gene scores and are thus prioritized. While this method works in all cases analyzed in the manuscript, It is based on a complex heuristic that propagates the effects through the network. For this heuristic it is hard to prove convergence (when one group of genes has high gene scores while the other has very low). Furthermore the results might be sensitive to the initial values of the edges. This means that for some specific datasets the method might not converge (in final time) to a solution or extensive testing of the initial values of the edges has to be done in order to find a satisfactory solution. Furthermore, this strategy of exploring the search space does not guarantee to find the most optimal gene sets as it is prone to local optima. A possible alternative to explore the search space would be to enumerate and evaluate all possible paths of a fixed length against an objective function using a random walk approach and subsequently check the nodes which occur in a large number of high scoring gene sets for larger interesting gene sets as such an approach would exhaustively check the network for gene sets of a fixed size and does not rely on convergence. Such an approach is currently under development and preliminary results show an increase in PPV in comparison with other methods when analyzing large populations and populations for which germline mutations are available.

The calculation of the MES score for a specific gene set is shown in **equation 7.1**. This equation reflects three important aspects of a desirable gene set: mutual exclusivity of the observed mutations in the patients (more mutual exclusive is more desirable), coverage (more mutations in the genes is more desirable) and a uniform distribution of mutated genes over the patients (more uniform is more desirable). The equation is rather complex as it requires the patients in *S* to be sorted in a specific way prior to computation and *S* is altered during execution. Therefore pseudocode for the formula is provided in **Figure 9**. This complexity can lead to confusion in cases were multiple patients have an identical number of mutations as the score of the gene set can be different depending on the ordering of such patients. Therefore, the algorithm will compute all possible orderings and take the mean of them as the score for the gene set. This, together with the observation that the three important aspects of the formula cannot be independently tuned which might prove useful in different use cases, prompted us to design a more elegant objective function for use in a future implementation. This function will certainly retain the three aspects as they have proven to work well but could, for example, be a weighted sum of these aspects so the function can be easily tuned for other cases.

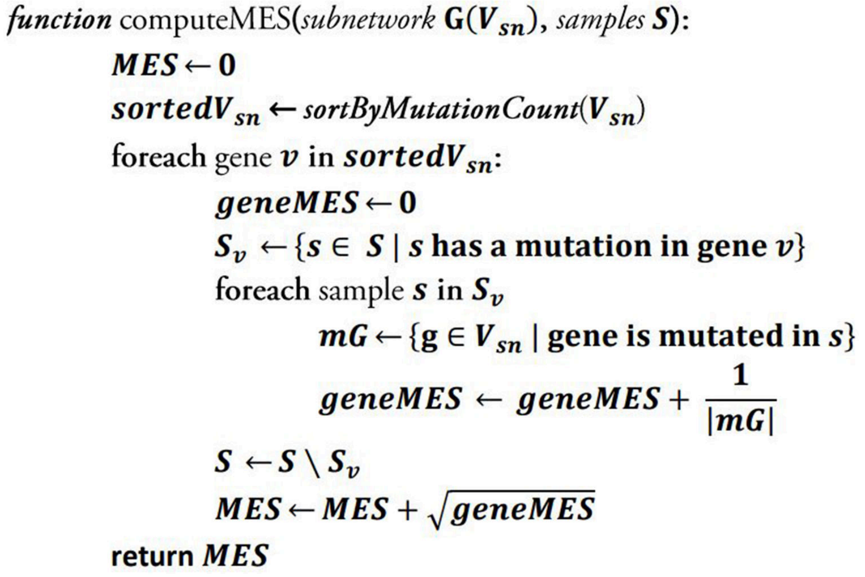

```
function computeMES(subnetwork $\mathbf{G}(V_{sn})$, samples $S$):
    $MES \leftarrow 0$
    $sortedV_{sn} \leftarrow sortByMutationCount(V_{sn})$
    foreach gene $v$ in $sortedV_{sn}$:
        $geneMES \leftarrow 0$
        $S_v \leftarrow \{s \in S \mid s \text{ has a mutation in gene } v\}$
        foreach sample $s$ in $S_v$
            $mG \leftarrow \{g \in V_{sn} \mid \text{gene is mutated in } s\}$
            $geneMES \leftarrow geneMES + \frac{1}{|mG|}$
        $S \leftarrow S \setminus S_v$
        $MES \leftarrow MES + \sqrt{geneMES}$
    return $MES$
```

*Figure 9:* ***Pseudocode for MES calculation.***

# 8

# Overall conclusions and perspectives

## 8.1 Conclusions

This thesis embodies work done over the past four years. During this time the aim was to develop three subnetwork inference methods which could cope with the analysis of omics data from different experimental designs. Each of these methods uses the (biological) specificities of the experimental design at hand together with an interaction network of the organism under research to infer a subnetwork of the interaction network which explains the observed omics data. All three were successfully tested and validated on publicly available or in-house data.

In chapter 4 it was shown that an in-house subnetwork inference method, PheNetic [6, 162], could be applied to differential expression datasets, even in the context of a naturally occurring multi-species consortium. This consortium consisted of three bacterial species which together were capable to efficiently degrade the herbicide linuron but could not do so efficiently in isolation. Therefore, RNA-seq data was generated for the bacteria degrading linuron in consortium conditions and in isolation. By performing differential expression analysis, using PheNetic, multiple metabolic pathways which were likely involved in the studied mechanism were uncovered. Having obtained this proof-of-concept, it was realized that the method could be adapted for use in different experimental designs.

The network-based method developed in chapter 4 roughly consists of three steps: first the network is weighted based on the available data, then a pathfinding step in which paths between differentially expressed genes are gathered, based on a biologically motivated definition, is performed. The edges of the network are weighted based on 1) differential expression data which is obtained from measuring expression data for a population in two different conditions and 2) the topology of the network. The found paths are given probabilities based on the weights of their edges. Finally, an optimization step in which the method reasons about which is the optimal subnetwork is performed. The optimal subnetwork is found by optimizing an objective function using the paths found in the pathfinding step. In order to achieve the aim of analyzing experiments with different experimental designs, in chapters 5 and 6 the network weighting and pathfinding steps are adapted to incorporate the available data and biological specificities of these datasets. The results are methods which respectively can be used with expression data coupled with genomics data from evolution experiments and with solely genomics data from evolution experiments which include hypermutator phenotypes. The following two paragraphs briefly explain how the method was altered to allow analysis of these experiments.

In chapter 5 two evolution experiments were analyzed: one in which four populations of an *E. coli* strain were evolved to resist the drug Amikacin and one in which a population of an *E. coli* strain diverged into two stably co-existing ecotypes during an evolution experiment in conditions with an elevated citrate concentration. In order to cope with these experimental designs, the method's path definition was adapted to analyze differential expression data coupled with genomics data. This was done by changing the pathfinding step to now search for all paths which start in a mutated gene and end in any significantly differentially expressed gene, keeping into account that a path should always go downstream (the mutation should be the cause and the differentially expressed gene the effect). In addition, the aim was to also allow ranking of the mutated genes as this is of importance when designing follow-up experiments in the lab. Ranking was based on how strongly a mutated gene is connected to the expression data, and thus how likely it is that it explains part of the phenotype. By performing a parameter sweep of the edge cost in the optimization function, optimal subnetworks were identified for very stringent settings (only selecting very small subnetworks) to very relaxed settings (selecting large subnetworks). We reasoned that mutated genes which were identified in stringent settings as well as relaxed settings were more strongly connected to the differential expression data than mutated genes which were only selected in relaxed settings. The resulting method was effective in reconstructing the relevant molecular processes and in the prioritization of mutated genes in two publicly available datasets. The method is available at http://bioinformatics.intec.ugent.be/phenetic/#/index.

In chapter 6 a very specifically designed evolution experiment was analyzed: 16 different populations of a strain of *E. coli* were independently evolved in the presence of increasing concentrations of ethanol. The ethanol tolerance of these populations, in terms of in what concentration of ethanol they could still grow, was constantly assessed and the populations were sequenced before and after each adaptive sweep (when a population significantly increases its tolerance). There was, however, no expression data available because it was both costly and possibly useless as all these populations had developed a mutator phenotype. By thoroughly redesigning the pathfinding step, such challenging datasets consisting only of mutation data and containing a lot of hypermutator phenotypes, were addressed. As in this case the expression data could not be used to weight the interaction network and drive the search for paths, a solution was found in the incorporation of additional data in the form of functional impact data (the predicted effect a mutation has on the protein it encodes) and frequency increase (the increase in frequency of a specific mutation during an adaptive sweep). This requires the sequencing of clonal populations before and after an adaptive event, as was done, in order to derive the frequency increase. On top of that, the definition of a biologically valid path was changed to ”any path starting in a gene which is mutated in a population and ending in any gene which is mutated in another population” because clusters of mutations within a population are not interesting but molecular pathways which are mutated in several populations are. This method, called IAMBEE, prioritized several interesting mutated genes and gave insight in the molecular mechanisms involved. It even allowed to generate a hypothesis about epistasis on the level of molecular pathways. The most promising of these mutations were validated in the wet-lab. IAMBEE is available at http://bioinformatics.intec.ugent.be/IAMBEE.

In chapter 7 we proposed a network-based method for the identification of molecular pathways that lie at the basis of certain cancer types. This was done by looking for patterns of mutations in molecular pathways which are mutually exclusive (have at most one mutation in a cancerous cell) as it is known that molecular pathways causal to cancer often exhibit this pattern. But while the network-based methods derived from PheNetic perform well on datasets from (clonal) evolution experiments, they could not be used directly to search for patterns of mutual exclusivity in human cancer datasets. This is the case because mutual exclusivity is a property of gene sets, not of individual genes and it is thus impossible to combine the different found paths during the optimization step as the path scores do not hold when combining them. As such, in the case of mutual exclusivity the combination of two paths, which are both very mutual exclusive by themselves, is not necessarily mutual exclusive. Instead, a multi-agent system using a heuristic approach in the domain of reinforcement learning, called SSA-ME was developed. SSA-ME was applied to all 12 cancer datasets in the TCGA PAN-cancer project [124] and was able to recover important molecular pathways involved in cancer while simultaneously predicting few rarely mutated possible cancer genes. As SSA-ME was built modular and the specificities for mutual exclusivity are just an objective function, SSA-ME can be used in different settings where subnetworks need to be inferred based on a metric which is a property of a set. SSA-ME is available at github (https://github.com/spulido99/SSA).

The successful development of these methods shows that network-based methods are useful to analyze omics data in multiple experimental designs, but that no one general method exists which is suitable in all cases. The method needs to exploit the data as well as the underlying biological mechanisms of the specific experiment. It is therefore important that these methods are designed modular such that specific parts can easily be adapted and additional functionality easily added. In this thesis the most common experimental designs in evolution experiments as well as genomics data in cancer were addressed.

## 8.2 Limitations

**Interaction networks**

While the developed methods performed well in the datasets presented in chapters 4 through 7, the availability of interactomics data for the organism is a prerequisite for any network-based method to function properly. This limitation was clear in chapter 4, where no complete interaction network could be constructed for *Variovorax paradoxus* WDL1 or *Comamonas testosteroni* WDL7. In order to construct an interaction network, metabolic interactions of closely related organisms were used but no transcriptional interactions and only a very limited amount of signaling interactions could be recovered. However, for model organisms such as human, *Escherichia coli*, *Bacillus subtilis* and *Arabidopsis thaliana* high quality interaction networks are available. Therefore, when planning (evolution) experiments in which the specific organism is not of primordial importance (for example when the mode of action of resistance to a specific compound is studied in gram negative bacteria one could design the experiment using *Escherichia coli*) one should opt for the use of a model organism. Luckily this is already common practice as the wealth of information generated for model organisms in the past, such as gene and GO annotation, are indispensable when analyzing experimental results in general.

For the study of naturally occurring organisms/populations on the other hand, there is no choice and network-based analysis might be limited. As shown in chapter 3, when working with organisms that have not been sequenced yet, the genome can be assembled and annotated [97, 361] prior to reconstructing a network. This network will be limited as regulatory and signaling interactions are typically species-specific and cannot be inferred from mapping annotated genes to curated interaction pathways, except when such interactions are available for a closely related species. On top of that, specific metabolic interactions (such as for example the catabolism of xenobiotics) will be missing. It was shown that even with this limited (largely metabolic) network, network-based analysis could be performed on omics data and yields interesting but possibly incomplete results.

### Comparison between different subnetwork inference methods

A multitude of subnetwork inference methods, which are usable in a variety of experimental designs, are now available but there is no consensus on which methodologies work best. This has three main reasons: 1) it is hard to compare different subnetwork inference method due to the lack of a proper benchmark dataset, 2) subnetwork inference methods are often developed for a specific experimental design or at least for use with specific input data and 3) the results of subnetwork inference methods are dependent on the provided interaction network. Some methods might be more robust towards more noisy, overconnected networks while others may perform better in slightly underconnected networks which lack some interactions. As interaction networks continue to grow, it is thus hard to propose a benchmark interaction network.

It is possible that two subnetwork inference methods generate different subnetworks when run on the same data set. Because of the reasons mentioned above it is often hard to tell which of the methods performs best. Therefore, subnetwork inference methods are rarely compared to each other. Validation is performed by either reconstructing the results of a small-scale experiments [118,311,362], by studying well-known mechanisms so results can be easily compared to literature [312,363] and/or by using synthetic data [7].

### Use of network-based methods

While it is shown that network-based methods can effectively analyze large omics datasets in multiple experimental designs, it is important to emphasize that these results should be used to guide further research, not replace it. Critical analysis of the results is still needed as false positives are likely to be amongst the results. However, in large and often complicated clonal omics datasets these methods can significantly reduce the time and resources needed to analyze the results and in some cases (as with hypermutators) analysis would be near-impossible without the help of network-based methods.

## 8.3 Perspectives

### Non-coding part of genomes

All networks used in this thesis use protein coding genes as nodes. This means that information on non-coding entities such as long non-coding RNA and miRNA cannot be used as it cannot be mapped to any gene. However, in principle this data could be added to the networks, provided that information regarding the position of these components in the genome and interactions between these components and genes (as it is known that these entities often have gene regulatory properties [364]) is known. As this data is becoming available with the construction of online databases such as lncrnadb [365] it can now be readily added to these networks and used provided whole-genome sequencing data is generated for the dataset to be analyzed.

**Networks in multi-organisms studies**

Efforts such as the study of the human gut [366, 367] and other bacterial ecology studies [368, 369] have been made in order to elucidate interactions between multiple species in bacterial communities. In these, often large, communities of species 16S rRNA is traditionally used to characterize the constituents of these communities [370]. This data can then be used to correlate the presence/abundance of taxonomic groups to clinical factors [371]. As these communities can be very complex, containing up to 5000 unique genes [372], more recently meta-transcriptomics studies have been performed on these communities in order to gain a deeper understanding of these systems and how their constituents interact [373, 374]. combining omics data such as RNA-seq data of the entire community with an interaction network might help to further uncover the functional characteristics of such communities. As in practice it is impossible to readily have interaction networks available for all identified (possibly unknown) species in a community sample, a representation of the community would most likely be assembled through functional annotation of the identified genes in the community together with known consensus pathways in the identified higher taxonomic groups. In the past, using this reasoning only a limited number of network representations to study metagenomics datasets have been proposed [375]. However, as a cell is a closed system, metabolites and signaling molecules must be exchanged between cells through the environment, using diffusion or active transport mechanisms to expel or obtain them. This implies that a meta-interaction network should explicitly model the interactomes of the taxonomic groups separately, together with the environment in which chemical interactions can occur [376, 377]. This makes the assembly of a meta-interaction network challenging but once available, they can be integrated with the network-based approaches presented here in the context of bacterial datasets through minimal adaptation of the methods. The incorporation of these meta-interaction networks in network-based methods is the logical next step to expand the methods to new experimental designs and more complex biological systems.

**Increasing the resolution of interaction networks**

Traditionally, the nodes of a biological interaction network represent genes/gene products and the edges represent the interactions between these nodes [109]. This implies that all data must be mapped to genes/gene products for use in the interaction network. The drawback of this approach is that only genes, not individual mutations, can be selected. However, it would be interesting if one could pinpoint the part of the gene (for example a causal mutation or a region in which causal mutations occur) in which mutations can be responsible for some phenotype. For example in human cancer a specific *BRAF* mutation was correlated to a specific drug treatment while other mutations in the same gene were not [378]. A possibility for assessing such effects would be to expand the network representation by duplicating the nodes which correspond to genes in which different ”subclasses” of mutations can be identified (for example when multiple mutational hotspots [307] can be identified within one gene or when a significant number of mutations of specific types are found within one gene). Doing so, network-based methods could select one specific ”subclass” of mutations in that gene.

**From static to dynamic networks**

Most available network-based methods, including the ones proposed in this thesis, use static interaction networks [111, 124, 269, 362]. Static refers to the fact that these networks are compiled a priori from available interactomics data and are not changed during analysis. It is however known that mutations can cause interaction networks to ”rewire”, as is required for evolution [379–381]. This rewiring can potentially create interactions which are important to explain the observed phenotype, leading to the inability of network-based methods which utilize static interaction networks to explain the phenotype. A possible solution is to abandon static interaction networks and allow the networks to be dynamic by encouraging the method to infer new interactions while analyzing the data. A possible way to achieve this would be to a priori propose a set of possible (and potentially weighted) new interactions based on the data, for example by looking at mutations within promotor regions or the DNA-binding domains of transcription factors. Given the data, a network-based method can then decide whether one or more of the proposed interactions contributes significantly to an explanation of the data, possibly inferring the existence of the new interaction.

**Condition/tissue-specific interaction networks**

Interaction networks are commonly compiled from publicly available databases which gather interactomics data for specific organisms in different conditions, and from different tissue types in case of multicellular organisms such as human [64, 80, 90, 100]. By merging this data without keeping into account in which conditions/from which tissues the interactions were obtained, valuable information is discarded and the resulting network will potentially be overconnected. This is particularly true when investigating human cells, which are differentiated to use a specific subset of molecular pathways. In the past efforts have been made to construct condition-dependent and tissue-dependent interaction networks [382–385]. However, most network-based methods still do not use condition-dependent or tissue-dependent interaction networks. As more experiments are being performed and more condition/tissue-specific interaction data becomes available it will become interesting to use them.

It can be concluded that network-based methods, although they have their limitations, are useful in clonal systems to analyze a multitude of different experimental designs involving different types of input data. This thesis specifically illustrated its use to discover differentially expressed molecular pathways between two conditions, to perform genotype-phenotype mapping in evolution experiments and to find patterns of mutual exclusive mutated genes in cancer genomes. It is expected that over the years to come these methods will be further expanded to include additional types of data such as proteomics and methylation data. Also, the networks and perhaps network representations will most likely expand as more data concerning non-coding elements and molecular interactions will become available. As more heterogeneous data will be incorporated in these methods, it is my opinion that network-based methods will have to employ more explicit biological reasoning when searching the interaction network as to assure that the found mechanisms make biological sense and can be explained in a mechanistic manner.

# Curriculum Vitae

### Personalia

| | |
|---|---|
| Name | Bram Weytjens |
| Date of birth | September 16, 1990 |
| Place of birth | Genk |
| Nationality | Belgian |
| E-mail | bweytjens@gmail.com |

---

### Education

11/2013-10/2017 joint PhD in bioinformatics and bioengineering

Thesis:*"Network-based identification of driver pathways in clonal systems"*

Promotors: Prof.Dr. Kathleen Marchal & Prof. Dr. Ir. Jozef Vanderleyden

Centre of Microbial and Plant Genetics & Department of Plant Biotechnology and Bioinformatics

UGent,Gent,Belgium & KU Leuven,Leuven, Belgium

09/2011-06/2013 Master of Engineering: Chemical Technology

Thesis:*"PheNEtic2:subnetwork inference in physical* *interaction networks by using E. coli single mutants differential expression data"*

Promotor: Prof. Dr. Ir. Jozef Vanderleyden

KU Leuven, Leuven, Belgium

09/2010-06/2016 Bachelor in biology

Thesis:*"Screening for aluminium tolerant yeast strains by fermentation; isolation of segregants & Further characterization of gene Dnmt-1 in Schistocera gregaria"*

Promotor: Prof. Dr. Johan Thevelein & Prof. Dr. Liliane Schoofs

KU Leuven, Leuven, Belgium

09/2008-06/2011 Bachelor of Engineering Technology
KU Leuven, Leuven, Belgium

---

**Publication list**

Swings T[†], **Weytjens, B**[†], Schalck T, Bonte C, Verstraeten N, Marchal K.[§], Michiels J.[§] 2017. Network-Based Identification of Adaptive Pathways in Evolved Ethanol-Tolerant Bacterial Populations. Molecular Biology and Evolution, msx228.
[†] these authors contributed equally to this paper
[§] these authors contributed equally to this paper

Albers P[†], **Weytjens B**[†], De Mot R, Marchal K, Springael D. 2017. Molecular processes underlying synergistic linuron mineralization in a triple-species bacterial consortium biofilm revealed by differential transcriptomics. Submitted to MicrobiologyOpen.
[†] these authors contributed equally to this paper

Babaki B, Van Daele D, **Weytjens B**, Guns T. A Branch-and-Cut Algorithm for Constrained Graph Clustering. Paper presented at data science meets optimisation CEC/CPAIOR (2017), Padova, Italy

De Maeyer D†, **Weytjens B**†, De Raedt L, Marchal K. 2016. Network-Based Analysis of eQTL Data to Prioritize Driver Mutations. Genome Biology and Evolution 8 (3). Doi: 10.1093/gbe/evw010
†These authors contributed equally to this work

Pulido-Tamayo S†,**Weytjens B**†, De Maeyer D, Marachal K. 2016. SSA-ME Detection of cancer driver genes using mutual exclusivity by small subnetwork analysis. Scientific reports, 6.
†These authors contributed equally to this work

Gerits E, Blommaert E, Lippell A, ONeill A J, **Weytjens B**, De Maeyer D, Carolina Fierro A, Marchal K, Marchand A, Chaltin P, Spincemaille P, De Brucker K, Thevissen K, Cammue B.P.A, Swings T, Liebens V, Fauvart M, Verstraeten N, Michiels J. 2016. Elucidation of the Mode of Action of a New Antibacterial Compound Active against Staphylococcus aureus and Pseudomonas aeruginosa. PloS one, 11(5), e0155139.

De Maeyer D, **Weytjens B**, Renkens J, De Raedt L, Marchal K. 2015. PheNetic: network-based interpretation of molecular profiling data. Nucleic acids research, gkv347.

---

## Awards

First place in the Flemish Biology Olympiad 2008

---

## Oral presentations at conferences

Automatic identification of causal mechanisms underlying experimentally evolved populations. **Weytjens B** (Presented). EMBL: new model systems for linking evolution and ecology. Heidelberg, Germany. May 10 2016.

Automatic identification of causal mechanisms underlying experimentally evolved populations. **Weytjens B** (Presented). SETAC - iEOS environmental omics & epigenetics. Ghent, Belgium. September 12 2016.

---

### Poster presentations at conferences

Automatic identification of causal mechanisms underlying experimentally evolved populations. **Weytjens B** (presented), De Maeyer D, Vanderschaeve S. EMBL: New approaches and concepts in microbiology. Heidelberg, Germany. October 13 2015.

Computational reasoning on genomics and transcriptomics data using interaction networks. **Weytjens B** (presented), De Maeyer D, De Raedt L, Marchal K. BIG N2N annual symposium. Ghent (zwijnaarde). May 21 2015. Poster: Automatic identification of causal mechanisms underlying experimentally

PheNetic: Omics Interpretation Using Interaction Networks. De Maeyer D, **Weytjens B** (presented), Renkens J, De Raedt L, Marchal K. 22nd Annual International Conference on Intelligent Systems for Molecular Biology (ISMB). Boston, Ma. July 13 2014.

---

### Attendance of symposia and conferences

SETAC - iEOS environmental omics & epigenetics. Ghent, Belgium. September 12 2016.

BIG N2N annual symposium. Ghent (zwijnaarde). May 19 2016.

EMBL: new model systems for linking evolution and ecology. Heidelberg, Germany. May 10 2016.

BIG N2N annual symposium. Ghent (zwijnaarde). May 21 2015.

EMBL: New approaches and concepts in microbiology. Heidelberg, Germany. October 13 2015.

22nd Annual International Conference on Intelligent Systems for Molecular Biology (ISMB). Boston, Ma. July 13 2014.

### Courses and training followed

Sollicitatiegesprek (KU Leuven human resources). January 13 2017.

FLAMES summer school in statistics. Writing packages in R. September 5- September 9 2016.

FLAMES summer school in statistics. Multilevel analysis. September 5- September 9 2016.

Multi-Agent Systems (B-KUL-H02H4A). Second semester of academic year 2014-2015.

Introductie leidinggeven voor doctorandi (KU Leuven human resources). May 29 2015.

Summerschool of microbial evolution: theory, simulation and experiment. May 6 May 7 2015.

Time and self management (KU Leuven human resources). May 19 2014.

### Involvement in educational activities

Assisting at exercise sessions on principal component analysis, data clustering and cluster validation at UGent first semester of academic year 2015-2016 and second semester of academic year 2016-2017.

Chaired a session at the Microbial Evolution: theory, simulation and experiment summer school. May 6- May 7 2015.

Thesis supervision of master thesis of Shauni Doms (Master Bioinformatics and systems biology at UGent) title:” Het vinden van mutaties onder positieve selectie door biologisch netwerk analyse”. September 2015 - June 2016.

Thesis Supervision of master thesis of Steven Vanderschaeve (Master Bioinformatics and systems biology at UGent) titled: ”Netwerk-gebaseerde data-analyse voor identificatie van antibiotica resistentie mechanismen in Escherichia coli”. September 2014 - June 2015.

# A

# Additions to chapter 4

## A.1 Additional results

### A.1.1 Transcriptional responses in *Variovorax sp.* WDL1 when grown in consortium conditions

Genes involved in polyhydroxybutyrate (PHB) synthesis from acetoacetyl-CoA (K03821, K00626 and K00023) were overexpressed in consortium conditions as well as a large fraction of the genes determining the anabolic pentose phosphate pathway (K00615, K01623, K00616, K01835, K00036 and K00033) including genes encoding the conversion of -D-glucose-6P to D-ribulose-5P and of D217 glyceraldehyde-3P to D-ribulose-5P and/or D-ribose-5P (**Additional Figure A1**). Another important fraction (88 CDS) of the enzyme encoding genes that were differentially expressed, were involved in amino acid metabolism and PheNetic selected several differentially expressed pathways related to amino acid metabolism. Genes encoding interconversion reactions between molecules of the glutamate family were differentially expressed (**Additional Figure A2**). Similarly, genes involved in the degradation of phenylacetate to acetyl-CoA in the phenylalanine metabolism were largely overexpressed in consortium conditions (**Additional Figure A3**. Moreover, in cysteine and methionine metabolism, several genes that were involved in cycling of the central metabolite S- adenosylmethionine (K01251, K00548, K00549, K00789) and genes involved in cysteine synthesis (K12339, K00640) were underexpressed in consortium conditions (**Additional Figure A4**. The differential expression of several genes encoding transporters involved in the uptake of amino acid and carbohydrate molecules was also indicative of a metabolic response upon co-culturing. Most of the transporters are members of the ATP-binding cassette (ABC) superfamily. Changes in general cell metabolism were further suggested by altered expression in pathways involved in sulfur and nitrogen transport and metabolism. Pathways involved in sulfur transport and metabolism were underexpressed in consortium conditions such as the synthesis of the sulfur containing metabolite thiamine (K03147, K0315-4) as well as an operon spanning three genes (K00390, K00381, K00957) involved in assimilatory sulfate reduction. Differentially expressed genes associated with nitrogen metabolism included genes involved in ammonium and nitrate/nitrite transport (K03320, K02575), assimilation of inorganic nitrogen via glutamine synthetase (K00370, K00373 and K01915) and several nitrogen regulatory and sensor proteins (K07673, K07712 and K07708).

Also DNA metabolism appeared to be affected. Increased DNA synthesis in WDL1 when grown in consortium conditions is suggested by the underexpression of degradation of purine and pyrimidine nucleotides (K00758, K01081), and overexpression of formation of deoxynucleotides (K02343, K02338, K01494, K00525). See **Additional Figure A5** and **Additional Figure A6**. In accordance with the suggested increased DNA synthesis of WDL1, 20 genes involved in different mechanisms of DNA repair and recombination were overexpressed (**Figure 4.5 in chapter 4**). Also, a part of the porphyrin metabolism was selected by PheNetic. Additional manual analysis showed that genes involved in heme production (K01599, K02495, K02492 and K01698) were overexpressed in consortium conditions. See **Additional Figure A7**.

Besides the metabolic pathways that were mainly identified by Phenetic, additional cellular systems were found to be differentially expressed between growth conditions in WDL1 (**Figure 4.5 in chapter 4**). Several of those systems are related to cell-to-cell interactions. These included overexpression under consortium conditions of eight out of thirteen genes coding for a type VI secretion system (T6SS), two genes that encode a toxin/antitoxin pair participating in systems mediating contact- dependent inhibition (CDI), a gene encoding a putative adhesin and genes encoding a putative quorum sensing circuit (**Figure 4.5 in chapter 4**). Interestingly, the latter are located just downstream of linuron hydrolase encoding gene hylA and encode a LuxR-type transcriptional regulator (K18098) and LuxI-type acyl-homoserine lactone (AHL) synthase (K18096).

Another set of genes with altered expression are associated with stress response indicating that WDL1 experiences cellular stress in consortium conditions. *rpoH* and *hrcA* were overexpressed in consortium compared to monoculture conditions. *rpoH* encodes sigma factor s32 which controls genes involved in heat shock response and protein homeostasis. Genes encoding chaperones *DnaK*, *DnaJ*, *GroEL*, *GroES*, *HtpG* and *ClpB* and a zinc protease were all overexpressed, whereas *grpE* was underexpressed. The log2-fold change values of all genes mentioned in this paragraph can be found in **Table 4.2 in chapter 4**

### A.1.2 Transcriptional responses elicited in *C. testosteroni* WDL7 when grown in consortium biofilms

Another operon that was strongly affected in WDL7 in consortium conditions was the glycerate biosynthesis operon (*gcl*; K01608, K00042, K01816). This operon is involved in the conversion of glyoxylate to glycerate and showed clear overexpression in consortium versus monoculture conditions. Its overexpression in consortium conditions was confirmed by transcriptional fusion reporter analysis (**Supplementary Figure S4.2 B in chapter 4**). Furthermore, seventeen out of 53 genes coding for ribosomal proteins in WDL7 were overexpressed in consortium conditions. Nearly one third of the genes belonging to an unknown prophage element were underexpressed. In contrast to WDL1, no differentially expressed genes involved in cell-to-cell interaction were identified in WDL7 while overexpression was observed for only one gene that is related to stress (*dnaK*, log2-fold change of -1.3) and underexpression for one gene related to DNA repair and recombination (K01247, log2-fold change of 1.1). The log2-fold change values of all genes mentioned in this paragraph can be found in **Table 4.2 in chapter 4**

## A.2 Additional discussion

### A.2.1 Semi-synthetic benchmarking set

The WDL1 *hylA* gene encoding linuron hydrolase showed strong overexpression in consortium conditions. The higher expression of *hylA* per cell in WDL1 under consortium conditions is remarkable but can be at least partially explained by recent observations that (i) WDL1 consists of two subpopulations, one carrying *hylA* and lacking the 3,4-DCA downstream pathway and one that carries only the 3,4-DCA pathway, and (ii) the linuron-hydrolyzing WDL1 subpopulation becomes more abundant (up to 10 fold) when grown in consortium conditions than when grown in monoculture, as shown by qPCR targeting *hylA* and the dca gene cluster in other identically operated biofilm experiments (P. Albers, unpublished results). Regardless of the dynamics of the linuron-hydrolyzing WDL1 subpopulation, the overall higher abundance of *hylA* transcripts in consortium conditions suggests an increased production of *HylA*, which can obviously be linked with the enhanced degradation of linuron in consortium biofilms. The pcaFIJ operon consisting of three genes encoding the last steps in linuron conversion to TCA cycle intermediates, was underexpressed in WDL1 in consortium conditions. As in *Sinorhizobium meliloti*, the pca operon of WDL1 is preceded by a regulatory gene that encodes an IclR-type regulator which upon interaction with 3-oxoadipate results in induction of the sinorhizobial pca operon [387]. This suggests that the pca operon in WDL1 is also inducible by 3-oxoadipate and that underexpression is possibly due to less 3-oxoadipate being used by WDL1 cells during consortium growth. On the other hand, it could be speculated that a lower expression of the pca operon in WDL1 is a consequence of catabolic repression by metabolic waste products or nutrients supplied by the other strains [388]. Regarding the linuron catabolic genes in WDL7, *dcaB* was the only gene of the dca operon of WDL7 that was slightly underexpressed in consortium condition. Other genes of the linuron catabolic operons of WDL7 were all highly but not differentially expressed, supporting the assumption that 3,4- DCA is a major carbon source for WDL7, not alone in monoculture, but also in consortium biofilm conditions [172]. This observation further confirms that there is metabolic association between WDL1 and WDL7 during linuron degradation.

## A.3 Additional experimental procedures

#### A.3.0.1 Draft genome sequence of the consortium members

Cell cultures of strains WDL1, WDL6 and WDL7 for sequencing were prepared as follows. WDL1 was plated from a cryoculture and grown on R2A [389] supplemented with 20 mg L-1 linuron for 4 days at 25°C. WDL6 was plated and grown on MMO agar plates supplemented with 1% (vol/vol) methanol [197] for 6 days at 25C; WDL7 was plated and grown on Luria-Bertani (LB) agar [390] overnight at 25°C. A smear of colonies of WDL1, WDL6 and a colony of WDL7 was inoculated in R2B supplemented with 20 mg L$^{-1}$ linuron, in liquid MMO supplemented with 1% (vol/vol) methanol and in LB, respectively and cultures were grown for 4 days, 4 days and overnight, respectively until exponential phase. Genomic DNA was extracted from the cultures using the Puregene Core kit A (Qiagen) following the manufacturers instructions. A paired-end library (90 bp reads with an insert length of 500 bp) of WDL6 genomic DNA was sequenced by BGI Tech Solutions (Hong Kong) using the Illumina Hi-seq platform resulting into 418 MB of sequence information. Sequencing of the WDL7 and WDL1 genomes was performed by Baseclear (The Netherlands) using Illumina Hi-seq based on 75 cycle paired-ended reads with an insert length of 400 bp resulting in a total of 751 MB of WDL7 and 300 MB of WDL1 genomic sequence information. Nucleotides with a PHRED quality score $<$ 20 were trimmed from the end of raw reads and trimmed reads with a length $<$ 10 were discarded using the FASTX-Toolkit-0.0.12 software (http://hannonlab.cshl.edu/fastx_toolkit/). Draft genome sequences were obtained by assembling the trimmed paired-end reads into contigs using Velvet (version 1.2.01) with an optimized k-mer length of 41, 51 and 41 for WDL1, WDL6 and WDL7, respectively and a minimal contig length of 100 bp [391]. The draft genomes were annotated using the web-based RAST server [203]. The PHAST web server was used to identify prophages in the bacterial genomes [392]. Undetected or erroneously annotated linuron catabolic genes were identified and reannotated manually. The details of the draft genome assemblies are summarized in **Additional Table A1**.

#### A.3.0.2 RNA extraction, library preparation and sequencing

Biofilm cells were flushed out of the flow chambers by injecting and pipetting up and down (10 times) 1 mL of ice cold RNase-stop solution (5% water-saturated phenol/95% ethanol mixture diluted (1:5 v/v) in deionized water). The cells were snap frozen in liquid nitrogen and stored at -80°C. After thawing on ice, biofilm biomass was pelleted by centrifugation at 15,000 g for 2 min at 4°C and total RNA was extracted using the SV total RNA Isolation kit (Promega) with minor modifications. Briefly, the pellet was resuspended in 100 L lysis buffer containing 50 mg mL$^{-1}$ chicken egg white lysozyme (Sigma-Aldrich) and incubated for 4 minutes at room temperature. Further extraction was performed according to the manufacturers instructions, except that after washing and dissolving in RNase-free water, the nucleic acid extract was treated twice with TURBO DNase using a TURBO DNA-free kit (Ambion). Lack of DNA contamination was verified by conventional PCR targeting the 16S rRNA gene of WDL1 and WDL7 as described in Supporting Experimental Procedures. rRNA was removed from the RNA extracts through subtractive hybridization using the MICROBExpressTM kit (Ambion) according to the manufacturers protocol. The rRNA-depleted RNA was dissolved in nuclease-free water. RNA quality and concentration were estimated by spectrophotometry (NanoDrop) and gel electrophoresis (Experion, Bio-Rad) before and after rRNA depletion.

1.0 -1.5 ng of rRNA-depleted RNA was used to construct RNAseq libraries using the ScriptSeqTMv2 RNAseq Library Preparation kit (Epicentre) for three consortium biofilms, three WDL7 monoculture biofilms and one WDL1 monoculture biofilm. Only one WDL1 biofilm RNA extract was used since insufficient RNA was extracted from the other two WDL1 monoculture biofilm samples. Index reads were added to the libraries using the Scriptseq Index PCR Primers (Epicentre) and the barcoded libraries were PCR amplified according to the manufacturers instructions. The Agencourt AMPure XP system (Beckman Coulter) was used to purify both the 3-terminal-tagged cDNA and the final RNAseq library. Size distribution of the libraries was assessed by agarose gel electrophoresis. Library cDNA concentrations were quantified using a QubitTM fluorometer (Invitrogen) and adjusted to 2 nM. Since WDL6 represents about 10% of the total biovolume in consortium samples [174], the seven equimolar consortium and monoculture libraries were multiplexed in a 5:1 volume ratio prior to sequencing to obtain sufficient transcript reads of all strains in the consortium samples. Hundred cycle paired-ended reads were obtained by Illumina Hiseq sequencing at the Genomics Core UZ Leuven facility (KU Leuven).

#### A.3.0.3 Verification of differential transcription using transcriptional gene fusions

Transcriptional gene fusions between the promotor regions of the glycerate biosynthesis operon (gcl) and of the 3-oxoadipate catabolic operon (pca) of WDL7 with the promoterless *gfpmut3.1* in the broad host range vector pRU1097 were constructed in WDL7 and tested for expression in WDL7 monoculture and WDL1-WDL7-WDL6 consortium biofilms as reported in Supporting Experimental Procedures.

#### A.3.0.4 Nucleotide sequence accession numbers

The draft genome sequences of *Variovorax sp.* WDL1, *C. testosteroni* WDL7 and *H. sulfonivorans* WDL6 have been deposited at DDBJ/EMBL/GenBank under the accession numbers LMTS00000000, LMXT00000000 and LMTR00000000.

## A.4 Additional figures and tables

*Table A1:* ***Summary of draft genome sequencing results.*** **PExx = Paired-end sequencing followed by a number that refers to the read length.*

| | WDL1 | WDL6 | WDL7 |
|---|---|---|---|
| N50 | 76000 | 94254 | 106400 |
| Contigs>100bp | 493 | 109 | 151 |
| Coverage | 24 | 44 | 45 |
| Genome size (bp) | 8,170,112 | 3,705,164 | 5,541,122 |
| GC content (%) | 66.4 | 61.1 | 61.5 |
| Number of CDSs | 7759 | 3496 | 5069 |
| Sequencing details* | PE 75 | PE90 | PE75 |
| Total data size | 575 MB | 418 MB | 751 MB |

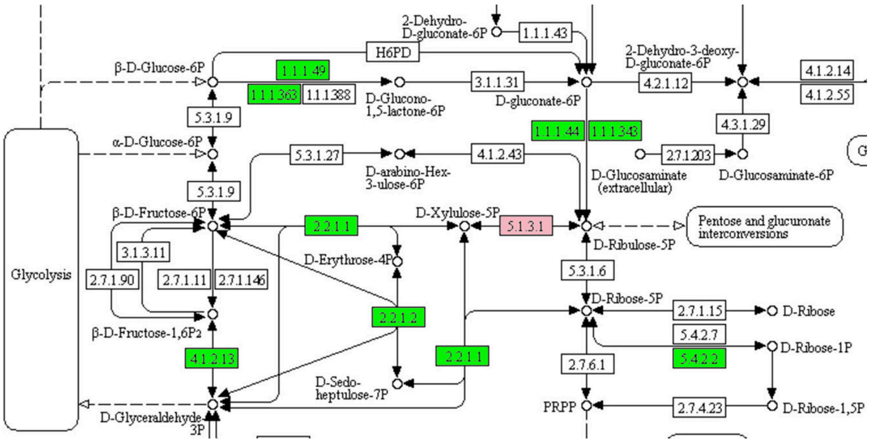

*Figure A1:* ***Phenetic inferred map of part of the pentose phosphate pathway.*** *Overexpressed and underexpressed WDL1 genes in consortium conditions compared to monoculture conditions in green and red, respectively.*

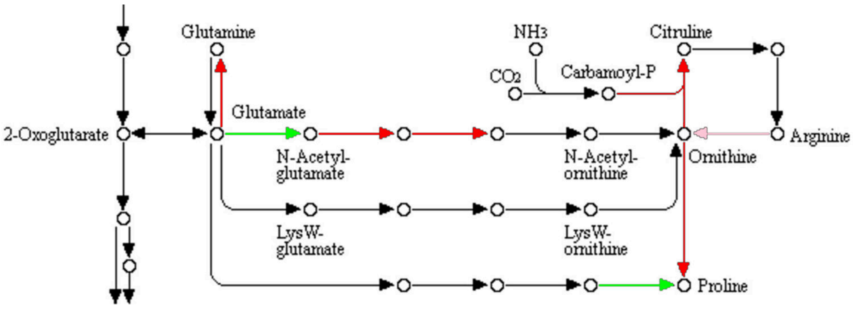

*Figure A2:* ***Phenetic inferred map of interconversion glutamate family.*** *Overexpressed and underexpressed WDL1 genes in consortium conditions compared to monoculture conditions in green and red, respectively.*

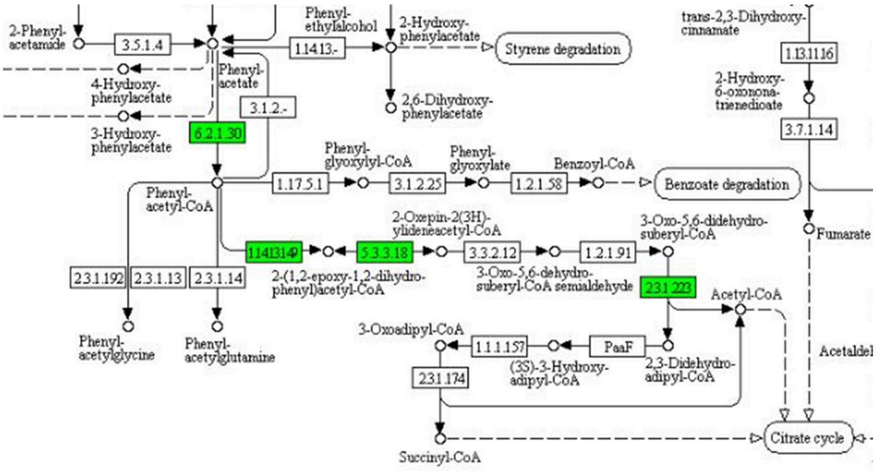

*Figure A3:* ***Phenetic inferred map of part of the phenylalanine metabolism.*** *Overexpressed and underexpressed WDL1 genes in consortium conditions compared to monoculture conditions in green and red, respectively.*

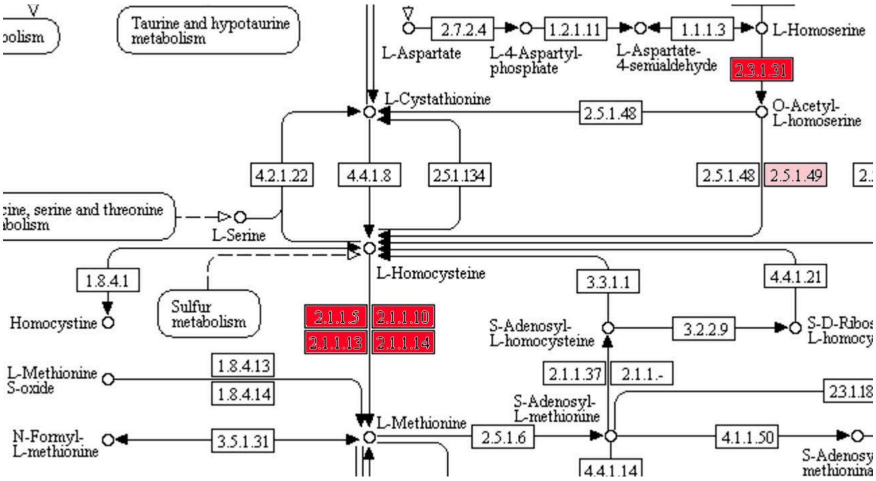

*Figure A4:* ***Phenetic inferred map of part of the cysteine/methionine metabolism.*** *Overexpressed and underexpressed WDL1 genes in consortium conditions compared to monoculture conditions in green and red, respectively.*

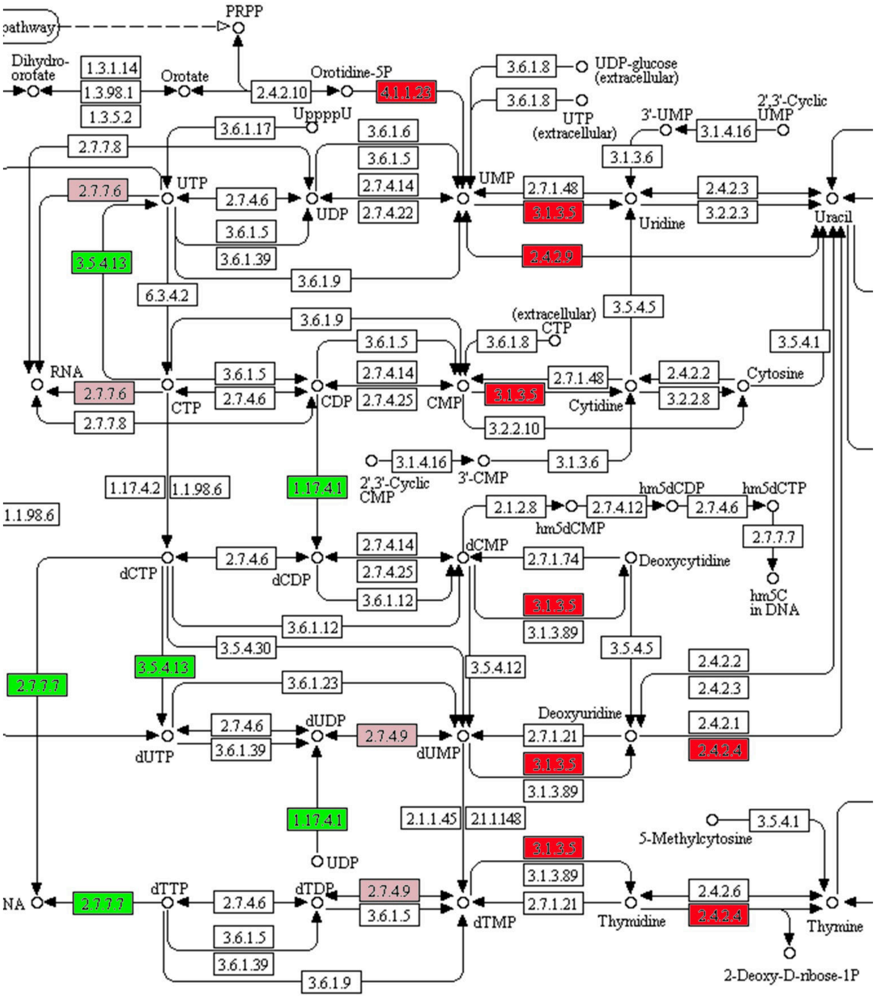

*Figure A5:* ***Phenetic inferred map of part of the pyrimidine metabolism.*** *Overexpressed and under-expressed WDL1 genes in consortium conditions compared to monoculture conditions in green and red,respectively.*

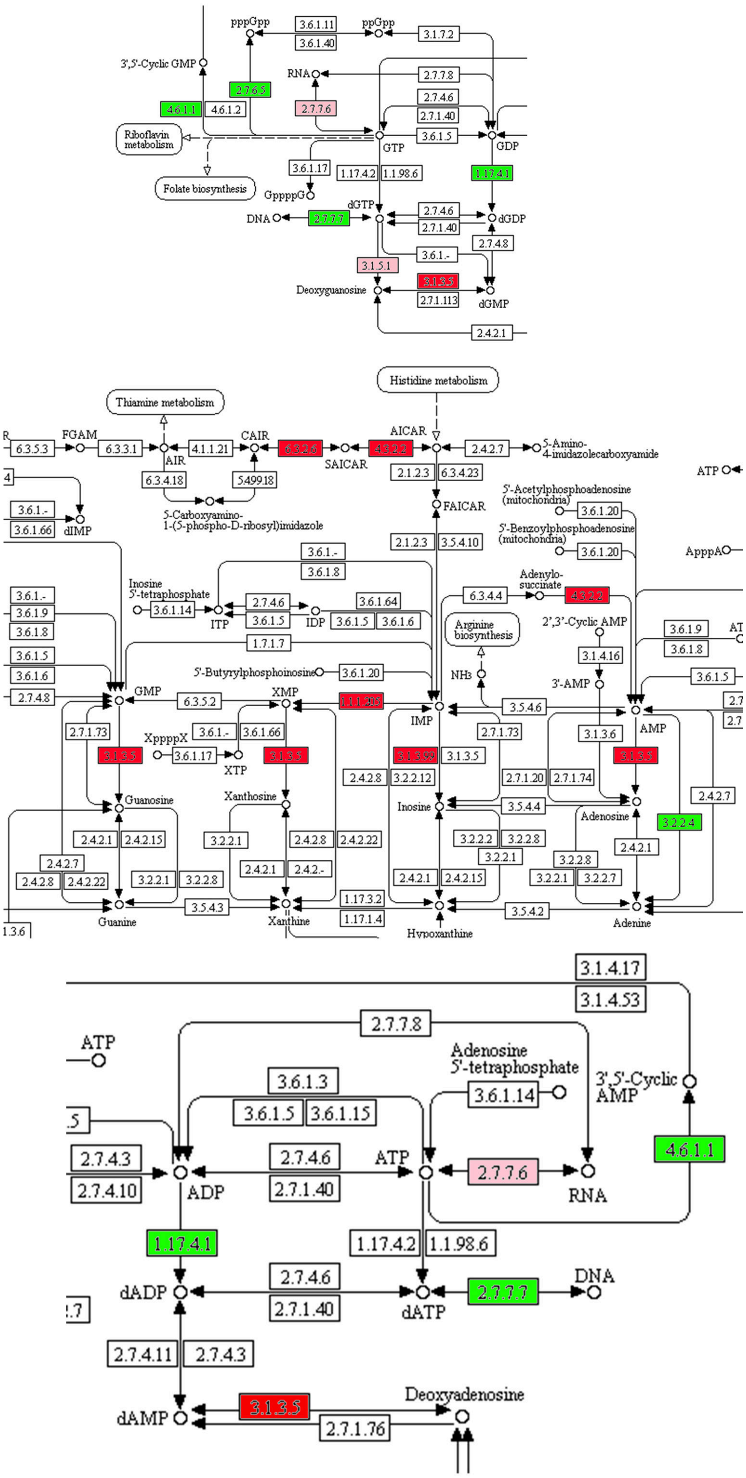

*Figure A6:* ***Phenetic inferred map of multiple parts of the purine metabolism.***

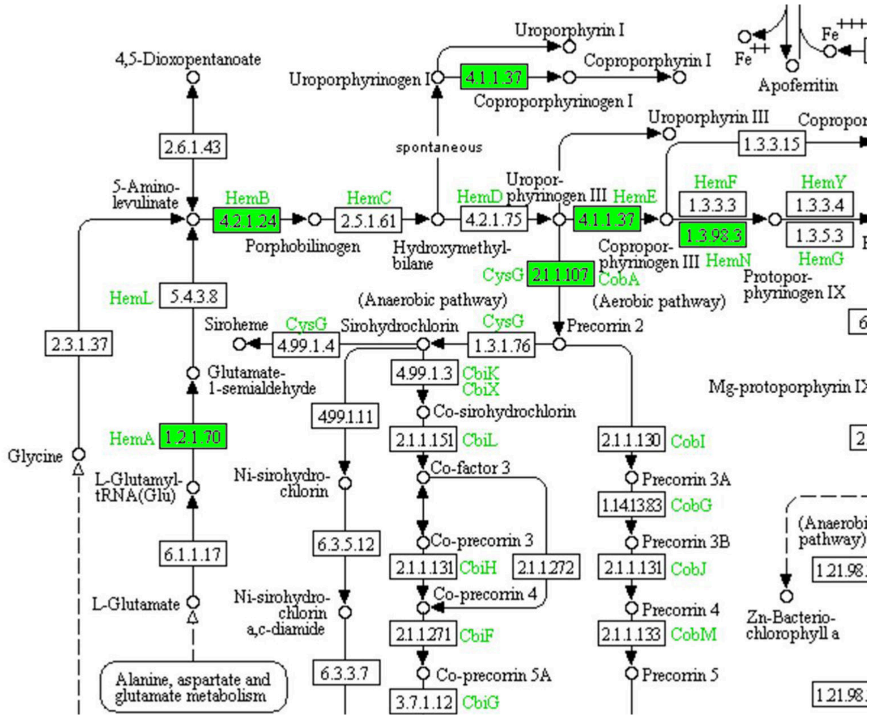

*Figure A7:* ***Phenetic inferred map of part of the porphyrin metabolism*** *Overexpressed and underexpressed WDL1 genes in consortium conditions compared to monoculture conditions in green and red, respectively.*

# B

# Additions to chapter 6

## B.1 Additional results

### B.1.1 Hypothetical ethanol tolerance related pathways

Our analysis was able to select several molecular pathways that were previously linked to the response to ethanol stress and to increasing ethanol tolerance. These results show the potential of IAMBEE to comprehensively analyze complex mutational datasets and select molecular pathways that are involved in the trait of interest. Additionally, IAMBEE selected few molecular pathway that were not previously directly linked to ethanol tolerance, but that could hypothetically play a role. These pathways are important, as they can provide new routes to genetically engineer higher ethanol tolerance in industrially relevant strains. In what follows we will shortly discuss some of these newly identified pathways and their possible role in ethanol tolerance.

### B.1.2 Transcription and translation

Other highly prioritized pathways are linked to transcription and translation. We found a frequently mutated connected network component containing several well-known genes involved in transcription termination and anti-termination (*rho*, *nusG* and *nusA*). Additionally, we found a frequently mutated subnetwork containing translation-linked genes encoding for 30S ribosomal subunit proteins (*rpsL*, *rpsD*, *rpsB* and *rpsH*) and the protein chain initiation factor *infB*. Selection of these pathways further corroborates earlier results that demonstrate early ethanol-induced transcription termination and ethanol-induced translational misreading during protein synthesis. Mutations in genes involved in transcription or translation might confer higher ethanol tolerance through compensation for these toxic effects [393–395].

Remarkably, we observed co-occurrence of mutations prioritized in transcription (anti-) termination factors, such as *rho*, *nusA* and *nusG* and ribosomal genes, such as *rpsB*, *rpsD*, *rpsL* and *rpsH*. These are consistently observed in the same populations and follow the same trajectories, suggesting that they are dependent on each other in driving the observed tolerance towards ethanol (**Figure 6.4**, **Figure 6.5 in chapter 6**). This observation suggests an epistatic interaction that corresponds to previous findings of Freddolino *et al.* who showed that mutations in rpsL increase ethanol tolerance in a mutant *rho* background [396] and Haft *et al.* who demonstrated the role in ethanol tolerance of epistatic interactions between a mutation in *rho* and *rpsQ* [393].

### B.1.3 Osmotic stress response

Of note, also the *envZ-ompR* two-component system that regulates outer membrane porin genes in response to changes in extracellular osmotic pressure was prioritized [273, 274]. Ethanol increases membrane fluidity, thereby causing leakage and osmotic stress as shown by Goodarzi *et al.* [260]. Mutations in *envZ* and *ompR* suggest adaptations to the increased osmotic stress under high ethanol conditions.

### B.1.4 Amino acid biosynthesis

Finally, several of the prioritized pathways and genes are involved in amino acid biosynthesis, such as isoleucine and valine biosynthesis (*ilvD*, *ilvC*, *ilvB*, *ilvE*, *ilvI*, *tdcB*), alanine and phenylalanine biosynthesis (*ilvE*, *alaA*), methionine biosynthesis (*metE*, *metB*, *metH*), biosynthesis of tetrahydrofolic acid, which is a precursor in the metabolism of amino acids (*folD*, *purH*), a gene involved in arginine biosynthesis (*argH*), and a gene involved in threonine and glycine biosynthesis (*itaE*) [397]. A role of amino acid biosynthesis and transport in tolerance towards ethanol stress has previously been suggested in yeast, because of impaired delivery of amino acids into the cell as a result of membrane functions being disrupted by ethanol [398, 399]. Our results are also in line with those of Horinouchi *et al.*

(2015) [400] who observed in their adapted ethanol tolerant strains upregulation of several genes involved in amino acid biosynthesis. They attributed the upregulation of amino acid biosynthesis genes to a significant decrease in expression of genes related to the tricarboxylic acid (TCA) cycle and consequently of precursors in amino acid biosynthesis [400].

### B.1.5 DNA damage and repair

A molecular pathway of particular interest is the pathway containing genes involved in DNA damage and repair, such as *umuC*, *umuD*, *recF* and *recA*. Both UmuC and UmuD are subunits of the error-prone polymerase PolV, which is specialized in trans-lesion synthesis [401]. This polymerase has a LexA binding motif in its promoter region and is consequently regulated by the SOS response [402]. Upon DNA damage, RecA binds to the single stranded DNA gap and induces cleavage of the LexA repressor, resulting in activation of SOS genes necessary for repair of the damaged DNA [403]. The selection of these genes strongly suggest that ethanol causes DNA lesions and adaptation might occur through mutations in genes involved in the repair. Interestingly, the *rapA* gene was also linked to this pathway. RapA is an RNA polymerase recycling factor that enables recycling of stalled RNA polymerases [404]. The selection of this gene further corroborates the role of mutations found in *rho*, *nusA* and *nusG*, transcription termination or anti-termination factors as described above.

### B.1.6 Protein stress

Another interesting pathway contains genes involved in protein stress and protein misfolding, such as *dnaK*, *htpG* and *rpoH*. Both DnaK (Hsp70) and HtpG (Hsp90 family) are chaperones involved in folding polypeptide chains and rescue of misfolded proteins [405,406]. They also interact with RpoH, the alternative sigma factor $\sigma^{32}$, to control the heat shock response in response to temperature and increase in misfolded proteins in *E. coli* [407]. Interestingly, overexpression of GroESL, another chaperone system, was recently linked to increased viability upon exposure to various organic solvents, such as ethanol and butanol [408]. Finally, the selection of this pathway substantiates the role of mutations found in *rpsL rpsD*, *rpsB* and *rpsH* that possibly increase accuracy of translation by ribosomes as previously discussed.

### B.1.7 Acid stress response

The resulting pathways also include one that contains *rstA*, which encodes for a transcriptional regulator. RstA is involved in many biological processes, such as acid tolerance [409]. Upregulation of genes involved in the acid stress response in response to ethanol stress was previously reported [259, 260].

### B.1.8 Pyrroloquinoline quinone biosynthesis

A rather peculiar pathway that was selected contains genes *cyoB* and *pqqL*. Little is known on the function of PqqL. Interestingly, *pqqL* from *E. coli* was able to complement *pqqE* and *pqqF* mutants from *Methylobacterium organophilum* [410]. The *pqqEF* genes are required for pyrroloquinoline quinone (PQQ) biosynthesis in *Methylobacterium extorquens* [411]. PQQ on his turn is a prosthetic group that is required for many bacterial dehydrogenases, including alcohol dehydrogenases [411, 412]. Hypothetically, *pqqL* might also play a role in PQQ cofactor synthesis that is required for the function of alcohol dehydrogenases in *E. coli*. Goodarzi *et al.* (2010) previously discovered ethanol degradation through *adhE* as an adaptive strategy to high ethanol stress [260]. The mutated *pqqL* might confer a similar resistance mechanism by activating an alcohol dehydrogenase through its PQQ cofactor. Alternatively, it was found that PqqL interacts with proteins involved in ribosome biogenesis, which might suggest an additional role in translation [413].

### B.1.9 Biofilm formation

A final molecular pathway of particular interest contains the *tamAB* genes. Both genes are frequently mutated in different parallel populations and mutations rise in frequency in the initial selective sweep as well as in the second selective sweep. TamA and TamB are components of a translocation and assembly complex. TamA is the outer membrane protein while TamB is the inner membrane protein. The complex is involved in secretion of the adhesin protein Ag43 [414]. Ag43 is involved in biofilm formation by promoting cell-to-cell aggregation [415, 416]. Exposure to stress conditions promotes to activation of biofilm formation, possibly to decrease exposure to the stress and increase the chances to survive [417]. Altering the biofilm formation capabilities through mutations in the *tamAB* genes might confer higher resistance to the ethanol stress.

# B.2 Additional methods

## B.2.1 Experimental evolution

We used a set of 16 parallel evolved *E. coli* populations. Of these highly ethanol-tolerant populations, 7 originated from our previously conducted evolution experiment [44]) and we initiated a new experiment using the same workflow to add an additional 9 populations to the final dataset. All populations acquired a hypermutator phenotype, which is necessary to enable evolution under near-lethal stress conditions [44]). For ease of reading, we renamed al populations HT1-16 (High Tolerance). In brief, all parallel populations originated from the same ancestral strains SX4 and SX25. We used lysogeny broth (LB) supplemented with 5% (v/v) ethanol as primary stress conditions to initiate the evolution experiment. We maintained growth in exponential phase in each population. As parameters to monitor evolution, we used both the optical density ($A_{595nm}$) and the time to reach a specific optical density, typical for exponential growth. When a population reached exponential phase ($A_{595nm}$ around 0.2) within 24 hours, we transferred it to fresh LB medium that was supplemented with an additional 0.5% (v/v) ethanol. If the population needed more than 24 hours but less than 14 days to reach exponential growth, we transferred it to fresh medium with the same percentage of ethanol. In case the strain did not grow within 14 days, we revived the sample from the previous time point from the -80C stock and used it to restart the evolving population in fresh medium with a 0.5% reduced ethanol concentration. Upon each transfer to fresh medium, a sample was stored in a -80C glycerol stock for further analysis. Based on the adaptation trajectories of these populations (**Figure S6.1 in chapter 6**) we decided to analyze both the selective sweep from 5% to 6% ethanol and the selective sweep from 6% to 6.5% ethanol in order to also gain insight into the temporal aspects of the adaptive pathways.

## B.2.2 Sequencing and mutation calling

High-quality genomic DNA from overnight cultures of the ancestor and intermediate points of evolved populations was isolated (DNeasy Blood & Tissue kit, Qiagen). 100 bp paired-end sequencing libraries with an average insert size of 200 bp were prepared at GeneCore (EMBL, Heidelberg) and used for massive parallel sequencing with the Illumina HiSeq2000. We used CLC Genomics Workbench version 7.6 (https://www.qiagenbioinformatics.com) (RRID:SCR_011853) for analysis of the sequences. Following quality assessment of the raw data, reads were trimmed using quality scores of the individual bases (quality limit = 0.01; maximum number of ambiguous bases = 2). Reads shorter than 15 bases were discarded from the set. We used the CLC Assembly Cell 4.0 algorithm to map the trimmed reads to the *E. coli* MG1655 reference genome (NC_000913.1) yielding a minimal coverage of 150x (mismatch cost = 2; insertion cost = 3; deletion cost = 3; length fraction = 0.8; similarity fraction = 0.8). Mutations were called using the CLC Low Frequency Variant Detector (required significance = 1%; minimum coverage = 10; minimum frequency = 10%). Finally, the mutations in the SX4 compared to the MG1655 reference genome were discarded.

### B.2.3 Mapping of mutations to genes

The mapped mutations were checked for anomalies. Around position 570000-580000 (DLP12 prophage) and position 1600000-1700000 (Qin prophage) we found a very large number of mutations (**Additional Figure B1 a**). As the calling of mutations in these prophage regions is likely erroneous, mutations in and between prophage-related genes (i.e. *aaaD*, *exoD*, *nohD*, *nohB*, *nohQ*, *rrrD*, *rzpD*, *yecD*, *yfdL* and *ylcH*) were filtered out (**Additional Figure B1 b**). There was also a bias towards mutations in HT4, HT3, HT8, HT2, HT5 and HT9. In these populations 204 identical SNVs or INDELS were detected while these mutations did not occur in one of the other populations. These populations originated from the new evolution experiment. As opposed to the populations that we previously reported on [44], these new populations were all initiated from a single ancestral population. As these mutations are not independent from each other (**Additional Figure B2**), we removed them from the analysis. Lastly, the *lacZ* gene shows a high number of mutations throughout the experiments but this was due to a known insertion element ( [44, 252, 418]), which CLC did not call correctly. As such, mutations in the *lacZ* gene were also discarded.

## B.3 Additional figures

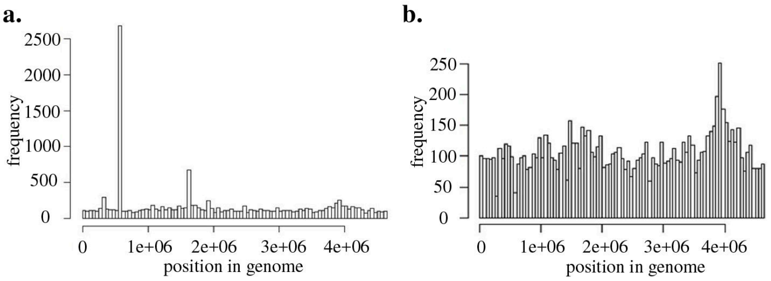

*Figure B1:* ***Mutational profile of all mutations from the 16 evolved populations. a****, Before filtering of mutations in prophage regions. It can be seen that there are an unusual amount of mutations around region 570000-580000 and region 1600000-1700000. As these are prophage regions, mutations in prophage regions were filtered out.* ***b****, After filtering of mutations in prophage regions the profile is more balanced.*

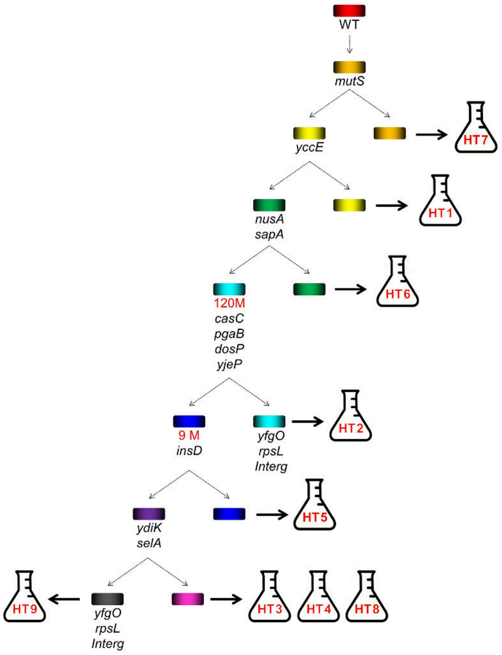

*Figure B2:* ***Lineage tracking of HT1-9 populations show common predecessor.*** *The graph shows the common mutations and InDels found in these populations. It is clear that a mutS mutation initially occurred and all populations evolved further from this mutator mutant. Interestingly, populations HT2, HT3, HT4, HT5, HT8 and HT9 shared a set of specific mutations. Identical SNPs and InDels which were found at least 4 times in these populations but not in any other population were discarded from the dataset as these mutations did not arise independently during evolution.*

# C
# Additions to chapter 7

## C.1 Literature-based evidence for frequently predicted cancer drivers in the TCGA PAN-cancer datasets

We also analyzed data from BLCA, COADREAD, GBM, HNSC, KIRC, LAML, LUAD, LUSC, OV, UCEC and STAD datasets. These results can be found in the online version of the paper presented in chapter 7. All datasets used for these analyses were downloaded from GDAC firehose. Here we only focus on a detailed description of genes that were prioritized recurrently in these datasets and that were not yet mentioned as drivers in the used cancer gene reference databases.

Versican (*VCAN*) was selected in three out of twelve different pan-cancer datasets (LUAD STAD, BLCA) and fell just below the PPV cutoff value in UCEC. *VCAN* is a major component of the extracellular matrix (EM) involved in cell adhesion, proliferation, migration and angiogenesis. Increased *VCAN* expression has been observed in a wide range of malignant

tumors and has been associated with both cancer relapse and poor patient outcomes [419–421]. Despite its well documented role in triggering tumor proliferation [422, 423], *VCAN* itself is not frequently mutated (mutations in 215 samples on a total of

5986 samples in the used pan-cancer datasets). In the LUAD dataset, *VCAN* was interacting and mutual exclusive with *EGFR*, *BCL9* and *CTNNB1* (b1 catenin). *CTNNB1* is a well-known driver gene that plays a central molecule in the wnt pathway and that is involved in the transcriptional regulation of *VCAN* [424]. The uncovered mutual exclusivity pattern can be seen in **Supplementary figure S7.4 in chapter 7**.

*BCL2L1* (BCL2 like 1, BCLX, BCLXL), belongs together with Mcl-1 to the Bcl2 family. *BCL2L1* is an anti-apoptotic gene that has just like *MCL1* has been observed to be amplified in a variety of cancers. This is in accordance with our findings where *BCL2L1* was selected as a potential driver gene in 66% of the pan-cancer datasets (OV, BLCA, COADREAD, LUAD, UCEC and LUSC) in which it mostly had gains of copy number. Overexpression of anti-apoptotic Bcl-2 proteins in cancers tilts the apoptosis signaling pathway towards cell survival. *BCL2L1* is, next to its role in promoting cancer cell survival by suppressing apoptosis, also involved in promoting metastasis in a way that is independent of the anti-apoptotic activity [341].

*UBE2I* Was prioritized in the ovarium (OV) and in the stomach adenocarcinoma (STAD) pan-cancer datasets (as a linker gene). The ubiquitin-conjugating enzyme 9 (Ubc9), the sole conjugating enzyme for sumoylation, regulates protein function and plays an important role in sumoylation-mediated cellular pathways. Sumoylation plays a key role in DNA repair and tumorigenesis. Indeed, overexpressing *Ubc9* has been shown to contribute to EOC progression and cell proliferation through the PI3K/Akt pathway [425]. In addition, the SUMO pathway mediated by *Ubc9* was shown to critically contribute to the transformed phenotype of *KRAS* mutant cells [418]. *UBE2I* was prioritized in OV because of its association with *TP53* and *RNF144B*. The latter protein is an E3 ubiquitin-protein ligase that accepts ubiquitin from the E2 ubiquitin-conjugating enzymes *UBE2L3* and *UBE2L6* and then directly transfers the ubiquitin to targeted substrates, thereby promoting their degradation. It induces apoptosis via a p53/*TP53*-dependent mechanism and affects cell death by affecting the ubiquitin-dependent stability of BAX, a pro-apoptotic protein [426].

# References

[1] Jason A Reuter, Damek V Spacek, and Michael P Snyder. *High-throughput sequencing technologies*. Molecular cell, 58(4):586–597, 2015.

[2] Hui Ge, Albertha JM Walhout, and Marc Vidal. *Integrating omicinformation: a bridge between genomics and systems biology*. TRENDS in Genetics, 19(10):551–560, 2003.

[3] Andrew R Joyce and Bernhard Ø Palsson. *The model organism as a system: integrating'omics' data sets*. Nature reviews. Molecular cell biology, 7(3):198, 2006.

[4] Bernhard Palsson and Karsten Zengler. *The challenges of integrating multi-omic data sets*. Nature chemical biology, 6(11):787, 2010.

[5] David Gomez-Cabrero, Imad Abugessaisa, Dieter Maier, Andrew Teschendorff, Matthias Merkenschlager, Andreas Gisel, Esteban Ballestar, Erik Bongcam-Rudloff, Ana Conesa, and Jesper Tegnér. *Data integration in the era of omics: current and future challenges*. BMC systems biology, 8(2):I1, 2014.

[6] Dries De Maeyer, Bram Weytjens, Joris Renkens, Luc De Raedt, and Kathleen Marchal. *PheNetic: network-based interpretation of molecular profiling data*. Nucleic acids research, page gkv347, 2015.

[7] Dries De Maeyer, Bram Weytjens, Luc De Raedt, and Kathleen Marchal. *Network-based analysis of eqtl data to prioritize driver mutations*. Genome biology and evolution, 8(3):481–494, 2016.

[8] Sergio Pulido-Tamayo, Bram Weytjens, Dries De Maeyer, and Kathleen Marchal. *SSA-ME Detection of cancer driver genes using mutual exclusivity by small subnetwork analysis*. Scientific reports, 6, 2016.

[9] Francis Crick. *Central dogma of molecular biology*. Nature, 227(5258):561–563, 1970.

[10] Fan Liu, Kate van Duijn, Johannes R Vingerling, Albert Hofman, André G Uitterlinden, A Cecile JW Janssens, and Manfred Kayser. *Eye color and the prediction of complex phenotypes from genotypes*. Current Biology, 19(5):R192–R193, 2009.

[11] Stephen J Chanock, Teri Manolio, Michael Boehnke, Eric Boerwinkle, David J Hunter, Gilles Thomas, Joel N Hirschhorn, Goncalo Abecasis, David Altshuler, Joan E Bailey-Wilson, et al. *Replicating genotype–phenotype associations*. Nature, 447(7145):655–660, 2007.

[12] Ray Wu. *Nucleotide sequence analysis of DNA: I. Partial sequence of the cohesive ends of bacteriophage $\lambda$ and 186 DNA*. Journal of molecular biology, 51(3):501–521, 1970.

[13] F Sanger, S Nicklen, and AR Coulson. *DNA sequencing with chain-terminating inhibitors*. Proc. Natl. Acad. Sci. USA, 74:5463–5467, 1977.

[14] Mark P Sawicki, Ghassan Samara, Michael Hurwitz, and Edward Passaro. *Human genome project*. The American journal of surgery, 165(2):258–264, 1993.

[15] Michael L Metzker. *Sequencing technologiesthe next generation*. Nature reviews genetics, 11(1):31–46, 2010.

[16] Chengwei Luo, Despina Tsementzi, Nikos Kyrpides, Timothy Read, and Konstantinos T Konstantinidis. *Direct comparisons of Illumina vs. Roche 454 sequencing technologies on the same microbial community DNA sample*. PloS one, 7(2):e30087, 2012.

[17] Sara Goodwin, John D McPherson, and W Richard McCombie. *Coming of age: ten years of next-generation sequencing technologies*. Nature Reviews Genetics, 17(6):333–351, 2016.

[18] Phillip EC Compeau, Pavel A Pevzner, and Glenn Tesler. *How to apply de Bruijn graphs to genome assembly*. Nature biotechnology, 29(11):987–991, 2011.

[19] Ben Langmead and Steven L Salzberg. *Fast gapped-read alignment with Bowtie 2*. Nature methods, 9(4):357–359, 2012.

[20] Kai Ye, Marcel H Schulz, Quan Long, Rolf Apweiler, and Zemin Ning. *Pindel: a pattern growth approach to detect break points of large deletions and medium sized insertions from paired-end short reads*. Bioinformatics, 25(21):2865–2871, 2009.

[21] Petr Danecek, Adam Auton, Goncalo Abecasis, Cornelis A Albers, Eric Banks, Mark A DePristo, Robert E Handsaker, Gerton Lunter, Gabor T Marth, Stephen T Sherry, et al. *The variant call format and VCFtools*. Bioinformatics, 27(15):2156–2158, 2011.

[22] Mark A DePristo, Eric Banks, Ryan Poplin, Kiran V Garimella, Jared R Maguire, Christopher Hartl, Anthony A Philippakis, Guillermo Del Angel, Manuel A Rivas, Matt Hanna, et al. *A framework for variation discovery and genotyping using next-generation DNA sequencing data*. Nature genetics, 43(5):491–498, 2011.

[23] Stephan J Sanders, Michael T Murtha, Abha R Gupta, John D Murdoch, Melanie J Raubeson, A Jeremy Willsey, A Gulhan Ercan-Sencicek, Nicholas M DiLullo, Neelroop N Parikshak, Jason L Stein, et al. *De novo mutations revealed by whole exome sequencing are strongly associated with autism*. Nature, 485(7397):237, 2012.

[24] Kaya Bilgüvar, Ali Kemal Öztürk, Angeliki Louvi, Kenneth Y Kwan, Murim Choi, Burak Tatli, Dilek Yalnizoğlu, Beyhan Tüysüz, Ahmet Okay Çağlayan, Sarenur Gökben, et al. *Whole exome sequencing identifies recessive WDR62 mutations in severe brain malformations*. Nature, 467(7312):207, 2010.

[25] Hubing Shi, Gatien Moriceau, Xiangju Kong, Mi-Kyung Lee, Hane Lee, Richard C Koya, Charles Ng, Thinle Chodon, Richard A Scolyer, Kimberly B Dahlman, et al. *Melanoma whole exome sequencing identifies V600EB-RAF amplification-mediated acquired B-RAF inhibitor resistance*. Nature communications, 3:724, 2012.

[26] Francis O Walker. *Huntington's disease*. The Lancet, 369(9557):218–228, 2007.

[27] Haichun Gao, Zamin K Yang, Terry J Gentry, Liyou Wu, Christopher W Schadt, and Jizhong Zhou. *Microarray-based analysis of microbial community RNAs by whole-community RNA amplification*. Applied and environmental microbiology, 73(2):563–571, 2007.

[28] Zhong Wang, Mark Gerstein, and Michael Snyder. *RNA-Seq: a revolutionary tool for transcriptomics*. Nature reviews genetics, 10(1):57–63, 2009.

[29] Latha Ramdas, Kevin R Coombes, Keith Baggerly, Lynne Abruzzo, W Edward Highsmith, Tammy Krogmann, Stanley R Hamilton, and Wei Zhang. *Sources of nonlinearity in cDNA microarray expression measurements*. Genome Biology, 2(11):research0047–1, 2001.

[30] Y Tu, G Stolovitzky, and U Klein. *Quantitative noise analysis for gene expression microarray experiments*. Proceedings of the National Academy of Sciences, 99(22):14031–14036, 2002.

[31] Gordon Smyth. *Limma: linear models for microarray data*. Bioinformatics and computational biology solutions using R and Bioconductor, pages 397–420, 2005.

[32] Hao Wu, M Kathleen Kerr, Xiangqin Cui, and Gary A Churchill. *MAANOVA: a software package for the analysis of spotted cDNA microarray experiments*. In The analysis of gene expression data, pages 313–341. Springer, 2003.

[33] Simon Anders, Paul Theodor Pyl, and Wolfgang Huber. *HTSeqa Python framework to work with high-throughput sequencing data*. Bioinformatics, 31(2):166–169, 2015.

[34] Michael I Love, Wolfgang Huber, and Simon Anders. *Moderated estimation of fold change and dispersion for RNA-seq data with DESeq2*. Genome biology, 15(12):550, 2014.

[35] Cole Trapnell, Adam Roberts, Loyal Goff, Geo Pertea, Daehwan Kim, David R Kelley, Harold Pimentel, Steven L Salzberg, John L Rinn, and Lior Pachter. *Differential gene and transcript expression analysis of RNA-seq experiments with TopHat and Cufflinks*. Nature protocols, 7(3):562–578, 2012.

[36] Richard E Lenski, Michael R Rose, Suzanne C Simpson, and Scott C Tadler. *Long-term experimental evolution in Escherichia coli. I. Adaptation and divergence during 2,000 generations*. The American Naturalist, 138(6):1315–1341, 1991.

[37] Michael Georg Hoesl, Stefan Oehm, Patrick Durkin, Elise Darmon, Lauri Peil, Hans-Rudolf Aerni, Juri Rappsilber, Jesse Rinehart, David Leach, Dieter Söll, et al. *Chemical evolution of a bacterial proteome*. Angewandte Chemie International Edition, 54(34):10030–10034, 2015.

[38] Bram Van den Bergh, Joran E Michiels, and Jan Michiels. *Experimental Evolution of Escherichia coli Persister Levels Using Cyclic Antibiotic Treatments*. Bacterial Persistence: Methods and Protocols, pages 131–143, 2016.

[39] Molly K Burke, Joseph P Dunham, Parvin Shahrestani, Kevin R Thornton, Michael R Rose, and Anthony D Long. *Genome-wide analysis of a long-term evolution experiment with Drosophila*. Nature, 467(7315):587, 2010.

[40] Martin Dragosits and Diethard Mattanovich. *Adaptive laboratory evolution–principles and applications for biotechnology*. Microbial cell factories, 12(1):64, 2013.

[41] Olivier Tenaillon, Alejandra Rodríguez-Verdugo, Rebecca L Gaut, Pamela McDonald, Albert F Bennett, Anthony D Long, and Brandon S Gaut. *The molecular diversity of adaptive convergence*. Science, 335(6067):457–461, 2012.

[42] Takaaki Horinouchi, Kuniyasu Tamaoka, Chikara Furusawa, Naoaki Ono, Shingo Suzuki, Takashi Hirasawa, Tetsuya Yomo, and Hiroshi Shimizu. *Transcriptome analysis of parallel-evolved Escherichia coli strains under ethanol stress*. BMC genomics, 11(1):579, 2010.

[43] James D Winkler, Carlos Garcia, Michelle Olson, Emily Callaway, and Katy C Kao. *Evolved osmotolerant Escherichia coli mutants frequently exhibit defective N-acetylglucosamine catabolism and point mutations in cell shape-regulating protein MreB*. Applied and environmental microbiology, 80(12):3729–3740, 2014.

[44] Toon Swings, Bram Van den Bergh, Sander Wuyts, Eline Oeyen, Karin Voordeckers, Kevin J Verstrepen, Maarten Fauvart, Natalie Verstraeten, and Jan Michiels. *Adaptive tuning of mutation rates allows fast response to lethal stress in Escherichia coli*. eLife, 6:e22939, 2017.

[45] Charles J Vaske, Stephen C Benz, J Zachary Sanborn, Dent Earl, Christopher Szeto, Jingchun Zhu, David Haussler, and Joshua M Stuart. *Inference of patient-specific pathway activities from multi-dimensional cancer genomics data using PARADIGM*. Bioinformatics, 26(12):i237–i245, 2010.

[46] Elina Zorde Khvalevsky, Racheli Gabai, Itzhak Haim Rachmut, Elad Horwitz, Zivia Brunschwig, Ariel Orbach, Adva Shemi, Talia Golan, Abraham J Domb, Eylon Yavin, et al. *Mutant KRAS is a druggable target for pancreatic cancer*. Proceedings of the National Academy of Sciences, 110(51):20723–20728, 2013.

[47] Alberto Ocaña and Atanasio Pandiella. *Identifying breast cancer druggable oncogenic alterations: lessons learned and future targeted options*. Clinical Cancer Research, 14(4):961–970, 2008.

[48] Manish A Shah and Jaffer A Ajani. *Gastric canceran enigmatic and heterogeneous disease*. Jama, 303(17):1753–1754, 2010.

[49] K David Voduc, Maggie CU Cheang, Scott Tyldesley, Karen Gelmon, Torsten O Nielsen, and Hagen Kennecke. *Breast cancer subtypes and the risk of local and regional relapse*. Journal of Clinical Oncology, 28(10):1684–1691, 2010.

[50] Mel Greaves and Carlo C Maley. *Clonal evolution in cancer*. Nature, 481(7381):306, 2012.

[51] Ivana Bozic, Tibor Antal, Hisashi Ohtsuki, Hannah Carter, Dewey Kim, Sining Chen, Rachel Karchin, Kenneth W Kinzler, Bert Vogelstein, and Martin A Nowak. *Accumulation of driver and passenger mutations during tumor progression*. Proceedings of the National Academy of Sciences, 107(43):18545–18550, 2010.

[52] Robert Weinberg. *Tumor suppressor genes*. Neuron, 11(2):191–196, 1993.

[53] Douglas Hanahan and Robert A Weinberg. *The hallmarks of cancer*. cell, 100(1):57–70, 2000.

[54] Athanasia Pavlopoulou, Demetrios A Spandidos, and Ioannis Michalopoulos. *Human cancer databases (Review)*. Oncology reports, 33(1):3–18, 2015.

[55] John N Weinstein, Eric A Collisson, Gordon B Mills, Kenna R Mills Shaw, Brad A Ozenberger, Kyle Ellrott, Ilya Shmulevich, Chris Sander, Joshua M Stuart, Cancer Genome Atlas Research Network, et al. *The cancer genome atlas pan-cancer analysis project*. Nature genetics, 45(10):1113–1120, 2013.

[56] Thomas J Hudson, Warwick Anderson, Axel Aretz, Anna D Barker, Cindy Bell, Rosa R Bernabé, MK Bhan, Fabien Calvo, Iiro Eerola, Daniela S Gerhard, et al. *International network of cancer genome projects*. Nature, 464(7291):993–998, 2010.

[57] Ronald S Burt, Martin Kilduff, and Stefano Tasselli. *Social network analysis: Foundations and frontiers on advantage*. Annual review of psychology, 64:527–547, 2013.

[58] Stephen P Borgatti, Ajay Mehra, Daniel J Brass, and Giuseppe Labianca. *Network analysis in the social sciences*. science, 323(5916):892–895, 2009.

[59] Jürgen Schmidhuber. *Deep learning in neural networks: An overview*. Neural networks, 61:85–117, 2015.

[60] Lore Cloots and Kathleen Marchal. *Network-based functional modeling of genomics, transcriptomics and metabolism in bacteria*. Current opinion in microbiology, 14(5):599–607, 2011.

[61] Aminael Sánchez-Rodríguez, Lore Cloots, and Kathleen Marchal. *Omics derived networks in bacteria*. Current Bioinformatics, 8(4):489–495, 2013.

[62] Patrik Dhaeseleer, Shoudan Liang, and Roland Somogyi. *Genetic network inference: from co-expression clustering to reverse engineering*. Bioinformatics, 16(8):707–726, 2000.

[63] Arun K Ramani, Zhihua Li, G Traver Hart, Mark W Carlson, Daniel R Boutz, and Edward M Marcotte. *A map of human protein interactions derived from co-expression of human mRNAs and their orthologs*. Molecular systems biology, 4(1):180, 2008.

[64] Damian Szklarczyk, Andrea Franceschini, Stefan Wyder, Kristoffer Forslund, Davide Heller, Jaime Huerta-Cepas Milan Simonovic, Alexander Roth, Alberto Santos, Kalliopi P. Tsafou, Michael Kuhn, Peer Bork, and Lars J. Jensen Christian von Mering. *STRING v10: proteinprotein interaction networks, integrated over the tree of life*. Nucleic Acid Research, 2015.

[65] Robert Hoffmann, Martin Krallinger, Eduardo Andres, Javier Tamames, Christian Blaschke, and Alfonso Valencia. *Text mining for metabolic pathways, signaling cascades, and protein networks*. Sci STKE, 283:e21, 2005.

[66] Sofie Van Landeghem, Filip Ginter, Yves Van de Peer, and Tapio Salakoski. *EVEX: a PubMed-scale resource for homology-based generalization of text mining predictions*. In Proceedings of BioNLP 2011 workshop, pages 28–37. Association for Computational Linguistics, 2011.

[67] Tomas Klingström and Dariusz Plewczynski. *Protein–protein interaction and pathway databases, a graphical review*. Briefings in bioinformatics, 12(6):702–713, 2011.

[68] Michael E Cusick, Haiyuan Yu, Alex Smolyar, Kavitha Venkatesan, Anne-Ruxandra Carvunis, Nicolas Simonis, Jean-François Rual, Heather Borick, Pascal Braun, Matija Dreze, et al. *Literature-curated protein interaction datasets*. Nature methods, 6(1):39–46, 2009.

[69] Sandra Orchard, Samuel Kerrien, Sara Abbani, Bruno Aranda, Jignesh Bhate, Shelby Bidwell, Alan Bridge, Leonardo Briganti, Fiona SL Brinkman, Gianni Cesareni, et al. *Protein interaction data curation: the International Molecular Exchange (IMEx) consortium*. Nature methods, 9(4):345–350, 2012.

[70] Soon-Hyung Yook, Zoltán N Oltvai, and Albert-László Barabási. *Functional and topological characterization of protein interaction networks*. Proteomics, 4(4):928–942, 2004.

[71] Erik RP Zuiderweg. *Mapping protein- protein interactions in solution by NMR spectroscopy*. Biochemistry, 41(1):1–7, 2002.

[72] SH Sleigh, PR Seavers, AJ Wilkinson, JE Ladbury, and JRH Tame. *Crystallographic and calorimetric analysis of peptide binding to OppA protein*. Journal of molecular biology, 291(2):393–415, 1999.

[73] Tord Berggård, Sara Linse, and Peter James. *Methods for the detection and analysis of protein–protein interactions*. Proteomics, 7(16):2833–2842, 2007.

[74] Stanley Fields and Rolf Sternglanz. *The two-hybrid system: an assay for protein-protein interactions*. Trends in Genetics, 10(8):286–292, 1994.

[75] Mike P Williamson and Michael J Sutcliffe. *Protein–protein interactions*, 2010.

[76] Orland Gonzalez. *Protein–Protein Interaction Databases*. In Encyclopedia of Systems Biology, pages 1786–1790. Springer, 2013.

[77] Baolin Liu and Bo Hu. *HPRD: a high performance RDF database*. International Journal of Parallel, Emergent and Distributed Systems, 25(2):123–133, 2010.

[78] Johannes Goll, Seesandra V Rajagopala, Shen C Shiau, Hank Wu, Brian T Lamb, and Peter Uetz. *MPIDB: the microbial protein interaction database*. Bioinformatics, 24(15):1743–1744, 2008.

[79] Andrew Chatr-Aryamontri, Bobby-Joe Breitkreutz, Rose Oughtred, Lorrie Boucher, Sven Heinicke, Daici Chen, Chris Stark, Ashton Breitkreutz, Nadine Kolas, Lara O'donnell, et al. *The BioGRID interaction database: 2015 update*. Nucleic acids research, 43(D1):D470–D478, 2015.

[80] Bruno Aranda, Hagen Blankenburg, Samuel Kerrien, Fiona SL Brinkman, Arnaud Ceol, Emilie Chautard, Jose M Dana, Javier De Las Rivas, Marine Dumousseau, Eugenia Galeota, et al. *PSICQUIC and PSISCORE: accessing and scoring molecular interactions*. Nature methods, 8(7):528–529, 2011.

[81] Denis Thieffry, Araceli M Huerta, Ernesto Pérez-Rueda, and Julio Collado-Vides. *From specific gene regulation to genomic networks: a global analysis of transcriptional regulation in Escherichia coli*. Bioessays, 20(5):433–440, 1998.

[82] Gerd Anders, Sebastian D Mackowiak, Marvin Jens, Jonas Maaskola, Andreas Kuntzagk, Nikolaus Rajewsky, Markus Landthaler, and Christoph Dieterich. *doRiNA: a database of RNA interactions in post-transcriptional regulation*. Nucleic acids research, 40(D1):D180–D186, 2012.

[83] Michael J Buck and Jason D Lieb. *ChIP-chip: considerations for the design, analysis, and application of genome-wide chromatin immunoprecipitation experiments*. Genomics, 83(3):349–360, 2004.

[84] Terrence S Furey. *ChIP–seq and beyond: new and improved methodologies to detect and characterize protein–DNA interactions*. Nature Reviews Genetics, 13(12):840–852, 2012.

[85] Dominic Schmidt, Michael D Wilson, Christiana Spyrou, Gordon D Brown, James Hadfield, and Duncan T Odom. *ChIP-seq: using high-throughput sequencing to discover protein–DNA interactions*. Methods, 48(3):240–248, 2009.

[86] S Balaji, M Madan Babu, Lakshminarayan M Iyer, Nicholas M Luscombe, and L Aravind. *Comprehensive analysis of combinatorial regulation using the transcriptional regulatory network of yeast.* Journal of molecular biology, 360(1):213–227, 2006.

[87] Jason Ernst, Qasim K Beg, Krin A Kay, Gábor Balázsi, Zoltán N Oltvai, and Ziv Bar-Joseph. *A semi-supervised method for predicting transcription factor–gene interactions in Escherichia coli.* PLoS Comput Biol, 4(3):e1000044, 2008.

[88] Karen Lemmens, Tijl De Bie, Thomas Dhollander, Sigrid C De Keersmaecker, Inge M Thijs, Geert Schoofs, Ami De Weerdt, Bart De Moor, Jos Vanderleyden, Julio Collado-Vides, et al. *DISTILLER: a data integration framework to reveal condition dependency of complex regulons in Escherichia coli.* Genome biology, 10(3):R27, 2009.

[89] Riet De Smet and Kathleen Marchal. *Advantages and limitations of current network inference methods.* Nature Reviews Microbiology, 8(10):717–729, 2010.

[90] Heladia Salgado, Martin Peralta-Gil, Socorro Gama-Castro, Alberto Santos-Zavaleta, Luis Muñiz-Rascado, Jair S García-Sotelo, Verena Weiss, Hilda Solano-Lira, Irma Martínez-Flores, Alejandra Medina-Rivera, et al. *RegulonDB v8. 0: omics data sets, evolutionary conservation, regulatory phrases, cross-validated gold standards and more.* Nucleic acids research, 41(D1):D203–D213, 2013.

[91] Mark B Gerstein, Anshul Kundaje, Manoj Hariharan, Stephen G Landt, Koon-Kiu Yan, Chao Cheng, Xinmeng Jasmine Mu, Ekta Khurana, Joel Rozowsky, Roger Alexander, et al. *Architecture of the human regulatory network derived from ENCODE data.* Nature, 489(7414):91–100, 2012.

[92] Hong-Mei Zhang, Hu Chen, Wei Liu, Hui Liu, Jing Gong, Huili Wang, and An-Yuan Guo. *AnimalTFDB: a comprehensive animal transcription factor database.* Nucleic acids research, 40(D1):D144–D149, 2012.

[93] Pavel S Novichkov, Olga N Laikova, Elena S Novichkova, Mikhail S Gelfand, Adam P Arkin, Inna Dubchak, and Dmitry A Rodionov. *RegPrecise: a database of curated genomic inferences of transcriptional regulatory interactions in prokaryotes.* Nucleic acids research, 38(suppl_1):D111–D118, 2010.

[94] You-Kwan Oh, Bernhard O Palsson, Sung M Park, Christophe H Schilling, and Radhakrishnan Mahadevan. *Genome-scale reconstruction of metabolic network in Bacillus subtilis based on high-throughput phenotyping and gene essentiality data.* Journal of Biological Chemistry, 282(39):28791–28799, 2007.

[95] John W Pinney, Martin W Shirley, Glenn A McConkey, and David R Westhead. *metaSHARK: software for automated metabolic network prediction from DNA sequence and its application to the genomes of Plasmodium falciparum and Eimeria tenella.* Nucleic acids research, 33(4):1399–1409, 2005.

[96] Ross Overbeek, Robert Olson, Gordon D Pusch, Gary J Olsen, James J Davis, Terry Disz, Robert A Edwards, Svetlana Gerdes, Bruce Parrello, Maulik Shukla, et al. *The SEED and the Rapid Annotation of microbial genomes using Subsystems Technology (RAST).* Nucleic acids research, 42(D1):D206–D214, 2014.

[97] Yuki Moriya, Masumi Itoh, Shujiro Okuda, Akiyasu C Yoshizawa, and Minoru Kanehisa. *KAAS: an automatic genome annotation and pathway reconstruction server.* Nucleic acids research, 35(suppl 2):W182–W185, 2007.

[98] Shujiro Okuda, Takuji Yamada, Masami Hamajima, Masumi Itoh, Toshiaki Katayama, Peer Bork, Susumu Goto, and Minoru Kanehisa. *KEGG Atlas mapping for global analysis of metabolic pathways*. Nucleic acids research, 36(suppl 2):W423–W426, 2008.

[99] Peter D Karp, Suzanne M Paley, Markus Krummenacker, Mario Latendresse, Joseph M Dale, Thomas J Lee, Pallavi Kaipa, Fred Gilham, Aaron Spaulding, Liviu Popescu, et al. *Pathway Tools version 13.0: integrated software for pathway/genome informatics and systems biology*. Briefings in bioinformatics, 11(1):40–79, 2010.

[100] Minoru Kanehisa, Yoko Sato, Masayuki Kawashima, Miho Furumichi, and Mao Tanabe. *KEGG as a reference resource for gene and protein annotation*. Nucleic Acid Research, 2016.

[101] Ida Schomburg, Antje Chang, and Dietmar Schomburg. *BRENDA, enzyme data and metabolic information*. Nucleic acids research, 30(1):47–49, 2002.

[102] Ron Caspi, Richard Billington, Luciana Ferrer, Hartmut Foerster, Carol A Fulcher, Ingrid M Keseler, Anamika Kothari, Markus Krummenacker, Mario Latendresse, Lukas A Mueller, et al. *The MetaCyc database of metabolic pathways and enzymes and the BioCyc collection of pathway/genome databases*. Nucleic acids research, 44(D1):D471–D480, 2016.

[103] Kun Ping Lu, Yih-Cherng Liou, and Xiao Zhen Zhou. *Pinning down proline-directed phosphorylation signaling*. Trends in cell biology, 12(4):164–172, 2002.

[104] Wangsen Cao, Clare Bao, Elizaveta Padalko, and Charles J Lowenstein. *Acetylation of mitogen-activated protein kinase phosphatase-1 inhibits Toll-like receptor signaling*. Journal of Experimental Medicine, 205(6):1491–1503, 2008.

[105] Gregory M Barton and Ruslan Medzhitov. *Toll-like receptor signaling pathways*. Science, 300(5625):1524–1525, 2003.

[106] Matthias Mann and Ole N Jensen. *Proteomic analysis of post-translational modifications*. Nature biotechnology, 21(3):255–261, 2003.

[107] Jesper V Olsen, Blagoy Blagoev, Florian Gnad, Boris Macek, Chanchal Kumar, Peter Mortensen, and Matthias Mann. *Global, in vivo, and site-specific phosphorylation dynamics in signaling networks*. Cell, 127(3):635–648, 2006.

[108] Arnon Paz, Zippora Brownstein, Yaara Ber, Shani Bialik, Eyal David, Dorit Sagir, Igor Ulitsky, Ran Elkon, Adi Kimchi, Karen B Avraham, et al. *SPIKE: a database of highly curated human signaling pathways*. Nucleic acids research, 39(suppl_-1):D793–D799, 2011.

[109] Albert-Laszlo Barabasi and Zoltan N Oltvai. *Network biology: understanding the cell's functional organization*. Nature reviews genetics, 5(2):101–113, 2004.

[110] Enrico Glaab, Anaïs Baudot, Natalio Krasnogor, Reinhard Schneider, and Alfonso Valencia. *EnrichNet: network-based gene set enrichment analysis*. Bioinformatics, 28(18):i451–i457, 2012.

[111] Omer Basha, Shoval Tirman, Amir Eluk, and Esti Yeger-Lotem. *ResponseNet2. 0: revealing signaling and regulatory pathways connecting your proteins and genesnow with human data*. Nucleic acids research, 41(W1):W198–W203, 2013.

[112] Lieven PC Verbeke, Lore Cloots, Piet Demeester, Jan Fostier, and Kathleen Marchal. *EPSILON: an eQTL prioritization framework using similarity measures derived from local networks*. Bioinformatics, 29(10):1308–1316, 2013.

[113] Roded Sharan, Igor Ulitsky, and Ron Shamir. *Network-based prediction of protein function*. Molecular systems biology, 3(1):88, 2007.

[114] Ulrich Stelzl, Uwe Worm, Maciej Lalowski, Christian Haenig, Felix H Brembeck, Heike Goehler, Martin Stroedicke, Martina Zenkner, Anke Schoenherr, Susanne Koeppen, et al. *A human protein-protein interaction network: a resource for annotating the proteome*. Cell, 122(6):957–968, 2005.

[115] Falk Schreiber and Henning Schwöbbermeyer. *MAVisto: a tool for the exploration of network motifs*. Bioinformatics, 21(17):3572–3574, 2005.

[116] Roded Sharan and Trey Ideker. *Modeling cellular machinery through biological network comparison*. Nature biotechnology, 24(4):427–433, 2006.

[117] David Warde-Farley, Sylva L Donaldson, Ovi Comes, Khalid Zuberi, Rashad Badrawi, Pauline Chao, Max Franz, Chris Grouios, Farzana Kazi, Christian Tannus Lopes, et al. *The GeneMANIA prediction server: biological network integration for gene prioritization and predicting gene function*. Nucleic acids research, 38(suppl 2):W214–W220, 2010.

[118] Oved Ourfali, Tomer Shlomi, Trey Ideker, Eytan Ruppin, and Roded Sharan. *SPINE: a framework for signaling-regulatory pathway inference from cause-effect experiments*. Bioinformatics, 23(13):i359–i366, 2007.

[119] Steven Maere, Karel Heymans, and Martin Kuiper. *BiNGO: a Cytoscape plugin to assess overrepresentation of gene ontology categories in biological networks*. Bioinformatics, 21(16):3448–3449, 2005.

[120] Stephen Oliver. *Proteomics: guilt-by-association goes global*. Nature, 403(6770):601–603, 2000.

[121] David Altshuler, Mark Daly, and Leonid Kruglyak. *Guilt by association*. Nature genetics, 26(2):135–138, 2000.

[122] François Fouss, Kevin Francoisse, Luh Yen, Alain Pirotte, and Marco Saerens. *An experimental investigation of kernels on graphs for collaborative recommendation and semisupervised classification*. Neural networks, 31:53–72, 2012.

[123] Lieven PC Verbeke, Jimmy Van den Eynden, Ana Carolina Fierro, Piet Demeester, Jan Fostier, and Kathleen Marchal. *Pathway relevance ranking for tumor samples through network-based data integration*. PloS one, 10(7):e0133503, 2015.

[124] Mark DM Leiserson, Fabio Vandin, Hsin-Ta Wu, Jason R Dobson, Jonathan V Eldridge, Jacob L Thomas, Alexandra Papoutsaki, Younhun Kim, Beifang Niu, Michael McLellan, et al. *Pan-cancer network analysis identifies combinations of rare somatic mutations across pathways and protein complexes*. Nature genetics, 47(2):106–114, 2015.

[125] Chen-Hsiang Yeang, Trey Ideker, and Tommi Jaakkola. *Physical network models*. Journal of computational biology, 11(2-3):243–262, 2004.

[126] Paul Shannon, Andrew Markiel, Owen Ozier, Nitin S Baliga, Jonathan T Wang, Daniel Ramage, Nada Amin, Benno Schwikowski, and Trey Ideker. *Cytoscape: a software environment for integrated models of biomolecular interaction networks*. Genome research, 13(11):2498–2504, 2003.

[127] Bobby-Joe Breitkreutz, Chris Stark, and Mike Tyers. *Osprey: a network visualization system*. Genome biology, 4(3):R22, 2003.

[128] Athanasios Theocharidis, Stjin Van Dongen, Anton J Enright, and Tom C Freeman. *Network visualization and analysis of gene expression data using BioLayout Express3D*. Nature protocols, 4(10):1535–1550, 2009.

[129] Gabriela Bindea, Bernhard Mlecnik, Hubert Hackl, Pornpimol Charoentong, Marie Tosolini, Amos Kirilovsky, Wolf-Herman Fridman, Zlatko Trajanoski, Jérôme Galon, et al. *ClueGO: a Cytoscape plug-in to decipher functionally grouped gene ontology and pathway annotation networks*. Bioinformatics, 25(8):1091–1093, 2009.

[130] Jason Montojo, Khalid Zuberi, Harold Rodriguez, Farzana Kazi, George Wright, Sylva L Donaldson, Quaid Morris, and Gary D Bader. *GeneMANIA Cytoscape plugin: fast gene function predictions on the desktop*. Bioinformatics, 26(22):2927–2928, 2010.

[131] William S Bush and Jason H Moore. *Genome-wide association studies*. PLoS Comput Biol, 8(12):e1002822, 2012.

[132] Jacob J Michaelson, Salvatore Loguercio, and Andreas Beyer. *Detection and interpretation of expression quantitative trait loci (eQTL)*. Methods, 48(3):265–276, 2009.

[133] Xinwei Chen, Christine A Hackett, Rients E Niks, Peter E Hedley, Clare Booth, Arnis Druka, Thierry C Marcel, Anton Vels, Micha Bayer, Iain Milne, et al. *An eQTL analysis of partial resistance to Puccinia hordei in barley*. PLoS One, 5(1):e8598, 2010.

[134] Shuang-Xia Zhao, Wei Liu, Ming Zhan, Zhi-Yi Song, Shao-Ying Yang, Li-Qiong Xue, Chun-Ming Pan, Zhao-Hui Gu, Bing-Li Liu, Hai-Ning Wang, et al. *A refined study of FCRL genes from a genome-wide association study for Graves disease*. PloS one, 8(3):e57758, 2013.

[135] Daniel J Kvitek and Gavin Sherlock. *Whole genome, whole population sequencing reveals that loss of signaling networks is the major adaptive strategy in a constant environment*. PLoS Genet, 9(11):e1003972, 2013.

[136] Jungeui Hong and David Gresham. *Molecular specificity, convergence and constraint shape adaptive evolution in nutrient-poor environments*. PLoS Genet, 10(1):e1004041, 2014.

[137] J Arjan GM de Visser and Daniel E Rozen. *Clonal interference and the periodic selection of new beneficial mutations in Escherichia coli*. Genetics, 172(4):2093–2100, 2006.

[138] Katy C Kao and Gavin Sherlock. *Molecular characterization of clonal interference during adaptive evolution in asexual populations of Saccharomyces cerevisiae*. Nature genetics, 40(12):1499, 2008.

[139] Troy G Hammerstrom, Kathryn Beabout, Thomas P Clements, Gerda Saxer, and Yousif Shamoo. *Acinetobacter baumannii Repeatedly Evolves a Hypermutator Phenotype in Response to Tigecycline That Effectively Surveys Evolutionary Trajectories to Resistance*. PloS one, 10(10):e0140489, 2015.

[140] Robert Woods, Dominique Schneider, Cynthia L Winkworth, Margaret A Riley, and Richard E Lenski. *Tests of parallel molecular evolution in a long-term experiment with Escherichia coli*. Proceedings of the National Academy of Sciences, 103(24):9107–9112, 2006.

[141] Paul M Magwene, John H Willis, and John K Kelly. *The statistics of bulk segregant analysis using next generation sequencing*. PLoS computational biology, 7(11):e1002255, 2011.

[142] Jürgen Claesen, Lieven Clement, Ziv Shkedy, Maria R Foulquié-Moreno, and Tomasz Burzykowski. *Simultaneous mapping of multiple gene loci with pooled segregants*. PLoS One, 8(2):e55133, 2013.

[143] Jeffrey E Barrick, Dong Su Yu, Sung Ho Yoon, Haeyoung Jeong, Tae Kwang Oh, Dominique Schneider, Richard E Lenski, and Jihyun F Kim. *Genome evolution and adaptation in a long-term experiment with Escherichia coli*. Nature, 461(7268):1243–1247, 2009.

[144] Gregory I Lang, Daniel P Rice, Mark J Hickman, Erica Sodergren, George M Weinstock, David Botstein, and Michael M Desai. *Pervasive genetic hitchhiking and clonal interference in 40 evolving yeast populations*. Nature, 500(7464):571, 2013.

[145] Lucinda Notley-McRobb, Shona Seeto, and Thomas Ferenci. *Enrichment and elimination of mutY mutators in Escherichia coli populations*. Genetics, 162(3):1055–1062, 2002.

[146] Lucinda Notley-McRobb, Rachel Pinto, Shona Seeto, and Thomas Ferenci. *Regulation of mutY and nature of mutator mutations in Escherichia coli populations under nutrient limitation*. Journal of bacteriology, 184(3):739–745, 2002.

[147] Jeffrey E Barrick and Richard E Lenski. *Genome-wide mutational diversity in an evolving population of Escherichia coli*. In Cold Spring Harbor symposia on quantitative biology, pages sqb–2009. Cold Spring Harbor Laboratory Press, 2009.

[148] Erick Denamur and Ivan Matic. *Evolution of mutation rates in bacteria*. Molecular microbiology, 60(4):820–827, 2006.

[149] Michael J Wiser, Noah Ribeck, and Richard E Lenski. *Long-term dynamics of adaptation in asexual populations*. Science, 342(6164):1364–1367, 2013.

[150] Jeffrey E Barrick and Richard E Lenski. *Genome dynamics during experimental evolution*. Nature Reviews Genetics, 14(12):827–839, 2013.

[151] Antoine Giraud, Miroslav Radman, Ivan Matic, and François Taddei. *The rise and fall of mutator bacteria*. Current opinion in microbiology, 4(5):582–585, 2001.

[152] Adam Eyre-Walker and Peter D Keightley. *The distribution of fitness effects of new mutations*. Nature reviews. Genetics, 8(8):610, 2007.

[153] Sébastien Wielgoss, Jeffrey E Barrick, Olivier Tenaillon, Michael J Wiser, W James Dittmar, Stéphane Cruveiller, Béatrice Chane-Woon-Ming, Claudine Médigue, Richard E Lenski, and Dominique Schneider. *Mutation rate dynamics in a bacterial population reflect tension between adaptation and genetic load*. Proceedings of the National Academy of Sciences, 110(1):222–227, 2013.

[154] Gilles Thomas, Kevin B Jacobs, Meredith Yeager, Peter Kraft, Sholom Wacholder, Nick Orr, Kai Yu, Nilanjan Chatterjee, Robert Welch, Amy Hutchinson, et al. *Multiple loci identified in a genome-wide association study of prostate cancer*. Nature genetics, 40(3):310–315, 2008.

[155] Paul DP Pharoah, Ya-Yu Tsai, Susan J Ramus, Catherine M Phelan, Ellen L Goode, Kate Lawrenson, Melissa Buckley, Brooke L Fridley, Jonathan P Tyrer, Howard Shen, et al. *GWAS meta-analysis and replication identifies three new susceptibility loci for ovarian cancer*. Nature genetics, 45(4):362–370, 2013.

[156] David J Hunter, Peter Kraft, Kevin B Jacobs, David G Cox, Meredith Yeager, Susan E Hankinson, Sholom Wacholder, Zhaoming Wang, Robert Welch, Amy Hutchinson, et al. *A genome-wide association study identifies alleles in FGFR2 associated with risk of sporadic postmenopausal breast cancer*. Nature genetics, 39(7):870–874, 2007.

[157] John S Witte. *Genome-wide association studies and beyond*. Annual review of public health, 31:9–20, 2010.

[158] Aisha I Khan, Duy M Dinh, Dominique Schneider, Richard E Lenski, and Tim F Cooper. *Negative epistasis between beneficial mutations in an evolving bacterial population*. Science, 332(6034):1193–1196, 2011.

[159] Hsin-Hung Chou, Hsuan-Chao Chiu, Nigel F Delaney, Daniel Segrè, and Christopher J Marx. *Diminishing returns epistasis among beneficial mutations decelerates adaptation*. Science, 332(6034):1190–1192, 2011.

[160] K Al-Saktawi, M McLaughlin, M Klugmann, A Schneider, JA Barrie, MC McCulloch, P Montague, D Kirkham, K-A Nave, and IR Griffiths. *Genetic background determines phenotypic severity of the Plp rumpshaker mutation*. Journal of neuroscience research, 72(1):12–24, 2003.

[161] Guy Van den Broeck, Ingo Thon, Martijn Van Otterlo, and Luc De Raedt. *DT-ProbLog: A decision-theoretic probabilistic Prolog*. In Proceedings of the twenty-fourth AAAI conference on artificial intelligence, pages 1217–1222. AAAI Press, 2010.

[162] Dries De Maeyer, Joris Renkens, Lore Cloots, Luc De Raedt, and Kathleen Marchal. *PheNetic: network-based interpretation of unstructured gene lists in E. coli*. Molecular BioSystems, 9(7):1594–1603, 2013.

[163] Paul D Sniegowski, Philip J Gerrish, and Richard E Lenski. *Evolution of high mutation rates in experimental populations of E. coli*. Nature, 387(6634):703, 1997.

[164] Aaron C Shaver, Peter G Dombrowski, Joseph Y Sweeney, Tania Treis, Renata M Zappala, and Paul D Sniegowski. *Fitness evolution and the rise of mutator alleles in experimental Escherichia coli populations*. Genetics, 162(2):557–566, 2002.

[165] Giovanni Ciriello, Ethan Cerami, Chris Sander, and Nikolaus Schultz. *Mutual exclusivity analysis identifies oncogenic network modules*. Genome research, 22(2):398–406, 2012.

[166] Maria A Svensson, Christopher J LaFargue, Theresa Y MacDonald, Dorothee Pflueger, Naoki Kitabayashi, Ashley M Santa-Cruz, Karl E Garsha, Ubaradka G Sathyanarayana, Janice P Riley, Chol S Yun, et al. *Testing mutual exclusivity of ETS rearranged prostate cancer*. Laboratory investigation, 91(3):404–412, 2011.

[167] Benjamin Horemans, Karolien Bers, Erick Ruiz Romero, Eva Pose Juan, Vincent Dunon, René De Mot, and Dirk Springael. *Functional redundancy of linuron degradation in microbial communities in agricultural soil and biopurification systems*. Applied and environmental microbiology, 82(9):2843–2853, 2016.

[168] Stuart A West, Ashleigh S Griffin, and Andy Gardner. *Social semantics: altruism, cooperation, mutualism, strong reciprocity and group selection*. Journal of evolutionary biology, 20(2):415–432, 2007.

[169] Kevin R Foster and Thomas Bell. *Competition, not cooperation, dominates interactions among culturable microbial species*. Current biology, 22(19):1845–1850, 2012.

[170] Alexander H Rickard, Robert J Palmer, David S Blehert, Shawn R Campagna, Martin F Semmelhack, Paul G Egland, Bonnie L Bassler, and Paul E Kolenbrander. *Autoinducer 2: a concentration-dependent signal for mutualistic bacterial biofilm growth*. Molecular microbiology, 60(6):1446–1456, 2006.

[171] Takefumi Shimoyama, Souichiro Kato, Shun'ichi Ishii, and Kazuya Watanabe. *Flagellum mediates symbiosis*. Science, 323(5921):1574–1574, 2009.

[172] Winnie Dejonghe, Ellen Berteloot, Johan Goris, Nico Boon, Katrien Crul, Siska Maertens, Monica Höfte, Paul De Vos, Willy Verstraete, and Eva M Top. *Synergistic degradation of linuron by a bacterial consortium and isolation of a single linuron-degrading Variovorax strain*. Applied and Environmental Microbiology, 69(3):1532–1541, 2003.

[173] Karolien Bers, I Batisson, Paul Proost, R Wattiez, René De Mot, and Dirk Springael. *HylA, an alternative hydrolase for initiation of catabolism of the phenylurea herbicide linuron in Variovorax sp. strains*. Applied and environmental microbiology, 79(17):5258–5263, 2013.

[174] Philip Breugelmans, Kim Bundvig Barken, Tim Tolker-Nielsen, Johan Hofkens, Winnie Dejonghe, and Dirk Springael. *Architecture and spatial organization in a triple-species bacterial biofilm synergistically degrading the phenylurea herbicide linuron*. FEMS microbiology ecology, 64(2):271–282, 2008.

[175] Simone Dealtry, Eman H Nour, Peter N Holmsgaard, Guo-Chun Ding, Viola Weichelt, Vincent Dunon, Holger Heuer, Lars H Hansen, Søren J Sørensen, Dirk Springael, et al. *Exploring the complex response to linuron of bacterial communities from biopurification systems by means of cultivation-independent methods*. FEMS microbiology ecology, 92(2):fiv157, 2016.

[176] Paolina Garbeva, Mark W Silby, Jos M Raaijmakers, Stuart B Levy, and Wietse De Boer. *Transcriptional and antagonistic responses of Pseudomonas fluorescens Pf0-1 to phylogenetically different bacterial competitors*. The ISME journal, 5(6):973–985, 2011.

[177] José Pérez, Alex Buchanan, Brett Mellbye, Rebecca Ferrell, Jeffrey H Chang, Frank Chaplen, Peter J Bottomley, Daniel J Arp, and Luis A Sayavedra-Soto. *Interactions of Nitrosomonas europaea and Nitrobacter winogradskyi grown in co-culture*. Archives of microbiology, 197(1):79–89, 2015.

[178] Vera Tai, Ian T Paulsen, Katherine Phillippy, D Aaron Johnson, and Brian Palenik. *Whole-genome microarray analyses of Synechococcus–Vibrio interactions*. Environmental microbiology, 11(10):2698–2709, 2009.

[179] Adam Z Rosenthal, Eric G Matson, Avigdor Eldar, and Jared R Leadbetter. *RNA-seq reveals cooperative metabolic interactions between two termite-gut spirochete species in co-culture*. The ISME journal, 5(7):1133–1142, 2011.

[180] Alexander S Beliaev, Margie F Romine, Margrethe Serres, Hans C Bernstein, Bryan E Linggi, Lye M Markillie, Nancy G Isern, William B Chrisler, Leo A Kucek, Eric A Hill, et al. *Inference of interactions in cyanobacterial–heterotrophic co-cultures via transcriptome sequencing*. The ISME journal, 8(11):2243–2255, 2014.

[181] Jorge Frias-Lopez and Ana Duran-Pinedo. *Effect of periodontal pathogens on the metatranscriptome of a healthy multispecies biofilm model*. Journal of bacteriology, 194(8):2082–2095, 2012.

[182] Yichao Wu, Anee Mohanty, Wu Siang Chia, and Bin Cao. *Influence of 3-Chloroaniline on the Biofilm Lifestyle of Comamonas testosteroni and its Implications on Bioaugmentation*. Applied and environmental microbiology, 82(14):4401–4409, 2016.

[183] Douglas B Kell, Marie Brown, Hazel M Davey, Warwick B Dunn, Irena Spasic, and Stephen G Oliver. *Metabolic footprinting and systems biology: the medium is the message*. Nature Reviews Microbiology, 3(7):557–565, 2005.

[184] Tony L Palama, I Canard, Gilles JP Rautureau, C Mirande, S Chatellier, and Bénédicte Elena-Herrmann. *Identification of bacterial species by untargeted NMR spectroscopy of the exo-metabolome*. Analyst, 141(15):4558–4561, 2016.

[185] Dawei Ren. *Synergistic interactions in multispecies biofilms*. PhD thesis, University of Copenhagen, Unpublished.

[186] Daniel Cerqueda-García, León P Martínez-Castilla, Luisa I Falcón, and Luis Delaye. *Metabolic analysis of Chlorobium chlorochromatii CaD3 reveals clues of the symbiosis in Chlorochromatium aggregatum.* The ISME journal, 8(5):991–998, 2014.

[187] Roland Wenter, Katharina Hütz, Dörte Dibbern, Tao Li, Veronika Reisinger, Matthias Plöscher, Lutz Eichacker, Brian Eddie, Thomas Hanson, Donald A Bryant, et al. *Expression-based identification of genetic determinants of the bacterial symbiosis Chlorochromatium aggregatum*. Environmental microbiology, 12(8):2259–2276, 2010.

[188] Jun Teramoto, Yoko Yamanishi, El-Shimy H Magdy, Akiko Hasegawa, Ayako Kori, Masahiro Nakajima, Fumihito Arai, Toshio Fukuda, and Akira Ishihama. *Single live-bacterial cell assay of promoter activity and regulation*. Genes to cells, 15(11):1111–1122, 2010.

[189] Pedro González-Torres, Leszek P Pryszcz, Fernando Santos, Manuel Martínez-García, Toni Gabaldón, and Josefa Antón. *Interactions between closely related bacterial strains are revealed by deep transcriptome sequencing*. Applied and environmental microbiology, 81(24):8445–8456, 2015.

[190] CB Ward and DA Glaser. *Correlation between rate of cell growth and rate of DNA synthesis in Escherichia coli B/r*. Proceedings of the National Academy of Sciences, 68(5):1061–1064, 1971.

[191] Darja Žgur-Bertok. *DNA damage repair and bacterial pathogens*. PLoS Pathog, 9(11):e1003711, 2013.

[192] Daniel J Dwyer, Michael A Kohanski, Boris Hayete, and James J Collins. *Gyrase inhibitors induce an oxidative damage cellular death pathway in Escherichia coli*. Molecular systems biology, 3(1):91, 2007.

[193] Alistair B Russell, S Brook Peterson, and Joseph D Mougous. *Type VI secretion system effectors: poisons with a purpose*. Nature reviews microbiology, 12(2):137–148, 2014.

[194] Erin C Garcia, Andrew I Perault, Sara A Marlatt, and Peggy A Cotter. *Interbacterial signaling via Burkholderia contact-dependent growth inhibition system proteins*. Proceedings of the National Academy of Sciences, 113(29):8296–8301, 2016.

[195] Nikole E Kimes, Mario López-Pérez, Eva Ausó, Rohit Ghai, and Francisco Rodriguez-Valera. *RNA sequencing provides evidence for functional variability between naturally co-existing Alteromonas macleodii lineages*. BMC genomics, 15(1):938, 2014.

[196] Benjamin Horemans, Erik Smolders, and Dirk Springael. *Carbon source utilization profiles suggest additional metabolic interactions in a synergistic linuron-degrading bacterial consortium*. FEMS microbiology ecology, 84(1):24–34, 2013.

[197] Nico Boon, Johan Goris, Paul De Vos, Willy Verstraete, and Eva M Top. *Genetic Diversity among 3-Chloroaniline-and Aniline-Degrading Strains of theComamonadaceae*. Applied and environmental microbiology, 67(3):1107–1115, 2001.

[198] Benjamin Horemans, Johan Hofkens, Erik Smolders, and Dirk Springael. *Biofilm formation of a bacterial consortium on linuron at micropollutant concentrations in continuous flow chambers and the impact of dissolved organic matter*. FEMS microbiology ecology, 88(1):184–194, 2014.

[199] Daniel C Ilut, Jeremy E Coate, Amelia K Luciano, Thomas G Owens, Gregory D May, Andrew Farmer, and Jeff J Doyle. *A comparative transcriptomic study of an allotetraploid and its diploid progenitors illustrates the unique advantages and challenges of RNA-seq in plant species*. American journal of botany, 99(2):383–396, 2012.

[200] Robert K Colwell, Anne Chao, Nicholas J Gotelli, Shang-Yi Lin, Chang Xuan Mao, Robin L Chazdon, and John T Longino. *Models and estimators linking individual-based and sample-based rarefaction, extrapolation and comparison of assemblages*. Journal of plant ecology, 5(1):3–21, 2012.

[201] Shingo Suzuki, Takaaki Horinouchi, and Chikara Furusawa. *Prediction of antibiotic resistance by gene expression profiles*. Nature communications, 5, 2014.

[202] Minoru Kanehisa, Susumu Goto, Yoko Sato, Miho Furumichi, and Mao Tanabe. *KEGG for integration and interpretation of large-scale molecular data sets*. Nucleic acids research, 40(D1):D109–D114, 2012.

[203] Ramy K Aziz, Daniela Bartels, Aaron A Best, Matthew DeJongh, Terrence Disz, Robert A Edwards, Kevin Formsma, Svetlana Gerdes, Elizabeth M Glass, Michael Kubal, et al. *The RAST Server: rapid annotations using subsystems technology*. BMC genomics, 9(1):75, 2008.

[204] Jeremy R Dettman, Nicolas Rodrigue, Anita H Melnyk, Alex Wong, Susan F Bailey, and Rees Kassen. *Evolutionary insight from whole-genome sequencing of experimentally evolved microbes*. Molecular ecology, 21(9):2058–2077, 2012.

[205] Tadeusz J Kawecki, Richard E Lenski, Dieter Ebert, Brian Hollis, Isabelle Olivieri, and Michael C Whitlock. *Experimental evolution*. Trends in ecology & evolution, 27(10):547–560, 2012.

[206] Matthew D Herron and Michael Doebeli. *Parallel evolutionary dynamics of adaptive diversification in Escherichia coli*. PLoS Biol, 11(2):e1001490, 2013.

[207] Patricia L Foster. *Stress-induced mutagenesis in bacteria*. Critical reviews in biochemistry and molecular biology, 42(5):373–397, 2007.

[208] Li Ding, Michael C Wendl, Joshua F McMichael, and Benjamin J Raphael. *Expanding the computational toolbox for mining cancer genomes*. Nature Reviews Genetics, 15(8):556–570, 2014.

[209] Gregory I Lang and Michael M Desai. *The spectrum of adaptive mutations in experimental evolution*. Genomics, 104(6):412–416, 2014.

[210] Jimmy Lin, Christine M Gan, Xiaosong Zhang, Siân Jones, Tobias Sjöblom, Laura D Wood, D Williams Parsons, Nickolas Papadopoulos, Kenneth W Kinzler, Bert Vogelstein, et al. *A multidimensional analysis of genes mutated in breast and colorectal cancers*. Genome research, 17(9):000–000, 2007.

[211] Laura D Wood, D Williams Parsons, Siân Jones, Jimmy Lin, Tobias Sjöblom, Rebecca J Leary, Dong Shen, Simina M Boca, Thomas Barber, Janine Ptak, et al. *The genomic landscapes of human breast and colorectal cancers*. Science, 318(5853):1108–1113, 2007.

[212] Jessica Plucain, Thomas Hindré, Mickaël Le Gac, Olivier Tenaillon, Stéphane Cruveiller, Claudine Médigue, Nicholas Leiby, William R Harcombe, Christopher J Marx, Richard E Lenski, et al. *Epistasis and allele specificity in the emergence of a stable polymorphism in Escherichia coli*. Science, 343(6177):1366–1369, 2014.

[213] Luc De Raedt, Angelika Kimmig, and Hannu Toivonen. *ProbLog: A Probabilistic Prolog and Its Application in Link Discovery*. In IJCAI, volume 7, pages 2462–2467, 2007.

[214] Jianxing Feng, Clifford A Meyer, Qian Wang, Jun S Liu, X Shirley Liu, and Yong Zhang. *GFOLD: a generalized fold change for ranking differentially expressed genes from RNA-seq data*. Bioinformatics, 28(21):2782–2788, 2012.

[215] Yudi Pawitan, Stefan Michiels, Serge Koscielny, Arief Gusnanto, and Alexander Ploner. *False discovery rate, sensitivity and sample size for microarray studies*. Bioinformatics, 21(13):3017–3024, 2005.

[216] Adnan Darwiche and Pierre Marquis. *A knowledge compilation map*. Journal of Artificial Intelligence Research, 17(1):229–264, 2002.

[217] Adnan Darwiche and Pierre Marquis. *A perspective on knowledge compilation*. In IJCAI, volume 1, pages 175–182, 2001.

[218] Anthony Gitter, Judith Klein-Seetharaman, Anupam Gupta, and Ziv Bar-Joseph. *Discovering pathways by orienting edges in protein interaction networks*. Nucleic Acids Res, 2011.

[219] Saket Navlakha, Anthony Gitter, and Ziv Bar-Joseph. *A Network-based Approach for Predicting Missing Pathway Interactions*. PLOS Computational Biology, 2012.

[220] Anna Stincone, Nazish Daudi, Ayesha S Rahman, Philipp Antczak, Ian Henderson, Jeffrey Cole, Matthew D Johnson, Peter Lund, and Francesco Falciani. *A systems biology approach sheds new light on Escherichia coli acid resistance*. Nucleic acids research, 39(17):7512–7528, 2011.

[221] Kristof Engelen, Qiang Fu, Pieter Meysman, Aminael Sánchez-Rodríguez, Riet De Smet, Karen Lemmens, Ana Carolina Fierro, and Kathleen Marchal. *COLOMBOS: access port for cross-platform bacterial expression compendia*. PLoS One, 6(7):e20938, 2011.

[222] Erik Garrison and Gabor Marth. *Haplotype-based variant detection from short-read sequencing*. arXiv preprint arXiv:1207.3907, 2012.

[223] Mickaël Le Gac, Jessica Plucain, Thomas Hindré, Richard E Lenski, and Dominique Schneider. *Ecological and evolutionary dynamics of coexisting lineages during a long-term experiment with Escherichia coli*. Proceedings of the National Academy of Sciences, 109(24):9487–9492, 2012.

[224] Gordon K Smyth et al. *Linear models and empirical bayes methods for assessing differential expression in microarray experiments*. Stat Appl Genet Mol Biol, 3(1):3, 2004.

[225] Minoru Kanehisa, Susumu Goto, Yoko Sato, Masayuki Kawashima, Miho Furumichi, and Mao Tanabe. *Data, information, knowledge and principle: back to metabolism in KEGG*. Nucleic Acid Research, 2014.

[226] Lars J Jensen, Michael Kuhn, Manuel Stark, Samuel Chaffron, Chris Creevey, Jean Muller, Tobias Doerks, Philippe Julien, Alexander Roth, Milan Simonovic, et al. *STRING 8a global view on proteins and their functional interactions in 630 organisms*. Nucleic acids research, 37(suppl 1):D412–D416, 2009.

[227] Tobias Norström, Jonas Lannergård, and Diarmaid Hughes. *Genetic and phenotypic identification of fusidic acid-resistant mutants with the small-colony-variant phenotype in Staphylococcus aureus*. Antimicrobial agents and chemotherapy, 51(12):4438–4446, 2007.

[228] Tracy L Raivio, Shannon KD Leblanc, and Nancy L Price. *The Escherichia coli Cpx envelope stress response regulates genes of diverse function that impact antibiotic resistance and membrane integrity*. Journal of bacteriology, 195(12):2755–2767, 2013.

[229] Kyle R Allison, Mark P Brynildsen, and James J Collins. *Metabolite-enabled eradication of bacterial persisters by aminoglycosides*. Nature, 473(7346):216–220, 2011.

[230] Daniel E Rozen and Richard E Lenski. *Long-term experimental evolution in Escherichia coli. VIII. Dynamics of a balanced polymorphism*. The American Naturalist, 155(1):24–35, 2000.

[231] Daniel E Rozen, Dominique Schneider, and Richard E Lenski. *Long-term experimental evolution in Escherichia coli. XIII. Phylogenetic history of a balanced polymorphism*. Journal of Molecular Evolution, 61(2):171–180, 2005.

[232] Daniel E Rozen, Nadège Philippe, J Arjan de Visser, Richard E Lenski, and Dominique Schneider. *Death and cannibalism in a seasonal environment facilitate bacterial coexistence*. Ecology letters, 12(1):34–44, 2009.

[233] Gregory W Luli and WILLIAM R Strohl. *Comparison of growth, acetate production, and acetate inhibition of Escherichia coli strains in batch and fed-batch fermentations*. Applied and environmental microbiology, 56(4):1004–1011, 1990.

[234] Christine M Beatty, Douglas F Browning, Stephen JW Busby, and Alan J Wolfe. *Cyclic AMP receptor protein-dependent activation of the Escherichia coli acsP2 promoter by a synergistic class III mechanism*. Journal of bacteriology, 185(17):5148–5157, 2003.

[235] Sophie Maisnier-Patin, John R Roth, Åsa Fredriksson, Thomas Nyström, Otto G Berg, and Dan I Andersson. *Genomic buffering mitigates the effects of deleterious mutations in bacteria*. Nature genetics, 37(12):1376–1379, 2005.

[236] Darren J Burgess. *RNA stability: remember your driver*. Nature Reviews Genetics, 13(2):72–73, 2012.

[237] Andrey Alexeyenko, Woojoo Lee, Maria Pernemalm, Justin Guegan, Philippe Dessen, Vladimir Lazar, Janne Lehtiö, and Yudi Pawitan. *Network enrichment analysis: extension of gene-set enrichment analysis to gene networks*. BMC bioinformatics, 13(1):226, 2012.

[238] Haisu Ma, Eric E Schadt, Lee M Kaplan, and Hongyu Zhao. *COSINE: COndition-SpecIfic sub-NEtwork identification using a global optimization method*. Bioinformatics, 27(9):1290–1298, 2011.

[239] Minghong Fang, Xiaohua Hu, Tingting He, Yan Wang, Junmin Zhao, Xianjun Shen, and Jie Yuan. *Prioritizing disease-causing genes based on network diffusion and rank concordance*. In Bioinformatics and Biomedicine (BIBM), 2014 IEEE International Conference on, pages 242–247. IEEE, 2014.

[240] Alex Lan, Ilan Y Smoly, Guy Rapaport, Susan Lindquist, Ernest Fraenkel, and Esti Yeger-Lotem. *ResponseNet: revealing signaling and regulatory networks linking genetic and transcriptomic screening data*. Nucleic acids research, page gkr359, 2011.

[241] Sepideh Babaei, Marc Hulsman, Marcel Reinders, and Jeroen de Ridder. *Detecting recurrent gene mutation in interaction network context using multi-scale graph diffusion*. BMC bioinformatics, 14(1):29, 2013.

[242] Matan Hofree, John P Shen, Hannah Carter, Andrew Gross, and Trey Ideker. *Network-based stratification of tumor mutations*. Nature methods, 10(11):1108–1115, 2013.

[243] Fabio Vandin, Eli Upfal, and Benjamin J Raphael. *Algorithms for detecting significantly mutated pathways in cancer*. Journal of Computational Biology, 18(3):507–522, 2011.

[244] Mark DM Leiserson, Dima Blokh, Roded Sharan, and Benjamin J Raphael. *Simultaneous identification of multiple driver pathways in cancer*. PLoS Comput Biol, 9(5):e1003054, 2013.

[245] Fabio Vandin, Eli Upfal, and Benjamin J Raphael. *De novo discovery of mutated driver pathways in cancer*. Genome research, 22(2):375–385, 2012.

[246] Sean Michael Carroll and Christopher J Marx. *Evolution after introduction of a novel metabolic pathway consistently leads to restoration of wild-type physiology*. PLoS Genet, 9(4):e1003427, 2013.

[247] Alejandra Rodríguez-Verdugo, Olivier Tenaillon, and Brandon S Gaut. *First-step mutations during adaptation restore the expression of hundreds of genes*. Molecular biology and evolution, 33(1):25–39, 2016.

[248] Daniel J Kvitek and Gavin Sherlock. *Reciprocal sign epistasis between frequently experimentally evolved adaptive mutations causes a rugged fitness landscape*. PLoS Genet, 7(4):e1002056, 2011.

[249] Robert J Woods, Jeffrey E Barrick, Tim F Cooper, Utpala Shrestha, Mark R Kauth, and Richard E Lenski. *Second-order selection for evolvability in a large Escherichia coli population*. Science, 331(6023):1433–1436, 2011.

[250] JT Anderson, MR Wagner, CA Rushworth, KVSK Prasad, and T Mitchell-Olds. *The evolution of quantitative traits in complex environments*. Heredity, 112(1):4–12, 2014.

[251] Hans P Steenackers, Ilse Parijs, Kevin R Foster, and Jozef Vanderleyden. *Experimental evolution in biofilm populations*. FEMS microbiology reviews, page fuw002, 2016.

[252] Bram Van den Bergh, Joran E Michiels, Tom Wenseleers, Etthel M Windels, Pieterjan Vanden Boer, Donaat Kestemont, Luc De Meester, Kevin J Verstrepen, Natalie Verstraeten, Maarten Fauvart, et al. *Frequency of antibiotic application drives rapid evolutionary adaptation of Escherichia coli persistence*. Nature microbiology, 1:16020, 2016.

[253] Adam C Palmer and Roy Kishony. *Understanding, predicting and manipulating the genotypic evolution of antibiotic resistance*. Nature Reviews Genetics, 14(4):243–248, 2013.

[254] James D Winkler and Katy C Kao. *Recent advances in the evolutionary engineering of industrial biocatalysts*. Genomics, 104(6):406–411, 2014.

[255] Christian Schlötterer, R Kofler, E Versace, R Tobler, and SU Franssen. *Combining experimental evolution with next-generation sequencing: a powerful tool to study adaptation from standing genetic variation*. Heredity, 114(5):431–440, 2015.

[256] Adam Eyre-Walker. *Genetic architecture of a complex trait and its implications for fitness and genome-wide association studies*. Proceedings of the National Academy of Sciences, 107(suppl 1):1752–1756, 2010.

[257] Sutticha Na-Ranong Thammasittirong, Thanawan Thirasaktana, Anon Thammasittirong, and Malee Srisodsuk. *Improvement of ethanol production by ethanol-tolerant Saccharomyces cerevisiae UVNR56*. SpringerPlus, 2(1):583, 2013.

[258] Sarah Huffer, Christine M Roche, Harvey W Blanch, and Douglas S Clark. *Escherichia coli for biofuel production: bridging the gap from promise to practice*. Trends in biotechnology, 30(10):538–545, 2012.

[259] Ramon Gonzalez, Han Tao, JE Purvis, SW York, KT Shanmugam, and LO Ingram. *Gene array-based identification of changes that contribute to ethanol tolerance in ethanologenic Escherichia coli: comparison of KO11 (parent) to LY01 (resistant mutant)*. Biotechnology progress, 19(2):612–623, 2003.

[260] Hani Goodarzi, Bryson D Bennett, Sasan Amini, Marshall L Reaves, Alison K Hottes, Joshua D Rabinowitz, and Saeed Tavazoie. *Regulatory and metabolic rewiring during laboratory evolution of ethanol tolerance in E. coli*. Molecular Systems Biology, 6(1):378, 2010.

[261] Sergios A Nicolaou, Stefan M Gaida, and Eleftherios T Papoutsakis. *Exploring the combinatorial genomic space in Escherichia coli for ethanol tolerance*. Biotechnology journal, 7(11):1337–1345, 2012.

[262] Steve Swinnen, Kristien Schaerlaekens, Thiago Pais, Jürgen Claesen, Georg Hubmann, Yudi Yang, Mekonnen Demeke, María R Foulquié-Moreno, Annelies Goovaerts, Kris Souvereyns, et al. *Identification of novel causative genes determining the complex trait of high ethanol tolerance in yeast using pooled-segregant whole-genome sequence analysis*. Genome research, 22(5):975–984, 2012.

[263] Felix H Lam, Adel Ghaderi, Gerald R Fink, and Gregory Stephanopoulos. *Engineering alcohol tolerance in yeast*. Science, 346(6205):71–75, 2014.

[264] Michael S Lawrence, Petar Stojanov, Paz Polak, Gregory V Kryukov, Kristian Cibulskis, Andrey Sivachenko, Scott L Carter, Chip Stewart, Craig H Mermel, Steven A Roberts, et al. *Mutational heterogeneity in cancer and the search for new cancer-associated genes*. Nature, 499(7457):214–218, 2013.

[265] Nathan D Dees, Qunyuan Zhang, Cyriac Kandoth, Michael C Wendl, William Schierding, Daniel C Koboldt, Thomas B Mooney, Matthew B Callaway, David Dooling, Elaine R Mardis, et al. *MuSiC: identifying mutational significance in cancer genomes*. Genome research, 22(8):1589–1598, 2012.

[266] David Tamborero, Abel Gonzalez-Perez, and Nuria Lopez-Bigas. *OncodriveCLUST: exploiting the positional clustering of somatic mutations to identify cancer genes*. Bioinformatics, 29(18):2238–2244, 2013.

[267] Peter E Chen and B Jesse Shapiro. *The advent of genome-wide association studies for bacteria*. Current opinion in microbiology, 25:17–24, 2015.

[268] Timothy D Read and Ruth C Massey. *Characterizing the genetic basis of bacterial phenotypes using genome-wide association studies: a new direction for bacteriology*. Genome medicine, 6(11):109, 2014.

[269] Özgün Babur, Mithat Gönen, Bülent Arman Aksoy, Nikolaus Schultz, Giovanni Ciriello, Chris Sander, and Emek Demir. *Systematic identification of cancer driving signaling pathways based on mutual exclusivity of genomic alterations*. Genome biology, 16(1):45, 2015.

[270] Thanh Le Van, Matthijs van Leeuwen, Ana Carolina Fierro, Dries De Maeyer, Jimmy Van den Eynden, Lieven Verbeke, Luc De Raedt, Kathleen Marchal, and Siegfried Nijssen. *Simultaneous discovery of cancer subtypes and subtype features by molecular data integration*. Bioinformatics, 32(17):i445–i454, 2016.

[271] Ruben AT Mars, Karoline Mendonça, Emma L Denham, and Jan Maarten van Dijl. *The reduction in small ribosomal subunit abundance in ethanol-stressed cells of Bacillus subtilis is mediated by a SigB-dependent antisense RNA*. Biochimica et Biophysica Acta (BBA)-Molecular Cell Research, 1853(10):2553–2559, 2015.

[272] Toshihiro Suzuki, Kohei Seta, Chiaki Nishikawa, Eri Hara, Toshiya Shigeno, and Toshiaki Nakajima-Kambe. *Improved ethanol tolerance and ethanol production from glycerol in a streptomycin-resistant Klebsiella variicola mutant obtained by ribosome engineering*. Bioresource technology, 176:156–162, 2015.

[273] Sheng Jian Cai and Masayori Inouye. *EnvZ-OmpR interaction and osmoregulation in Escherichia coli*. Journal of Biological Chemistry, 277(27):24155–24161, 2002.

[274] Heather J Quinn, Andrew DS Cameron, and Charles J Dorman. *Bacterial regulon evolution: distinct responses and roles for the identical OmpR proteins of Salmonella Typhimurium and Escherichia coli in the acid stress response*. PLoS Genet, 10(3):e1004215, 2014.

[275] François Taddei, Miroslav Radman, J Maynard-Smith, Bruno Toupance, et al. *Role of mutator alleles in adaptive evolution*. Nature, 387(6634):700, 1997.

[276] Robert Vaser, Swarnaseetha Adusumalli, Sim Ngak Leng, Mile Sikic, and Pauline C Ng. *SIFT missense predictions for genomes*. Nature protocols, 11(1):1, 2016.

[277] Richard J Heath and Charles O Rock. *Roles of the FabA and FabZ $\beta$-hydroxyacyl-acyl carrier protein dehydratases in Escherichia coli fatty acid biosynthesis*. Journal of Biological Chemistry, 271(44):27795–27801, 1996.

[278] Burkhard Loffeld and Heribert Keweloh. *cis/trans isomerization of unsaturated fatty acids as possible control mechanism of membrane fluidity inPseudomonas putida P8*. Lipids, 31(8):811–815, 1996.

[279] Yong-Mei Zhang and Charles O Rock. *Membrane lipid homeostasis in bacteria*. Nature Reviews Microbiology, 6(3):222–233, 2008.

[280] Thomas M Buttke and Lonnie O'Neal Ingram. *Ethanol-induced changes in lipid composition of Escherichia coli: inhibition of saturated fatty acid synthesis in vitro*. Archives of biochemistry and biophysics, 203(2):565–571, 1980.

[281] Lian Hua Luo, Pil-Soo Seo, Jeong-Woo Seo, Sun-Yeon Heo, Dae-Hyuk Kim, and Chul Ho Kim. *Improved ethanol tolerance in Escherichia coli by changing the cellular fatty acids composition through genetic manipulation*. Biotechnology letters, 31(12):1867, 2009.

[282] David G White, John D Goldman, Bruce Demple, and Stuart B Levy. *Role of the acrAB locus in organic solvent tolerance mediated by expression of marA, soxS, or robA in Escherichia coli.* Journal of bacteriology, 179(19):6122–6126, 1997.

[283] Shota Atsumi, Tung-Yun Wu, Iara MP Machado, Wei-Chih Huang, Pao-Yang Chen, Matteo Pellegrini, and James C Liao. *Evolution, genomic analysis, and reconstruction of isobutanol tolerance in Escherichia coli.* Molecular systems biology, 6(1):449, 2010.

[284] Amanda C Bernardi, Claudia S Gai, Jingnan Lu, Anthony J Sinskey, and Christopher J Brigham. *Experimental evolution and gene knockout studies reveal AcrA-mediated isobutanol tolerance in Ralstonia eutropha*. Journal of bioscience and bioengineering, 122(1):64–69, 2016.

[285] M Ines Borges-Walmsley, Jeremy Beauchamp, Sharon M Kelly, Kornelia Jumel, Denise Candlish, Stephen E Harding, Nicholas C Price, and Adrian R Walmsley. *Identification of oligomerization and drug-binding domains of the membrane fusion protein EmrA*. Journal of Biological Chemistry, 278(15):12903–12912, 2003.

[286] Satoshi Nagakubo, Kunihiko Nishino, Takahiro Hirata, and Akihito Yamaguchi. *The putative response regulator BaeR stimulates multidrug resistance of Escherichia coli via a novel multidrug exporter system, MdtABC.* Journal of bacteriology, 184(15):4161–4167, 2002.

[287] Kunihiko Nishino and Akihito Yamaguchi. *EvgA of the two-component signal transduction system modulates production of the YhiUV multidrug transporter in Escherichia coli.* Journal of bacteriology, 184(8):2319–2323, 2002.

[288] Concetta C DiRusso, Tamra L Heimert, and Amy K Metzger. *Characterization of FadR, a global transcriptional regulator of fatty acid metabolism in Escherichia coli. Interaction with the fadB promoter is prevented by long chain fatty acyl coenzyme A.* Journal of Biological Chemistry, 267(12):8685–8691, 1992.

[289] Hye Yun Oh, Jae Ok Lee, and Ok Bin Kim. *Increase of organic solvent tolerance of Escherichia coli by the deletion of two regulator genes, fadR and marR*. Applied microbiology and biotechnology, 96(6):1619–1627, 2012.

[290] Jeremy J Minty, Ann A Lesnefsky, Fengming Lin, Yu Chen, Ted A Zaroff, Artur B Veloso, Bin Xie, Catie A McConnell, Rebecca J Ward, Donald R Schwartz, et al. *Evolution combined with genomic study elucidates genetic bases of isobutanol tolerance in Escherichia coli.* Microbial cell factories, 10(1):18, 2011.

[291] Kenneth Michael Dombek and LO Ingram. *Effects of ethanol on the Escherichia coli plasma membrane.* Journal of bacteriology, 157(1):233–239, 1984.

[292] Juan L Ramos, Estrella Duque, María-Trinidad Gallegos, Patricia Godoy, María Isabel Ramos-González, Antonia Rojas, Wilson Terán, and Ana Segura. *Mechanisms of solvent tolerance in gram-negative bacteria*. Annual Reviews in Microbiology, 56(1):743–768, 2002.

[293] Lonnie O'Neal Ingram and Thomas M Buttke. *Effects of alcohols on microorganisms*. Advances in microbial physiology, 25:253–300, 1985.

[294] Lonnie O Ingram. *Ethanol tolerance in bacteria*. Critical reviews in biotechnology, 9(4):305–319, 1989.

[295] Sarah Huffer, Melinda E Clark, Jonathan C Ning, Harvey W Blanch, and Douglas S Clark. *Role of alcohols in growth, lipid composition, and membrane fluidity of yeasts, bacteria, and archaea*. Applied and environmental microbiology, 77(18):6400–6408, 2011.

[296] Juan M Vanegas, Maria F Contreras, Roland Faller, and Marjorie L Longo. *Role of unsaturated lipid and ergosterol in ethanol tolerance of model yeast biomembranes*. Biophysical journal, 102(3):507–516, 2012.

[297] Socorro Gama-Castro, Heladia Salgado, Alberto Santos-Zavaleta, Daniela Ledezma-Tejeida, Luis Muiz-Rascado Jair Santiago Garca-Sotelo, Kevin Alquicira-Hernndez, Irma Martnez-Flores, Lucia Pannier Jaime Abraham Castro-Mondragn, Alejandra Medina-Rivera, Hilda Solano-Lira, Csar Bonavides-Martnez Ernesto Prez-Rueda, Shirley Alquicira-Hernndez, Liliana Porrn-Sotelo, Alejandra Lpez-Fuentes Anastasia Hernndez-Koutoucheva, Vctor Del Moral-Chvez, Fabio Rinaldi, and Julio Collado-Vides. *high-level integration of gene regulation, coexpression, motif clustering and beyond*. Nucleic Acid Research, 2016.

[298] Albert-Lszl Barabsi and Rka Albert. *Emergence of scaling in random networks*. Science, 1999.

[299] Pauline C Ng and Steven Henikoff. *Predicting deleterious amino acid substitutions*. Genome research, 11(5):863–874, 2001.

[300] Prateek Kumar, Steven Henikoff, and Pauline C Ng. *Predicting the effects of coding non-synonymous variants on protein function using the SIFT algorithm*. Nature protocols, 4(7):1073–1081, 2009.

[301] Boris Iglewicz and David Caster Hoaglin. *How to detect and handle outliers*. ASQC Quality Press, 1993.

[302] Luigi Fratta and Ugo Montanari. *A Boolean algebra method for computing the terminal reliability in a communication network*. IEEE Transactions on Circuit Theory, 1973.

[303] Jason L. Cook and Jose Emmanuel Ramirez-Marquez. *Two-terminal reliability analyses for a mobile ad hoc wireless network*. Reliability Engineering & System Safety, 2007.

[304] Cancer Genome Atlas Network et al. *Comprehensive molecular portraits of human breast tumors*. Nature, 490(7418):61, 2012.

[305] Abel Gonzalez-Perez and Nuria Lopez-Bigas. *Functional impact bias reveals cancer drivers*. Nucleic acids research, page gks743, 2012.

[306] Sam Ng, Eric A Collisson, Artem Sokolov, Theodore Goldstein, Abel Gonzalez-Perez, Nuria Lopez-Bigas, Christopher Benz, David Haussler, and Joshua M Stuart. *PARADIGM-SHIFT predicts the function of mutations in multiple cancers using pathway impact analysis*. Bioinformatics, 28(18):i640–i646, 2012.

[307] Jimmy Van den Eynden, Ana Carolina Fierro, Lieven PC Verbeke, and Kathleen Marchal. *SomInaClust: detection of cancer genes based on somatic mutation patterns of inactivation and clustering*. BMC bioinformatics, 16(1):125, 2015.

[308] Ludmil B Alexandrov, Serena Nik-Zainal, David C Wedge, Samuel AJR Aparicio, Sam Behjati, Andrew V Biankin, Graham R Bignell, Niccolo Bolli, Ake Borg, Anne-Lise Børresen-Dale, et al. *Signatures of mutational processes in human cancer*. Nature, 500(7463):415–421, 2013.

[309] William C Hahn and Robert A Weinberg. *Modelling the molecular circuitry of cancer*. Nature Reviews Cancer, 2(5):331–341, 2002.

[310] Bert Vogelstein, Nickolas Papadopoulos, Victor E Velculescu, Shibin Zhou, Luis A Diaz, and Kenneth W Kinzler. *Cancer genome landscapes*. science, 339(6127):1546–1558, 2013.

[311] Chen-Hsiang Yeang, Frank McCormick, and Arnold Levine. *Combinatorial patterns of somatic gene mutations in cancer*. The FASEB Journal, 22(8):2605–2622, 2008.

[312] Mark DM Leiserson, Hsin-Ta Wu, Fabio Vandin, and Benjamin J Raphael. *CoMEt: a statistical approach to identify combinations of mutually exclusive alterations in cancer*. Genome biology, 16(1):160, 2015.

[313] Sohrab P Shah, Andrew Roth, Rodrigo Goya, Arusha Oloumi, Gavin Ha, Yongjun Zhao, Gulisa Turashvili, Jiarui Ding, Kane Tse, Gholamreza Haffari, et al. *The clonal and mutational evolution spectrum of primary triple-negative breast cancers*. Nature, 486(7403):395–399, 2012.

[314] Cyriac Kandoth, Michael D McLellan, Fabio Vandin, Kai Ye, Beifang Niu, Charles Lu, Mingchao Xie, Qunyuan Zhang, Joshua F McMichael, Matthew A Wyczalkowski, et al. *Mutational landscape and significance across 12 major cancer types*. Nature, 502(7471):333–339, 2013.

[315] P Andrew Futreal, Lachlan Coin, Mhairi Marshall, Thomas Down, Timothy Hubbard, Richard Wooster, Nazneen Rahman, and Michael R Stratton. *A census of human cancer genes*. Nature Reviews Cancer, 4(3):177–183, 2004.

[316] Anke H Sillars-Hardebol, Beatriz Carvalho, Jeroen AM Beliën, Meike de Wit, Pien M Delis-van Diemen, Marianne Tijssen, Mark A van de Wiel, Fredrik Pontén, Remond JA Fijneman, and Gerrit A Meijer. *BCL2L1 has a functional role in colorectal cancer and its protein expression is associated with chromosome 20q gain*. The Journal of pathology, 226(3):442–450, 2012.

[317] YH Kim, L Girard, CP Giacomini, P Wang, T Hernandez-Boussard, R Tibshirani, JD Minna, and JR Pollack. *Combined microarray analysis of small cell lung cancer reveals altered apoptotic balance and distinct expression signatures of MYC family gene amplification*. Oncogene, 25(1):130–138, 2006.

[318] Yu-Ting Chou, Chih-Chan Lee, Shih-Hsin Hsiao, Sey-En Lin, Sheng-Chieh Lin, Chih-Hung Chung, Chi-Hsiu Chung, Yu-Rong Kao, Yuan-Hung Wang, Chien-Tsun Chen, et al. *The emerging role of SOX2 in cell proliferation and survival and its crosstalk with oncogenic signaling in lung cancer*. Stem cells, 31(12):2607–2619, 2013.

[319] Mariangela De Robertis, Luisa Loiacono, Caterina Fusilli, Maria Luana Poeta, Tommaso Mazza, Massimo Sanchez, Luigi Marchionni, Emanuela Signori, Giuseppe Lamorte, Angelo Luigi Vescovi, et al. *Dysregulation of EGFR pathway in EphA2*

*cell subpopulation significantly associates with poor prognosis in colorectal cancer*. Clinical Cancer Research, 23(1):159–170, 2017.

[320] Christian Perez-Llamas and Nuria Lopez-Bigas. *Gitools: analysis and visualisation of genomic data using interactive heat-maps*. PloS one, 6(5):e19541, 2011.

[321] Martin Kircher, Daniela M Witten, Preti Jain, Brian J O'roak, Gregory M Cooper, and Jay Shendure. *A general framework for estimating the relative pathogenicity of human genetic variants*. Nature genetics, 46(3):310–315, 2014.

[322] Michael S Lawrence, Petar Stojanov, Craig H Mermel, James T Robinson, Levi A Garraway, Todd R Golub, Matthew Meyerson, Stacey B Gabriel, Eric S Lander, and Gad Getz. *Discovery and saturation analysis of cancer genes across 21 tumour types*. Nature, 505(7484):495–501, 2014.

[323] Juan Carlos Oliveros. *Venny. An interactive tool for comparing lists with Venn's diagrams*, 2007-2015.

[324] Jishnu Das and Haiyuan Yu. *HINT: High-quality protein interactomes and their applications in understanding human disease*. BMC systems biology, 6(1):92, 2012.

[325] Thomas Rolland, Murat Taşan, Benoit Charloteaux, Samuel J Pevzner, Quan Zhong, Nidhi Sahni, Song Yi, Irma Lemmens, Celia Fontanillo, Roberto Mosca, et al. *A proteome-scale map of the human interactome network*. Cell, 159(5):1212–1226, 2014.

[326] David Croft, Antonio Fabregat Mundo, Robin Haw, Marija Milacic, Joel Weiser, Guanming Wu, Michael Caudy, Phani Garapati, Marc Gillespie, Maulik R Kamdar, et al. *The Reactome pathway knowledgebase*. Nucleic acids research, 42(D1):D472–D477, 2014.

[327] Broad Institute of MIT and Harvard. *road Institute TCGA Genome Data Analysis Center: Correlations between copy number and mRNA expression*, 2015.

[328] Broad Institute of MIT and Harvard. *Broad Institute TCGA Genome Data Analysis Center: SNP6 Copy number analysis (GISTIC2)*, 2015.

[329] Broad Institute of MIT and Harvard. *Broad Institute TCGA Genome Data Analysis Center (2016): Mutation Assessor*, 2016.

[330] Boris Reva, Yevgeniy Antipin, and Chris Sander. *Predicting the functional impact of protein mutations: application to cancer genomics*. Nucleic acids research, page gkr407, 2011.

[331] Craig H Mermel, Steven E Schumacher, Barbara Hill, Matthew L Meyerson, Rameen Beroukhim, and Gad Getz. *GISTIC2. 0 facilitates sensitive and confident localization of the targets of focal somatic copy-number alteration in human cancers*. Genome biology, 12(4):R41, 2011.

[332] Broad Institute of MIT and Harvard. *Broad Institute TCGA Genome Data Analysis Center: Mutation Analysis (MutSigCV v0.9)*, 2015.

[333] Broad Institute of MIT and Harvard. *Broad Institute TCGA Genome Data Analysis Center: Mutation Analysis (MutSig 2CV v3.1)*, 2015.

[334] Ngak-Leng Sim, Prateek Kumar, Jing Hu, Steven Henikoff, Georg Schneider, and Pauline C Ng. *SIFT web server: predicting effects of amino acid substitutions on proteins*. Nucleic acids research, 40(W1):W452–W457, 2012.

[335] Ivan A Adzhubei, Steffen Schmidt, Leonid Peshkin, Vasily E Ramensky, Anna Gerasimova, Peer Bork, Alexey S Kondrashov, and Shamil R Sunyaev. *A method and server for predicting damaging missense mutations*. Nature methods, 7(4):248–249, 2010.

[336] Huaiyu Mi, Qing Dong, Anushya Muruganujan, Pascale Gaudet, Suzanna Lewis, and Paul D Thomas. *PANTHER version 7: improved phylogenetic trees, orthologs and collaboration with the Gene Ontology Consortium*. Nucleic acids research, page gkp1019, 2009.

[337] Minoru Kanehisa, Michihiro Araki, Susumu Goto, Masahiro Hattori, Mika Hirakawa, Masumi Itoh, Toshiaki Katayama, Shuichi Kawashima, Shujiro Okuda, Toshiaki Tokimatsu, et al. *KEGG for linking genomes to life and the environment*. Nucleic acids research, 36(suppl 1):D480–D484, 2008.

[338] Satoko Yamamoto, Noriko Sakai, Hiromi Nakamura, Hiroshi Fukagawa, Ken Fukuda, and Toshihisa Takagi. *INOH: ontology-based highly structured database of signal transduction pathways*. Database, 2011:bar052, 2011.

[339] Guanming Wu, Xin Feng, and Lincoln Stein. *A human functional protein interaction network and its application to cancer data analysis*. Genome biology, 11(5):R53, 2010.

[340] Felix Rückert, Gihan Dawelbait, Christof Winter, Arndt Hartmann, Axel Denz, Ole Ammerpohl, Michael Schroeder, Hans Konrad Schackert, Bence Sipos, Günter Klöppel, et al. *Examination of apoptosis signaling in pancreatic cancer by computational signal transduction analysis*. PloS one, 5(8):e12243, 2010.

[341] Soyoung Choi, Zhengming Chen, Laura H Tang, Yuanzhang Fang, Sandra J Shin, Nicole C Panarelli, Yao-Tseng Chen, Yi Li, Xuejun Jiang, and Yi-Chieh Nancy Du. *Bcl-xL promotes metastasis independent of its anti-apoptotic activity*. Nature communications, 7, 2016.

[342] Franziska Ertel, Mai Nguyen, Anne Roulston, and Gordon C Shore. *Programming cancer cells for high expression levels of Mcl1*. EMBO reports, 14(4):328–336, 2013.

[343] Ldia Hernandez, Sarah Hsu, Ben Davidson, Michael J. Birrer, Elise C. Kohn, and Christina M. Annunziata. *Activation of NF-kappaB signaling by inhibitor of NF-kappaB kinase beta increases aggressiveness of ovarian cancer*. Cancer Research, 2010.

[344] Chen-Bo Ding, Wei-Na Yu, Ji-Hong Feng, and Jun-Min Luo. *Structure and function of Gab2 and its role in cancer (Review)*. Molecular medicine reports, 12(3):4007–4014, 2015.

[345] M Bocanegra, A Bergamaschi, YH Kim, MA Miller, AB Rajput, J Kao, A Langerød, W Han, D-Y Noh, SS Jeffrey, et al. *Focal amplification and oncogene dependency of GAB2 in breast cancer*. Oncogene, 29(5):774–779, 2010.

[346] Gerold Bepler and Angelika Koehler. *Multiple chromosomal aberrations and 11p allelotyping in lung cancer cell lines*. Cancer genetics and cytogenetics, 84(1):39–45, 1995.

[347] Outi Monni, Maarit Bärlund, Spyro Mousses, Juha Kononen, Guido Sauter, Mervi Heiskanen, Paulina Paavola, Kristiina Avela, Yidong Chen, Michael L Bittner, et al. *Comprehensive copy number and gene expression profiling of the 17q23 amplicon in human breast cancer*. Proceedings of the National Academy of Sciences, 98(10):5711–5716, 2001.

[348] Ganapathy Sriram and Raymond B Birge. *Emerging roles for crk in human cancer*. Genes & cancer, 1(11):1132–1139, 2010.

[349] Kelly E Fathers, Emily S Bell, Charles V Rajadurai, Sean Cory, Hong Zhao, Anna Mourskaia, Dongmei Zuo, Jason Madore, Anie Monast, Anne-Marie Mes-Masson, et al. *Crk adaptor proteins act as key signaling integrators for breast tumorigenesis*. Breast Cancer Research, 14(3):R74, 2012.

[350] Emily S Bell and Morag Park. *Models of crk adaptor proteins in cancer*. Genes & cancer, 3(5-6):341–352, 2012.

[351] Xiang Zhou, Qian Hao, Peng Liao, Shiwen Luo, Minhong Zhang, Guohui Hu, Hongbing Liu, Yiwei Zhang, Bo Cao, Melody Baddoo, et al. *Nerve growth factor receptor negates the tumor suppressor p53 as a feedback regulator*. Elife, 5:e15099, 2016.

[352] Alexander D Boiko, Olga V Razorenova, Matt van de Rijn, Susan M Swetter, Denise L Johnson, Daphne P Ly, Paris D Butler, George P Yang, Benzion Joshua, Michael J Kaplan, et al. *Human melanoma-initiating cells express neural crest nerve growth factor receptor CD271*. Nature, 466(7302):133–137, 2010.

[353] Gianluca Civenni, Anne Walter, Nikita Kobert, Daniela Mihic-Probst, Marie Zipser, Benedetta Belloni, Burkhardt Seifert, Holger Moch, Reinhard Dummer, Maries van den Broek, et al. *Human CD271-positive melanoma stem cells associated with metastasis establish tumor heterogeneity and long-term growth*. Cancer research, 71(8):3098–3109, 2011.

[354] Angela LM Johnston, Xueqing Lun, Jennifer J Rahn, Abdelhamid Liacini, Limei Wang, Mark G Hamilton, Ian F Parney, Barbara L Hempstead, Stephen M Robbins, Peter A Forsyth, et al. *The p75 neurotrophin receptor is a central regulator of glioma invasion*. PLoS Biol, 5(8):e212, 2007.

[355] Mariangela De Robertis, Luisa Loiacono, Caterina Fusilli, Maria Luana Poeta, Tommaso Mazza, Massimo Sanchez, Luigi Marchionni, Emanuela Signori, Giuseppe Lamorte, Angelo Luigi Vescovi, et al. *Dysregulation of EGFR pathway in EphA2 cell subpopulation significantly associates with poor prognosis in colorectal cancer*. Clinical Cancer Research, 23(1):159–170, 2017.

[356] Sarah Keppler, Susann Wei$\beta$bach, Christian Langer, Stefan Knop, Jordan Pischimarov, Miriam Kull, Thorsten Stühmer, Torsten Steinbrunn, Ralf Bargou, Hermann Einsele, et al. *Rare SNPs in receptor tyrosine kinases are negative outcome predictors in multiple myeloma*. Oncotarget, 7(25):38762, 2016.

[357] Lilly YW Bourguignon, Hongbo Zhu, Bo Zhou, Falko Diedrich, Patrick A Singleton, and Mien-Chie Hung. *Hyaluronan promotes CD44v3-Vav2 interaction with Grb2-p185HER2 and induces Rac1 and Ras signaling during ovarian tumor cell migration and growth*. Journal of Biological Chemistry, 276(52):48679–48692, 2001.

[358] Marco Ranzani, Stefano Annunziato, David J Adams, and Eugenio Montini. *Cancer gene discovery: exploiting insertional mutagenesis*. Molecular Cancer Research, 11(10):1141–1158, 2013.

[359] M Dorigo and Luca Maria Gambardella. *Ant-Q: a reinforcement learning approach to combinatorial optimization*. Universite Libre de Bruxelles, Belgium, 1995.

[360] Marco Dorigo and Luca Maria Gambardella. *Ant colony system: a cooperative learning approach to the traveling salesman problem*. IEEE Transactions on evolutionary computation, 1(1):53–66, 1997.

[361] David Hernandez, Patrice François, Laurent Farinelli, Magne Østerås, and Jacques Schrenzel. *De novo bacterial genome sequencing: millions of very short reads assembled on a desktop computer*. Genome research, 18(5):802–809, 2008.

[362] Silpa Suthram, Andreas Beyer, Richard M Karp, Yonina Eldar, and Trey Ideker. *eQED: an efficient method for interpreting eQTL associations using protein networks*. Molecular systems biology, 4(1):162, 2008.

[363] Esti Yeger-Lotem, Laura Riva, Linhui Julie Su, Aaron D Gitler, Anil G Cashikar, Oliver D King, Pavan K Auluck, Melissa L Geddie, Julie S Valastyan, David R Karger, et al. *Bridging high-throughput genetic and transcriptional data reveals cellular responses to alpha-synuclein toxicity*. Nature genetics, 41(3):316–323, 2009.

[364] John S Mattick and Igor V Makunin. *Non-coding RNA*. Human molecular genetics, 15(suppl_1):R17–R29, 2006.

[365] Xiu Cheng Quek, Daniel W Thomson, Jesper LV Maag, Nenad Bartonicek, Bethany Signal, Michael B Clark, Brian S Gloss, and Marcel E Dinger. *lncRNAdb v2. 0: expanding the reference database for functional long noncoding RNAs*. Nucleic acids research, 43(D1):D168–D173, 2014.

[366] Peter J Turnbaugh, Ruth E Ley, Micah Hamady, Claire Fraser-Liggett, Rob Knight, and Jeffrey I Gordon. *The human microbiome project: exploring the microbial part of ourselves in a changing world*. Nature, 449(7164):804, 2007.

[367] Ettje F Tigchelaar, Alexandra Zhernakova, Jackie AM Dekens, Gerben Hermes, Agnieszka Baranska, Zlatan Mujagic, Morris A Swertz, Angélica M Muñoz, Patrick Deelen, Maria C Cénit, et al. *Cohort profile: LifeLines DEEP, a prospective, general population cohort study in the northern Netherlands: study design and baseline characteristics*. BMJ open, 5(8):e006772, 2015.

[368] Luana Martins Perin, Maria Luisa Savo Sardaro, Luís Augusto Nero, Erasmo Neviani, and Monica Gatti. *Bacterial ecology of artisanal Minas cheeses assessed by culture-dependent and-independent methods*. Food Microbiology, 65:160–169, 2017.

[369] Eduardo Medina, Ilenys M Pérez-Díaz, Fred Breidt, Janet Hayes, Wendy Franco, Natasha Butz, and María Andrea Azcarate-Peril. *Bacterial Ecology of Fermented Cucumber Rising pH Spoilage as Determined by Nonculture-Based Methods*. Journal of food science, 81(1):M121–M129, 2016.

[370] David M Ward, Roland Weller, and Mary M Bateson. *16S rRNA sequences reveal numerous uncultured microorganisms in a natural community*. Nature, 345(6270):63, 1990.

[371] Gwen Falony, Marie Joossens, Sara Vieira-Silva, Jun Wang, Youssef Darzi, Karoline Faust, Alexander Kurilshikov, Marc Jan Bonder, Mireia Valles-Colomer, Doris Vandeputte, et al. *Population-level analysis of gut microbiome variation*. Science, 352(6285):560–564, 2016.

[372] Human Microbiome Project Consortium et al. *A framework for human microbiome research*. Nature, 486(7402):215–221, 2012.

[373] Jorge Frias-Lopez, Yanmei Shi, Gene W Tyson, Maureen L Coleman, Stephan C Schuster, Sallie W Chisholm, and Edward F DeLong. *Microbial community gene expression in ocean surface waters*. Proceedings of the National Academy of Sciences, 105(10):3805–3810, 2008.

[374] Jack A Gilbert, Dawn Field, Ying Huang, Robert A Edwards, Weizhong Li, Paul Gilna, and Ian Joint. *Detection of large numbers of novel sequences in the metatranscriptomes of complex marine microbial communities*. Handbook of Molecular Microbial Ecology II: Metagenomics in Different Habitats, pages 277–286, 2011.

[375] Bo Liu and Mihai Pop. *MetaPath: identifying differentially abundant metabolic pathways in metagenomic datasets*. In BMC proceedings, volume 5, page S9. BioMed Central, 2011.

[376] Olga V Kalinina, Oliver Wichmann, Gordana Apic, and Robert B Russell. *ProtChemSI: a network of protein–chemical structural interactions*. Nucleic acids research, 40(D1):D549–D553, 2012.

[377] Damian Szklarczyk, Alberto Santos, Christian von Mering, Lars Juhl Jensen, Peer Bork, and Michael Kuhn. *STITCH 5: augmenting protein–chemical interaction networks with tissue and affinity data*. Nucleic acids research, 44(D1):D380–D384, 2016.

[378] David B Solit, Levi A Garraway, Christine A Pratilas, Ayana Sawai, Gad Getz, Andrea Basso, Qing Ye, Jose M Lobo, Yuhong She, Iman Osman, et al. *BRAF mutation predicts sensitivity to MEK inhibition*. Nature, 439(7074):358–362, 2006.

[379] Jinho Kim, Inhae Kim, Seong Kyu Han, James U Bowie, and Sanguk Kim. *Network rewiring is an important mechanism of gene essentiality change*. Scientific reports, 2:900, 2012.

[380] Sourav Bandyopadhyay, Monika Mehta, Dwight Kuo, Min-Kyung Sung, Ryan Chuang, Eric J Jaehnig, Bernd Bodenmiller, Katherine Licon, Wilbert Copeland, Michael Shales, et al. *Rewiring of genetic networks in response to DNA damage*. Science, 330(6009):1385–1389, 2010.

[381] Hunter B Fraser, Aaron E Hirsh, Lars M Steinmetz, Curt Scharfe, and Marcus W Feldman. *Evolutionary rate in the protein interaction network*. Science, 296(5568):750–752, 2002.

[382] Omer Basha, Dvir Flom, Ruth Barshir, Ilan Smoly, Shoval Tirman, and Esti Yeger-Lotem. *MyProteinNet: build up-to-date protein interaction networks for organisms, tissues and user-defined contexts*. Nucleic acids research, 43(W1):W258–W263, 2015.

[383] Edward L Huttlin, Mark P Jedrychowski, Joshua E Elias, Tapasree Goswami, Ramin Rad, Sean A Beausoleil, Judit Villén, Wilhelm Haas, Mathew E Sowa, and Steven P Gygi. *A tissue-specific atlas of mouse protein phosphorylation and expression*. Cell, 143(7):1174–1189, 2010.

[384] Casey S Greene, Arjun Krishnan, Aaron K Wong, Emanuela Ricciotti, Rene A Zelaya, Daniel S Himmelstein, Ran Zhang, Boris M Hartmann, Elena Zaslavsky, Stuart C Sealfon, et al. *Understanding multicellular function and disease with human tissue-specific networks*. Nature genetics, 47(6):569–576, 2015.

[385] Yuanfang Guan, Dmitriy Gorenshteyn, Margit Burmeister, Aaron K Wong, John C Schimenti, Mary Ann Handel, Carol J Bult, Matthew A Hibbs, and Olga G Troyanskaya. *Tissue-specific functional networks for prioritizing phenotype and disease genes*. PLoS Comput Biol, 8(9):e1002694, 2012.

[386] JE Król, JT Penrod, H McCaslin, LM Rogers, H Yano, AD Stancik, W Dejonghe, CJ Brown, RE Parales, Stefan Wuertz, et al. *Role of IncP-1$\beta$ plasmids pWDL7::*

*rfp and pNB8c in chloroaniline catabolism as determined by genomic and functional analyses*. Applied and environmental microbiology, 78(3):828–838, 2012.

[387] Allyson M MacLean, Gordon MacPherson, Punita Aneja, and Turlough M Finan. *Characterization of the $\beta$-ketoadipate pathway in Sinorhizobium meliloti*. Applied and environmental microbiology, 72(8):5403–5413, 2006.

[388] Fenja S Bleichrodt, Rita Fischer, and Ulrike C Gerischer. *The $\beta$-ketoadipate pathway of Acinetobacter baylyi undergoes carbon catabolite repression, cross-regulation and vertical regulation, and is affected by Crc*. Microbiology, 156(5):1313–1322, 2010.

[389] D J Reasoner and EE Geldreich. *A new medium for the enumeration and subculture of bacteria from potable water.* Applied and environmental microbiology, 49(1):1–7, 1985.

[390] Joseph Sambrook, Edward F Fritsch, Tom Maniatis, et al. *Molecular cloning: a laboratory manual.* Cold spring harbor laboratory press, 1989.

[391] Daniel R Zerbino and Ewan Birney. *Velvet: algorithms for de novo short read assembly using de Bruijn graphs*. Genome research, 18(5):821–829, 2008.

[392] You Zhou, Yongjie Liang, Karlene H Lynch, Jonathan J Dennis, and David S Wishart. *PHAST: a fast phage search tool*. Nucleic acids research, page gkr485, 2011.

[393] Rembrandt JF Haft, David H Keating, Tyler Schwaegler, Michael S Schwalbach, Jeffrey Vinokur, Mary Tremaine, Jason M Peters, Matthew V Kotlajich, Edward L Pohlmann, Irene M Ong, et al. *Correcting direct effects of ethanol on translation and transcription machinery confers ethanol tolerance in bacteria*. Proceedings of the National Academy of Sciences, 111(25):E2576–E2585, 2014.

[394] Christopher M Burns and John P Richardson. *NusG is required to overcome a kinetic limitation to Rho function at an intragenic terminator*. Proceedings of the National Academy of Sciences, 92(11):4738–4742, 1995.

[395] Zvi Pasman and Peter H von Hippel. *Regulation of rho-dependent transcription termination by NusG is specific to the Escherichia coli elongation complex*. Biochemistry, 39(18):5573–5585, 2000.

[396] Peter L Freddolino, Hani Goodarzi, and Saeed Tavazoie. *Fitness landscape transformation through a single amino acid change in the Rho terminator*. PLoS Genet, 8(5):e1002744, 2012.

[397] Ingrid M Keseler, Amanda Mackie, Martin Peralta-Gil, Alberto Santos-Zavaleta, Socorro Gama-Castro, César Bonavides-Martínez, Carol Fulcher, Araceli M Huerta, Anamika Kothari, Markus Krummenacker, et al. *EcoCyc: fusing model organism databases with systems biology*. Nucleic acids research, 41(D1):D605–D612, 2013.

[398] Katsunori Yoshikawa, Tadamasa Tanaka, Chikara Furusawa, Keisuke Nagahisa, Takashi Hirasawa, and Hiroshi Shimizu. *Comprehensive phenotypic analysis for identification of genes affecting growth under ethanol stress in Saccharomyces cerevisiae*. FEMS yeast research, 9(1):32–44, 2009.

[399] Dragana Stanley, Ajith Bandara, Sarah Fraser, PJ Chambers, and Grant A Stanley. *The ethanol stress response and ethanol tolerance of Saccharomyces cerevisiae*. Journal of applied microbiology, 109(1):13–24, 2010.

[400] Takaaki Horinouchi, Shingo Suzuki, Takashi Hirasawa, Naoaki Ono, Tetsuya Yomo, Hiroshi Shimizu, and Chikara Furusawa. *Phenotypic convergence in bacterial adaptive evolution to ethanol stress*. BMC Evolutionary Biology, 15(1):180, 2015.

[401] Nina Bacher Reuven, Gali Arad, Ayelet Maor-Shoshani, and Zvi Livneh. *The mutagenesis protein UmuC is a DNA polymerase activated by UmuD, RecA, and SSB and is specialized for translesion replication*. Journal of Biological Chemistry, 274(45):31763–31766, 1999.

[402] Andrew Robinson, John P McDonald, Victor EA Caldas, Meghna Patel, Elizabeth A Wood, Christiaan M Punter, Harshad Ghodke, Michael M Cox, Roger Woodgate, Myron F Goodman, et al. *Regulation of mutagenic DNA polymerase V activation in space and time*. PLoS Genet, 11(8):e1005482, 2015.

[403] Anbu K Adikesavan, Panagiotis Katsonis, David C Marciano, Rhonald Lua, Christophe Herman, and Olivier Lichtarge. *Separation of recombination and SOS response in Escherichia coli RecA suggests LexA interaction sites*. PLoS Genet, 7(9):e1002244, 2011.

[404] Maxim V Sukhodolets, Julio E Cabrera, Huijun Zhi, and Ding Jun Jin. *RapA, a bacterial homolog of SWI2/SNF2, stimulates RNA polymerase recycling in transcription*. Genes & development, 15(24):3330–3341, 2001.

[405] Bernd Bukau and Arthur L Horwich. *The Hsp70 and Hsp60 chaperone machines*. Cell, 92(3):351–366, 1998.

[406] Jeffrey G Thomas and François Baneyx. *ClpB and HtpG facilitate de novo protein folding in stressed Escherichia coli cells*. Molecular microbiology, 36(6):1360–1370, 2000.

[407] Florence Arsène, Toshifumi Tomoyasu, and Bernd Bukau. *The heat shock response of Escherichia coli*. International journal of food microbiology, 55(1):3–9, 2000.

[408] Kyle A Zingaro and Eleftherios Terry Papoutsakis. *Toward a semisynthetic stress response system to engineer microbial solvent tolerance*. Mbio, 3(5):e00308–12, 2012.

[409] Hiroshi Ogasawara, Akiko Hasegawa, Emi Kanda, Takenori Miki, Kaneyoshi Yamamoto, and Akira Ishihama. *Genomic SELEX search for target promoters under the control of the PhoQP-RstBA signal relay cascade*. Journal of bacteriology, 189(13):4791–4799, 2007.

[410] E Turlin, F Gasser, and F Biville. *Sequence and functional analysis of an Escherichia coli DNA fragment able to complement pqqE and pqqF mutants from Methylobacterium organophilum*. Biochimie, 78(10):822–831, 1996.

[411] Amy L Springer, Roopa Ramamoorthi, and Mary E Lidstrom. *Characterization and nucleotide sequence of pqqE and pqqF in Methylobacterium extorquens AM1*. Journal of bacteriology, 178(7):2154–2157, 1996.

[412] Ronnie Machielsen, Agustinus R Uria, Servé WM Kengen, and John van der Oost. *Production and characterization of a thermostable alcohol dehydrogenase that belongs to the aldo-keto reductase superfamily*. Applied and environmental microbiology, 72(1):233–238, 2006.

[413] Alla Gagarinova, Geordie Stewart, Bahram Samanfar, Sadhna Phanse, Carl A White, Hiroyuki Aoki, Viktor Deineko, Natalia Beloglazova, Alexander F Yakunin, Ashkan

Golshani, et al. *Systematic Genetic Screens Reveal the Dynamic Global Functional Organization of the Bacterial Translation Machinery*. Cell Reports, 17(3):904–916, 2016.

[414] Joel Selkrig, Khedidja Mosbahi, Chaille T Webb, Matthew J Belousoff, Andrew J Perry, Timothy J Wells, Faye Morris, Denisse L Leyton, Makrina Totsika, Minh-Duy Phan, et al. *Discovery of an archetypal protein transport system in bacterial outer membranes*. Nature structural & molecular biology, 19(5):506–510, 2012.

[415] Kristian Kjærgaard, Mark A Schembri, Henrik Hasman, and Per Klemm. *Antigen 43 from Escherichia coli induces inter-and intraspecies cell aggregation and changes in colony morphology of Pseudomonas fluorescens*. Journal of bacteriology, 182r(17):4789–4796, 2000.

[416] Per Klemm, Louise Hjerrild, Morten Gjermansen, and Mark A Schembri. *Structure-function analysis of the self-recognizing antigen 43 autotransporter protein from Escherichia coli*. Molecular microbiology, 51(1):283–296, 2004.

[417] Paolo Landini. *Cross-talk mechanisms in biofilm formation and responses to environmental and physiological stress in Escherichia coli*. Research in microbiology, 160(4):259–266, 2009.

[418] Bing Yu, Stephen Swatkoski, Alesia Holly, Liam C Lee, Valentin Giroux, Chih-Shia Lee, Dennis Hsu, Jordan L Smith, Garmen Yuen, Junqiu Yue, et al. *Oncogenesis driven by the Ras/Raf pathway requires the SUMO E2 ligase Ubc9*. Proceedings of the National Academy of Sciences, 112(14):E1724–E1733, 2015.

[419] William Weidong Du, Ling Fang, Xiangling Yang, Wang Sheng, Bing L Yang, Arun Seth, Yaou Zhang, Burton B Yang, and Albert J Yee. *The role of versican in modulating breast cancer cell self-renewal*. Molecular Cancer Research, 11(5):443–455, 2013.

[420] William Weidong Du, Weining Yang, and Albert J Yee. *Roles of versican in cancer biologytumorigenesis, progression and metastasis*. Histol Histopathol, 28(6):701–713, 2013.

[421] Andrew J Sakko, Carmela Ricciardelli, Keiko Mayne, Wayne D Tilley, Richard G LeBaron, and David J Horsfall. *Versican accumulation in human prostatic fibroblast cultures is enhanced by prostate cancer cell-derived transforming growth factor $\beta$1*. Cancer research, 61(3):926–930, 2001.

[422] Kanda Fanhchaksai, Futoshi Okada, Naoko Nagai, Peraphan Pothacharoen, Prachya Kongtawelert, Sonoko Hatano, Shinji Makino, Tomoyuki Nakamura, and Hideto Watanabe. *Host stromal versican is essential for cancer-associated fibroblast function to inhibit cancer growth*. International Journal of Cancer, 138(3):630–641, 2016.

[423] Nidhi Gupta, Rehan Khan, Raman Kumar, Lalit Kumar, and Alpana Sharma. *Versican and its associated molecules: Potential diagnostic markers for multiple myeloma*. Clinica Chimica Acta, 442:119–124, 2015.

[424] Kohichi Takada, Di Zhu, Gregory H Bird, Kumar Sukhdeo, Jian-Jun Zhao, Mala Mani, Madeleine Lemieux, Daniel E Carrasco, Jeremy Ryan, David Horst, et al. *Targeted disruption of the BCL9/$\beta$-catenin complex inhibits oncogenic Wnt signaling*. Science translational medicine, 4(148):148ra117–148ra117, 2012.

[425] Mei Dong, Xiaoyan Pang, Yang Xu, Fang Wen, and Yi Zhang. *Ubiquitin-conjugating enzyme 9 promotes epithelial ovarian cancer cell proliferation in vitro*. International journal of molecular sciences, 14(6):11061–11071, 2013.

[426] Giovanni Benard, Albert Neutzner, Guihong Peng, Chunxin Wang, Ferenc Livak, Richard J Youle, and Mariusz Karbowski. *IBRDC2, an IBR-type E3 ubiquitin ligase, is a regulatory factor for Bax and apoptosis activation*. The EMBO journal, 29(8):1458–1471, 2010.